Photochemical reactions at atmospherically relevant interfaces

Liselotte Tinel

Thèse de l'Université de Lyon

Présentée devant
L'UNIVERSITÉ CLAUDE BERNARD – LYON1
ÉCOLE DOCTORALE DE CHIMIE

Pour l'obtention du
Diplôme de doctorat
(arrêté du 7 août 2006)

Soutenue et présentée publiquement le 07 décembre 2015

Par

Liselotte Tinel

Des réactions photochimiques aux interfaces atmosphériques

Photochemical reactions at atmospherically relevant interfaces

---

Directeur de thèse: Dr. Christian George

Jury :

Pr. Olivier PIVA	*Président*	*Université Claude Bernard – Lyon 1*
Pr. D. James DONALDSON	*Rapporteur*	*University of Toronto, Canada*
Dr. Marcello BRIGANTE	*Rapporteur*	*Université Blaise Pascal, Clermont-Ferrand*
Dr. Véronique DAËLE	*Examinatrice*	*ICARE, CNRS, Orléans*
Pr. Anne MONOD	*Examinatrice*	*Université Aix-Marseille, Marseille*
Dr. Christian GEORGE	*Directeur de thèse*	*IRCELYON, CNRS, Lyon*
Dr. Stéphane DUMAS	*Co-directeur de thèse*	*IRCELYON, CNRS, Lyon*

IRCELYON – UMR 5256 CNRS – Université de Lyon 1
2, Avenue Albert Einstein, 69626 VILLEURBANNE Cedex

UNIVERSITE CLAUDE BERNARD - LYON 1

Président de l'Université	**M. François-Noël GILLY**
Vice-président du Conseil d'Administration	M. le Professeur Hamda BEN HADID
Vice-président du Conseil des Etudes et de la Vie Universitaire	M. le Professeur Philippe LALLE
Vice-président du Conseil Scientifique	M. le Professeur Germain GILLET
Directeur Général des Services	M. Alain HELLEU

COMPOSANTES SANTE

Faculté de Médecine Lyon Est – Claude Bernard	Directeur : M. le Professeur J. ETIENNE
Faculté de Médecine et de Maïeutique Lyon Sud – Charles Mérieux	Directeur : Mme la Professeure C. BURILLON
Faculté d'Odontologie	Directeur : M. le Professeur D. BOURGEOIS
Institut des Sciences Pharmaceutiques et Biologiques	Directeur : Mme la Professeure C. VINCIGUERRA
Institut des Sciences et Techniques de la Réadaptation	Directeur : M. le Professeur Y. MATILLON
Département de formation et Centre de Recherche en Biologie Humaine	Directeur : Mme. la Professeure A-M. SCHOTT

COMPOSANTES ET DEPARTEMENTS DE SCIENCES ET TECHNOLOGIE

Faculté des Sciences et Technologies	Directeur : M. F. DE MARCHI
Département Biologie	Directeur : M. le Professeur F. FLEURY
Département Chimie Biochimie	Directeur : Mme Caroline FELIX
Département GEP	Directeur : M. Hassan HAMMOURI
Département Informatique	Directeur : M. le Professeur S. AKKOUCHE
Département Mathématiques	Directeur : M. le Professeur Georges TOMANOV
Département Mécanique	Directeur : M. le Professeur H. BEN HADID
Département Physique	Directeur : M. Jean-Claude PLENET
UFR Sciences et Techniques des Activités Physiques et Sportives	Directeur : M. Y.VANPOULLE
Observatoire des Sciences de l'Univers de Lyon	Directeur : M. B. GUIDERDONI
Polytech Lyon	Directeur : M. P. FOURNIER
Ecole Supérieure de Chimie Physique Electronique	Directeur : M. G. PIGNAULT
Institut Universitaire de Technologie de Lyon 1	Directeur : M. le Professeur C. VITON
Ecole Supérieure du Professorat et de l'Education	Directeur : M. le Professeur A. MOUGNIOTTE
Institut de Science Financière et d'Assurances	Directeur : M. N. LEBOISNE

Résume de thèse: Réactions photochimiques aux interfaces atmosphériques

Les travaux présentés dans ce manuscrit portent sur des réactions photochimiques aux interfaces atmosphériques et plus précisément des réactions troposphériques induites par la lumière entre la phase gazeuse et la phase condensée, que ce soit à la surface des aérosols ou de l'eau. La thèse est composée de sept parties en forme d'article et ce résumé présentera brièvement le contenu de chaque chapitre.

Le premier chapitre comporte une introduction au contexte scientifique avec plus précisément la présentation de la composition atmosphérique, les réactions chimiques qui la déterminent et l'importance de la photochimie dans l'atmosphère avec notamment l'exemple des réactions photosensibilisées. Le rôle des réactions hétérogènes et photochimiques dans l'atmosphère est discuté, montrant que ces réactions peuvent jouer un rôle important dans l'atmosphère terrestre. L'exemple le plus marquant étant celui des particules stratosphériques polaires qui sont responsables de l'émission des halogénures moléculaires photolabiles, responsables du trou dans la couche d'ozone. Mais les aérosols ne sont pas les seules interfaces où des réactions photochimiques impactant l'atmosphère peuvent avoir lieu, d'autres surfaces comme le sol, les surfaces des constructions ou la surface de l'eau superficielle constituent autant de sites potentiels pour cette chimie, dont peu de choses sont connu actuellement. L'interface océan-atmosphère, qui couvre 75% de notre planète, pourrait être particulièrement important pour ces réactions induites par la lumière et notamment les réactions ayant lieu dans la microcouche de surface, la couche de max. 1 mm d'épaisseur avec des propriétés physiques et chimiques particulières. Les travaux de cette thèse se sont concentrés sur les réactions photochimiques à la surface des aérosols et dans la microcouche de surface.

Le deuxième chapitre détaille les différents dispositifs expérimentaux et les méthodes utilisées dans les travaux. Ces méthodes incluent des techniques spectroscopiques, comme la photolyse laser, utilisée pour la détermination des cinétiques fondamentales entre une espèces excitée et un réactif. Une autre technique spectroscopique appliquée dans ces travaux est la fluorescence induite par impulsion laser

sous un angle oblique à la surface d'une solution. Cette technique, pratiquée lors d'une collaboration avec l'Université de Toronto, permet d'observer le comportement de photosensibilisateurs à la surface de l'eau avec ou sans couche d'organique à la surface. Les autres techniques analytiques utilisées sont différentes techniques de spectrométrie de masse. L'analyse des produits en phase condensé a été faite par la chromatographie liquide couplé à la spectrométrie de masse de haute résolution. Les produits en phase gazeuse ont été mesurés avec un spectromètre de masse à transfert protonique.

Dans le troisième chapitre, les résultats d'une étude cinétique d'un photosensibilisateur, le 2-carboxy-pterine, sont présentés sous forme d'article. Nos travaux ont montré que ce photosensibilisateur, d'une famille de composés présents à la surface de la mer, est capable d'oxyder des halogénures, notamment l'iodure, quand il est excité à l'état triplet, ce qui mène à la formation de halogènes radicalaires. La réaction avec des acides organiques passe plutôt par l'état excité singulet qu'avec l'état triplet du photosensibilisateur, comme observée par des mesures fluorimétriques. La réaction avec ces acides carboxyliques est rapide et il est suggéré que ces réactions passent par un transfert d'électron de l'acide vers le photosensibilisateur excité, comme dans le cas des halogénures. Il est montré que la réaction entre 2-carboxy-pterine et acides carboxyliques forme des produits d'oxydation et un mécanisme de formation est proposé. Les implications de telles réactions à la surface de aérosols ou de l'eau sont discutées.

Un autre photosensibilisateur est sous à l'étude dans le quatrième chapitre, présenté comme deux articles publiés. Ce photosensibilisateur, l'imidazole-2-carboxaldehyde, peut être catalysé *in situ* dans les particules à partir de deux composés très largement répandus, notamment l'ion d'ammonium, très présent dans les aérosols, et le glyoxal, produit d'oxydation de nombreux composés organiques gazeux. Ces composés peuvent donc donner naissance dans l'aerosol à la formation d'un photosensibilisateur, qui induit une croissance des aérosols, par l'oxydation des composés organiques volatiles (COVs) à la surface des aérosols, comme démontré dans une étude dans un tube à écoulement. Nous proposons un chemin réactionnel pour la formation photo-induite des produits hautement oxygénés observés dans les particules. Les caractéristiques physico-chimiques de ce nouveau photosensibilisateur efficace sont étudiés par photolyse laser et sa réactivité vis-à-vis les halogénures démontrée. Cette voie d'oxydation photo-active peut mener à la formation

d'espèces radicalaires des halogènes à la surface de l'eau, et même aux formes moléculaires très réactifs des halogènes qui peuvent passer en phase gazeuse.

Le cinquième chapitre, sous forme d'article publié, rapporte des travaux effectués pour caractériser les réactions à la surface d'une solution aqueuse contenant un surfactant bien décrit, le 1-octanol et deux photosensibilisateurs connus, l'acide 4-benzoylbenzoïque et l'imidazole-2-carboxaldehyde. Lors de ces expériences il a été démontré par de la spectrométrie infrarouge que des produits fonctionnalisés et insaturés se forment dans une couche mince de ce surfactant contenant le photosensibilisateur en question. De plus, la tendance du photosensibilisateur à diffuser vers la couche de 1-octanol à la surface d'une solution aqueuse est démontré par fluorescence induite par impulsion laser à la surface de la solution couverte par une monocouche de l'organique. Ensuite l'efficacité de la réaction photochimique est montrée par la mesure des composés produits par photochimie au-dessus d'une solution aqueuse contenant le surfactant et un photosensibilisateur. Une grande diversité de produits gazeux est observée, dont des produits insaturés. Ces produits sont particulièrement importants pour l'atmosphère car ils peuvent être oxydés et ainsi condenser plus facilement sur des aérosols et promouvoir leur croissance ou provoquer la nucléation de nouvelles particules. Un mécanisme réactionnel est proposé pour la formation de certains de ces produits.

La microcouche de surface est ensuite étudiée sous un autre angle dans le sixième chapitre, de nouveau sous forme d'article. Un acide carboxylique, l'acide nonanoïque est utilisé cette fois comme microcouche de surface synthétique et un photosensibilisateur, l'acide 4-benzoylbenzoïque ajouté dans la solution aqueuse. Lors de l'irradiation de cette solution, de nombreux produits, similaires à ceux observés avec l'octanol et décrits dans le chapitre 5, sont observés lors de l'analyse en parallèle des produits en phase gazeuse et en phase condensée. Afin de comprendre les mécanismes derrière cette chimie surfacique, des expériences sont effectuées dans un milieu pauvre en oxygène d'un côté et avec du peroxyde d'hydrogène de l'autre côté, démontrant ainsi qu'un arrachement d'hydrogène est l'étape initiale dans la formation des produits et mettant en évidence le rôle de l'oxygène dans la formation des produits par un mécanisme radicalaire. Mais l'importance des réactions radical-radical est aussi soulignée par ces expériences, des réactions favorisées dans la couche de surface qui représente un milieu concentré. Enfin, des expériences sans

photosensibilisateur, avec uniquement une solution contenant l'acide nonanoïque révèlent que ce composé est lui-même capable d'induire des réactions photochimiques, menant à la formation de composés insaturés en phase gaz. Les différentes pistes expliquant ce phénomène sont discutées.

Enfin le septième chapitre vient résumer les travaux décrits, leurs implications pour l'atmosphère et jette un œil sur l'avenir.

List of used abbreviations

AMS: Aerosol Mass Spectrometer

ATR-FTIR: Attenuated Total Reflectance-Fourier Transform InfraRed Spectroscopy

4-BBA: 4-benzoylbenzoic acid

CCN: Cloud Condensation Nuclei

CDOM: Chromophoric (or colored) Dissolved Organic Matter

CPC: Condensation Particle Counter

CPT: 6-carboxypterin

dGMP: 2'-deoxyguanosine 5'-monophosphate

DMA: Differential Mobility Analyser

DMSO: dimethylsulfoxide

DOM: Dissolved Organic Matter

ESR: Electron Spin Resonance

FTIR: Fourrier Transform InfraRed spectroscopy

GALIF: Glancing Angle Laser Induced Fluorescence

IC: imidazole-2-carboxaldehyde

IN: Ice Nuclei

IR: InfraRed

LFP: Laser Flash Photolysis

LIF: Laser Induced Fluorescence

MCP: MultiChannel Plate

NA: Nonanoic Acid

OPO: Optical Parametric Oscillator

P: Photosensitizer

^{3}P: triplet excited state of the photosensitizer

^{1}P: singlet state of the photosensitizer

PMT: Photon Multiplier Tube

POA: Primary Organic Aerosols

PTR-ToF-MS: Proton Transfer Reaction Time of Flight Mass Spectrometer

RH: Relative Humidity

SIFT: Selected Ion Flow Tube

SML: Surface MicroLayer

SMPS: Scanning Mobility Particle Sizer

SOA: Secondary Organic Aerosols

SRI-ToF-MS: Switchable Reagent Ionization Time of Flight Mass Spectrometer

UPLC-HESI-HRMS: Ultrahigh Performance Liquid Chromatography Heated Electrospray Ionization High Resolution Mass Spectrometer

UV: UltraViolet irradiation

Vis: Visible irradiation

VOC : Volatile Organic Compound

Table of contents

Chapter I: Scientific context

I.0. Motivation

Air is one of the most primordial needs of humankind and many lifeforms on Earth, although clean air is nowadays not always an evidence and the influence of this air on the global climate just starts to be understood. In this very complex global puzzle, the atmosphere is linked with global warming, health, oceans, land use, climate patterns and so many more. This chapter tries to dress the scene for the work presented in this thesis by introducing the important concepts for this work and by situating them on the global puzzle of the Earth's system.

Chapter I: Scientific context

I.1. The atmosphere

I.1.1. Structure of the atmosphere

One of the particularities of our planet Earth is the existence of a gaseous envelop around its globe, called the atmosphere. This gaseous envelop is the cradle of many chemical and physical transformations impacting the conditions on Earth and one of the most concerning effects of the atmosphere, is its role in the increase of the global temperature of the planet. The greenhouse effect has been known for almost four centuries and was brought in relation with the atmosphere of the Earth almost two centuries ago (Fleming, 1999; Fourier, 1824). In the past few decades it has gained considerable attention and is now considered one of the most prominent environmental causes of this century (IPCC, 2013). Therefore, great efforts have been made to improve the understanding of the physics and chemistry ruling in the atmosphere. The body of scientific knowledge over the chemical and physical reactions taking place in the atmosphere is substantial and only a very brief overview of the basic principles will be given here.

In general, the atmosphere can be vertically divided in five layers, each characterized amongst others by an inversion of a vertical gradient of temperature. Figure I-1 illustrates this stratification of the atmosphere defining the troposphere, stratosphere, mesosphere, thermosphere and exosphere (or space). The atmosphere interacts with other elements of the Earth's system, such as the oceans, the lithosphere, the pedosphere, biosphere and the cryosphere. In the whole Earth's climate system, the atmosphere responds the fastest to changes and in global mass it represents the smallest fraction. Nonetheless, changes in the atmosphere can greatly influence the global climate through its interactions with other elements of the Earth's system.

In this work we will only focus on the lowest atmospheric layer, the troposphere, extending from ground level to 7-15 km, depending on the latitude. It is the layer where the meteorological phenomena are observed and where emissions, anthropogenic and biogenic, take place. These emissions can be transformed through a wide variety of processes in the troposphere, be degraded, transported or deposited on the Earth's surface. The troposphere

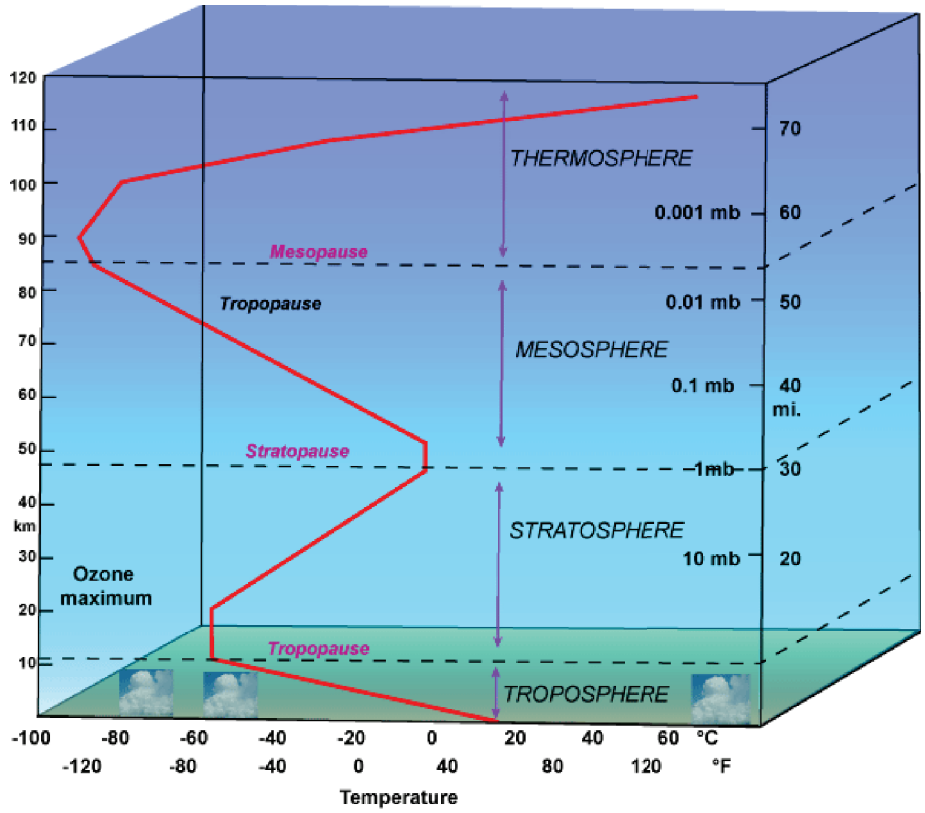

Figure I-1: Schematic of the stratification of the atmosphere and the temperature gradients in function of the altitude and pressure. From http://www.geog.ucsb.edu

is not an isolated layer and is influenced by the upper layers of the atmosphere, e.g., absorption of short wavelengths and can influence the upper layers, e.g., through direct exchange with the stratosphere, particularly at tropical latitudes.

I.1.2.Chemical composition of the atmosphere

The atmosphere of the Earth is composed mainly of a few gaseous species, N_2, O_2, Ar and water vapor, as can be seen from table I-1. Other gases are present as traces only. One of the main variables in the composition of the terrestrial atmosphere is the amount of water in the atmosphere; in liquid or gaseous form which varies with meteorological conditions, altitude and latitude. Water vapor is the most abundant greenhouse gas present in the atmosphere, with the second most abundant greenhouse gas being CO_2, whose concentration in the atmosphere is increasing steeply since the industrial revolution. Other important greenhouse gases are nitrous oxide and methane. Oxidants, such as oxygen, ozone or nitrogen dioxide, are very abundant in the atmosphere and therefore the atmosphere can be considered as a giant oxidizing reactor.

Table I-1: overview of the main constituents of the atmosphere at ground level (Delmas et al., 2005; Seinfeld and Pandis, 2012)

Species	Chemical formula	% of total volume	Mean atmospheric residence time
Nitrogen	N_2	78.084	15 x 10^{16} years
Oxygen	O_2	20.948	8 x 10^3 years
Water vapor	H_2O	0-4	6 - 15 days
Argon	Ar	0.934	infinite
Liquid water	H_2O	< 0.3	1 - 20 days
Carbon dioxide	CO_2	> 0.040	15 years
Neon	Ne	1.818 x 10^{-3}	infinite
Helium	He	1.818 x 10^{-3}	infinite
Methane	CH_4	± 1.7 x 10^{-4}	9 years
Hydrogen	H_2	± 5 x 10^{-5}	10 years
Nitrous oxide	N_2O	± 3.1 x 10^{-5}	150 years
Carbon monoxide	CO	± 1.2 x 10^{-5}	2 months
Ozone	O_3	2 - 200 x 10^{-6}	1-2 months
Ammonia	NH_3	± 0.1 - 1 x 10^{-6}	20 days
Nitrogen dioxide	NO_2	± 1 x 10^{-7}	1 day
VOC	$C_xH_yO_z$	± 0.1 - 1 x 10^{-6}	hours - days
Sulfur dioxide	SO_2	± 2 x 10^{-8}	1 day
Particles		< 10^{-5}	minutes - weeks

As it becomes clear from table I-1, the organic species, the so-called volatile organic compounds or VOCs, and particles represent only a minor fraction in the atmosphere's composition. But although only representing a minor fraction, these VOCs and particles are responsible for much of the chemistry occurring in the troposphere. Numerous chemical reactions take place with these VOCs and the transformation of these organic compounds can influence the formation or depletion of main oxidants, such as ozone and is strongly connected to the particulate fraction. The increase of emission of certain types of VOCs, together with other trace gases as NO_2 or SO_2, can have a global impact, affecting for instance the radiative forcing of the Earth (indirect effects), precipitation (acidity, quantity) and human health.

I.1.3 Atmospheric aerosols

An atmospheric aerosol is defined as a stable suspension of liquid or solid particles in a gas and *strictu sen*su there is a distinction between aerosol and particle, but very often both words are used to designate a particle. In this work, aerosol and particle will both be used indistinctly to designate particles. In atmospheric sciences, aerosols are commonly distinguished from cloud droplets and ice particles, which are named cloud particles or hydrometeors.

I.1.3.a. Sources and composition.

Atmospheric aerosols have many different sources. They can be emitted as a primary aerosol, meaning they are emitted in the atmosphere as a particle due to wind erosion from the soil, sea spray, a volcanic eruption, combustion etc. Aerosols can also be formed from gaseous precursors in the atmosphere and form secondary organic aerosols or SOA. Ultrafine particles with equivalent diameters below 0.1 µm, have the highest number density while the coarse particles, diameters > 1 µm, have the highest mass density. Secondary organic particles are mostly found in the smaller size ranges, POA constitute mainly the coarse mode. The size of the particles will also determine their residence time in the atmosphere and coarse particles can therefore have very short atmospheric lifetimes (minutes to hours).

Atmospheric particles are very complex chemical mixtures and even their physical state is still not well understood (Virtanen et al., 2010). The chemical characterization of the mineral components, accounting for around 30 to 70 % of the dry aerosol mass, is relatively well known and their sources can be apportioned (Delmas et al., 2005; Monks et al., 2009). The organic components are much less well characterized, due to their high complexity and very low individual concentrations. The organic fraction consists indeed of many thousands of different molecules, each presenting a small fraction of the particle mass (Hallquist et al., 2009). Nonetheless the organic fraction can account for a substantial part of the total particle mass (up to 60%) especially for and particle sizes lower than 1 µm (Zhang et al., 2007) influencing optical properties, chemical reactivity and toxicity of the particle. The complexity of the organic phase of a particle is illustrated through the different formation processes of SOA. SOA can be formed by new particles after the homogeneous nucleation of gaseous species or coagulation of different particles, condensation of low volatility species

on existing particles, partitioning of polar species in more polar water containing aerosols or reactive uptake of gaseous species through heterogeneous reactions at the surface of the particle. This is illustrated figure I-2 with the example of the gas phase oxidation of a biogenic monoterpene (α-pinene) and an anthropogenic aromatic compound (mesitylene) with different atmospheric oxidants, leading to oxidation products with different polarities and volatilities, which will influence the particulate phase. Besides, the particle is not a fixed chemical entity and chemical reactions, condensation or evaporation of species occur during its atmospheric journey; the so-called aerosol ageing.

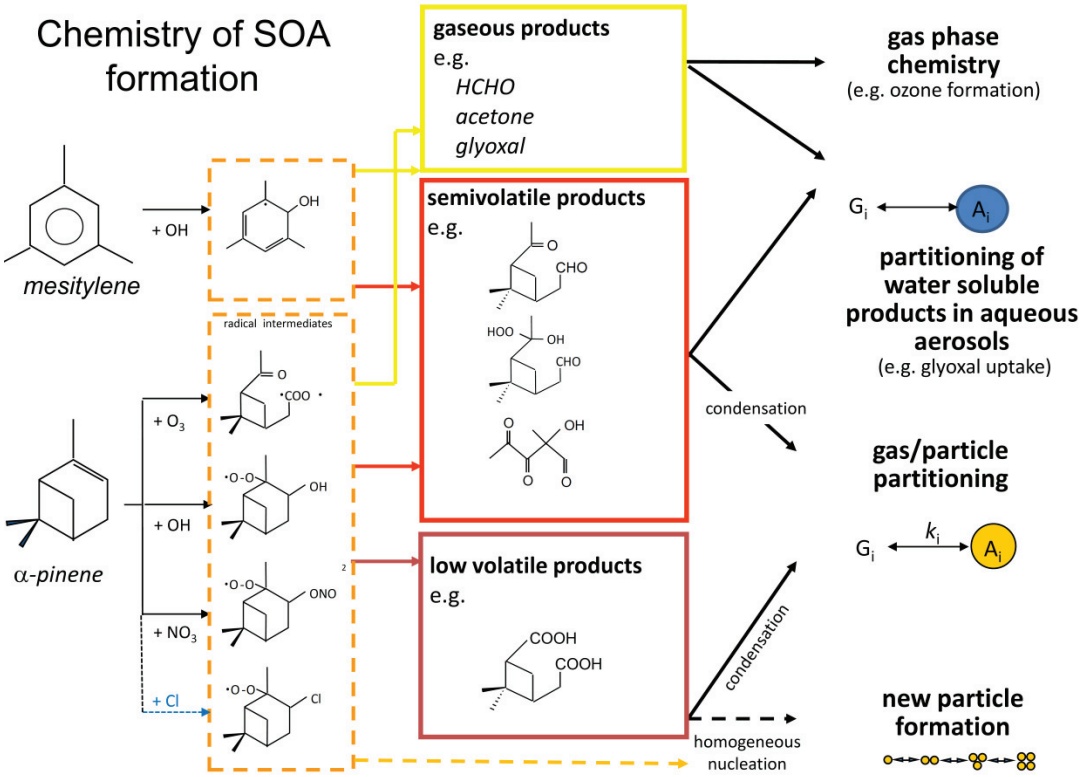

Figure I-2: overview of the gas phase oxidation products of two monoterpenes with different atmospheric oxidants and their atmospheric fates (Hoffmann, 2013)

Marine sources are the biggest natural sources of particles (Andreae and Rosenfeld, 2008). Although the super-micrometer particles are particularly rich in inorganic salts, especially sea salts such as sodium chloride, marine particles with diameters ≤ 500 nm, are highly enriched in organic matter, accounting for more than 50% of the dry mass of these smaller particles (Facchini et al., 2008; Hoffman and Duce, 1977). However, the production mechanisms, chemical composition and properties and the contribution of ocean-derived organic matter to the marine aerosols are not well understood (Law et al., 2013). As terrestrial aerosols,

marine aerosols undergo transformations in the atmosphere leading from very hydrophobic organic fractions in the freshly emitted particles to more water soluble organic fractions through the ageing process (Rinaldi et al., 2010), although the ageing of marine aerosols is through photochemical processes remains largely unexplored (Gantt and Meskhidze, 2013).

I.1.3.b. Impact of aerosols

The most obvious impact of aerosols is a decrease in the visibility. Indeed, despite their small volume and low concentration in the atmosphere, aerosols can strongly influence the transfer of radiant energy in through scattering and absorption (Eidels-Dubovoi, 2002; IPCC, 2013). They also influence global climate and meteorology through their role in cloud formation processes as cloud condensation nuclei (CCN) and ice nuclei (IN). Notably the presence of organic matter in the aerosol influences the capability of a particle to act as a CCN, but the role of many organic compounds on hygroscopicity and CCN capacity has yet to be determined (Cruz and Pandis, 1997; Sun and Ariya, 2006). The uncertainties of the background concentrations and composition of aerosols, especially in remote marine regions, and their role as CCN remains one of the main uncertainties of the aerosol-cloud-climate system (Gantt and Meskhidze, 2013; IPCC, 2013).

Particles are also a main factor determining air quality and form a challenge for public health in polluted areas. Respiratory problems, heart malfunctions and allergic diseases increase in populations exposed to aerosol loaded air and show correlation with an association of different properties of the particles, such as chemical composition, size and surface area (Pöschl, 2005). Ultrafine particles, diameter < 100 nm) are entrained deeper into the respiratory system and, due to their small size, even penetrate the membranes and enter blood circulation. Therefore these ultrafine particles are suspected to be particularly hazardous to human health, although more investigations are needed to elucidate their specific health impact (Davidson et al., 2005).

I.2. Surface microlayer

The previous section introduced the atmosphere as one main influence in climate regulation, another being the ocean, notably representing the main CO_2 sink. The influence of the ocean on the atmosphere and vice versa spans a broad range of processes, from nutrients balance for marine biology to regional weather patterns. As the oceans cover a large part of the Earth's surface, the ocean is also a major control on the atmospheric budget of many trace gasses. The exchanges of traces gases between atmosphere and the ocean influence both the chemistry and the physics of the atmosphere and the biogeochemistry of the oceans (Liss and Johnson, 2014). This work will focus on the exchange these gases, which are in many cases more reactive than the greenhouse gases, and to a lesser degree also on aerosols.

The air-sea exchange of trace gases is controlled by several physical, chemical and biological processes in the atmosphere and in the water. The wind speed is a very important factor in the air-sea exchange of gases, but other processes such as bubble bursting, waves, rain and surface films contribute largely (Garbe et al., 2014). As mentioned in the previous section, bubble bursting contributes largely to the marine aerosol budget through the injection of small droplets into the atmosphere (de Leeuw et al., 2011). Surface films influence the air-sea gas exchange via several mechanisms, due to their particular characteristics.

I.2.1. Definition

The sea surface film, or better called the sea surface microlayer (SML) is defined as the top 1µm to 1 mm of the ocean, as schematized figure I- 3. This region shows different chemical and physical properties than the underlying water, as an accumulation of organic and inorganic matter, mainly hydrophobic in nature, but also of associated microorganisms occurs due to reduced mixing in this region (Cunliffe et al., 2011; Liss and Duce, 1997). This surface layer is naturally reactive, since it is constituted for a large fraction of reactive organic material, such as dissolved organic matter (DOM), which contains a high proportion of functional groups such as carbonyls, aromatic moieties and carboxylic acids (Sempere and Kawamura, 2003; Stubbins et al., 2008) and can be conceived as a complex gelatinous film

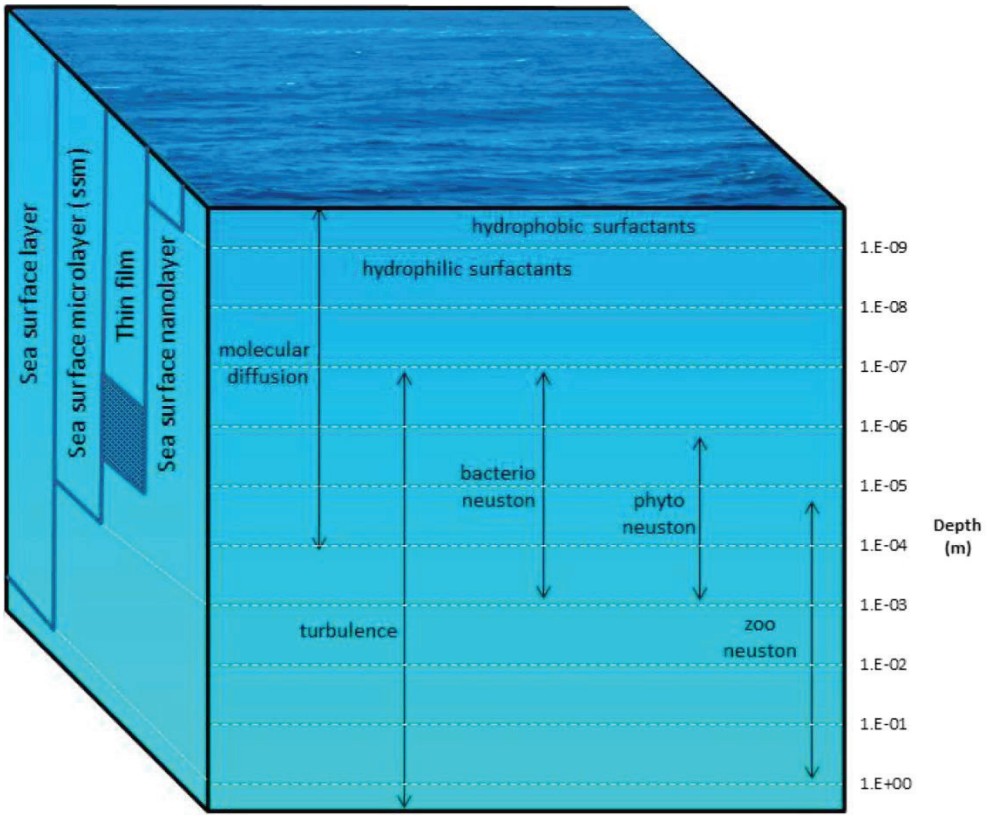

Figure I-3: Schematic representation of the sea-surface layer. (Carpenter and Nightingale, 2015)

(Cunliffe et al., 2013). The marine biology is a large contributor to the composition of the SML, through exudates and extracellular material (Liss and Duce, 1997). It is also a zone that is particularly undersampled, due to experimental difficulties and therefore much of the evidence of the chemistry taking place there comes from laboratory or modelling studies (Carpenter and Nightingale, 2015).

It has to be mentioned that the SML is distinguished from slicks in what follows. Slicks are visible films on the surface of the sea, typically of only 2-3 nm thickness that spontaneously form during increased supply of organic material to the SML. Although their composition is closely related to the SML composition, they tend to be enriched in lipids, particulate matter and surfactants (Cunliffe et al., 2013). Slick appears as patches on the surface, whereas the invisible SML is a more uniform layer on the top of the ocean. They also disrupt at lower wind speeds (4-5 m s^{-1}) (Cunliffe et al., 2013) than the more stable SML, for which enrichment in organic material has been measured by wind speeds of up to 10 m s^{-1} (Kuznetsova et al., 2004; Reinthaler et al., 2008).

As can be seen from figure I-3, the surface microlayer not only contains hydrophobic components, but also a large hydrophilic portion, composed essentially of proteins and carbohydrates, such as polysaccharides. Although lipids appeared to be less abundant in the SML than previously thought, they may still be important in affecting the physicochemical properties of the SML, notably through their surfactant capacity (Cunliffe et al., 2013). Typically, compounds in the SML are surface active and amphiphilic, with a polar head and a hydrophobic tail (Carpenter and Nightingale, 2015). The presence of these surface active compounds, or surfactants, lowers the surface tension of the water compared to the tension of clear water. Experiments showed that in presence of coastal SML, usually particularly enriched in organic matter, the surface tension measured was substantially lower (10-15 mN m^{-1}), but also open ocean SML behaves as a surfactant (Barger and Means, 1985; Bock and Frew, 1993). This surfactant property of the SML, where they are typically enriched by a factor of 3 compared to the underlying water, is particularly important for the air-sea gas exchange at low wind speeds (Carpenter and Nightingale, 2015).

I.2.2. Influence of the surface microlayer on the air-sea exchange

The air-sea gas exchange is driven by molecular and turbulent diffusion. Turbulent diffusion is defined by the turbulent eddies in bulk water and in air close to the air-water interface. At the scale of the SML, these turbulences are suppressed and the exchange at the interface is controlled by molecular diffusion (Upstill-Goddard, 2006). On either side of the interface, on the water and the gas side, the gas concentrations show gradients, the so-called diffusive sub-layers, through which gas transport rates constrain the air-water exchange (Cunliffe et al., 2013).

The sea surface microlayer, although an infinitely small fraction of the total water column, can thus significantly influence the air-sea gas transfer, by altering the hydrodynamic properties of the sea surface. The presence of the SML, and in particular the more soluble surfactant fraction, reduces the roughness of the sea surface, dampens wave breaking and lowers the sub-surface turbulence, and hence turbulent energy transfer. The surface microlayer indeed concentrates hydrophobic organic material, which is known to have a blocking effect on the evaporation of water and the uptake of gases into the water although the fundamental processes controlling this effect are not so well understood (Donaldson and George, 2012). In particular, the influence of complex mixtures of organics

on the gas exchange is not well documented. One of the first studies bringing into evidence the influence of the SML on air-sea gas exchange rates in the field, showed a substantial suppression of exchange rate in presence of natural DOM-rich films (Frew et al., 2004).

Another influence of an organic layer, as the SML, at the water interface on the gas exchange is to prevent the dissolution of a gas molecule impinging on the water surface, as shown for model compounds (Davidovits et al., 2006). Whereas a dissolution without a free energy barrier would occur in case of a bare water surface, on a coated surface the solvent shell that water would form around the gas molecule on the surface is not available, preventing its dissolution. On the other hand, certain atmospheric species can be more soluble in organic solvents, which would lead to an increase dissolution of these compounds in presence of an organic coating (Donaldson and Vaida, 2006). This enhanced solubilization can even lead to a build-up of hydrophobic organic compounds as polycyclic aromatic hydrocarbons (PAHs) at the surface (Donaldson and Valsaraj, 2010).

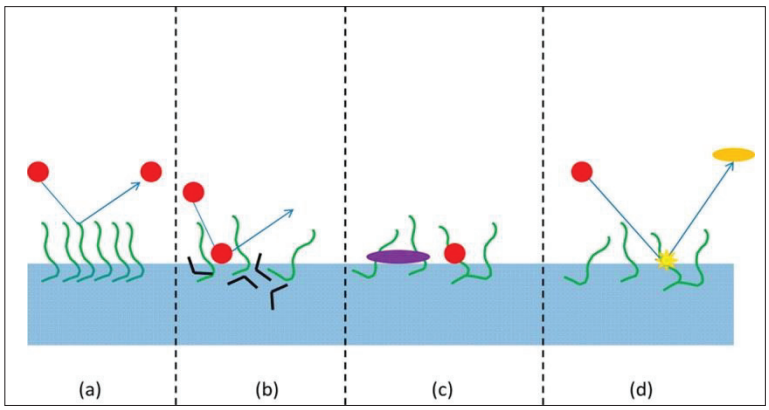

Figure I-4: Schematics of the different influences the presence of an organic coating (green) can have on gas exchange: (a) blocking effect of the gas molecule (red); (b) coating prevents dissolution; (c) coating enhances dissolution leading to enhanced surface concentrations (purple); (d) chemical reaction between gas molecule and coating (Donaldson and George, 2012)

But the SML can also impact air-sea gas exchange through chemical reactions, leading to the enhanced uptake of gases or at the contrary leading to gaseous emissions. It is for example well known that the surface of the seas is an important sink for ozone, higher than expected from its dissolution alone (Kramm et al., 1995). This was explained by reactive uptake processes of ozone with compounds, such as iodide, at the air-water interface (Chang et al., 2004; Ganzeveld et al., 2009). The different effects an organic coating on water can have on the gas-exchange, are schematized figure I-4.

As mentioned in the previous section, the SML will also contribute to the organic fraction of marine particles produced by bubble bursting or sea spray. The latter being coarse particles, their lifetime is reduced to minutes (Cunliffe et al., 2013) and their influence on the marine troposphere therefore more limited. Finer particles are produced by bubble bursting showing an organic content very similar to the composition of the SML (Law et al., 2013). These particles can, during their stay in the troposphere, influence the chemistry in the marine boundary layer, as schematized in figure I-5, illustrating that the influence of the SML on the atmospheric chemistry through gas exchange is not only strictly constrained to the air-sea interface.

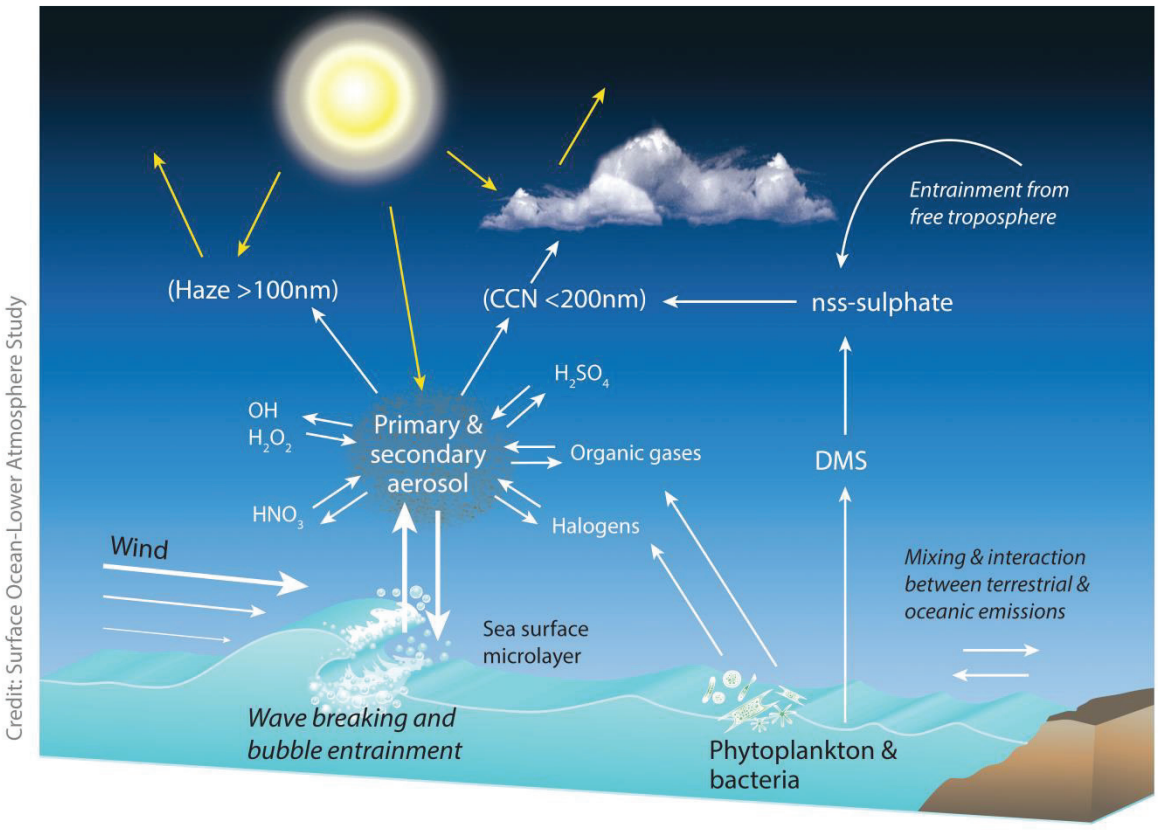

Figure I-5: Schematic representation of the interactions of the sea surface with the marine boundary layer (Law et al., 2013).

I.2.3. Photochemistry in the surface micro-layer

Due to the enrichment of organic matter in the SML and its wide exposure to sunlight, the SML is often considered as a very favorable venue for photochemical reactions, although little evidence for such reactions exist (Plane et al., 1997). However, there is evidence of enhanced organic and inorganic cycling in the surface ocean through photochemical oxidation of DOM (Carpenter and Nightingale, 2015; Cunliffe et al., 2013). This photochemical oxidation leads for instance to the release of carbon dioxide, monoxide and oxygenated volatile organic compounds as measured above the open oceans (Miller and Zepp, 1995; Mopper and Stahovec, 1986; Zafiriou et al., 2003).

Also inorganic compounds such as halides, nitrates and nitrites can undergo photolysis or oxidation at the sea surface layers. This has been shown for the reaction between halides and chlorophyll or simple aromatic ketones, leading to the release of highly reactive halogen atoms in the gas phase (Jammoul et al., 2009; Reeser et al., 2009a). Iodide in particular could be enhanced in the SML as it has a slight surfactant properties (Wren and Donaldson, 2010). Measurements of abnormally elevated concentrations of methyl iodide in the north and tropical Atlantic Ocean showed correlation with light intensities, pointing towards an important abiotic source of CH_3I (Happell and Wallace, 1996; Richter and Wallace, 2004). Methyl iodide is believed to be produced in part from the recombination of $I^{\bullet}$ with methyl radicals produced by the photo-oxidation of DOM (Moore and Zafiriou, 1994).

Although these studies provide evidence for the sunlight-driven oxidation of DOM, halides or the production of halogenated compounds, it is not clear if these mechanisms are predominantly occurring in the SML. Very few studies investigated the photochemical activity in the SML (Plane et al., 1997).

In one field study, Gever et al. used the sampled microlayer of a commercial rice field to study the photochemical degradation of a SML enriched pesticide, thiobencarb. They show that thiobencarb undergoes a quicker degradation in the SML containing sample than in the SML free sample (Gever et al., 1996). No information on the gas phase was collected during these experiments. Interestingly, they observed only one of the classically expected oxidation products of the pesticide in the microlayer after light exposure (Draper and Crosby, 1981), leading to think that particular chemistry might occur in the SML.

Other laboratory study showed that photochemical oxidation of lipids on aqueous solutions leads to the formation of polymers through cross-linking, showing the same properties as marine humic acids (Harvey et al., 1983; Harvey et al., 1984). It is also known that the sunlight exposure of surface films from crude oils leads to enhanced microbial toxicity (Pengerud et al., 1984), which was attributed to the formation of stable hydroperoxides (Larson et al., 1979).

The SML could thus play an important role as source for photochemical production of VOCs, but it can also be a sink for gases through reactive uptake. The photochemical processes leading to gas uptake at the air-sea interface, will be treated in the next section. The photochemistry occurring in the SML and the particular role of the SML in these photochemical processes leading to the release of volatile species, remains rather unknown (Donaldson and George, 2012; Donaldson and Vaida, 2006) and is the motivation behind the studies presented in this thesis.

I.3. Atmospheric photochemistry

Photochemistry is the study of interactions between radiant energy, coming from the sun if we consider the atmosphere, and chemical species. Photochemical processes are the key processes in the atmosphere where reactions are mostly driven by light. After a brief introduction to the basics of photochemistry, the importance of photochemistry at different levels in the atmosphere will be discussed.

I.3.1. Photochemistry: basic principles

1.3.1.a. Absorption and molecular electronically excited states.

Absorption of a photon by a molecule can lead to an excited energy state. This excited state is called a resonant state, meaning the molecule will absorb a photon when there exists a energy level above its ground state corresponding exactly to the energy of the photon. The absorbance of a molecule can be determined by spectrometry in which the difference in light intensity between the incoming $I_0(\lambda)$ and outgoing light beam $I(\lambda)$ passing through a sample measured for a given wavelength, applying the Beer-Lambert's law:

$$A = \log\left(\frac{I_0(\lambda)}{I(\lambda)}\right) = \varepsilon C l$$

(Equation I-1)

with: *A: absorbance*

$I_0(\lambda)$: light intensity of the incoming light at a given wavelength

$I(\lambda)$: light intensity of the outgoing light at the given wavelength

C: concentration of the absorber(s) (mol L^{-1})

ε: molar extinction coefficient (L mol-1 cm-1)

l : optical pathlength (cm)

It should be noted that in equation I-1 the expression of Beer-Lambert's law is $\log_{10}$ based, while many absorption cross sections for gaseous species in atmospheric sciences use the natural logarithm (e based). In this work, the photochemical active species considered are in the condensed phase and absorption will be express using the definition given equation I-1.

Once the molecule has absorbed a photon of the appropriate energy, its electrons can undergo transitions to an electronically excited state. The different electronically excited

states can be schematized in a Jablonski diagram, as shown figure I-6. The ground state S_0 makes the transition to the excited singlet states S_1 or S_2 of the same spin multiplicity upon absorption of light, where the vertical gap on the diagram between states represents their difference in energy. The S_1 excited state of the molecule can return to the ground state either through vibrational relaxation, symbolized by black wavy arrows on fig. I-6, or radiative relaxation, called fluorescence. Fluorescence is defined as the emission of light due to a spin-allowed transition and is therefore characterized by a short lifetime, 10^{-6} – 10^{-9} s (Braun et al., 1986). The singlet state excited molecule can also undergo spin forbidden transition to a triplet state by intersystem crossing (fig. I-6, violet wavy arrow). From the triplet excited state, the molecule can undergo either vibrational or radiative relaxation. The radiative transition from a triplet excited state to the singlet, called phosphorescence, is spin forbidden and therefore has a longer lifetime than singlet state emissions. The excited molecule can also undergo internal crossing, defined as intramolecular crossing from one excited state to another of the same multiplicity, without the radiative emission.

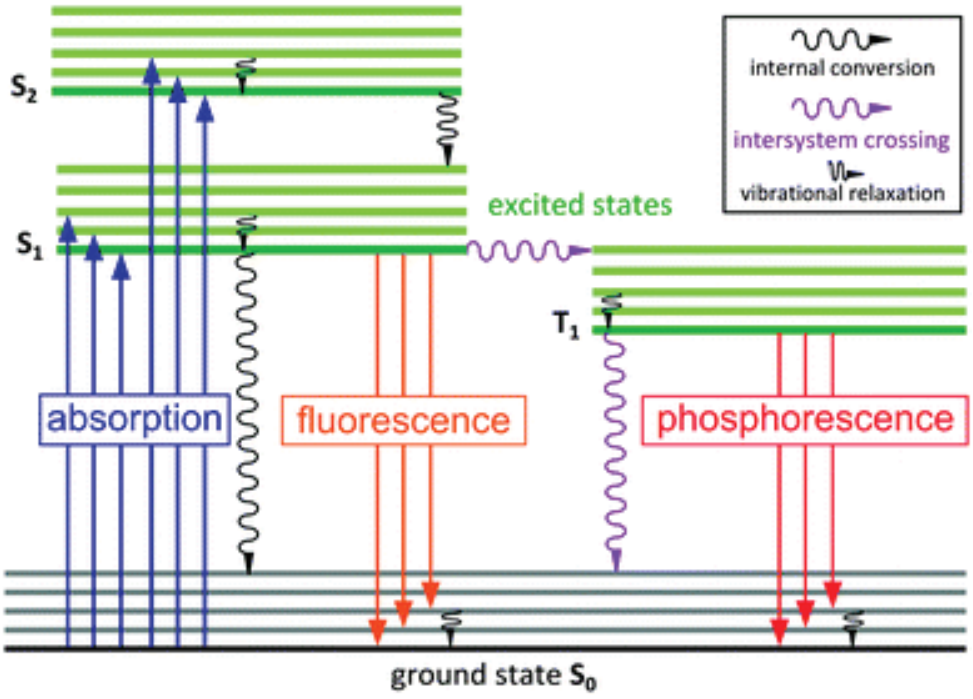

Figure I-6: Jablonski diagram showing basic photophysical processes (Heine and Muller-Buschbaum, 2013)

The electronically excited molecule can undergo different primary, photochemical or photophysical, processes. The different processes an excited molecule can undergo are summarized hereafter (Calvert and Pitts, 1966; Finlayson-Pitts and Pitts Jr, 1999):

$$AB + h\nu \rightarrow AB^* \quad (1)$$

$$AB^* \rightarrow AB + h\nu \quad (2)$$

$$AB^* + M \rightarrow AB + M \quad (3)$$

$$AB^* \rightarrow A + B \quad (4)$$

$$AB^* \rightarrow AB^{\#} / BA \quad (5)$$

$$AB^* + C \rightarrow AC + B \quad (6)$$

$$AB^* \rightarrow AB^+ + e^- \quad (7)$$

$$AB^* + M \rightarrow AB + M^* \quad (8)$$

Photophysical processes are processes in which the excited species formed in reaction (1) undergoes radiative transitions, i.e. fluorescence or phosphorescence (reaction 2) and non-radiative transitions, in which some or all of the energy of the excited molecule is converted to vibrational energy, and ultimately heat (reaction 3). The light emitted by the radiative relaxations will have a lower energy state than the light absorbed: $\lambda_{abs} < \lambda_{em}$. Photochemical processes are the processes in which the excited species dissociates (reaction 4), isomerizes (reaction 5), rearranges (reaction 5) or reacts with another molecule (reaction 6). Other high energetic radiation, such as X-rays, can cause the ionization of the molecule (reaction 7). These radiations are not present in the lower atmosphere and as such less important for our purpose here. Finally, the electronically excited molecule can also react through photosensitized reactions with surrounding molecules, as represented reaction (8). Intramolecular transitions are predominant at low pressure, where collisions are rather rare, but intermolecular transitions are more important at 1 atm or in liquid phase.

For atmospheric chemistry the most important electron excitations are those resulting in the dissociation of molecular bonds (reaction 4). In order to cause bond-breaking, the energy absorbed by a molecule has to be higher than 40 kcal/mol in most cases (Moortgat et al., 2013). The radiations containing this amount of energy are essentially the ultraviolet (UV) radiations, which are essentially absorbed in the higher atmosphere and by the stratospheric ozone layer. Though the quantity of UV radiation reaching the lower

troposphere and the surface of the earth is very small compared to the incoming radiation on the top of the atmosphere, this little amount of UV radiation will be the driving force for most of the chemical reactions in the troposphere (Finlayson-Pitts and Pitts Jr, 1999).

I.2.1.b. Photosensitized reactions

As mentioned in the previous section, an excited molecule can react through photosensitized reactions with other molecules, meaning the excited molecule induces photochemical reactions in molecules that are not photochemical reactive themselves, i.e., do not absorb light in the considered range of wavelengths. Photosensitized reactions can occur through different processes and mostly occur from triplet excited states, as these have a longer lifetime, increasing the probability to collide and react with another molecule. The efficiency of the a photosensitized reaction depends on (1) high absorption coefficient of the sensitizer in the considered spectral range, (2) the energy of the excited state of the photosensitizer, (3) a high quantum yield of the triplet state ($\Phi_T > 0.4$) and a long triplet lifetime ($\tau_T > 1$ µs) and (4) a high photostability, meaning that the photosensitizer self is not rapidly degraded through the initiated photochemistry. These type of reactions are more important in the liquid phase than in the gas phase as the number concentration of molecules in the gas phase is much lower, the probability of collision between the photosensitizer and his substrate is also much lower. But due to the high probability of collision, the excited photosensitizer can also easier undergo collisional quenching, provoking no chemical reaction.

The first type of photosensitized reaction is induced by energy transfer from the excited molecule to the ground state molecule, reaction (8) in the previous section. This energy transfer is rather rare in nature, with one notable exception, oxygen. Molecular oxygen can be photosensitized by a large range of photosensitizers through energy transfer mostly from their triplet excited state. For an efficient energy transfer to O_2 to yield singlet oxygen the energy of the excited state of the photosensitizer should be sufficiently high ($E \geq 95$ kJ mol^{-1}) and can be in competition with an electron transfer from oxygen to the photosensitizer to yield superoxide ($O_2^{\bullet -}$) (DeRosa and Crutchley, 2002). Photochemical reactions necessitating the production of singlet oxygen are known as indirect photosensitized reactions or the type II mechanism.

The type I mechanism is the direct reaction between a compound and the excited photosensitizer. This happens following two pathways, either by electron transfer or by hydrogen-atom abstraction and yields the production of free radicals. The type I

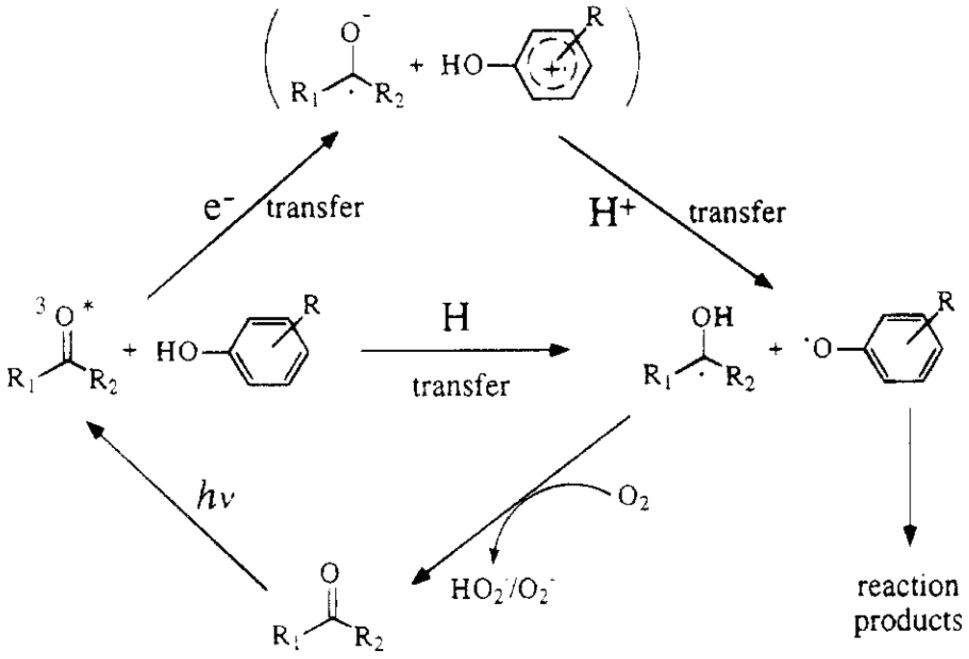

Figure I-7: Type I reaction photosensitized reaction mechanisms (Canonica et al., 1995)

photosensitized reactions are resumed in figure I-7, for a triplet excited state carbonyl as photosensitizer and a phenol as substrate. The reduced photosensitizer, the ketyl radical, can return to the ground state ketone through an oxidation in presence of O_2, leading to the formation of superoxide $O_2^{\bullet-}$ or $HO_2^{\bullet}$. Once the photosensitizer is regenerated in the ground state, a new excitation can start a new cycle of photooxidation. The number of cycles one molecule of the photosensitizer can initiate depends on the nature of the photosensitizer and the environment (deoxygenated, concentration of oxidants…).

I.2.2. Photochemistry and the atmosphere

I.2.2.a. Light source

This section will tread the briefly photochemical reactions influencing the troposphere, but first the driving force behind these reactions needs some specifications. The largest energy source available on our planet is the sun, driving the biosphere and virtually all chemical reactions in the atmosphere. The spectral distribution of incident solar

radiation spans a large range of wavelengths, from UV to the infrared, with a peak around 500 nm. Approximately 47% of the incident terrestrial solar irradiation is in the visible range, from 380 nm to 780 nm, approximately 46% in the infrared (IR, $\lambda > 780$ nm) and only about 7% of the incident radiation is in the ultraviolet region ($\lambda < 400$ nm) (Vignola et al., 2012). As mentioned before, only a very small part of that spectrum can initiate chemistry, mainly the most energetic radiations, which are in the shorter wavelengths, more precisely in the UV region.

The solar irradiance received on the surface of the Earth is largely variable depending on the angular position of the sun in the sky. This position can be defined by two angles, the solar zenith angle θ_0, the angle the local vertical makes with the sun, schematized figure I-5, and the solar azimuth angle φ_0, the angle measured from a horizontal reference direction, where only θ_0 will influence the actinic flux (Madronich and Flocke, 1999). The solar zenith angle is also determining the path length l of the light in the atmosphere as can be seen figure I-8. For each location with a given longitude and latitude, the solar zenith angle can be calculated, taking into account the time of the day, the solar declination accounting for the changing position of the sun towards the Earth's equatorial plate depending on the time of the year and the yearly cycle of the sun-Earth distance. The calculations taking into account all these factors are quite complex and beyond the scope of this introduction.

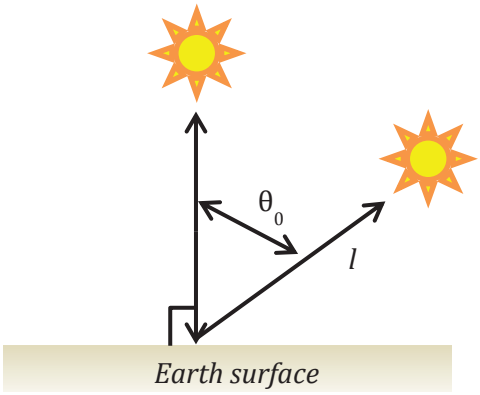

Figure I-8: Definition of the solar zenith angle

As the sunlight passes through the atmosphere, with a path length l, a large portion of the light is scattered and absorbed. The most important atmospheric absorbers are oxygen, absorbing light with $\lambda < 240$ nm, ozone, absorbing at $\lambda < 360$ nm and water vapor (Vis & IR). Other gaseous absorbers as sulfur, nitrogen dioxides or organic compounds can be mentioned as absorbers but will only have a significant effect on the light attenuation in

polluted areas. The actinic flux of solar light at the sea level of the Earth is thus very different of the incident solar irradiation at the top of the atmosphere, as illustrated figure I-9.

In contrast to laboratory collimated beam experiments, atmospheric radiation may be incident simultaneously from many different directions. Scattering, or redirecting, of solar photons leads to a complex angular redistribution of the sky radiation. Often the direct solar beam is only one component of the total radiation field, with large scattered contributions possible from clouds, aerosols, gaseous molecules, and surface reflections. Especially the scattering due to aerosols is very complex and depends on the size distribution, concentration and chemical composition. This scattering can lead to considerable changes in the actinic flux due to the directionality of the incident light beams and the orientation of the absorbers and especially for gaseous species can lead to much higher real actinic fluxes in the atmosphere then the irradiance measured on the horizontal flat surface of a radiometer (Madronich and Flocke, 1999). Estimations of the actinic flux at different altitudes in the atmosphere can be modelled, but will not be treated in detail here.

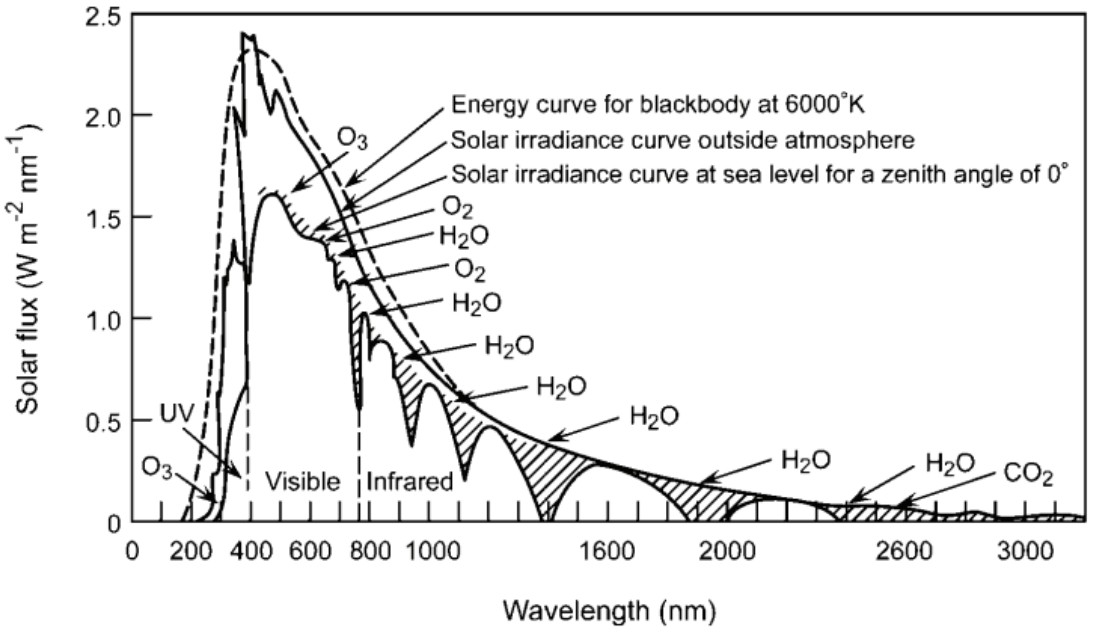

Figure I-9: Solar spectral radiation at the top of the atmosphere and at sea level, showing the most important absorbing species. Emission of a blackbody at 6000 K shown for comparison (Finlayson-Pitts and Pitts Jr., 1999).

I.2.2.b. Homogeneous photochemical reactions

As illustrated figure I-9, solar radiation at the top of the atmosphere differs largely of the solar radiation at sea level due to the absorption of many components in the atmosphere, and affects the UV region in particular mainly due to the absorption of ozone and molecular oxygen. These molecules, after absorption of a photon, will induce photochemical reactions in the atmosphere and constitute a first example of homogeneous gas phase photochemistry in the atmosphere. Here we will only treat the example of ozone, as this reaction is relevant for the troposphere. The absorption of molecular oxygen is only important at higher altitudes (stratosphere) where the short wavelengths ($\lambda < 242.2$ nm) are still available and therefore will not be detailed here (Okabe, 1978).

Gas-phase

Ozone (O_3) plays an important role in the atmosphere, first of all by its absorption of UV and IR light in the stratospheric ozone layer and notably in the Hartley bands (200-300 nm), hence protecting the biosphere from damaging solar irradiation at lower altitudes. On the other hand, it is also toxic for most lifeforms on Earth, since ozone is a highly reactive species, e.g. reacting readily with carbon-carbon double bonds in most organic compounds. Through its absorption of UV light, its electronically excited states provide the precursors for the formation of the hydroxyl radical ($OH^{\bullet}$), an ubiquitous and very reactive atmospheric oxidant. When O_3 absorbs light below 850 nm (reaction 9), it photolyzes in molecular and atomic oxygen. Depending on the wavelength of the light absorbed, the oxygen species formed can have different electronical states, as shown in reactions (10-)-(13) below:

$$O_3 + h\nu \longrightarrow O_3^* \quad (9)$$

$$O_3^* \longrightarrow O_2 ({}^3\Sigma g^-) + O({}^3P) \quad (10)$$

$$\longrightarrow O_2 ({}^1\Delta g \text{ or/and } {}^3\Sigma g^+) + O({}^3P) \quad (11)$$

$$\longrightarrow O_2 ({}^3\Sigma g^-) + O({}^1D) \quad (12)$$

$$\longrightarrow O_2 ({}^1\Delta g) + O({}^1D) \quad (13)$$

$$O({}^1D) + H_2O \longrightarrow 2\ OH^{\bullet} \quad (14)$$

$$O({}^3P) + O_2 \longrightarrow O_3 \quad (15)$$

For wavelengths greater than 440 nm, ozone dissociates mainly in molecular oxygen and atomic oxygen in the ground (triplet) state, reaction (10). Reaction (11) is the dissociation of ozone in excited triplet or the spin-forbidden singlet state molecular oxygen and a ground state oxygen atom. This is a minor pathway of photodissociation for wavelengths lower than 612 nm (Finlayson-Pitts and Pitts Jr, 1999). Another spin-forbidden reaction is reaction (12), leading to the formation of ground state molecular oxygen and singlet atomic oxygen, occurring as a minor pathway for wavelengths lower than 325 nm but a major source of singlet $O(^1D)$ for wavelengths between 325-329 nm. Reaction (13) is the main photolysis reaction of ozone leading to the formation of $O(^1D)$ for $\lambda < 325$ nm. The produced $O(^1D)$ will then react with water vapor to form hydroxyl radicals (14), causing a net ozone loss. Reactions (10) and (11) are insignificant in the troposphere, on one hand because the absorption coefficient of ozone is very low at these long wavelength and on the other hand because the $O(^3P)$ formed will react with O_2 to form ozone, leading to no net ozone loss (15).

The photochemistry of ozone and $OH^{\bullet}$ production is profoundly entwined with the chemistry of many other atmospheric compounds, as summarized figure I-10. The production of $OH^{\bullet}$ and/or ozone influences the oxidative capacity of the atmosphere and so

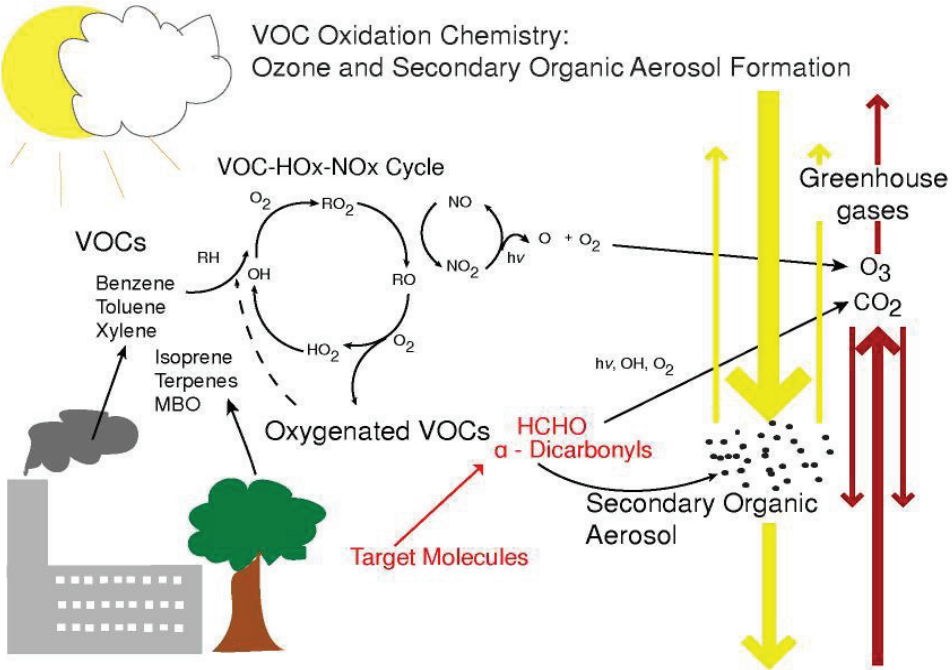

Figure I-10: VOC-HOx-NOx cycling (Keutsch, 2009)

the oxidation of organic species (VOCs), changing the NO-NO_2 cycling which can lead to a net ozone production, depending on the concentrations of NOx and VOCs in the atmosphere, and ultimately to the formation of SOA or CO_2.The example of photochemistry of ozone illustrates the importance of photochemical reactions in the troposphere, but also how complex photochemistry in this changing system can be.

Condensed phase

Homogeneous photochemistry is not limited to gas-phase reactions, but can also take place in liquid phase. Cloud droplets can undergo chemical changes through photochemical reactions and this is also holds for more liquid aerosols. The surface water receives a considerable amount of sunlight and therefore is also very affected by these photochemical reactions. In natural waters, the incident sunlight is rapidly attenuated through absorption and scattering. Light attenuation due to scattering is mostly important in natural water containing a high concentration of suspended solids. Table I-2 shows the fractions of the incident light at the surface of the ocean, measured at 310 nm for the UV-B and 500 nm for the visible light, transmitted through the water at different depths, for two types of water. As appears from table I-2, the UV-B light penetrates less deep in the water than the visible light and photochemical reactions driven mostly by this UV light can thus only be important in the surface waters. Generally, photochemical reactions in the natural water are significant in the photochemical zone, defined as the maximum depth where more than 0.1% of the incident light is transmitted (Faust, 1999).

Table I-2: Fractions of UV-B and Visible light transmitted at different water depths for two types of water (adapted from (Liss and Duce, 1997)

Type of water	water depth (m)					
	0.01	1	10	50	100	
Clearest open ocean	1.00	0.86	0.22	6×10^{-4}	-	UV-B
Moderately productive	0.99	0.40	1×10^{-4}	-	-	
Clearest open ocean	1.00	0.98	0.78	0.29	0.08	Visible
Moderately productive	1.00	0.90	0.33	4×10^{-3}	2×10^{-5}	

Many organic substances, designated with the general term dissolved organic matter (DOM), present in the water show absorption in the visible or UV region. As the chromophores involved in absorbing species are typically aromatic or carbonyl bearing species, excitation in natural waters typically involves the promotion of an electron from a n or π bonding orbital (for aromatic or carbonyl compounds) to a higher energy anti-bonding orbital, π* (Canonica et al., 1995; Osburn and Morris, 2003).

Direct photochemistry, not mediated by a photosensitizer, of these ubiquitous carbonyl bearing compounds is particularly relevant for liquid phase homogeneous reactions as this chemistry can lead to a variety of products and even induce free radical formation, but also occurs in the gas phase in the troposphere where carbonyls are well represented. These carbonyl bearing compounds absorb weakly around 280 nm, corresponding to a n⟶π* transition. Figure I-11 resumes the different mechanisms of direct photochemistry a carbonyl compound can undergo with the example of heptanone. After the absorption of a photon, the compounds forms an excited state. Then two main photochemical pathways can be followed, either the Norrish type I, leading to the formation of two free radicals or the Norrish type II. The latter proceeds through the formation of a bi-radical, which can then break the C-C bond in β-position to the carbonyl function to form an unsaturated alcohol and an alkene. Other products can also be formed from the initial bi-radical in this pathway, such as the Yang cyclisation shown figure I-11.

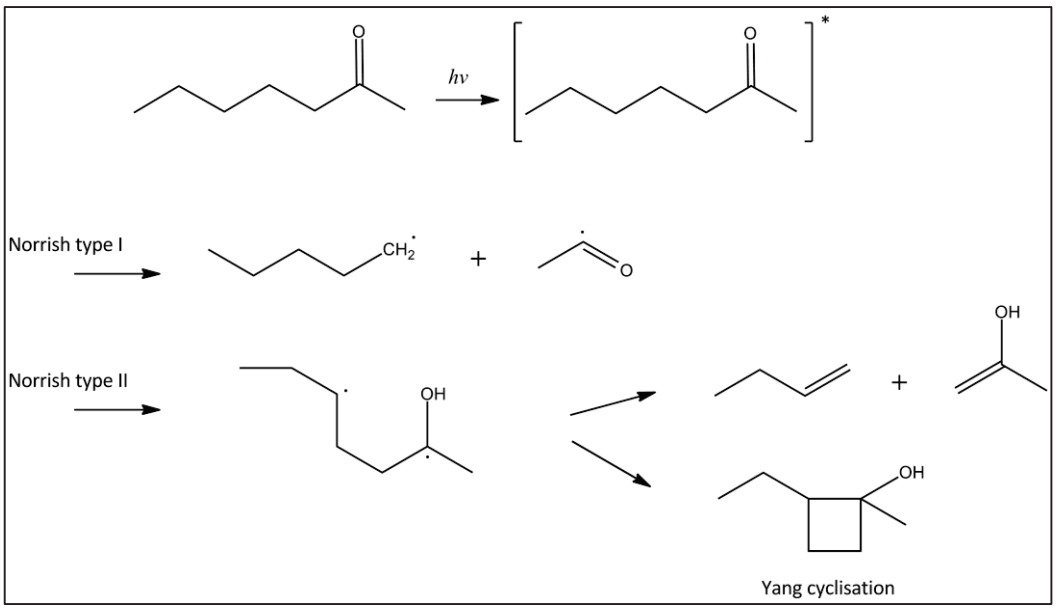

Figure I-11: Mechanisms for direct photolysis of carbonyl compounds (adapted from George et al., 2015)

Excited DOM in the liquid phase can thus undergo direct photolysis but can also act as photosensitizers. Photosensitized reactions are much more important in liquid phase than in the gas phase, as stated before, due to the much higher probability of collisions between molecules. Many studies have shown the importance of DOM in the photooxidation of other compounds which in many cases involves the implication of singlet oxygen, $O_2(^1\Delta_g)$ (Osburn and Morris, 2003; Vialaton and Richard, 2002; Zepp et al., 1985). This reaction was longtime thought to be the only important photosensitized reaction in natural waters, but Canonica and co-workers first brought into evidence that type I photosensitized reactions can be in competition with the singlet oxygen mediated oxidation in natural waters (Canonica et al., 1995). They showed that methyl-phenols, for example, can be efficiently oxidized through direct photosenitized reactions by excited humic acids in solutions with representative natural concentrations. These liquid phase photochemical reactions can also influence the gas phase composition, as discussed in the next section.

I.2.2.c. Heterogeneous photochemical reactions

As mentioned before, the atmosphere is not a homogeneous phase and many interactions between the gas phase and the condensed phase occur continuously. The most obvious example is the presence of rain drops, but also aerosols, ocean and many other surfaces can interact with the atmosphere through photochemical reactions. In the atmosphere, solar radiation can provide the energy to initiate reactions, as seen in the previous section, and condensed phases or surfaces can favor these reactions, for example by reducing the activation energy necessary for a given photochemical pathway by allowing a longer wavelength for reaction of species associated with the surface (George et al., 2015). These condensed phase are themselves mostly not perfectly homogeneous phases, but are often multiple mixed phase systems and aerosols can be cited as an example here. Aerosol particles are considered as internal mixtures of solids and liquids, and the liquids can be aqueous or organic or a mixture of both. Under experimental conditions where irradiation occurs simultaneously with gas phase oxidation, as is frequently the case for example in smog chambers, it is often very difficult to distinguished the part of gas phase photochemistry from the photochemistry in the organic condensed phase as both are so entwined. While gas phase reactions, generating free radicals and gas phase oxidants, are needed in these cases for the formation of the particles, the oxidants present in the gas

phase will compete through heterogeneous reactions with the photochemistry in the condensed organic phase. Many interfaces are available in the atmosphere, leading to a very broad range of heterogeneous reaction, and many of these remain still rather poorly known. Therefore, heterogeneous photochemical reactions will be treated here through several well-understood and relevant examples for this study, but do not claim to be the most representative or exhaustive.

Organic aerosols

A first effect light can have on aerosol particles, is the direct photolysis of light-absorbing compounds present in the organic phase of the particle, leading to the release of gas phase products and the loss of mass for the particle. Wong an co-workers, for example, generated SOA in an atmospheric reaction chamber from the ozonolysis of α-pinene, a biogenic monoterpene, which were collected and reinjected as aerosols in a second chamber without gas phase oxidants (Wong et al., 2015). The irradiation of the particles in the second chamber lead to a shift in the particle size distribution to lower masses. Aerosol mass spectrometry (AMS) monitored a loss of the organic fraction in the particles, due to the loss of volatile organic compounds explaining the loss of mass. The irradiated particles showed a smaller organic fraction bearing carbonyl functions and generally a higher oxidized organic content than before irradiation. Interestingly, photochemical induced mass loss was higher under higher relative humidity (RH), meaning that the photolysis in particles is enhanced by the presence of water. This can be due to either direct implication of water in the photochemical processes or to a change in the physical state of the particle, accelerating the chemical reactions taken place there. Other studies, using a denuder to strip most volatiles and gas-phase oxidants before reinjecting the aerosols, confirm that this photochemistry is essentially a condensed phase process (Epstein et al., 2014).

But particles can also show increase in mass under irradiance, due to uptake from volatile compounds from the gas phase. A study injecting seed particles containing organic photosensitizers, humic acids or 4-benzoylbenzoic acid, in an aerosol flow tube in presence of VOCs as isoprene or limonene, showed an increase in the particle size upon irradiation (Monge et al., 2012). This growth was explained by the reactive uptake of the VOC into the condensed phase, through photosensitized oxidation of the VOC by the excited photosensitizer present at the surface of the particle. The observed growth rates of the

particles (around 5 nm h^{-1}) implied that these processes could be a pathway for atmospheric particle growth.

Liquid interfaces

Although studies of direct photochemical reactions at liquid interfaces are still scarce, especially under atmospherically relevant conditions, photochemistry is for several reasons believed to be enhanced at the air-liquid interface (George et al., 2015). Firstly, it has been shown that the excited states of certain photoactive compounds, as eosin B, can attain much longer lifetimes at the liquid-liquid surface (alkane-water) than in the bulk, due to lower hydrogen-bond assisted deactivation of the excited state (Fita et al., 2011a; Fita et al., 2011b). Energy transfer between an excited molecule and a second compound could also be favored at the liquid-gas interface compared to the bulk. The intermolecular distances at the interface of liquids are smaller than in the bulk, which increases the efficiency of the energy transfer (Sitzmann and Eisenthal, 1989). Although these characteristics have only been shown at liquid-liquid interfaces, they can potentially favor photochemical reactions at the liquid-gas interface in a similar way.

Polymerization is one of the better known light enhanced reactions at the air-liquid interface. In an experiment with peptides containing an UV active group in their peptide sequence, polymerization of the peptides was observed under UV irradiation (de Samaniego and Miller, 2008). This photochemical reaction takes place in two steps; reorientation of the peptides followed by the crosslinking reaction. The reaction was shown to be faster and more extended in higher organized films, due to a closer molecular packing at the surface. Although this experiment was not done under environmentally relevant conditions, it points to the propensity of polymerization at the interface and to the importance of surface excess concentrations and organization of the film to mediate such reactions.

Photoenhancement has been observed in reactions with ozone at the air-water interface. In the dark, chlorophyll and pyrene present at the interface react heterogeneously with ozone following a Langmuir-Hinschelwood kinetics (Clifford et al., 2008; Henderson and Donaldson, 2012). When this reaction occurs under illuminated conditions, the kinetics are accelerated and the dependency on the gas phase ozone concentration seems to change (Reeser et al., 2009b; Styler et al., 2009). This enhanced reactivity has been explained as the results of an electron transfer from the excited organic compound at the interface, towards

an O_3 molecule; either in the gas-phase or adsorbed at the surface. The so formed ozonide anion ($O_3^{-\bullet}$) that rapidly forms an hydroxyl radical through hydrolysis.

One of the largest air-liquid interfaces where these photochemical reactions could occur is obviously the surface of the oceans, although little evidence for the photochemical reactions occurring there exist up to date (Plane et al., 1997)

I.4. Motivations for this study

As introduced briefly here, it becomes clear that there is a wide range of heterogeneous photochemical reactions that are to date not well understood. Moreover, field measurements of VOCs, such as halogenated species, in the marine boundary layer over the open ocean, show higher concentrations than expected and particle nucleation event over the open oceans are still not well explained (Carpenter & Nightingale, 2015; George & Donaldson , 2014). This points towards an unknown source which could be a photochemical production of these species in the surface microlayer. Since photochemical reactions this region are virtually undocumented, this study aims to do a first step towards a better understanding of the light-induced reactions taking place in the SML.

I.5. References

Andreae, M. and Rosenfeld, D., 2008. Aerosol–cloud–precipitation interactions. Part 1. The nature and sources of cloud-active aerosols. Earth-Science Reviews, 89(1): 13-41.

Barger, W.R. and Means, J.C., 1985. Clues to the structure of marine organic material from the study of physical properties of surface films. Marine and Estuarine Geochemistry, Lewis Publishers, Chelsea Michigan. 1985. p 47-67, 6 fig, 6 tab, 25 ref.

Bock, E.J. and Frew, N.M., 1993. Static and dynamic-response of natural multicomponent oceanic surface-films to compression and dilation - laboratory and field observations. Journal of Geophysical Research-Oceans, 98(C8): 14599-14617.

Braun, A.M., Maurette, M.-T. and Oliveros, E., 1986. Technologie photochimique. Presses polytechniques romandes.

Calvert, J.G. and Pitts, J.N., 1966. Photochemistry. Wiley.

Canonica, S., Jans, U., Stemmler, K. and Hoigne, J., 1995. Transformation Kinetics of Phenols in Water: Photosensitization by Dissolved Natural Organic Material and Aromatic Ketones. Environmental Science & Technology, 29(7): 1822-1831.

Carpenter, L.J. and Nightingale, P.D., 2015. Chemistry and Release of Gases from the Surface Ocean. Chemical Reviews, 115(10): 4015-4034.

Chang, W.N., Heikes, B.G. and Lee, M.H., 2004. Ozone deposition to the sea surface: chemical enhancement and wind speed dependence. Atmospheric Environment, 38(7): 1053-1059.

Clifford, D., Donaldson, D.J., Brigante, M., D'Anna, B. and George, C., 2008. Reactive uptake of ozone by chlorophyll at aqueous surfaces. Environmental Science & Technology, 42(4): 1138-1143.

Cruz, C.N. and Pandis, S.N., 1997. A study of the ability of pure secondary organic aerosol to act as cloud condensation nuclei. Atmospheric Environment, 31(15): 2205-2214.

Cunliffe, M. et al., 2013. Sea surface microlayers: A unified physicochemical and biological perspective of the airâ€“ocean interface. Progress in Oceanography, 109(0): 104-116.

Cunliffe, M., Upstill-Goddard, R.C. and Murrell, J.C., 2011. Microbiology of aquatic surface microlayers. Fems Microbiology Reviews, 35(2): 233-246.

Davidovits, P., Kolb, C.E., Williams, L.R., Jayne, J.T. and Worsnop, D.R., 2006. Mass accommodation and chemical reactions at gas-liquid interfaces. Chemical Reviews, 106(4): 1323-1354.

Davidson, C.I., Phalen, R.F. and Solomon, P.A., 2005. Airborne particulate matter and human health: a review. Aerosol Science and Technology, 39(8): 737-749.

de Leeuw, G. et al., 2011. Production flux of sea spray aerosol. Reviews of Geophysics, 49(2).

de Samaniego, M.S.S. and Miller, A.F., 2008. Two-dimensional polymerization of a polydiacetylene functionalized amphiphilic peptide at the air-water interface. Colloids and Surfaces a-Physicochemical and Engineering Aspects, 321(1-3): 271-274.

Delmas, R., Megie, G. and Peuch, V. (Editors), 2005. Physique et chimie de l'atmosphère. Belin, 640 pp.

DeRosa, M.C. and Crutchley, R.J., 2002. Photosensitized singlet oxygen and its applications. Coordination Chemistry Reviews, 233: 351-371.

Donaldson, D.J. and George, C., 2012. Sea-Surface Chemistry and Its Impact on the Marine Boundary Layer. Environmental Science & Technology, 46(19): 10385-10389.

Donaldson, D.J. and Vaida, V., 2006. The influence of organic films at the air-aqueous boundary on atmospheric processes. Chemical Reviews, 106(4): 1445-1461.

Donaldson, D.J. and Valsaraj, K.T., 2010. Adsorption and Reaction of Trace Gas-Phase Organic Compounds on Atmospheric Water Film Surfaces: A Critical Review. Environmental Science & Technology, 44(3): 865-873.

Draper, W.M. and Crosby, D.G., 1981. Hydrogen-peroxide and hydroxyl radical - intermediates in indirect photolysis reactions in water. Journal of Agricultural and Food Chemistry, 29(4): 699-702.

Eidels-Dubovoi, S., 2002. Aerosol impacts on visible light extinction in the atmosphere of Mexico City. Science of the Total Environment, 287(3): 213-220.

Epstein, S.A., Blair, S.L. and Nizkorodov, S.A., 2014. Direct Photolysis of a-Pinene Ozonolysis Secondary Organic Aerosol: Effect on Particle Mass and Peroxide Content. Environmental Science & Technology, 48(19): 11251-11258.

Facchini, M.C. et al., 2008. Primary submicron marine aerosol dominated by insoluble organic colloids and aggregates. Geophysical Research Letters, 35(17).

Faust, B.C., 1999. Aquatic Photochemical Reactions in Atmospheric, Surface, and Marine Waters: Influences on Oxidant Formation and Pollutant Degradation. In: P. Boule (Editor), Environmental Photochemistry. The Handbook of Environmental Chemistry. Springer Berlin Heidelberg, pp. 101-122.

Finlayson-Pitts, B.J. and Pitts Jr, J.N., 1999. Chemistry of the upper and lower atmosphere: theory, experiments, and applications. Academic press.

Fita, P., Fedoseeva, M. and Vauthey, E., 2011a. Hydrogen-Bond-Assisted Excited-State Deactivation at Liquid/Water Interfaces. Langmuir, 27(8): 4645-4652.

Fita, P., Fedoseeva, M. and Vauthey, E., 2011b. Ultrafast Excited-State Dynamics of Eosin B: A Potential Probe of the Hydrogen-Bonding Properties of the Environment. Journal of Physical Chemistry A, 115(12): 2465-2470.

Fleming, J.R., 1999. Joseph Fourier, the 'greenhouse effect', and the quest for a universal theory of terrestrial temperatures. Endeavour, 23(2): 72-75.

Fourier, J., 1824. Remarques générales sur les températures du globe terrestre et des espèces planétaires. Annales Chimique Physique, 27(31): 136-167.

Frew, N.M. et al., 2004. Air-sea gas transfer: Its dependence on wind stress, small-scale roughness, and surface films. Journal of Geophysical Research-Oceans, 109(C8).

Gantt, B. and Meskhidze, N., 2013. The physical and chemical characteristics of marine primary organic aerosol: a review. Atmospheric Chemistry and Physics, 13(8): 3979-3996.

Ganzeveld, L., Helmig, D., Fairall, C.W., Hare, J. and Pozzer, A., 2009. Atmosphere-ocean ozone exchange: A global modeling study of biogeochemical, atmospheric, and waterside turbulence dependencies. Global Biogeochemical Cycles, 23.

Garbe, C.S. et al., 2014. Transfer across the air-sea interface, Ocean-Atmosphere Interactions of Gases and Particles. Springer, pp. 55-112.

George, C., Ammann, M., D'Anna, B., Donaldson, D.J. and Nizkorodov, S.A., 2015. Heterogeneous Photochemistry in the Atmosphere. Chemical Reviews, 115(10): 4218-4258.

Gever, J.R., Mabury, S.A. and Crosby, D.G., 1996. Rice field surface microlayers: Collection, composition and pesticide enrichment. Environmental Toxicology and Chemistry, 15(10): 1676-1682.

Hallquist, M. et al., 2009. The formation, properties and impact of secondary organic aerosol: current and emerging issues. Atmospheric Chemistry and Physics, 9(14): 5155-5236.

Happell, J.D. and Wallace, D.W.R., 1996. Methyl iodide in the Greenland/Norwegian Seas and the tropical Atlantic Ocean: Evidence for photochemical production. Geophysical Research Letters, 23(16): 2105-2108.

Harvey, G.R., Boran, D.A., Chesal, L.A. and Tokar, J.M., 1983. The structure of marine fulvic and humic acids. Marine Chemistry, 12(2-3): 119-132.

Harvey, G.R., Boran, D.A., Piotrowicz, S.R. and Weisel, C.P., 1984. Synthesis of marine humic substances from unsaturated lipids. Nature, 309(5965): 244-246.

Heine, J. and Muller-Buschbaum, K., 2013. Engineering metal-based luminescence in coordination polymers and metal-organic frameworks. Chemical Society Reviews, 42(24): 9232-9242.

Henderson, E.A. and Donaldson, D.J., 2012. Influence of Organic Coatings on Pyrene Ozonolysis at the Air–Aqueous Interface. The Journal of Physical Chemistry A, 116(1): 423-429.

Hoffman, E.J. and Duce, R.A., 1977. Organic Carbon in Marine Atmospheric Particulate Matter - Concentration And Particle-Size Distribution. Geophysical Research Letters, 4(10): 449-452.

Hoffmann, T., 2013. Chemistry of Organic Aerosols, SESAC 2013, Taicang, China.

IPCC (Editor), 2013. The Physical Science Basis. Contribution of Working Group I to the fifth Assesment Report of the Intergovernmental Panel on Climate Change. Cambridge University Press, Cambridge and New York, 1535 pp.

Jammoul, A., Dumas, S., D'Anna, B. and George, C., 2009. Photoinduced oxidation of sea salt halides by aromatic ketones: a source of halogenated radicals. Atmospheric Chemistry and Physics, 9(13): 4229-4237.

Keutsch, F.N., 2009.

Kramm, G. et al., 1995. On the dry deposition of ozone and reactive nitrogen species. Atmospheric Environment, 29(21): 3209-3231.

Kuznetsova, M., Lee, C., Aller, J. and Frew, N., 2004. Enrichment of amino acids in the sea surface microlayer at coastal and open ocean sites in the North Atlantic Ocean. Limnology and Oceanography, 49(5): 1605-1619.

Larson, R.A., Bott, T.L., Hunt, L.L. and Rogenmuser, K., 1979. Photo-oxidation products of a fuel-oil and their anti-microbial activity. Environmental Science & Technology, 13(8): 965-969.

Law, C.S. et al., 2013. Evolving research directions in Surface Ocean-Lower Atmosphere (SOLAS) science. Environmental Chemistry, 10(1): 1-16.

Liss, P.S. and Duce, R.A. (Editors), 1997. Sea Surface and Global Change. Cambridge University Press, Cambridge, 509 pp.

Liss, P.S. and Johnson, M.T., 2014. Ocean-Atmosphere Interactions of Gases and Particles. Springer.

Madronich, S. and Flocke, S., 1999. The Role of Solar Radiation in Atmospheric Chemistry. In: P. Boule (Editor), Environmental Photochemistry. The Handbook of Environmental Chemistry. Springer Berlin Heidelberg, pp. 1-26.

Miller, W.L. and Zepp, R.G., 1995. Photochemical production of dissolved inorganic carbon from terrestrial organic-matter - significance to the oceanic organic-carbon cycle. Geophysical Research Letters, 22(4): 417-420.

Monge, M.E. et al., 2012. Alternative pathway for atmospheric particles growth. Proceedings of the National Academy of Sciences of the United States of America, 109(18): 6840-6844.

Monks, P.S. et al., 2009. Atmospheric composition change - global and regional air quality. Atmospheric Environment, 43(33): 5268-5350.

Moore, R.M. and Zafiriou, O.C., 1994. Photochemical production of methyl-iodide in seawater. Journal of Geophysical Research-Atmospheres, 99(D8): 16415-16420.

Moortgat, G.K., Barnes, A.J., Le Bras, G. and Sodeau, J.R., 2013. Low-temperature Chemistry of the Atmosphere, 21. Springer Science & Business Media.

Mopper, K. and Stahovec, W.L., 1986. Sources and sinks of low-molecular-weight organic carbonyl-compounds in seawater. Marine Chemistry, 19(4): 305-321.

Okabe, H., 1978. Photochemistry of small molecules, 431. Wiley New York.

Osburn, C.L. and Morris, D.P., 2003. Photochemistry of chromophoric dissolved organic matter in natural waters. UV effects in aquatic organisms and ecosystems, 1: 185-217.

Pengerud, B., Thingstad, F., Tjessem, K. and Aaberg, A., 1984. Photoinduced toxicity of north-sea crude oils toward bacterial-activity. Marine Pollution Bulletin, 15(4): 142-146.

Plane, J. et al., 1997. Photochemistry in the seasurface micro layer. The Sea Surface and Global Change. Cambridge Univsersity Press, Cambridge: 71-92.

Pöschl, U., 2005. Atmospheric Aerosols: Composition, Transformation, Climate and Health Effects. Angewandte Chemie International Edition, 44(46): 7520-7540.

Reeser, D.I., George, C. and Donaldson, D.J., 2009a. Photooxidation of Halides by Chlorophyll at the Air-Salt Water Interface. Journal of Physical Chemistry A, 113(30): 8591-8595.

Reeser, D.I. et al., 2009b. Photoenhanced Reaction of Ozone with Chlorophyll at the Seawater Surface. Journal of Physical Chemistry C, 113(6): 2071-2077.

Reinthaler, T., Sintes, E. and Herndl, G.J., 2008. Dissolved organic matter and bacterial production and respiration in the sea-surface microlayer of the open Atlantic and the western Mediterranean Sea. Limnology and Oceanography, 53(1): 122-136.

Richter, U. and Wallace, D.W.R., 2004. Production of methyl iodide in the tropical Atlantic Ocean. Geophysical Research Letters, 31(23).

Rinaldi, M. et al., 2010. Primary and Secondary Organic Marine Aerosol and Oceanic Biological Activity: Recent Results and New Perspectives for Future Studies. Advances in Meteorology.

Seinfeld, J.H. and Pandis, S.N., 2012. Atmospheric chemistry and physics: from air pollution to climate change. John Wiley & Sons.

Sempere, R. and Kawamura, K., 2003. Trans-hemispheric contribution of C-2-C-10 alpha, omega-dicarboxylic acids, and related polar compounds to water-soluble organic carbon in the western Pacific aerosols in relation to photochemical oxidation reactions. Global Biogeochemical Cycles, 17(2).

Sitzmann, E.V. and Eisenthal, K.B., 1989. Dynamics of intermolecular electronic-energy transfer at an air liquid interface. journal of Chemical Physics, 90(5): 2831-2832.

Stubbins, A. et al., 2008. Relating carbon monoxide photoproduction to dissolved organic matter functionality. Environmental Science & Technology, 42(9): 3271-3276.

Styler, S.A., Brigante, M., D'Anna, B., George, C. and Donaldson, D.J., 2009. Photoenhanced ozone loss on solid pyrene films. Physical Chemistry Chemical Physics, 11(36): 7876-7884.

Sun, J. and Ariya, P.A., 2006. Atmospheric organic and bio-aerosols as cloud condensation nuclei (CCN): A review. Atmospheric Environment, 40(5): 795-820.

Upstill-Goddard, R.C., 2006. Air-sea gas exchange in the coastal zone. Estuarine Coastal and Shelf Science, 70(3): 388-404.

Vialaton, D. and Richard, C., 2002. Phototransformation of aromatic pollutants in solar light: Photolysis versus photosensitized reactions under natural water conditions. Aquatic Sciences, 64(2): 207-215.

Vignola, F., Michalsky, J. and Stoffel, T., 2012. Solar Resource Definitions and Terminology, Solar and Infrared Radiation Measurements. Energy and the Environment. CRC Press, pp. 7-34.

Virtanen, A. et al., 2010. An amorphous solid state of biogenic secondary organic aerosol particles. Nature, 467(7317): 824-827.

Wong, J.P.S., Zhou, S. and Abbatt, J.P.D., 2015. Changes in Secondary Organic Aerosol Composition and Mass due to Photolysis: Relative Humidity Dependence. Journal of Physical Chemistry A, 119(19): 4309-4316.

Wren, S.N. and Donaldson, D.J., 2010. Glancing-angle Raman spectroscopic probe for reaction kinetics at water surfaces. Physical Chemistry Chemical Physics, 12(11): 2648-2654.

Zafiriou, O.C., Andrews, S.S. and Wang, W., 2003. Concordant estimates of oceanic carbon monoxide source and sink processes in the Pacific yield a balanced global "blue-water'' CO budget. Global Biogeochemical Cycles, 17(1).

Zepp, R.G., Schlotzhauer, P.F. and Sink, R.M., 1985. Photosensitized transformations involving electronic energy transfer in natural waters: role of humic substances. Environmental Science & Technology, 19(1): 74-81.

Zhang, Q. et al., 2007. Ubiquity and dominance of oxygenated species in organic aerosols in anthropogenically-influenced Northern Hemisphere midlatitudes. Geophysical Research Letters, 34(13).

Chapter II: Experimental set-up and methods

II.0. Motivation.

The experimental set-ups and methods used for the work presented in this thesis will all be described in this chapter. The general set-up and theoretical principles behind the used techniques and methods will be presented here. The specific analytical methods and experimental details are addressed in the following chapters dealing with the results. For the one technique of mass spectrometry applied in this work, some specific method development was done which will be given special attention here.

Chapter II: Experimental set-up and methods

II.1.Spectroscopic methods

II.1.1. Choice of the photo active compounds

As stated in chapter I, the surface microlayer contains a large variety of compounds with finally little knowledge over molecular speciation in the SML (Hedges et al., 2000). This makes the choice of representative compounds rather difficult, and especially for potential photosensitizers. The photo-active chosen here were selected because of their potential photochemical properties, but of course also for their probable presence at the air-sea interface. For example, compounds bearing a carbonyl group were privileged since the presence of such a chemical functionality is known to promote triplet state excitation, opening the possibility photochemical reactions. Another very important criteria of selection was their light absorbing properties in the UV-A or visible regions, since this is the actinic region at the surface of the oceans. An overview of the different type of photosensitizers used in different set-ups is given in table 1. The listed solubilities given are those theoretically predicted in water at pH=7 and 293.15K (Hou et al., 2004). The next sections briefly introduce each photosensitizer.

Table II-1: overview of studied photosensitizers

Compound	Chemical structure	Supplier	Purity	Solubility
imidazole-2-carboxaldehyde (IC)	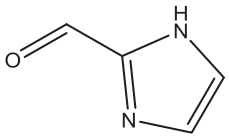	Sigma-Aldrich	97%	4.78 M
2-carboxy-pterine (CPT)	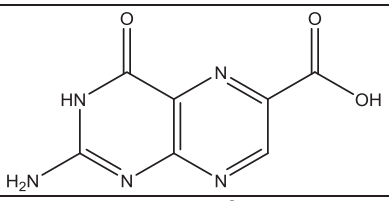	Schircks laboratories	>97.5%	3.54 M
4-benzoyl-benzoic acid (4-BBA)	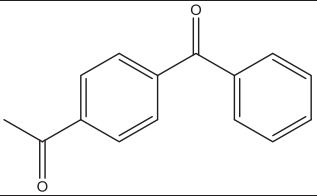	Sigma-Aldrich	99%	0.21 M

II.1.1.a. Imidazole-2-carboxaldehyde:

Nitrogen containing compounds formed in glyoxal based SOA are reported to alter the optical properties of these particles (Kampf et al., 2012; Nozière et al., 2008; Shapiro et al., 2009; Yu et al., 2011). These nitrogen containing compounds, amongst which imidazole-2-carboxaldehyde (IC), can be formed *in situ* in the condensed phase in presence of glyoxal and ammonium ions through a catalytic reaction, as shown in figure II-1. A recent laboratory study in our group showed that the formation of imidazole-2-carboxaldehyde (IC) in SOA leads to light induced growth of the particles without the presence of a gas-phase oxidant (Aregahegn et al., 2013). This particle growth has been explained by a heterogeneous reaction between the light excited photosensitizer and the VOC present leading to a reactive uptake of the VOC into the particulate phase. To further elucidate the role of IC in the particle growth, the photochemical properties of IC were studied using the laser flash photolysis (LFP) set-up and the results are presented chapter IV.

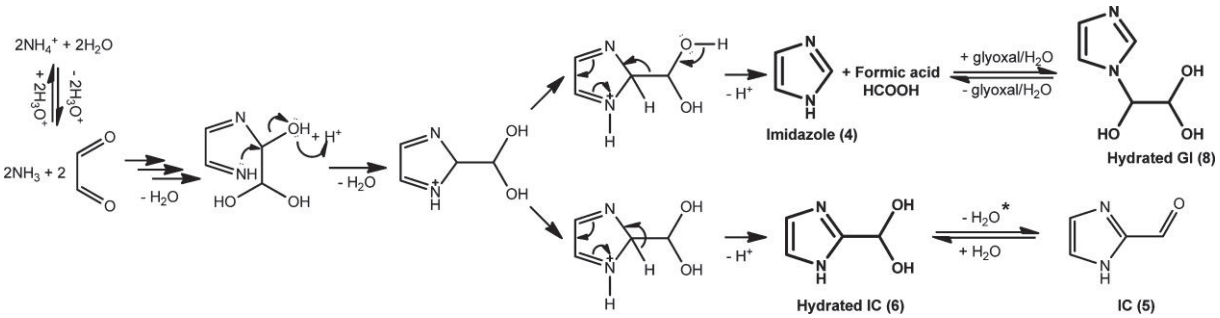

Figure II-1: Formation mechanism of IC in condensed phase as proposed by Yu and co-workers (Yu et al., 2011)

Imidazoles are also produced by marine biology, have been measured in sea water and could thus be present in the SML. Furthermore, both reactants necessary for the formation of IC are also present in the marine boundary layer. Glyoxal was measured over the Pacific Ocean (Sinreich et al., 2010; van Pinxteren and Herrmann, 2013) and ammonium salts are a very common compound in marine aerosols (Facchini et al., 2008; Huebert et al., 1996). This motivated the laser flash photolysis study of the reactivity of IC with halides, because photochemical reactions involving halides at the surface of aerosols or the sea can

potentially lead to the release of very reactive species in the gas phase, such as molecular halogens or radical anions (X_2^-) (Jammoul et al., 2009; Reeser et al., 2009).

But upon UV absorption, showing a maximum at 286 nm with shoulders up to 335 nm, IC also emits a very intense fluorescence signal. This fluorescence could be used to probe the behavior of this photoactive compound at the air/water surface by means of a glancing angle laser induced fluorescence set-up and evaluate the influence of an organic coating at the water surface.

It should be noted that both fluorescence and triplet state formation of imidazole-2-carboxaldehyde are significantly decreased under acidic conditions (pH < 3.5). This can probably be explained by the acid-base equilibrium between the diol and the aldehyde form of IC. Indeed, under very acidic conditions, the equilibrium will be shifted towards the formation of the diol form. As the π-π* transition is related to the carbonyl-function of an aromatic ring (Calvert and Pitts, 1966), the shift towards a fully hydrated geminal diol form inhibits this transition, which explains the lower signals observed in acidic medium. This was confirmed by UV-Vis absorption spectra of aqueous solutions of ground state IC at different pH, figure II-2, showing clearly a much lower absorbance at low pH for the absorption band centred at 285 nm (fig II-2). Another feature evidenced on this figure, the increase of absorption with increasing pH as indicated by the arrows. This shift is accompanied by a shift towards longer wavelengths (318 nm) of the absorption maximum for pH > 9.6. When after this pH is decreased again, as indicated by the arrows, the maximum absorption wavelength is shifted towards its initial maximum (286 nm), but the absorbance is much higher than for a non-alkaline solution. This indicates that a chemical change occurs in IC at high pH conditions. Different hypothesis can be emitted to explain this phenomenon, such as tautomerisation or diol formation, but time limited our research to the forms of IC in neutral pH and no further investigation has been done to elucidate this point.

In a preliminary study of ^{3}IC reacting with small atmospheric relevant carboxylic acids, the main difficulty was the acidification of the solution, which inhibited the triplet state absorption. The use of buffer solution was tested, but the phosphate anions present in the buffer quenched chemically the triplet state of IC. As of today, no satisfactory solution has been found for the spectroscopic study of IC in presence of acids.

The results presented in chapter IV will treat the photochemical reactions of IC with halides and an organic. The fluorescent properties of the molecule will used to study surface photochemistry, as presented chapter VI.

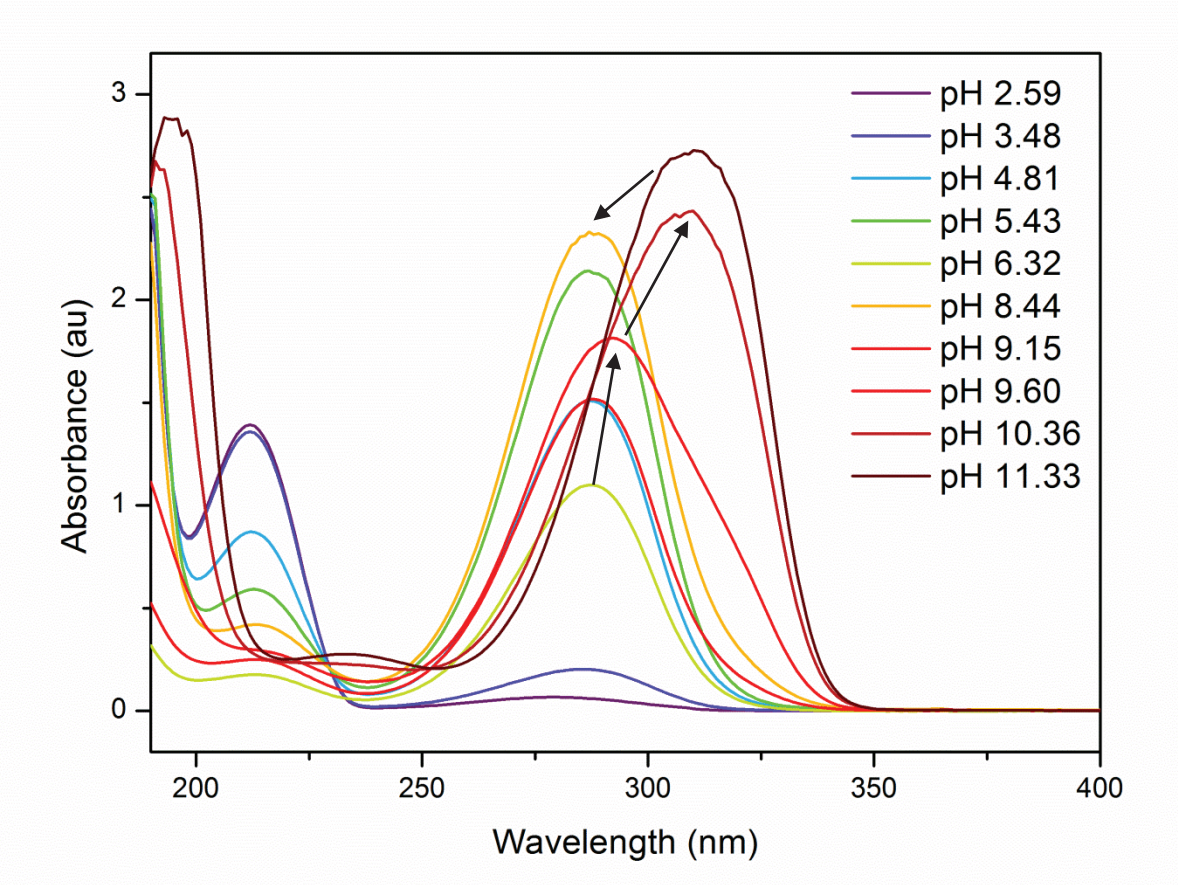

Figure II-2: Absorption spectra of aqueous solutions of 0.25 mM IC at different pH

II.1.1.b. 6-carboxy-pterin:

Pterins are a group of heterocyclic compounds, derivatives of 2-amino-4-hydroxypteridine and widespread in biological systems, whose photochemical properties are quite well documented (Lorente and Thomas, 2006). Several pterins have also been measured in seawater and the SML, amongst which 6-carboxy-pterin (CPT) and showed reactivity upon UV-A irradiation (Momzikoff et al., 1983). Early studies showed that some triplet excited pterins have the capacity to react with oxygen to form singlet oxygen (Chahidi et al., 1981; Ledbetter et al., 1995) and light induced oxidation of phosphate and iodide anions by pterins, CPT amongst others, has also been reported (Laura Dantola et al., 2010; Swarna et al., 2012). Pterins are also studied for their role in the development of the human skin disease Vitiligo and, especially CPT, for their role in the degradation of DNA *via*

photosensitized reactions (Hirakawa et al., 2003; Ito and Kawanishi, 1997; Rokos et al., 2002; Serrano et al., 2015).

Little is known though about the direct (type I) photochemical reactivity of pterins with organics other than specific DNA sequences. The choice of CPT as representative photosensitizer for the pterins present in the SML was motivated by its interesting photochemical properties, notably its capacity to induce photochemical reactions *via* electron transfer with DNA and also by its stability towards photooxidation at relevant (alkaline) pH. Although photobleaching through decarboxylation occurs upon irradiation, especially when oxygen is present (Suarez et al., 2000). It is also interesting to note that reactivity of CPT has been shown for singlet and triplet excited states (Song and Hwang, 2007; Swarna et al., 2012).

Pterins behave like weak acids in aqueous solutions and the pH of the solution influences largely their photophysical properties. The dominant equilibrium in environmentally relevant conditions involves an amine group (acid form) and a phenolate group (basic form). The pK_a of this equilibrium lays around 8 for the most pterin derivatives

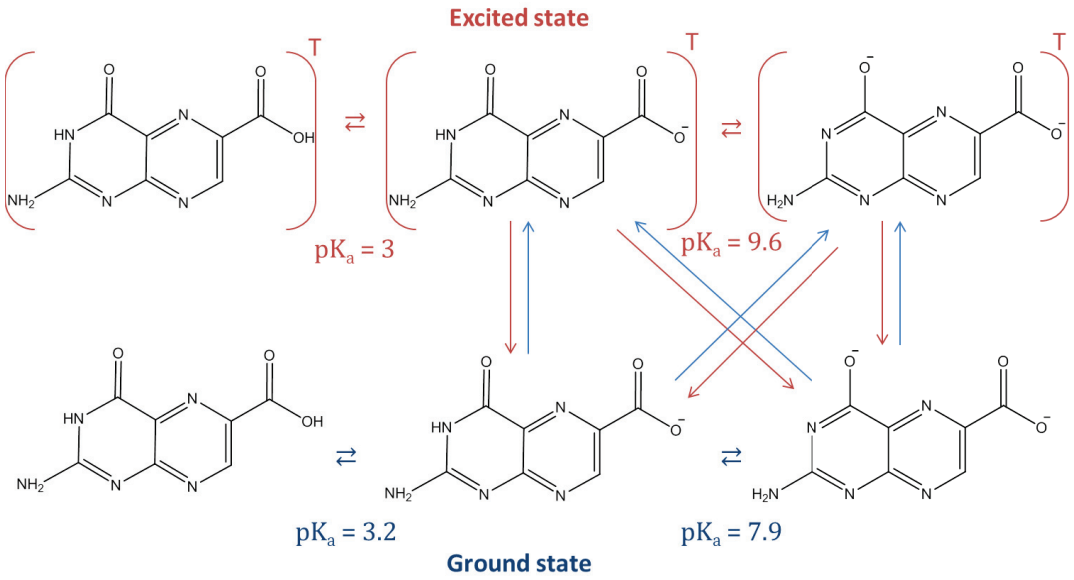

Figure II-3: Relevant acid-base equilibria of 6-carboxy-pterin in ground state and excited state in aqueous solution

and pK_a=7.9 for CPT (Lorente and Thomas, 2006). The carboxyl group of CPT has a pK_a around 3.2, which means that under environmental conditions it will be present as a carboxylate group. The 2-amino group and other ring nitrogen-functions have pK_a values

below 2.3. Figure II-3 shows the different equilibria under relevant pH conditions for ground and excited state CPT based on pK_a values from the literature (Chahidi et al., 1981; Pfleider.W et al., 1970; Suarez et al., 2000). Upon excitation, Chahidi and co-workers proposed that deprotonation occurs for neutral pterin, causing the shift in pK_a between ground state and triplet state. As CPT shows very similar photophysical properties, the same shift in pK_a can be expected here (Thomas et al., 2002). Under environmental conditions, CPT will thus be present, in function of the pH, under its mono-ionic and/or under bi-ionic form.

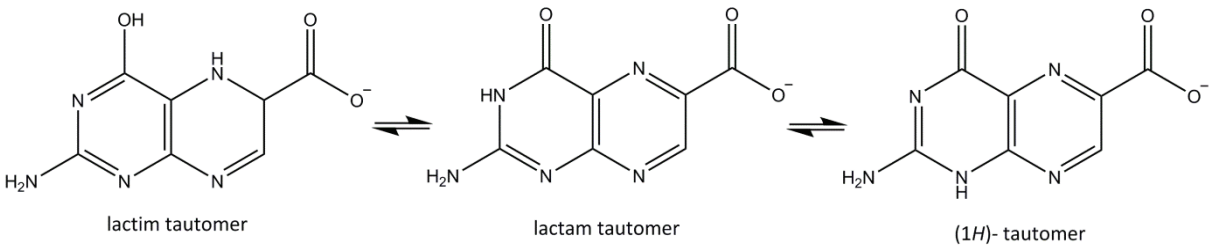

Figure II-4: three tautomeric forms of 6-carboxy-pterin

Several tautomers exist for CPT and the best known are the lactim and lactam form on the carbonyl group at position 4, as shown figure II-4. Lactim and lactam tautomers have been thought to be responsible for the existence of two triplet states, as has been demonstrated for pterin and also suggested for biopterin (Chahidi et al., 1981; Ledbetter et al., 1993; Ledbetter et al., 1995). But recent theoretical calculations showed that a third tautomer was more probably involved in chemical reactions, confirming an older NMR study stating that the lactam tautomer is the most important at neutral pH (Benkovic et al., 1985; Soniat and Martin, 2008). Indeed, the calculated Gibbs energy (ΔG) was found to be lowest for the lactam tautomer of pterin and only slightly higher (0.7-1.3 kcal/mol) for the (1*H*)-tautomer. The Gibbs free energy for the lactim pterin tautomer was found to be –surprisingly- 5.7-11.2 kcal/mol higher than the lactam tautomer. The existence of tautomers for CPT also seems to explain the bi-exponential decay rates of triplet state CPT in dimethylsulfoxide (DMSO) (Song and Hwang, 2007).

Chemical quenching of singlet state of pterins by anions, such as phosphate, present in commonly used buffers has been reported in literature (Lorente et al., 2004). Therefore, in

our studies pH has been adjusted by dropwise addition of a concentrated solution of NaOH. The reactivity of singlet and triplet CPT with halides and an organic compound has been investigated by means of laser flash photolysis and fluorescence. The results of this study are presented in chapter III.

II.1.1.c. 4-benzoyl-benzoic acid:

Aromatic ketones, such as benzophenone or 4-benzoyl-benzoic acid (4-BBA), can be used as a model sensitizers for the DOM since carbonyl functions are believed to represent an important fraction of the DOM (Canonica et al., 1995). 4-BBA shows very similar photophysical properties as benzophenone, a widely used photosensitizer, but has the advantage of a slightly higher solubility in water. The triplet state yield of 4-BBA is close to unity and shows a reactivity towards a wide range of organics, such as phenols or organosulfides, through type I and type II (implying singlet oxygen) photochemical reactions (Aregahegn et al., 2013; Latour et al., 2005). The radiative relaxation of the singlet state of 4-BBA is very low -hence the high triplet state yield- but this also implies that 4-BBA shows only a very weak and undefined fluorescence peak and is not adapted for the fluorescent techniques. The absorption maximum of 4-BBA lays around 265 nm, irradiation that will be scarcely available in the lower atmosphere, but the absorption spectrum shows a non-negligible tail up to 330 nm. Since its maximum is at the lower end of UV spectrum available at ground level, 4-BBA is probably the less representative as photosensitizer in the SML. Nevertheless, 4-BBA can give us interesting information about the mechanistic pathways leading to the formation of the photoproducts, since its reactivity upon excitation is well understood. Therefore, 4-BBA has been used in this study as a reference photosensitizer in different systems.

II.1.2.UV-Vis absorption and fluorescence

To start the investigation of new photosensitizers, the absorption spectrum of these under the appropriate conditions (solvent, pH) must of course be known. This has been done with a classical Agilent 8453 UV-Vis spectrometer (deuterium-tungsten lamps, photodiode array) in 1 cm quartz cuvettes for the photosensitizers used. The absorbance of the solutions, A_{10}, was recorded between 190 and 1100 nm.

The fluorescence of IC and CPT has also been studied and therefore steady state fluorescence spectra were measured with a Perkin Elmer(LS 45) fluorimeter. Additionally, during my stay at the University of Toronto a second fluorimeter (Photon Technology International QuantMaster 40) equipped with a 75W Xe-arc lamp as light source and an analog photon counting detection system was used. In both cases, the samples were introduced in closed quartz cuvettes of 1 cm and no thermoregulation was used. Both excitation and emission spectra were recorded. Excitation spectra are spectra obtained by monitoring a fixed emission wavelength over a range of excitation wavelengths; emission spectra are obtained by fixing one excitation wavelength and scanning a range of emission wavelengths.

To investigate the properties of the singlet state of CPT and establish its reactivity towards halides and some organics, the Perkin Elmer Fluorimeter has been used. Blank measurements with pure water showed an intense peak at 400 nm due to harmonics of the fluorescent excitation source, but who did not interfere with our measurements. Regular control measurements of pure water and the solution containing only CPT showed some temperature dependence of the fluorescent intensity (up to 3 %) and spectra were corrected for this.

Different types of reactivity can lead to fluorescence quenching: dynamic and static quenching. The latter is caused by a chemical complex being formed between the quencher and the fluorophore in its ground state; there is no reaction involving light. Dynamic quenching is due to collisional encounters between the excited fluorophore and the quencher. The dynamic type of fluorescence quenching can be evaluated using the Stern-Volmer equation (equation II-1).

$$I_F^0/I_F = 1 + K_{SV}[Q] = 1 + kq\,\tau_F^0\,[Q] \qquad \textit{(equation II-1)}$$

with : I_F^0 *: Fluorescence intensity without quencher present (au)*

I_F*: Fluorescence intensity in presence of the quencher (au)*

K_{SV}*: Stern-Volmer constant* (M^{-1})

[Q]: concentration of the quencher (M)

k_q*: bimolecular quenching rate coefficient* ($M^{-1}\,s^{-1}$)

τ_F^0*: fluorescence lifetime in the absence of a quencher (s)*

The observation of a linear relation for the Stern-Volmer plot alone, does not provide a direct evidence about the nature of the quenching process, since both dynamic and static quenching processes can show linear behavior. Indeed, if static quenching occurs, the equilibrium for the complexation might be reached at each concentration of quencher used, in which case the K_{SV} measured reflects the equilibrium constant of the complex formation (Calvert and Pitts, 1966). To establish whether the quenching process involved is a dynamic or static one, the UV-Vis absorbance spectrum of the solution were taken in presence and in absence of the quencher. If complex formation is involved, a change in the UV-Vis absorption spectrum should occur. Another way of assessing the dynamic character of the quenching process is monitoring the fluorescence lifetime in presence of different concentrations of the quencher. If the quenching is static, then $\tau_F^0/\ \tau_F = 1$ whereas for dynamic quenching $\tau_F^0/\ \tau_F = I_F^0/I_F$. With the laser flash photolysis set-up, time resolved fluorescence signals can be acquired to monitor the fluorescence lifetime, but the system is of limited use for fluorescence signals. Indeed, fluorescence lifetimes of pterins are of the order of 5-10 ns and the pulsewidth of the laser impulse is 5-6 ns. This means the fluorescence will partly be masked by the electronical interferences caused by the laser impulse in the system.

II.1.3. Glancing angle laser induced fluorescence

This rather unique spectroscopic technique was developed at the University of Toronto by the Donaldson group (Mmereki and Donaldson, 2002; Mmereki and Donaldson, 2003) and all experiments with this technique have been performed there. As for a classical laser induced fluorescence set-up, a laser impulse is used to excite a molecule to the singlet state. The laser used in the Donaldson group was a Nd:YAG laser, but by using an optical parametric oscillator (OPO, Vibrant 355, Opotek) pumped by the laser at 355 nm, the output wavelength is tunable for a range of wavelength going from 245-355 nm. When the excited molecule returns to the ground state by emitting a photon and thus fluoresces at a certain wavelength, the signal is transmitted to a photomultiplier tube (R2496 Hamamatsu) by means of a liquid light-guide. The wavelength detected is selected by a monochromator, as shown figure (figure II-5).

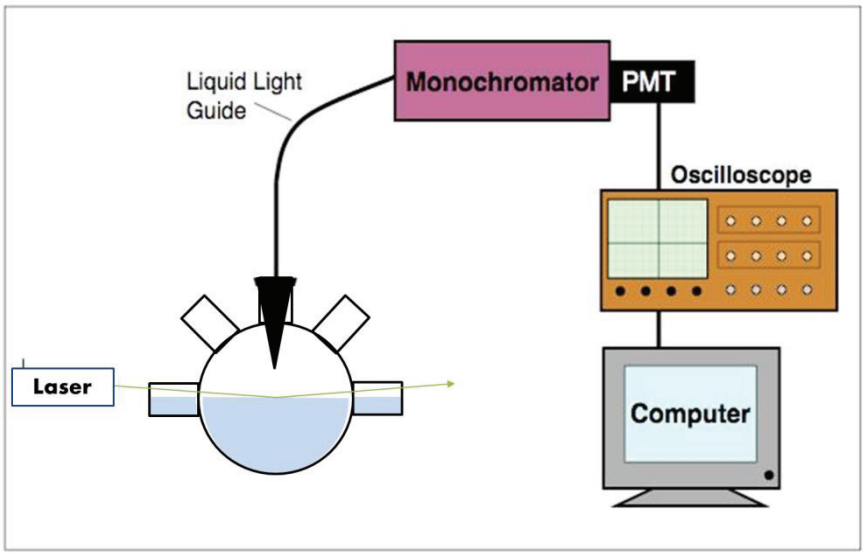

Figure II-5: Schematic representation of the glancing angle laser induced fluorescence set-up

The solution of interest is introduced in a three-neck round-bottom Pyrex flask, provided with 2 quartz windows at the sides. The incoming laser beam impinges on the surface of the solution with a very flat angle (>85°) such as to make a glancing reflection on the surface. The liquid light guide is introduced into the bottle by one of the necks and fixed approximately 1 cm above the place where the laser impacts the surface. The two additional necks of the round bottom flask can be used to introduce a gas flow above the surface, but were left open for the experiments presented.

The Pyrex bottle is then filled with 100 mL of the aqueous solution containing the photosensitizer under study without organic coating. The solution is left to stabilize for 10 minutes before registering the spectra on a pure water surface. Then, an organic surfactant is added, in our case octanol or nonanoic acid and the solution is left to stabilize for 20 minutes, after which the fluorescence spectra are taken. To obtain the adsorption isotherms, showing the surface behavior of the photosensitizer, the solution in the flask will be diluted with a second aqueous solution, containing only the organic and no photosensitizer. This is done by pipetting 10 mL of the solution from the flask and adding 10 mL of the second solution without sensitizer. After each dilution the solution is left to stabilize before taking the spectra. These consecutive dilutions are continued until the fluorescence signal is too weak to be detected. The same was done for a solution without any organic surfactant,

diluting with pure water. Once the pure water IC solution was diluted, the reverse was done; i.e. re-concentrating the solution until the initial concentration was reached by adding 10 mL of solution containing IC. This validated the procedure using successive dilutions, since the profile for the isotherm found when using the re-concentrations was the same as when diluting, within experimental errors, as illustrated figure II-6.

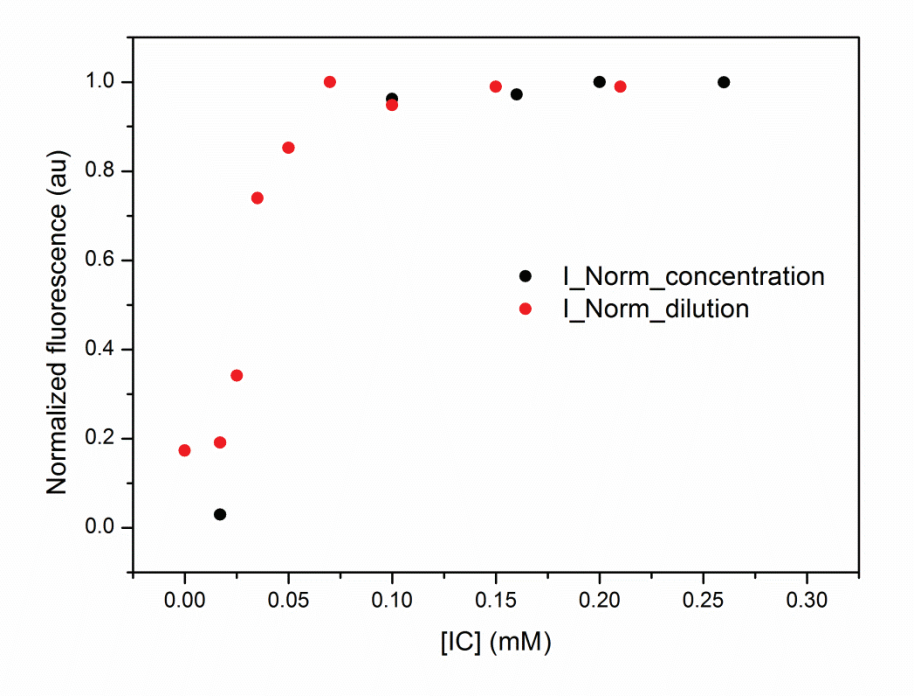

Figure II-6: Comparison of the normalized maximum surface fluorescence at the surface of a pure water solution of IC in function of different bulk concentration of IC, obtained by dilution (red) and concentration (black)

If the system is probing the surface, then the expected isotherms of the fluorescence intensity in function of the concentration of the photosensitizer would be well described by the Langmuir-Hinshelwood adsorption equation:

$$I = \frac{N^{surf}\,[P]}{b + [P]}$$

(equation II-2)

with: *I: fluorescence intensity (arbitrary units)*

N^{surf}: maximum number of surface adsorption sites

[P]: concentration of the photosensitizer (M-1)

In which the constant b is directly related to the inverse of the adsorption equilibrium constant from solution (Donaldson and Anderson, 1999; Mmereki and Donaldson, 2003). If the presence of an organic surface layer enhances the presence of the photosensitizer at the surface compared to a pure water surface, b will thus decrease, since the adsorption equilibrium constant is higher in the case of an organic coated surface.

To verify and validate the OPO laser set-up, a comparison with the commercial fluorimeters was done. Therefore, the set-up was slightly changed to be comparable to a classical fluorimeter set-up. The Pyrex flask was replaced by a classical 1 cm quartz cuvette, with the laser impulse arriving in the bulk of the solution. The liquid light guide was mounted at an angle of 90° with the laser incoming beam. Excitation and emission spectra could be recorded with the signal treatment described above. For the first measurements done, the excitation spectrum, the difference with the commercial fluorimeters is considerable, showing a very flat spectrum with a maximum emission (at 325 nm) for an excitation at 265 nm, as shown figure II-7a. This can be explained by the high variability of the intensity of the laser for this measurement over the range of wavelengths considered. Also the excitation spectra were taken before the emission spectra and the fixed wavelength (325 nm and 380 nm) for the emission was not the maximum of the fluorescence emission for this set-up. After the measurements for the excitation spectra, the laser output was optimized and a lower variability for the laser output was obtained. The output varied from 1.7 mJ/pulse to 2.1 mJ/pulse in the 250-310 nm wavelength range, with a maximum output around 290 nm and an output at a fixed wavelength stable within 10% over 300 pulses, which was measured before each measurement.

The comparison of the methods (figure II-7) also shows differences between both fluorimeters; for the Toronto fluorimeter the maximum in the excitation spectrum is seen at 282 nm, whereas maximum emission in Lyon was measured for an excitation at 275 nm. For the emission spectra, the OPO set-up bulk measurements are in better agreement with the fluorimeter measurements. Maxima were measured at 330 nm and 338 nm for the Toronto and Lyon fluorimeters respectively. The OPO measurement shows 2 maxima, one around

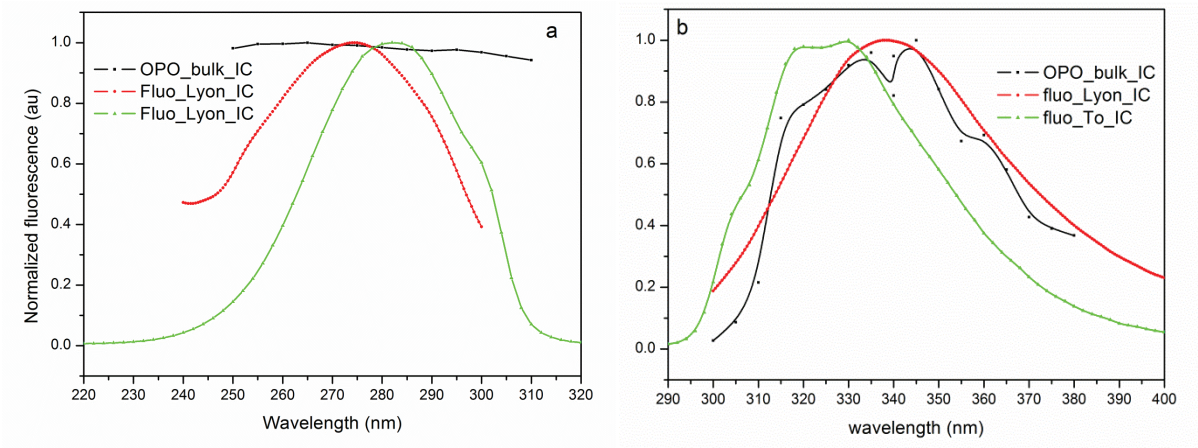

Figure II-7: Comparison of excitation (a) and emission (b) spectra for aqueous solutions of IC measured with the different set-ups: OPO laser set-up in black, the Perkin Elmer fluorimeter in Lyon in red and the PTI fluorimeter in Toronto in green

335 nm and another around 345 nm. The point at 345 nm seems rather abnormal with respect to the measurements with the fluorimeters and further bulk measurements with the OPO set-up done in coated solutions, where always one maximum was found (see results chapter V and VI).

It becomes clear from this inter-comparison that the fluorimeters and the OPO set-up show differences in the measured wavelengths, but for the emission spectra in particular the OPO set-up seems to agree better with the fluorimeter in Lyon than both fluorimeters among each other. A comparison with a fourth fluorimeter in Lyon showed a maximum at 336 nm for the same solution (table II-2). This data is not shown here, since there is no digital output for this instrument. As three methods showed very close values for the maxima of the emission spectra table II-2, we concluded that the monochromator of the fluorimeter used in the University of Toronto probably needed a calibration and that the OPO set-up was valid, if the variability of the laser output was well taken into account.

Table II-2: Wavelength of the maximum emission for excitation and emission spectra measured by different methods

	Max. excitation spectrum (nm)	Max. emission spectrum (nm)
OPO set-up	265	335 (345)
Fluorimeter Toronto	282	330
Fluorimeter Lyon	274.5	338
Old fluorimeter Lyon	279	336

II.1.4. Laser flash photolysis

Laser flash photolysis (LFP), a well-known spectroscopic method for the kinetic study of short-lived species, was developed in 1947 by George Porter and Ronald G.W. Norrish (Nobel prize 1967). This technique provides direct transient measurement of reactions involving species such as radicals, excited states or ions and is widely used in physics, chemistry and biology. The principle LFP reposes on the excitation by a very short light impulse of the transient species, whose change in absorption (or emission) spectrum is measured in the beam of a second analyzing light source. The short light impulse is delivered by the output of a laser, providing single-wavelength excitation and nanosecond time resolution. Upon the excitation by the laser light, the photosensitizer will from a triplet state, whose difference in absorption compared to ground state will be measured with time-resolved spectroscopy. When adding a second reactant to the solution, the triplet state of the photosensitizer can react with this compound, which will lead to a shorter lifetime of the triplet state absorption.

In the set-up used for the experiments presented here, schematized in figure II-8, a pulsed Nd:YAG laser (Surelite II-10, Continuum) provides the exciting light pulse, at four possible wavelengths (266nm, 355 nm, 532 nm and 1064 nm). The laser pulse will excite the photosensitizer, placed in a quartz flow cell (450 µL, 1 cm path length) at 13 cm distance of the laser output and in the optical path of the analyzing light, provided here by a Xenon arc lamp (75 W, Lot-Oriel). The solution is deoxygenized before introduction in the flow cell by bubbling the solution with N_2 before each experiment and kept under N_2 purge flow during the measurements. The degassed solution is then introduced in the flow cell by means of a peristaltic pump, ensuring a complete purge of the exposed volume every 17 seconds, to avoid photolysis of the photosensitizer and limit heating. The light then enters a monochromator (DK240, Spectral Products) and is detected by a photomultiplier tube (H7732-01, Hamamatsu). After amplification by a high speed current amplifier-discriminator (Femto), the AC component of the signal is recorded by a oscilloscope (TDS3032c, Tektronix).

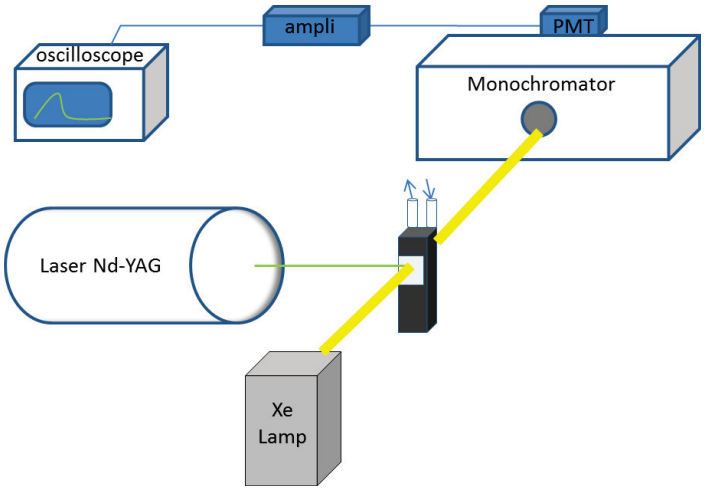

Figure II-8: Schematic representation of the laser flash photolysis set-up

The signals obtained were averaged over 16 laser pulses and the lifetimes of the triplet state determined by fitting the transient signal with an adapted function using OriginPro (version 8.0988). For the kinetic measurements the probe wavelengths corresponds to the maximum absorption wavelengths of the triplet state of the considered photosensitizer.

Since the two photosensitizers studied with LFP, 6-carboxypterin and imidazole-2-carboxaldehyde, showed quite different behavior, the experimental conditions had to be adapted in function of the photosensitizer studied. The optimized experimental conditions are specified in the sections treating the results of these experiments (Chapter III for CPT and Chapter IV for IC).

II.2. Chemical characterization

II.2.1 Set-up and chemical compounds under study

II. 2.1.b. Set-up

In order to analyze the gaseous and liquid phase products formed by the photo-initiated reactions, the second part of the thesis focused on mass spectrometry methods for the identification of these products. The set-up used for these studies, schematized figure II-9, was a small cylindrical quartz reactor, with a volume of 14 mL, mounted at 13 cm of a Xenon arc lamp. The reactor was filled only half-way to optimize the surface area to volume ratio while keeping almost equal volumes for the gas-and bulk phase. A Xenon arc lamp (Lot-Oriel, 100 W) was used for the irradiation, since these lamps reproduce the spectrum of the solar irradiation available in the lower troposphere. A quartz water filter of 1 cm thickness was placed at the exit of the lamp to filter part of the infrared irradiation, avoiding excessive heating.

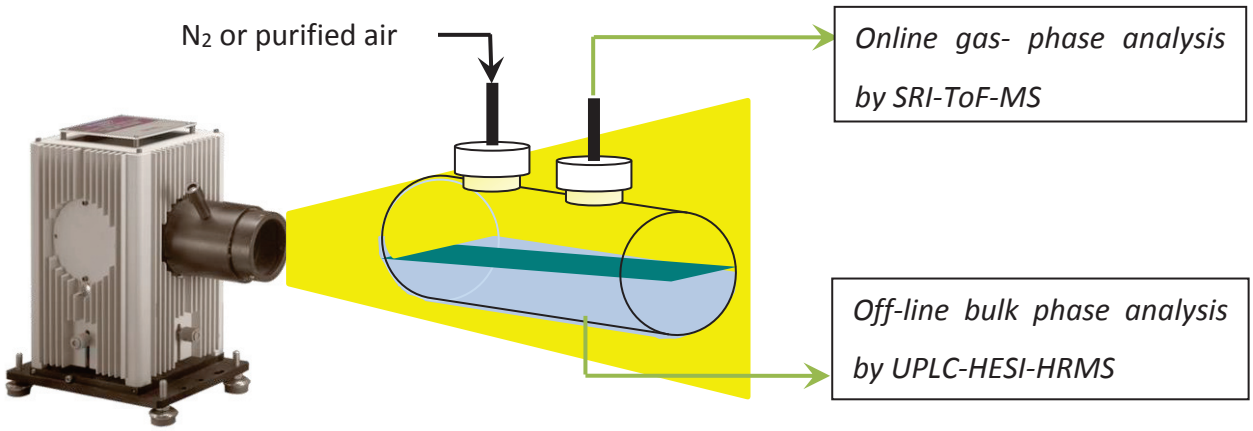

Figure II-9: Schematic representation of the set-up

II.2.1.b Choice of the organic coatings

Two surfactants have been used as proxies for the SML: nonanoic acid (NA) and 1-octanol. Octanol is a classical compound used as a model in surfactant studies, especially to describe the partitioning of compounds between aqueous and organic phases. NA, a saturated linear carboxylic acid, can be representative of the many fatty acids found in the SML. Though most natural fatty acids contain a pair number of carbons, nonanoic acid has been identified

in a rice-field microlayer in a Californian field study previously (Gever et al., 1996). NA can also be produced by the oxidation reaction of oleic acid, a very common natural fatty acid, at the surface of water reacting quickly with ozone to produce nonanoic acid remaining at the interface (King et al., 2009).

The 1-octanol used was provided by Sigma Aldrich with a 99% purity. Most experiments were done with NA provided by Alfa Aesar, purity 97% but some experiments were performed with ultra pure NA (99.5 %, Sigma Aldrich) and the type of NA used for the experiments will be specified. Due to its poor solubility, theoretically predicted around 1-1.5 mM at pH 4-5, NA quickly forms a layer at the interface water-air. As discussed in the introduction, measuring the surface tension for different bulk concentrations of NA gives a clear indication at which concentration the excess concentration of NA forms a surface layer. As can be seen on figure II-10a, the surface tension changes level out for a bulk concentration of about 1 mM, meaning that for concentrations beyond 1mM, the surface is covered entirely with nonanoic acid (Ciuraru et al., 2015). For 1-octanol, the surface excess concentration as a function of bulk concentration shows a plateau from 0.9 mM bulk concentration onwards, figure II-10b, and theoretically a mono-layer regime is reached for a concentration of around 2.5 mM (Mmereki and Donaldson, 2003). In our experiments, the typical concentrations were 2 mM for NA and 1-2.5 mM for octanol.

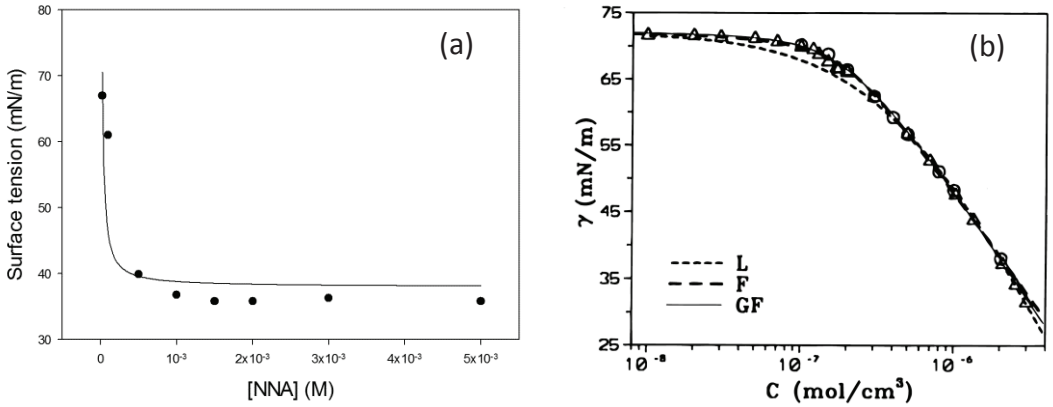

Figure II-10: Surface tension in function of bulk concentration for (a) nonanoic acid (adapted from Ciuraru et al., 2015) and (b) 1-octanol (Lin et al., 1997)

The pH of the bulk aqueous phase will play an important role on the solubility of the surfactant and thus on the formation of the surface microlayer. At very alkaline pH (>10), it is expected that 2 mM of NA will be dissolved completely and no surface excess will be

available at the surface. On the contrary, at pH lower than 3, the maximum solubility of NA decreases to around 1 mM and surface excess will thus be favored. The pH of the solution will influence less the surface excess in case of octanol, as the solubility of an alcohol is not pH dependent. In our experiments, pH was not corrected and was measured to be between 4.1 - 5.4, depending on the photosensitizer used.

From what is known about the absorption of saturated carboxylic acids and long-chain alcohols, no photochemical reactions should be initiated by the sole surfactant and a photoactive compound must be added in order to trigger the photochemistry. But surprisingly, during our study it will become clear that photochemistry is occurring merely in the presence of the surfactant NA, without addition of a photosensitizer. The possible mechanism behind this and its implications will be discussed in length in chapter VI.

II.2.1.c. Choice of the photoactive compounds

Three different photoactive compounds were used in this study with the goal to understand the molecular mechanism behind the formation of the observed products. Firstly, a well-known model photosensitizer, 4-benzoyl-benzoic acid (4-BBA), was used as presented section II.1.1.c. The second photosensitizer used was imidazole-2-carboxaldehyde (IC), since this photosensitizer could be measured by fluorescence directly at the surface by GALIF and therefore more direct proof from its reactivity at the surface was available (see section II.1.1.a). The third compound used, hydrogen peroxide, is not a photosensitizer, but will be photolysed when irradiated with UV light to form OH-radicals. These radicals can then initiate radical reactions through hydrogen abstraction on the substrate (NA or 1-octanol). H_2O_2 (Sigma-Aldrich, 37 wt %, solution in water) was used to verify the hypothesis that the reactions were initiated by hydrogen abstraction and that products were formed through radical chain reactions.

II.2.2 Condensed phase analysis

The condensed phase was analyzed with an off-line method using ultra-performance liquid chromatography (UPLC) coupled to a high resolution mass spectrometer (HRMS) with an ionisation by heated electrospray (HESI) in the positive and negative modes (UPLC-(+/-)HESI-HRMS). The UPLC unit is a commercially available Dionex Ultimate 3000 (Thermo Scientific, USA) mounted with a HSS T3 Acquity UPLC column (1.8 µm, 2.1 × 100 mm). The high

resolution mass spectrometer is a commercially available Q-Exactive (Thermo Scientific, USA) of the Orbitrap type, providing analysis with a nominative resolution of 140 000 at m/z 200. The HRMS was run on the full scan mode over a mass range of m/z 50-750. Further analytical details will be given in each section discussing condensed phase results. In the next paragraph the principles of this type of HRMS will be briefly discussed.

II.2.2.a. Operating principles

The electrospray ionization mode is based the generation of a spray at the end of a capillary guiding the sample into an electric field. The electric field is applied between the end of the capillary and a counter electrode. Depending on the polarity of the field applied, the sample droplets will contain an excess of positive and negative charges. The solvent evaporates under the action of the temperature and the sheath flow of N_2 applied in the source and the droplets shrink to a critical size. The non-volatile ionized analytes are concentrated in the droplets and when the droplet attains the Rayleigh limit, repulsive forces between like charges in the droplet cause an Coulombic explosion, giving birth to smaller spherical charged droplets. Eventually all solvent evaporates and only the charged analyte remains. Another mechanism explaining the ESI ionization is the atmospheric pressure ion-evaporation process, proposing a field desorption model. Both are schematized figure II-11.

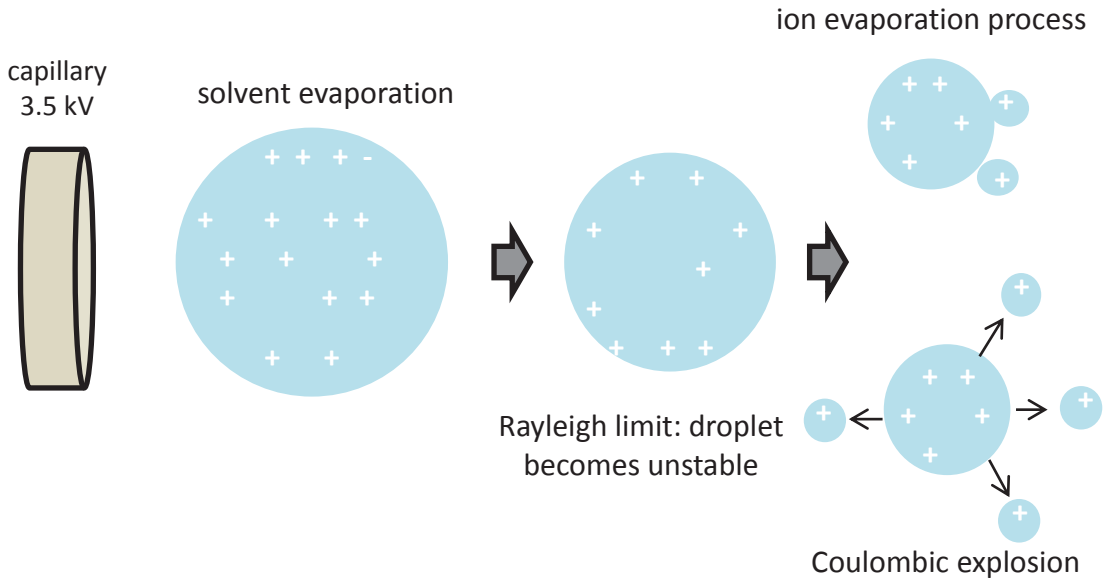

Figure II-11: Schematic representation of the ESI ionization process

The ions formed this way will enter a transfer tube and pass through the stack of lenses (S-lens) as showed figure II-12, guiding the ions into the flatapole. This bent flatapole applies a oscillating voltage on the incoming ions much like a quadrupole, but is used here essentially for transmission. The combination of flatapole and quadrupole provides a first mass filter, permitting to select a certain mass range for single ion scan almost instantaneously (Michalski et al., 2011). The ions are then extracted towards the C-trap, where the ions are stored and cooled before being injected in the Orbitrap. In the C-trap rotational frequencies of the ions are rapidly ramped down and an electric field is applied to accelerate the ions and extract them into the Orbitrap

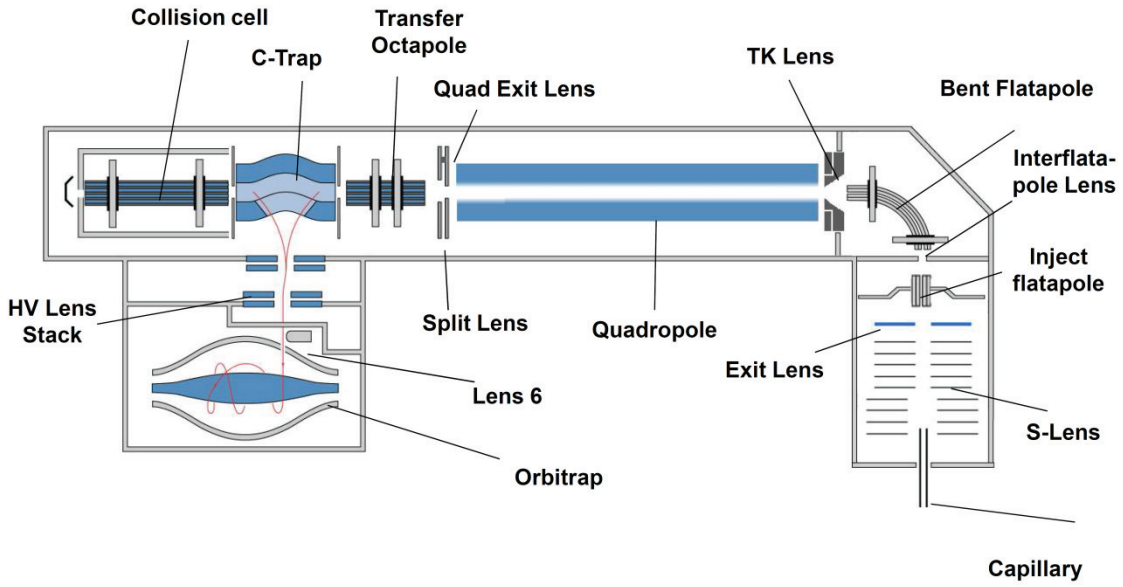

Fig. II-12: Schematic representation of the HRMS (Michalski et al., 2011) .

The Orbitrap consists of a central electrode and an outside barrel-shaped surface, between which a static electrostatic field is applied (unlike the dynamic electrostatic field created in case of a quadrupole). The electric field is inhomogeneous with a minimum in the center of the Orbitrap, where the space between the electrodes is highest, and the vectors of the electric field are non-parallel, as schematized figure II-13. The axial oscillations are initiated by the dynamic injection pulse and no further excitation is needed; the mass-dependent axial oscillations are maintained by the inhomogeneous electric field. When a short packet of ions of enters the field tangentially and off-equator, the ions are squeezed towards the central electrode by a decrease in voltage. In the axial direction, ions are forced to move

towards the equator by the electric field and start the axial oscillations. The frequency of the natural oscillation along the *z*-axis is mass dependent according to equation II-6 (Watson and Sparkman, 2008):

$$\omega_z = \sqrt{\frac{k}{m/z}} \qquad \textit{(equation II-3)}$$

with: ω_z : *the oscillatory frequency along the z-axis (Hz)*

k : constant

m: the mass number of the ion

z: charge number of the ion

Because the rotational frequency is strongly dependent on ion energy, angles and position the ion packet will form a rotating ring. The frequency of axial oscillations of each ring induces an image on split outer electrodes. The time-domain signal thus obtained, formed by frequencies of the oscillating image current are then treated by modified Fourier transform.

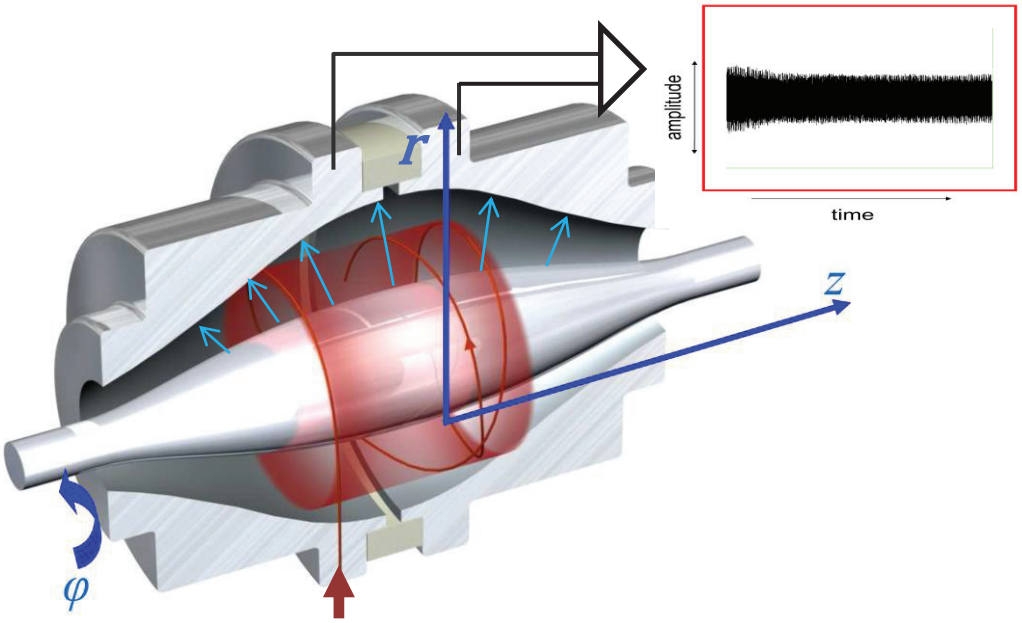

Figure II-13: Schematic representation of the orbitrap showing the injection point, illustrating the inhomogeneous electric field and the signal output (adapted from Watson & Sparkman, 2008)

The Q-Exactive also permits to obtain MS/MS spectra by using the high energy collision cell, which will lead to fragmentation of the selected ions. Fragmentation patterns can give interesting information about the structure of the parent ion.

This type of mass analyzer has a very high resolving capacity combined with a low detection limit (in the 10^{-9} M range, depending on the compound). Due to the soft ionization by HESI, the mass spectra show little fragmentation and most ions will be detected at their molar mass plus or minus 1 (in positive and negative ionization mode respectively). Ionization efficiency depends on the matrix, making quantification difficult in very variable matrices, especially when no chromatographic separation is used, the so-called direct injection (Chambers et al., 2007). The vacuum requirements for the Orbitrap are very high with a pressure of only 10^{-10} mbar and makes it a rather laboratory-bound instrument.

II.2.2.b. Sample preparation: derivatization

The details of the analysis are given in each chapter treating MS results, but one point of the sample preparation, i.e., the derivatization, maybe needs a little more explanation. For the condensed phase, samples were split in two. Part of the sample was injected without derivatization and the other part was added to a solution of 1 mg mL^{-1} O-(2,3,4,5,6-penta-fluorophenyl)methyl-hydroxylamine hydrochloride solution (PFBHA). This well-known derivatization method selective for ketones and aldehydes forms PFBHA-oximes on the carbonyl groups as illustrated by the figure II-14 (Cancilla and Hee, 1992).

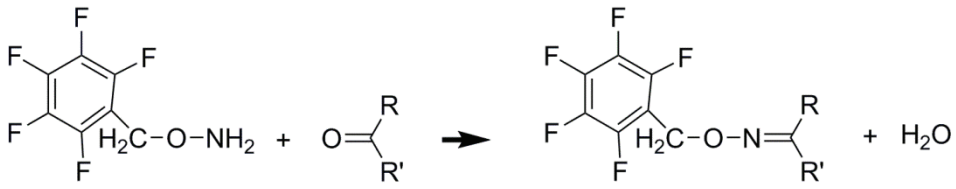

Figure II-14: Reaction mechanism for the derivatization of carbonyls with PFBHA

This derivatization not only gives exclusion on the presence of a carbonyl presence, but also increases the sensitivity of the detection, as derivatized compounds are very easily ionized and better transmitted due to the heavier molecular mass. Relative intensities for the derivatized samples and the non-derivatized samples can thus show several orders of magnitude difference.

II.2.3. Gas-phase analysis

The on-line monitoring of changes in the gas-phase was done with a high resolution time of flight mass spectrometer coupled to a switchable reagent ionization source (SRI-ToF-MS, Ionicon 8000, Austria). The SRI-ToF-MS is equipped with a variant of the proton transfer reaction source, using besides H_3O^+ alternative primary ions, here NO^+ and O_2^+ to chemically ionize the analytes. In our experiments, only H_3O^+ and NO^+ ionization modes were used. This type of mass spectrometer allows for a real time monitoring of most VOCs with a nominative resolution of 8000, a high sensitivity and a detection limit of pptV level. The theory behind the PTR and SRI mass spectrometer will be briefly discussed in the next section. Full details on the experimental conditions will be given in each section where SRI-ToF-MS results are treated..

II.2.3.a. Operating principles

The first mass spectrometers with proton transfer reaction ionization were developed in the late 90s by the Austrian group of Professor Lindinger (Lindinger et al., 1998a; Lindinger et al., 1998b) and are now widely adopted, particularly in atmospherical research (de Gouw and Warneke, 2007). On figure II-15 the different parts of the SRI-ToF-MS are schematized.

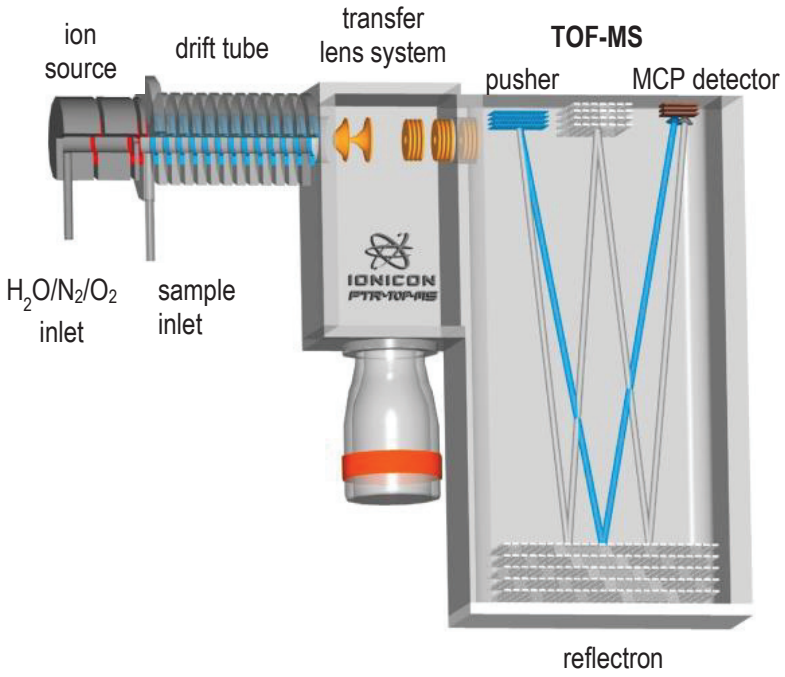

Figure II-15: Schematic representation of the SRI-ToF-MS (adapted from ionicon.com)

First of all, the primary ions are generated in the ion source, consisting of a hollow cathode (Hansel et al., 1995). Then the H_3O^+ (or NO^+ or O_2^+) ions generated are extracted towards a reactor of 9.3 cm length, called drift tube, where the analytes are also introduced and the reaction between VOCs and primary ions takes place. The extraction of the primary ions is done by means of two elements at different voltages, avoiding the backwards diffusion of sampled air into the ion source region. The backwards diffusion of sampled air into the ion source causes impurities in the primary ion production and explains e.g., the presence of NO^+ and O_2^+ impurity peaks in the H_3O^+ ionization mode spectra. For the NO^+ ionization mode these impurities will mainly be O_2, NO_2 and H_3O^+. The drift tube consists of a number of stainless steel rings, separated by Teflon rings, working as electronically and vacuum seals. Each ring is connected to a resistor network building up a homogeneous electric field inside the drift tube, characterized by the overall drift tube voltage. The drift voltage guides the ions towards the exit of the drift tube reactor, but also provides the kinetic energy necessary to avoid excessive cluster formation in the reactor. This drift tube voltage can also be expressed as E, the gradient of the electric field per centimeter. An important parameter for SRI-ToF-analysis is E/N, unity Townsend (1 Td = 10^{-17} V cm^2) where N represents the number density of the gas in the drift tube. N will depend on the pressure, generally set at 2.24 mbar in our experiments and temperature in the drift tube. In general, high E/N values lead to more fragmentation whereas low E/N values lead to more water cluster formation.

The now ionized VOCs are extracted at the end of the drift tube by a system of transfer lenses and enter the time-of-flight mass spectrometer. This mass spectrometer is based on the principle that the time of flight in a 'field free region' of an accelerated ion will depend directly of its mass to charge ratio. By measuring the time between the accelerating pulse given at the extraction of the ions and the arrival of an ion on the detector, the m/z can be determined, theoretically without any limitation of m/z range (Watson and Sparkman, 2008). In the ToF-MS used in our instrument, the ions are accelerated orthogonally and then enter a reflector to obtain higher resolution. The reflector corrects the velocity of ions having the same m/z but different kinetic energies. The reflector, also called ion mirror, consists of an electric field opposed to the pusher and of greater magnitude then the field in the accelerator region. When the accelerated ions with greater kinetic energy (m^+_{high}) enter the opposing electric field, they will penetrate deeper into the

reflector, as they have the highest velocity, while ions with lower kinetic (m^+_{low})energy will

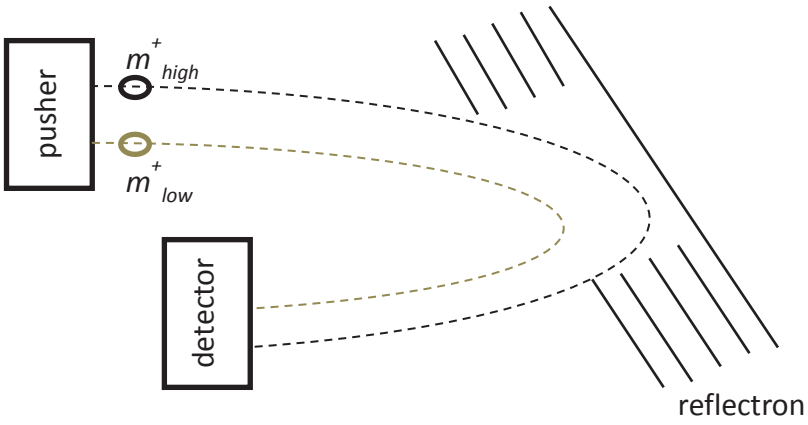

Figure II-16: Illustration of the principles of a reflectron

penetrate less far in the reflector, as schematized figure II-16. When their kinetic energy reaches zero, they will start to get accelerated again by the opposing electric field. Ions with high initial kinetic energy acquire more kinetic energy during reacceleration than ions with a low initial kinetic energy, as they penetrated further in the reflector electric field and due to this longer flight trajectory, ions of the same m/z with different kinetic energies will reach the detector at the same time. The flight trajectory is typically a V-shape but can also be W-shape, which almost doubles the resolution but with a loss of sensitivity. The detector of this type of mass spectrometer is most commonly a MCP, micro channel plate which have the advantage of having a fast response time.

II.2.3.b. H_3O^+ ion chemistry in the drift tube

The specificity of the SRI-ToF-MS is of course its ionization mode. As mentioned before, primary ions produced in the ion source enter the reactor to ionize the analytes introduced there. In the classical PTR, the primary ions are thus hydronium ions, H_3O^+. In this case, the VOCs introduced will be ionized by a proton transfer (reaction (1) in the reaction scheme below) if their proton affinities (PA) are higher than the proton affinity of water, PA = 691 kJ mol^{-1} (or 166.5 kcal mol^{-1}) (Blake et al., 2009). If the reaction is energetically allowed, it proceeds at a rate close to the collision rate, generally between 1.5 x 10^{-9} cm^3 s^{-1} ≤ k ≥ 4 x 10^{-9} cm^3 s^{-1} (Lindinger et al., 1998a). Proton transfer rate coefficients for many VOCs have been determined experimentally by selected ion flow tube mass spectrometry (SIFT-MS)

measurements (Smith and Spanel, 2005a) or theoretically (Cappellin et al., 2012). One of the advantages of PTR is that most of the VOCs present in the air have proton affinities higher than water, but not the most common components of air, such as O_2, N_2 or CO_2. Another advantage of using H_3O^+ as primary ions is that many of their proton transfer reactions are non-dissociative so that most VOCs will be detected at the protonated molecular mass, simplifying the mass spectra. Even though proton transfer is a soft ionization mode, fragmentation occurs but it frequently follows a rather straightforward pattern, e.g. the loss of a water molecule from alcohols, although larger molecules tend to follow more complicated fragmentation patterns (Buhr et al., 2002; Tani et al., 2003).

Fragmentation is also function of the humidity of the sampled air since water clusters, reaction (2) below, may intervene in the fragmentation of the compounds. Several authors report the influence of humidity on the sensitivity and the fragmentation ratios of different compounds which seem to be very variable depending on the compounds considered and operational setting (notably E/N). For instance, Baasandorj and co-workers report higher fragmentation in high relative humidity (RH) samples and lower sensitivity of formic acid and acetic acid in PTR-MS measurements at E/N=125, but higher sensitivity at lower E/N values (E/N < 100) (Baasandorj et al., 2015). The lower sensitivities observed are attributed to enhanced water-driven fragmentation under high RH. Several authors report higher sensitivities under high RH conditions for a series of alcohols and aldehydes emitted from green leaves, pyrrole and a series of monoterpenes .(Pang, 2015; Sinha et al., 2009; Tani et al., 2004). Higher sensitivities are thought be due to proton transfer and ligand switching reactions of VOCs with water clusters as shown in reactions (3a) and (3b):

$$H_3O^+ + R \longrightarrow RH^+ + H_2O \quad (1)$$

$$H_3O^+ + nH_2O \rightleftarrows H_3O^+(H_2O)_n \quad (2)$$

$$H_3O^+(H_2O)_n + R \longrightarrow RH^+ + (n+1)H_2O \quad (3a)$$

$$H_3O^+(H_2O)_n + R \longrightarrow H^+(H_2O)_mR + (n\text{-}m+1)H_2O \quad (3b)$$

The proton transfer reaction (3a) is more selective than in reaction (1) since the proton affinities of the water clusters $(H_2O)_n$ are higher than for H_2O. Species with a low PA, as e.g. formaldehyde, whose PA is only 22 kJ mol^{-1} above that of water, will thus not undergo proton transfer from water clusters. Ligand switching reaction (3b) highly depends on the

polarity of the VOC. For many VOCs ionization rates for reaction with water clusters will be similar to the rates for reaction (1), with the notable exceptions of species with a low PA and species with a low polarity, e.g. benzene (de Gouw and Warneke, 2007).

As fragmentation patterns and sensitivity are so dependent on the sample humidity and operational settings (E/N in particular), care must be taken to assess these issues correctly for the operational settings of the instrument and the sample humidity. For our experiments, the fragmentation patterns of the main products were examined by measuring the signals of liquid standards in water, under the same experimental conditions as the experiment (without any irradiation). Small volumes (< 2 µL, in function of the volatility and instrument response) of a standard were added to ultra-pure water, after acquisition of a blank spectrum in presence of ultra-pure water only. Although these results are not sufficient to correct for a difference in sensitivity, they do provide a good approach to establish the fragmentation pattern and branching ratios under experimental conditions. Table II-3 lists the fragmentation pattern for 8 different standards under our working conditions and also shows the mass accuracy for each ion (Δ m/z). Only peaks with an intensity higher than 10% of the major ion for the considered compound are taken into account.

The rather extensive fragmentation clearly demonstrates that fragmentation should be taken into account in our measurements, even for this soft ionization method. It becomes clear form table II-3 that certain fragments are common to several compounds and can also be protonated product ions for other compounds, e.g. m/z 69.069. This fragment is common to nonenal and octanal, but can also be the protonated product ion for isoprene, or any other compound with the same molecular formula (C_5H_8). It has to be noted here that the proposed fragmentation patterns are based on common fragmentations pathways, such as loss of H_2O, CO or OH. The other neutral reaction products proposed are confirmed by their ionized equivalents and where this is not the case, speculative neutral products are proposed in italics.

The interpretation of the mass spectra in experiments is complicated by the presence of the many fragment ions. Therefore care must be taken when attributing a molecular formula to a certain mass, especially for the smaller masses, to rule out their origin as fragments of bigger ions which is possible by using the branching ratios of the major products for the experimental conditions. The identity of the detected ions is also

Table II-3: product ion distribution for the reaction of H_3O^+ with 8 standard compounds under our experimental conditions (E/N= 135 Td). In bold are the protonated product ions, speculative fragmentation patterns are in italic.

Compound	Formula	Purity (%)	MW	Detected ions [and proposed reaction channel]	Branching ratio (%)	Expected m/z (amu)	Δ m/z (x 10^{-3} amu)
1-nonanol	$C_9H_{20}O$	98	144.15	$C_9H_{19}^+$ [+ H_2O]	1.9	127.1481	0.2
				$C_6H_{13}^+$ [+C_3H_7 + H_2O]	5.1	85.1012	0.1
				$C_5H_{11}^+$ [+ C_4H_8 + H_2O]	13.9	71.0855	0.7
				$C_4H_9^+$ [+ C_5H_{10} + H_2O]	26.47	57.0699	1.6
				$C_3H_7^+$ [+ C_6H_{12} + H_2O]	33.3	43.0542	1.9
				$C_3H_5^+$ [+ C_6H_{14} + H_2O]	19.4	41.0386	1.3
trans-2-nonenal	$C_9H_{16}O$	97	140.12	**$(C_9H_{16}O)H^+$**	31.6	141.1274	0
				$C_9H_{15}^+$ [+ H_2O]	26.4	123.1168	1
				$C_6H_9^+$ [+ C_3H_7 + H_2O]	15.1	81.0704	0.6
				$C_5H_9^+$ [+ C_4H_6 + H_2O]	4.95	69.0699	0.1
				$C_5H_7^+$ [+ C_4H_7 + H_2O]	8.4	67.0542	1
				$C_3H_5O^+$ *[+ C_5H_{12}]*	13.5	57.0335	0
1-octanol	$C_8H_{18}O$	≥ 99	144.15	$C_8H_{17}^+$	0.2	113.1325	0.5
				$C_5H_{11}^+$ [+ C_3H_6 + H_2O]	1.7	71.0855	2.4
				$C_4H_9^+$ [+ C_4H_8 + H_2O]	93.5	57.0699	5.9
				$C_3H_7^+$ [+ C_5H_{10} + H_2O]	2.6	43.0542	2.5
				$C_3H_5^+$ [C_5H_{12} + H_2O]	1.9	41.0386	2
octanal	$C_8H_{16}O$	99	128.22	**$(C_8H_{16}O)H^+$**	12.6	129.1274	-7.8
				$C_8H_{15}^+$[+ H_2O]	27.4	111.1168	0.3
				$C_5H_9^+$ [+ C_3H_5 +H_2O]	50	69.0699	-1.1
				$C_3H_5^+$ [+ C_5H_9 +H_2O]	10.0	41.0386	-0.8
trans-2-octenal	$C_8H_{14}O$	≥ 95	126.10	**$(C_8H_{14}O)H^+$**	33.4	127.1117	0
				$C_8H_{13}^+$ [+ H_2O]	39.4	109.1012	-1.2
				$C_5H_7^+$ *[+ C_3H_6 + H_2O]*	7.4	67.0542	0.4
				$C_3H_5O^+$ *[+ C_5H_{10}]*	19.9	57.0335	-1.3
2 -4 -octadienal	$C_8H_{12}O$	≥ 95	124.09	**$(C_8H_{12}O)H^+$**	90.6	125.0961	0.5
				$C_8H_{11}^+$ [+ H_2O]	9.4	107.0855	2.7
heptanoic acid	$C_7H_{14}O_2$	> 98	130.14	**$(C_7H_{14}O_2)H^+$**	30.4	131.1066	0.2
				$C_7H_{14}O^+$ [+ H_2O]	8.1	113.0961	-0.6
				$C_6H_{13}^+$ [+ CO + H_2O]	3.8	85.1012	-0.3
				$C_3H_7O^+$ *[+ C_4H_6 + H_2O]*	48.9	59.0491	0.4
				$C_3H_7^+$ [+C_3H_6+ CO+H_2O]	8.8	43.0542	0.4
hexanoic acid	$C_6H_{12}O_2$	> 98	116.08	**$(C_6H_{12}O_2)H^+$**	28.5	117.0910	-1.1
				$C_6H_{11}O^+$ [+ H_2O]	4.5	99.0804	0.5
				$C_5H_{11}^+$ [+ CO + H_2O]	9.0	71.0855	-0.5
				$C_2H_4O_2^+$ [+ C_4H_9]	18.1	60.0206	0.4
				$C_4H_9^+$ [+$C_2H_4O_2$]	8.6	57.0699	0.3
				$C_3H_7^+$ *[+C_2H_4+CO+ H_2O]*	17.2	43.0542	0.2
				$C_3H_5^+$ *[+C_2H_6+CO+ H_2O]*	14.0	41.0386	0.1

ascertained by comparison with a second ionization mode, in our case with NO^+ as primary ion, which is described in the next section.

The quantification of the compounds in our experiments has been theoretically determined. When the rate coefficient *k* of the proton transfer between hydronium ions and a reactant is known, the concentration of the protonated reactants can be calculated as follows:

$$[RH^+] = [H_3O^+]_0 \{1-\exp(-k\,[R]\Delta t)\} \approx [H_3O^+]\,k\,[R]\,\Delta t \qquad \textit{(equation II-4)}$$

with: [RH+]: *concentration of the protonated reactant (ppbV)*

$[H_3O^+]_0$*: concentration of hydronium ions with no reactants present (ppbV)*

k: rate coefficient for the proton transfer ($cm^3\ s^{-1}$)

Δt: reaction time in the drift tube (s)

[R]: *concentration of neutral reactants (ppbV)*

The reaction time of the analyte in the drift tube, *Δt* , depends of the pressure and temperature in the drift tube, the length of the drift tube and the strength of the electric field E. Further details about the estimation of *Δt* are given in the literature (de Gouw and Warneke, 2007; Warneke et al., 2001). The concentration $[H_3O^+]_0$ is the concentration of hydronium ions at the end of the drift tube when no neutral reactant are presents. The approximation in equation II-7 is justified if [R] consists of very small densities of trace gases, meaning that $[RH^+] \ll [H_3O^+]$ and $[H_3O^+] \approx [H_3O^+]_0$ is constant. Under these conditions the concentration of $[RH^+]$ measured at the end of the drift tube is directly proportional to the concentration of R in the sample and by measuring $i(RH^+)$ and $i(H_3O^+)$, the count rates for RH^+ and H_3O^+ respectively, the volume mixing ratio of a reactant in the sample can be determined using equation II-5:

$$\frac{i(RH^+)}{i(H_3O^+)} = VMR \times k \times \Delta t \times N \times \frac{T_{RH^+}}{T_{H3O^+}}$$

(equation II-5)

with: $i(RH^+)$*: count rate for the protonated reactant (cps)*

$i(H_3O^+)$*: count rate for the hydronium ion (cps)*

VMR: volume mixing ratio (ppbV)

N: number density of the gas in the drift tube (molecules cm^{-3})

T_{RH+}*: transmission efficiency of protonated reactants*

T_{H3O+}: transmission efficiency of hydronium ions

The transmission efficiencies of RH^+ and H_3O^+ depend on the extraction efficiency of the ions from the drift tube into the ToF-MS, their transmission inside the ToF-MS and the detection efficiency and their values ranges between 0 and 1. The instrument is regularly calibrated with a standard mixture of VOCs (57 VOCs, PAMs mix, Restek, USA) to correct for these transmission efficiencies.

The theoretical determination of the volume mixing ratios of VOCs is subject to several approximations. First of all the reaction rate *k*, which is known for a great number of VOCs but is often approximated for others by the canonical $2x10^9$ cm^3 s^{-1}. It should be noted that rate coefficients determined under thermal conditions at 300K, as applicable for SIFT-MS, are not a good approximation for the thermal conditions of the PTR-MS. Not only is the temperature in the drift often much higher than the temperatures used in SIFT-MS, but the rate coefficient also depends on the electric field strength in the drift tube, inducing more energetic collisions (Cappellin et al., 2012; Smith and Spanel, 2011). The second source of errors induced by the calculation of the volume mixing ratios is the influence of humidity on the sensitivity and ion-cluster reactions. These issues are mostly addressed by using an external calibration for the targeted compounds.

In our case the multiple products of the studied reactions were unknown and the absence of a versatile calibration system at that time and the cost of custom-made gas standards were preventing an external calibration. As a consequence, the quantifications given in this work are only corrected for fragmentation branching ratios and global uncertainties on absolute quantification of up to 40 % can be expected (Herndon et al., 2006). Therefore most quantifications given here are relative and should be interpreted with caution.

II.2.3.c. NO^+ ion chemistry in the drift tube

The second ionization mode used in this study is the ionization by NO^+. The reactions of this ion with VOCs are more varied than those of H_3O^+, but provide valuable complementary information about the molecular structure. NO^+ is also a harder ionization mode than H_3O^+ and although NO^+ will, as the hydronium ions, not ionize the most common constituents of ambient air (N_2, O_2,…) it can ionize compounds like organosulfurs which would not be ionized by H_3O^+. Different reactions of organics with NO^+ include charge transfer, hydride ion

(H^-) transfer, hydroxide transfer (OH^-) alkoxide ion transfer (OR^-) and association. Charge transfer will only occur if the ionization potential of the VOCs is lower than that of NO^+ (IP = 9.26 eV), which is the case only for selected VOCs, such as isoprene (IP = 8.84 eV). Table II-4 provides an overview of the different product ions expected for different types of organic molecules as determined by SIFT-MS analysis since relatively little is known about the NO^+ reaction with VOCs in SRI-ToF-MS conditions.

Table II-4: overview of the different ionization reactions of NO^+ with different types of organic molecules, adapted from Smith & Spanel 2005 (Smith and Spanel, 2005a)

VOC	**NO^+ product ions** [a]
Alcohols	$(M-H)^+$; $(M-OH)^+$
Diols	$(M-H)^+$; $(M-OH_3)^+$
Phenols	$M^{+\bullet}$
Saturated / unsaturated aldehydes	$(M-H)^+$ / $(M-H)^+$; MNO^+
Ketones	MNO^+ ; $M^{+\bullet}$
Carboxylic acids	MNO^+ ; $(M-OH)^+$
Esters / ethers	MNO^+ ; $(M-OR)^+$ / $(M-H)^+$
Organosulphur	$M^{+\bullet}$
Aliphatic / aromatic hydrocarbons	$(M-H)^+$ (alkanes); M^+ (alkenes) / $M^{+\bullet}$
Monoterpenes	$M^{+\bullet}$; $(M-R)^+$
Aliphatic & aromatic halocarbons	$(M-X)^+$; $M^{+\bullet}$; MNO^+

[a]: M stands for the reactant molecule, X for a halogen and R for a fragment. Product ions are designated as follows: loss of fragments is indicated between brackets; $M^{+\bullet}$ is a radical parent cation, MNO^+ is an adduct.

This variability of product ions will in certain cases help to understand the molecular structure of the VOC considered. Ketones and aldehydes for example can clearly be distinguished in this ionization mode in SRI-ToF-MS, since ketones will be detected almost exclusively as an adduct ion whereas aldehydes show more complex fragmentation (Mochalski et al., 2014a; Mochalski et al., 2014b). It is also expected that the saturated aldehydes fragment less in reaction with NO^+ than with H_3O^+ (Mochalski et al., 2014a). Other applications of NO^+ as primary ion are the selective detection of atmospherically relevant compounds such as isoprene and 2-methyl-3-buten-2-ol or 1,3-butadiene which are subject

to interferences in the H_3O^+ ionization mode (Karl et al., 2012; Knighton et al., 2009). An additional advantage of the NO^+ ionization is the relative independence of fragmentation patterns on the relative humidity of the sample, as shown by Mochalski and co-authors (Mochalski et al., 2014b), making comparison under different humidity conditions easier.

As for the H_3O^+ mode, the ion products of eight standards were examined under our experimental conditions and the fragmentation patterns are detailed in table II-5. All values are corrected for a background of pure water. Table II-5 clearly shows the diversity of product ions and the more extensive fragmentation with NO^+. It has to be noted that the fragmentation patterns proposed here are based on the loss of hydride or hydroxide ion, as has been proposed for SIFT reactions and for which the energetics are favorable (Smith and Spanel, 2005b). The reaction products of these reactions strongly indicate that under our conditions, as in SIFT, the NO^+/VOC reactions proceed via close interactions and the formation of an initial $(MNO^+)^*$ excited charge complex. But unlike under thermalized SIFT-MS conditions, these ions are not the exclusive products of the reaction with NO^+ and the energy for the supplementary fragmentation must be due to the elevated ion-molecule interaction energies in the drift tube. Mochalski and co-workers showed that the fragmentation of propanal in the NO^+ ionization mode leads to the formation of neutral reaction products that are very endothermic, by up to 3.2 eV (Mochalski et al., 2014b) and de Gouw and co-workers showed that the water cluster H_2O-H_3O^+, with a binding energy of 1.4 eV, is entirely dissociated in a drift tube with E/N =130 Td (de Gouw et al., 2003). These results clearly point out the highly energetic environment of the drift tube which favors endothermic reactions. This makes the proposition of fragmentation pathways problematic, especially as the kinetic energy distribution in the drift tube remains highly uncertain. The speculative character of the fragmentation channels proposed here is marked by the use of italics. The other proposed patterns follow the loss of common groups (CO_2, H_2O, H or OH) or are confirmed by the detection of their ionized equivalents.

The loss of a hydride ion or the adduct of a NO^+ are not the main fragmentation products for the standards used here, except for the unsaturated aldehydes and often the main product ions are non-characteristic ions common to many compounds. This complicates identification and quantification of trace gases when mass spectra of complex

Table II-5: product ion distribution for the reaction of NO^+ with 8 standard compounds under our experimental conditions (E/N= 135 Td). In bold are the products of hydride ion transfer, speculative fragmentation patterns are in italic.

Compound	Formula	Purity (%)	MW	Detected ions [and proposed reaction channel]	Branching ratio (%)	Expected m/z (amu)	Δ m/z (x 10^{-3} amu)
1-nonanol	$C_9H_{20}O$	98	144.15	**$C_9H_{19}O^+$** [+HNO]	15.0	143.1430	0.3
				$C_9H_{17}^+$ [+ H_2O + HNO]	5.5	125.132	1.6
				$C_6H_{11}^+$ *[+ C_3H_9O + NO]*	11.8	83.0855	1.2
				$C_5H_9^+$ [C_4H_9 +H_2O + NO]	39.3	69.0699	1.6
				$C_4H_9^+$ [C_5H_9+H_2O+NO]	9.7	57.0699	0.0
				$C_4H_7^+$ *[$C_5H_{13}O$ + NO]*	7.3	55.0542	-0.8
				$C_3H_5^+$ *[$C_6H_{15}O$ + NO]*	11.4	41.0386	-0.2
trans-2-nonenal	$C_9H_{16}O$	97	140.12	**$C_9H_{15}O^+$** [+ HNO]	57.6	139.1117	-0.5
				$C_5H_9O^+$ *[+ C_4H_7 + NO]*	4.7	85.0648	34
				$C_5H_9^+$ *[+ C_4H_7O + NO]*	6.8	69.0699	-2
				$C_3H_3O^+$ *[+ C_6H_{13} + NO]*	8.8	55.0178	-2
				$C_2H_3O^+$ *[+ C_7H_{13} + NO]*	15.3	43.0178	-1.3
				$C_3H_5^+$ *[+ $C_6H_{11}O$ + NO]*	6.8	41.0386	-1.2
1-octanol	$C_8H_{18}O$	≥ 99	144.15	**$C_8H_{17}O^+$** [+ HNO]	11.6	129.1274	0
				$C_8H_{15}^+$ [+ H_2O + HNO]	1. 99	111.1168	0.1
				$C_5H_9^+$ *[C_3H_9O + NO]*	48.2	69.0699	1.7
				$C_4H_7^+$ *[+ $C_4H_{11}O$ + NO]*	4.8	55.0542	0.6
				$C_3H_5^+$ *[+$C_5H_{13}O$ + NO]*	15.4	41.0386	0.1
octanal	$C_8H_{16}O$	99	128.22	**$C_8H_{15}O^+$** [+HNO]	24.4	127.1117	-4.7
				$C_8H_{13}^+$ [+ H_2O + HNO]	5.2	109.1012	6.7
				$C_4H_9^+$ *[+ C_4H_7O + NO]*	62.7	57.0699	-0.3
				$C_3H_5^+$ *[+ $C_5H_{11}O$ + NO]*	7.6	41.0386	-1.3
trans-2-octenal	$C_8H_{14}O$	≥ 95	126.10	**$C_8H_{13}O^+$** [+ HNO]	82.8	125.0961	-2
				$C_3H_3O^+$ [C_5H_{11} + NO]	17.2	55.0178	0.5
2 -4 - octadienal	$C_8H_{12}O$	≥ 95	124.09	$C_8H_{12}O_2^+$ *[+ NO]**	2.5	139.0754	-2.2
				$C_8H_{11}O^+$ [+ HNO]	24.3	123.0804	0.2
				$C_7H_{11}O^+$ *[+ CH + NO]**	6.5	111.0804	-1.8
				$C_5H_5O^+$ *[+C_3H_7 + NO]*	52.8	81.0335	1.3
				$C_4H_4O^+$ *[+C_4H_8 + NO]*	6.5	68.0257	-0.1
				$C_3H_7^+$ [+ C_5H_5O + NO]	7.3	43.0542	-0.7
heptanoic acid	$C_7H_{14}O_2$	> 98	130.14	$C_7H_{14}O_2$•NO^+	8.3	160.0968	-0.2
				$C_7H_{13}O^+$ [+ HNO_2]	13.3	113.0961	-1.2
				$C_7H_{11}^+$ *[+ 2OH + HNO]*	2.1	95.0855	-1.4
				$C_6H_{13}^+$ [+ CO_2 + HNO]	8.3	85.1012	-0.8
				$C_4H_9^+$ *[+ $C_3H_5O_2$ + NO]*	17.1	57.0699	-0.5
				$C_3H_7^+$ *[+ $C_4H_7O_2$ + NO]*	31.4	43.0542	-0.5
				$C_3H_5^+$ *[+ $C_4H_9O_2$ + NO]*	19.4	41.0386	-0.5
hexanoic acid	$C_6H_{12}O_2$	> 98	116.08	$C_6H_{12}O_2$•NO^+	5.0	146.0812	-0.5
				$C_6H_{11}O^+$ [+ HNO_2]	7.8	99.0804	0.2
				$C_6H_{11}^+$ *[+ O_2 + HNO]*	4.8	83.0855	-1.0
				$C_5H_{11}^+$ [+ CO_2 + HNO]	13.4	71.0855	-0.1
				$C_5H_9^+$ *[+ CO_2+H_2+HNO]*	16.3	69.0699	-0.5
				$C_3H_7^+$ *[+ $C_3H_5O_2$ + NO]*	29.2	43.0542	-0.1
				$C_3H_5^+$ *[+ $C_3H_7O_2$ + NO]*	23.6	41.0386	-0.7

*ions probably due to impurities

mixtures are analyzed. On the other hand the different ion distribution for example of saturated and unsaturated aldehydes provides a useful complement to confirm the identity of these compounds, especially as in H_3O^+ mode the loss of a water molecule makes it difficult to distinguish aldehydes from protonated alkenes or alcohols who lost a hydroxyl group. In case of the acids, the association with NO^+ is , although a minor ion, a very valuable help in the confirmation of the molecular structure

This ionization mode was only used as a qualifying tool and no attempt was made to quantify. Where for H_3O^+ the concentrations in the sample can reasonably well be calculated from the measurement of H_3O^+ and $VOCH^+$, for NO^+ uncertainties prevent theoretical calculation when using this primary ion. The reaction rates between NO^+ and VOCs are much less well known, although SIFT measurements with different types of VOCs have been done. But as discussed in the previous section for H_3O^+, these rate constants are not necessarily valid under drift tube conditions. Also, the reactions of NO^+ with VOCs cannot be assumed to proceed at collision rate, since the different processes involved proceed sometimes at much lower rates (Smith and Spanel, 2005b). Therefore external calibration for NO^+ is necessary. In our experiments only normalized signals, expressed in normalized counts per second (ncps), will be reported for which the signals are normalized to a NO^+ signal of 10^6 ($i(NO^+)$= 10^6) and calculated according equation II-6:

$$\frac{i(R^+)}{i(NO^+)} = VMR \times \frac{T_{R^+}}{T_{NO^+}}$$

(*equation II-6)*

with: *$i(R^+)$: count rate for the ionized reactant (cps)*

$i(NO^+)$: count rate for NO^+ (cps)

VMR: volume mixing ratio (ppbV)

T_{R+}: transmission efficiency of ionized reactants

T_{NO+}: transmission efficiency of NO^+

The normalized signal takes the internal transmission of the ions into account and allows to compare relative intensities of ions over different experiments.

This approach enabled us to identify gas products formed in the interfacial processes studied and to propose a reaction mechanism for certain reactions, as will be described in chapters V and VI.

II.3. References

Aregahegn, K.Z., Noziere, B. and George, C., 2013. Organic aerosol formation photo-enhanced by the formation of secondary photosensitizers in aerosols. Faraday Discussions, 165: 123-134.

Baasandorj, M., Millet, D.B., Hu, L., Mitroo, D. and Williams, B.J., 2015. Measuring acetic and formic acid by proton-transfer-reaction mass spectrometry: sensitivity, humidity dependence, and quantifying interferences. Atmospheric Measurement Techniques, 8(3): 1303-1321.

Benkovic, S.J., Sammons, D., Armarego, W.L.F., Waring, P. and Inners, R., 1985. Tautomeric nature of quinonoid 6,7-dimethyl-7,8-dihydro-6h-pterin in aqueous-solution - a n-15-nmr study. Journal of the American Chemical Society, 107(12): 3706-3712.

Blake, R.S., Monks, P.S. and Ellis, A.M., 2009. Proton-transfer reaction mass spectrometry. Chemical Reviews, 109: 861-896.

Buhr, K., van Ruth, S. and Delahunty, C., 2002. Analysis of volatile flavour compounds by Proton Transfer Reaction-Mass Spectrometry: fragmentation patterns and discrimination between isobaric and isomeric compounds. . International Journal of Mass Spectrometry, 221(1): 1-7.

Calvert, J.G. and Pitts, J.N., 1966. Photochemistry, 1 Wiley, New York, 899 pp.

Cancilla, D.A. and Hee, S.S.Q., 1992. O-(2,3,4,5,6-pentafluorophenyl)methylhydroxylamine hydrochloride - a versatile reagent for the determination of carbonyl-containing compounds. Journal of Chromatography, 627(1-2): 1-16.

Canonica, S., Jans, U., Stemmler, K. and Hoigne, J., 1995. Transformation Kinetics of Phenols in Water: Photosensitization by Dissolved Natural Organic Material and Aromatic Ketones. Environmental Science & Technology, 29(7): 1822-1831.

Cappellin, L. et al., 2012. On Quantitative Determination of Volatile Organic Compound Concentrations Using Proton Transfer Reaction Time-of-Flight Mass Spectrometry. Environmental Science & Technology, 46(4): 2283-2290.

Chahidi, C., Aubailly, M., Momzikoff, A., Bazin, M. and Santus, R., 1981. Photophysical and photosensitizing properties of 2-amino-4 pteridinone - a natural pigment. Photochemistry and Photobiology, 33(5): 641-649.

Chambers, E., Wagrowski-Diehl, D.M., Lu, Z. and Mazzeo, J.R., 2007. Systematic and comprehensive strategy for reducing matrix effects in LC/MS/MS analyses. Journal of Chromatography B-Analytical Technologies in the Biomedical and Life Sciences, 852(1-2): 22-34.

Ciuraru, R. et al., 2015. Photosensitized production of functionalized and unsaturated organic compounds at the air-sea interface. Scientific Reports, 5: 12741.

de Gouw, J. and Warneke, C., 2007. Measurements of volatile organic compounds in the earth's atmosphere using proton-transfer-reaction mass spectrometry. Mass Spectrometry Reviews, 26: 223-257.

de Gouw, J. et al., 2003. Sensitivity and specificity of atmospheric trace gas detection by proton-transfer-reaction mass spectrometry. International Journal of Mass Spectrometry, 223(1-3): 365-382.

Donaldson, D.J. and Anderson, D., 1999. Adsorption of atmospheric gases at the air-water interface. 2. C-1-C-4 alcohols, acids, and acetone. Journal of Physical Chemistry A, 103(7): 871-876.

Facchini, M.C. et al., 2008. Important Source of Marine Secondary Organic Aerosol from Biogenic Amines. Environmental Science & Technology, 42: 9116-9121.

Gever, J.R., Mabury, S.A. and Crosby, D.G., 1996. Rice field surface microlayers: Collection, composition and pesticide enrichment. Environmental Toxicology and Chemistry, 15(10): 1676-1682.

Hansel, A. et al., 1995. Proton-transfer reaction mass-spectrometry - online trace gas-analysis at the ppb level. International Journal of Mass Spectrometry, 149: 609-619.

Hedges, J.I. et al., 2000. The molecularly-uncharacterized component of nonliving organic matter in natural environments. Organic Geochemistry, 31(10): 945-958.

Herndon, S.C. et al., 2006. Hydrocarbon emissions from in-use commercial aircraft during airport operations. Environmental Science & Technology, 40(14): 4406-4413.

Hirakawa, K., Suzuki, H., Oikawa, S. and Kawanishi, S., 2003. Sequence-specific DNA damage induced by ultraviolet A-irradiated folic acid via its photolysis product. Archives of Biochemistry and Biophysics, 410(2): 261-268.

Hou, T.J., Xia, K., Zhang, W. and Xu, X.J., 2004. ADME evaluation in drug discovery. 4. Prediction of aqueous solubility based on atom contribution approach. Journal of Chemical Information and Computer Sciences, 44(1): 266-275.

Huebert, B.J., Zhuang, L.Z., Howell, S., Noone, K. and Noone, B., 1996. Sulfate, nitrate, methanesulfonate, chloride, ammonium, and sodium measurements from ship, island, and aircraft during the Atlantic Stratocumulus Transition Experiment Marine Aerosol Gas Exchange. Journal of Geophysical Research-Atmospheres, 101(D2): 4413-4423.

Ito, K. and Kawanishi, S., 1997. Photoinduced hydroxylation of deoxyguanosine in DNA by pterins: Sequence specificity and mechanism. Biochemistry, 36(7): 1774-1781.

Jammoul, A., Dumas, S., D'Anna, B. and George, C., 2009. Photoinduced oxidation of sea salt halides by aromatic ketones: a source of halogenated radicals. Atmospheric Chemistry and Physics, 9: 4229-4237.

Kampf, C.J., Jakob, R. and Hoffmann, T., 2012. Identification and characterization of aging products in the glyoxal/ammonium sulfate system & implications for light-absorbing material in atmospheric aerosols. Atmospheric Chemistry and Physics, 12(14): 6323-6333.

Karl, T. et al., 2012. Selective measurements of isoprene and 2-methyl-3-buten-2-ol based on NO+ ionization mass spectrometry. Atmospheric Chemistry and Physics, 12(24): 11877-11884.

King, M.D. et al., 2009. Oxidation of oleic acid at the air-water interface and its potential effects on cloud critical supersaturations. Physical Chemistry Chemical Physics, 11(35): 7699-7707.

Knighton, W.B., Fortner, E.C., Herndon, S.C., Wood, E.C. and Miake-Lye, R.C., 2009. Adaptation of a proton transfer reaction mass spectrometer instrument to employ NO+ as reagent ion for the detection of 1,3-butadiene in the ambient atmosphere. Rapid Communications in Mass Spectrometry, 23(20): 3301-3308.

Latour, V., Pigot, T., Simon, M., Cardy, H. and Lacombe, S., 2005. Photo-oxidation of di-n-butylsulfide by various electron transfer sensitizers in oxygenated acetonitrile. Photochemical & Photobiological Sciences, 4(2): 221-229.

Laura Dantola, M. et al., 2010. Electron-transfer processes induced by the triplet state of pterins in aqueous solutions. Free Radical Biology and Medicine, 49(6): 1014-1022.

Ledbetter, J.W., Pfleiderer, W. and Freisheim, J.H., 1993. Laser-sensitized tautomers in dihydrofolate reductase. Advances in experimental medicine and biology, 338: 499-502.

Ledbetter, J.W., Pfleiderer, W. and Freisheim, J.H., 1995. Photosensitized reduction of l-biopterin in the active ternary complex of dihydrofolate reductase. Photochemistry and Photobiology, 62(1): 71-81.

Lin, S.-Y., Wang, W.-J. and Hsu, C.-T., 1997. Adsorption Kinetics of 1-Octanol at the Air−Water Interface. Langmuir, 13(23): 6211-6218.

Lindinger, W., Hansel, A. and Jordan, A., 1998a. On-line monitoring of volatile organic compounds at pptv levels by means of proton-transfer-reaction mass spectrometry (PTR-MS) - Medical applications, food control and environmental research. International Journal of Mass Spectrometry, 173(3): 191-241.

Lindinger, W., Hansel, A. and Jordan, A., 1998b. Proton-transfer-reaction mass spectrometry (PTR-MS): on-line monitoring of volatile organic compounds at pptv levels. Chemical Society Reviews, 27(5): 347-354.

Lorente, C., Capparelli, A.L., Thomas, A.H., Braun, A.M. and Oliveros, E., 2004. Quenching of the fluorescence of pterin derivatives by anions. Photochemical & Photobiological Sciences, 3(2): 167-173.

Lorente, C. and Thomas, A.H., 2006. Photophysics and photochemistry of pterins in aqueous solution. Accounts of Chemical Research, 39(6): 395-402.

Michalski, A. et al., 2011. Mass Spectrometry-based Proteomics Using Q Exactive, a High-performance Benchtop Quadrupole Orbitrap Mass Spectrometer. Molecular & Cellular Proteomics, 10(9).

Mmereki, B.T. and Donaldson, D.J., 2002. Laser induced fluorescence of pyrene at an organic coated air-water interface. Physical Chemistry Chemical Physics, 4(17): 4186-4191.

Mmereki, B.T. and Donaldson, D.J., 2003. Direct observation of the kinetics of an atmospherically important reaction at the air-aqueous interface. Journal of Physical Chemistry A, 107(50): 11038-11042.

Mochalski, P., Unterkofler, K., Hinterhuber, H. and Amann, A., 2014a. Monitoring of Selected Skin-Borne Volatile Markers of Entrapped Humans by Selective Reagent Ionization Time of Flight Mass Spectrometry in NO+ Mode. Analytical Chemistry, 86(8): 3915-3923.

Mochalski, P., Unterkofler, K., Španěl, P., Smith, D. and Amann, A., 2014b. Product ion distributions for the reactions of NO+ with some physiologically significant aldehydes obtained using a SRI-TOF-MS instrument. International Journal of Mass Spectrometry, 363(0): 23-31.

Momzikoff, A., Santus, R. and Giraud, M., 1983. A study of the photosensitizing properties of seawater. Marine Chemistry, 12(1): 1-14.

Nozière, B., Dziedzic, P. and Córdova, A., 2008. Products and Kinetics of the Liquid-Phase Reaction of Glyoxal Catalyzed by Ammonium Ions (NH4+). The Journal of Physical Chemistry A, 113(1): 231-237.

Pang, X., 2015. Biogenic volatile organic compound analyses by PTR-TOF-MS: Calibration, humidity effect and reduced electric field dependency. Journal of Environmental Sciences-China, 32: 196-206.

Pfleider.W, Zondler, H. and Mengel, R., 1970. Pteridines .39. synthesis and structure of pterin-6-carboxylic and pterin-7-carboxylic acids. Annalen Der Chemie-Justus Liebig, 741: 64-&.

Reeser, D.I., George, C. and Donaldson, D.J., 2009. Photooxidation of Halides by Chlorophyll at the Air-Salt Water Interface. Journal of Physical Chemistry A, 113: 8591-8595.

Rokos, H., Beazley, W.D. and Schallreuter, K.U., 2002. Oxidative stress in vitiligo: Photo-oxidation of pterins produces H2O2 and pterin-6-carboxylic acid. Biochemical and Biophysical Research Communications, 292(4): 805-811.

Serrano, M.P., Lorente, C., Borsarelli, C.D. and Thomas, A.H., 2015. Unraveling the Degradation Mechanism of Purine Nucleotides Photosensitized by Pterins: The Role of Charge-Transfer Steps. Chemphyschem, 16(10): 2244-2252.

Shapiro, E.L. et al., 2009. Light-absorbing secondary organic material formed by glyoxal in aqueous aerosol mimics. Atmospheric Chemistry and Physics, 9(7): 2289-2300.

Sinha, V., Custer, T.G., Kluepfel, T. and Williams, J., 2009. The effect of relative humidity on the detection of pyrrole by PTR-MS for OH reactivity measurements. International Journal of Mass Spectrometry, 282(3): 108-111.

Sinreich, R., Coburn, S., Dix, B. and Volkamer, R., 2010. Ship-based detection of glyoxal over the remote tropical Pacific Ocean. Atmospheric Chemistry and Physics, 10(23): 11359-11371.

Smith, D. and Spanel, P., 2005a. Selected ion flow tube mass spectrometry (SIFT-MS) for on-line trace gas analysis. Mass Spectrometry Reviews, 24: 661-700.

Smith, D. and Spanel, P., 2005b. Selected ion flow tube mass spectrometry (SIFT-MS) for on-line trace gas analysis. Mass Spectrometry Reviews, 24(5): 661-700.

Smith, D. and Spanel, P., 2011. Direct, rapid quantitative analyses of BVOCs using SIFT-MS and PTR-MS obviating sample collection. Trac-Trends in Analytical Chemistry, 30(7): 945-959.

Song, Q.H. and Hwang, K.C., 2007. Direct observation for photophysical and photochemical processes of folic acid in DMSO solution. Journal of Photochemistry and Photobiology a-Chemistry, 185(1): 51-56.

Soniat, M. and Martin, C.B., 2008. Theoretical Study on the Relative Energies of Neutral Pterin Tautomers. Pteridines, 19(4): 120-124.

Suarez, G., Cabrerizo, F.M., Lorente, C., Thomas, A.H. and Capparelli, A.L., 2000. Study of the photolysis of 6-carboxypterin in acid and alkaline aqueous solutions. Journal of Photochemistry and Photobiology a-Chemistry, 132(1-2): 53-57.

Swarna, S., Lorente, C., Thomas, A.H. and Martin, C.B., 2012. Rate constants of quenching of the fluorescence of pterins by the iodide anion in aqueous solution. Chemical Physics Letters, 542: 62-65.

Tani, A., Hayward, S., Hansel, A. and Hewitt, C.N., 2004. Effect of water vapour pressure on monoterpene measurements using proton transfer reaction-mass spectrometry (PTR-MS). International Journal of Mass Spectrometry, 239(2-3): 161-169.

Tani, A., Hayward, S. and Hewitta, C.N., 2003. Measurement of monoterpenes and related compounds by proton transfer reaction mass spectrometry (PTR-MS). International Journal of Mass Spectrometry, 223(1-3): 561-578.

Thomas, A.H. et al., 2002. Fluorescence of pterin, 6-formylpterin, 6-carboxypterin and folic acid in aqueous solution: pH effects. Photochemical & Photobiological Sciences, 1(6): 421-426.

van Pinxteren, M. and Herrmann, H., 2013. Glyoxal and methylglyoxal in Atlantic seawater and marine aerosol particles: method development and first application during the Polarstern cruise ANT XXVII/4. Atmospheric Chemistry and Physics, 13(23): 11791-11802.

Warneke, C., van der Veen, C., Luxembourg, S., de Gouw, J.A. and Kok, A., 2001. Measurements of benzene and toluene in ambient air using proton-transfer-reaction mass spectrometry: calibration, humidity dependence, and field intercomparison. International Journal of Mass Spectrometry, 207(3): 167-182.

Watson, J.T. and Sparkman, O.D., 2008. The Mass Spectrometer, Introduction to Mass Spectrometry. John Wiley & Sons, Ltd, pp. 53-172.

Yu, G. et al., 2011. Glyoxal in Aqueous Ammonium Sulfate Solutions: Products, Kinetics and Hydration Effects. Environmental Science & Technology, 45(15): 6336-6342.

Chapter III: Photosensitized reactions initiated by 6-carboxypterin: singlet and triplet reactivity

III.0. Motivations:

The following chapter in the form of an article, soon to be submitted, treats the photochemistry of a pterin. Pterins, derivatives of 2-aminopteridin-4(3*H*)-one, are natural photosensitizers, common to many biological systems. Indications that these photosensitizers are also present in the sea-surface microlayer have been reported, motivating the study of the photophysical and photochemical properties of 6-carboxypterin (CPT), chosen as model compound for this group of photoactive compounds. The kinetics of excited CPT in singlet and triplet state in presence of halides and organics were studied in aqueous solutions at neutral pH by means of steady state fluorescence and laser flash photolysis. The fluorescence of CPT was efficiently quenched by 2 halides, iodide and bromide, and by 4 carboxylic acids, lactic, malonic, propionic and citric acid with reaction rates close to the diffusion controlled limit. In the triplet state, the triplet absorption spectrum was measured and its pH dependence shown. The triplet state excited CPT showed quite high reactivity with iodide, but no reaction with bromide and chloride could be seen. The singlet or triplet state quenching in presence of limonene could not be evidenced. A reaction mechanism is proposed with an initiative step of electron transfer from the quencher towards the excited photosensitizer. This type of photo-induced reactions in the sea surface microlayer can trigger the production of many oxidized species including halogen atoms in the bulk and gaseous phase.

Chapter III: Photosensitized reactions initiated by 6-carboxypterin: singlet and triplet reactivity

Authors: Liselotte Tinel, Stéphanie Rossignol, Stéphane Dumas, Christian George

Article soon to be submitted

III.1. Introduction

Pterins are widespread throughout many biological systems and play roles ranging from pigments to coenzymes, *e.g.* folic acid (Pfleiderer, 1993). Also, photosensitized reactions initiated by pterin-derived compounds are involved in numerous photobiological processes. The so called pterins are a group of heterocyclic compounds derived from 2-aminopteridin-4(3*H*)-one, or pterin, with most commonly a substituent at position 6 if they are unconjugated.

Pterins have been quite extensively studied in the past for their photophysical properties. Especially their intense fluorescence has been applied for analytical purposes. For instance the detection of folic acid has been achieved through the fluorescence of 6-carboxy-pterin or more recently, pterin-based fluorescent probes were designed for DNA incorporation (Hawkins et al., 2001; Herbert and Bertino, 1967; Seibert et al., 2002). During the development of vitiligo, a human depigmentation disease of the skin, pterins amongst which 6-carboxy-pterin, are detected in the skin, indicating that excited states of pterins are generated *in vivo* (Rokos et al., 2002; Schallreuter et al., 2001; Schallreuter et al., 1994). Photosensitized reaction of some pterins can lead to DNA damage by photooxidation through electron transfer and/or hydrogen abstraction (type I mechanism) or through the generation of singlet oxygen (type II mechanism). The presence of 6-carboxy-pterin produced by the photodegradation of folic acid, could play an important role in this UV-A induced DNA damage (Hirakawa et al., 2003). Pterins not only play a role in human biology, but are thought to be chromophores in blue-light antennas of certain superior plants but also in some species of for example flagellates and fungi (Brodhun and Hader, 1990; Galland and Senger, 1988; Hohl et al., 1992). In the marine environment their presence in ascidians and their excretions has been demonstrated (Gaill and Momzikoff, 1975).

Pterins are thus present in marine biology and have been identified, amongst others, to cause the observed enhanced UV-absorption in the upper layers of the sea-water and induce photo-oxidative reactions (Momzikoff et al., 1983). It is indeed known that the presence of chromophores is enriched in the upper layer of the ocean, especially in the sea-surface microlayer (SML) (Peter S. Liss, 1997). The SML, defined as the organic enriched thin interfacial layer of the sea of a few tens of µm thickness, plays an important though still unclear role in the air-sea chemical interactions (Carpenter and Nightingale, 2015)

It is estimated, for example, that dry deposition of ozone on the sea-surface accounts for approximately one third of the global annual ozone deposition (Fairall et al., 2007; Ganzeveld et al., 2009). Although ozone loss is reigned by physical processes at higher wind speeds (Gallagher et al., 2001), at low wind speed and low surface turbulence the chemical loss processes of ozone at the sea surface become relatively more important (Chang et al., 2004). Martino and co-workers showed that both iodine and dissolved organic compounds present at the surface contribute significantly to the reactive uptake of ozone at the surface (Martino et al., 2012) and other studies demonstrated the importance of ozone loss on the surface due to light-driven reactive uptake by biogenic compounds, such as chlorophyll (Clifford et al., 2008; D'Anna et al., 2009; Reeser et al., 2009).

Halogen atoms in the gas phase, iodine and bromine especially, also influence largely the ozone concentration in the marine boundary layer (MBL) by initiating catalytic cycles of ozone destruction (Carpenter, 2003; von Glasow et al., 2003). These gas-phase halogen atoms can be emitted by different mechanisms, such as photolysis of poly-halogenated compounds emitted by algae and phytoplankton (Dixneuf et al., 2009; Saiz-Lopez and von Glasow, 2012), heterogeneous chemistry of ozone or NO_y on snow or sea-salt particles (Abbatt et al., 2012) and heterogeneous photochemical reactions at the sea-air interface, in particular for chlorine (Thomas et al., 2006).

However there still seems to be an ubiquitous missing source of iodine in the MBL, that is only partially explained by recently proposed reaction between hypoiodious acid (HOI) and dissolved organic matter (DOM) leading to the production of volatile organoiodine compounds(Martino et al., 2009; Shaw and Carpenter, 2013). Another source of gas-phase halogens, accounting for part of the halogens measured, could be the photochemical oxidation of halides present in surface water or in aerosols in the MBL (O'Dowd and de

Leeuw, 2007). Photoactivated aromatic carbonyls, like benzophenone and imidazole-2-carboxaldehyde (Jammoul et al., 2009; Tinel et al., 2014), or biogenic compounds such as chlorophyll (Reeser et al., 2009), can lead to the formation of reactive radical anions ($X_2^{\bullet-}$) and ultimately to the release of molecular halogens in the gas-phase. Photosensitizers in the SML can thus, through their reactions with halides and ozone, influence the oxidative capacity of the MBL and contribute to the formation of aerosols.

But photosensitizers in the SML also have the capacity to react with organics, as well with volatile organic compounds in the gas-phase (VOCs) as with organics present in the SML or in the underlying bulk-water phase. These reactions may be favored by the nature of the SML, where organics are concentrated at the interface, leading to the uptake of hydrophobic compounds from the gas phase, as demonstrated for the uptake of ozone by polyaromatic hydrocarbons (PAH) in presence of an organic coating (Donaldson and Vaida, 2006; Mmereki et al., 2004). Another implication of photochemical active compounds in the SML, is their entrainment in marine aerosols through bubble bursting and sea spray (Facchini et al., 2008; O'Dowd et al., 2004; Putaud et al., 2000). There, they can modify the composition of particulate phase through heterogeneous reactions at the air-particle interface. Such light induced heterogeneous reactions at the surface of aerosols can participate in particle growth through the formation of low-volatility products (Aregahegn et al., 2013; Monge et al., 2012; Rossignol et al., 2014). But still little is known about the importance of these reactions and their environmental influence.

The photosensitizer selected for this study, 6-carboxy-pterin (CPT), shows like most unconjugated pterins strong absorption in the UV-A, at the lower end of the actinic solar flux at sea level. Upon UV-A absorption, the CPT can be excited to the short-lived singlet state and upon relaxation emit a photon, measured as fluorescence. The singlet excited state of CPT (^{1}CPT) can also participate in fast reactions: (1) oxidation of DNA specific sequences probably through electron transfer (Hirakawa et al., 2003) (2) oxidation through electron transfer from acetate, phosphate and iodide anion (Lorente et al., 2004; Swarna et al., 2012). The calculated quantum yield of fluorescence of CPT is 0.18 in basic medium and 0.28 in acidic medium, with an estimated energy of 2.87-2.90 eV (Thomas et al., 2003; Thomas et al., 2002). But CPT also can also form a longer-lived triplet state upon excitation. Triplet excited state CPT (^{3}CPT) can also participate in photosensitized reactions, as reported for the

degradation of a nucleotide (dGMP) through type I (electron transfer) and type II mechanisms (Serrano et al., 2012). Unlike ^{1}CPT, ^{3}CPT is an efficient photosensitizer of $O_2(^1\Delta_g)$, singlet oxygen, and can thus induce singlet oxygen mediated reactions (type II mechanism) (Thomas et al., 2003). The same authors estimate the energy of the triplet state CPT at 2.45 eV.

In this work, light-induced reactions between a naturally occurring photosensitizer, 6-carboxy-pterin, and three common sea-salts, NaI, NaBr and NaCl in aqueous solutions are studied. The reaction of CPT with 4 small organic acids and a monoterpene, limonene, was also examined. The small carboxylic acids studied i.e., lactic acid, propionic acid, malonic and citric acid, represent the small carboxylic acids ubiquitously present in the troposphere, and aerosols (Chebbi and Carlier, 1996). In the MBL these acids have been related to biological activity and measured in gas- and particulate phase (Miyazaki et al., 2014). Limonene is a model compound for biogenic VOCs and a known hydrogen donor in photosensitized reactions (Rossignol et al., 2014). The reaction kinetics were determined by means of laser-flash photolysis and fluorimetry, while reaction products were analyzed using ultra-performance liquid chromatography coupled through a heated electrospray ionization (positive and negative modes) source to high resolution mass spectrometer [UPLC-(+/-)HESI-HRMS].

III.2. Experimental

III.2.1 Chemicals

Malonic acid (MA; 99%), citric acid (CA; 99%) and limonene ((R)-(+)-limonene 97%) were provided by Sigma Aldrich, propionic acid (PA; ≥99.5%)and lactic acid (LA; 90%) by Fluka and 6-carboxy-pterin (pterin-6-carboxylic acid, >97.5%) was purchased from Schircks laboratories (Jona, Switzerland). For the chromatographic analysis, water, formic acid and acetonitrile were all Optima® LC/MS grade and provided by Fischer Scientific, U.K. The carbonyl derivatization was done using O-(2,3,4,5,6-pentafluorophenyl)methylhydroxylamine hydrochloride solutions (PFBHA, ≥ 99.0%, Fluka).

All chemicals were used as purchased without further purification. Solutions were freshly prepared in 18-MΩ ultra pure water (Elga), 10 minutes of sonication was needed to obtain complete dissolution of CPT. The solutions containing limonene were made in a water-acetonitrile mixture (1:1, a v/v, Elga ultrapure water, France/Fischer Chemical, U.K.). A 1M solution of sodium hydroxide (NaOH, ≥98% reagent grade, Sigma Aldrich) was added dropwise to the solutions to obtain the desired pH. Fluorescence and laser flash photolysis experiments were performed at pH = 7-7.3. At this pH, propionic acid and lactic acid are in their carboxylate form. Citric acid and malonic acid will be almost entirely (at >95%) under their completely deprotonated forms. CPT who has a pK_a of 7.9 on the pterin ring, is mainly in its carboxylate monoanionic form as illustrated figure III-1. The UV-Vis absorption spectrum taken at different pH shows two maxima, with a shift towards longer wavelengths in more alkaline (pH > 9) conditions (figure III-S1, section III.6. Supplementary Information). One could argue in sight of figure III-S1 that more basic conditions enhance further the absorption of the lower energy absorption peak and emphasise the peak shift towards the longer wavelengths. However, several reasons motivate the choice of a more neutral pH: (1) reactions at a more neutral pH are more environmentally relevant (2) if the studied reaction involves an electron transfer from *e.g.* a halide X^- towards ^{3}CPT, than this reaction might be favored in presence of the mono-ionic form of ^{3}CPT (3) precautions at high alkalinity must be taken, since OH^- quenching of the singlet excited state has been shown (Thomas et al., 2002). UV-Vis absorption spectra of the prepared solutions were taken with an Agilent 8453

UV-Vis spectrometer in 1 cm quartz cuvettes. All experiments were performed at room temperature.

III.2.2 Laser flash photolysis

The transient absorption spectrum of the excited CPT was measured with a classical laser flash photolysis (LFP) apparatus (Jammoul et al., 2009). The photolysis excitation source was the second harmonic (355 nm, pulse width ±7 ns) of a Nd:YAG laser (Surelite II 10, Continuum, U.S.) operated in the single-shot mode. The excitation wavelength was chosen at the most environmentally relevant absorption maximum of the absorption spectrum of CPT, which lays around 347 nm. During the experiments, the laser pulse energy was limited at 45 mJ/pulse (±159 mJ/cm^2) to limit as much as possible photolysis of the photosensitizer and therefore possible interferences of its products on the studied chemistry. Therefore, the laser output passed through a partially closed iris and went then through the aperture in the short axis (4 mm path length) of a fully masked quartz flow cell, mounted at 13 cm of the laser output. The solution containing the photosensitizer was introduced in the flow cell of 450 µL by means of a peristaltic pump, with a flow of 1.6 mL/min, ensuring a complete purge of the exposed volume every 17 s. This limited the exposition of the introduced solution to 3–4 laser shots and maintained a constant temperature in the flow cell. The working solutions containing 0.2 mM CPT, were deoxygenated by bubbling N_2 at least 30 minutes before the start of the experiment and continuously kept under N_2 flow during the experiment. All connections where made from either glass or PTFE tubing, ensuring a clean liquid flow. Transient species produced by the pulsed laser beam were monitored by means of time-resolved absorption spectroscopy. The analyzing light, provided by a 75 W high-pressure Xenon arc lamp (LOT-Oriel), passed through the two apertures of the long axis of the flow cell (1 cm path length). The light was then collected by a ¼-m monochromator (Spectral Products DK240) equipped with a 2400 grooves/mm grating and detected by a photo-multiplier (Hamamatsu H7732-01). The PMT signal was passed through a high-speed current amplifier/discriminator (Femto) and the AC component recorded on a 300 MHz oscilloscope (Tektronix TDS3032c). The digitalized signal was then transferred to a computer for further processing. Typically, 32 measurements were averaged at each wavelength to obtain a transient absorption spectrum, with an accuracy of 3%. The full transient absorption

spectrum was then reconstructed from the steady and transient signals. For construction of an absorption spectrum, measurements were repeated every 5–20 nm between 380 nm and 700 nm, limits determined by the measuring system and the absorption of ^{3}CPT. For the kinetic measurements, the probe wavelengths for the transient absorption decay of triplet state of CPT were 400 and 425 nm, two maxima in the triplet state absorption spectra.

III.2.3 Steady-state fluorescence

Steady state fluorescence were performed using a commercial fluorimeter (Perkin Elmer, LS 45). Solutions containing 0.1 µM CPT were pH adjusted and introduced in a quartz cell (path length 1 cm) without deoxygenation. The excitation wavelength was set at 350 nm and emission spectra were registered between 360 nm and 540 nm. The absorbance of the solutions at the excitation wavelength was kept below 0.1, to keep irradiance homogeneous within the cuvette. The emission spectrum showed a maximum at 438 nm at pH = 7.2, in good agreement with the literature values (Thomas et al., 2002) for the acid, monoanionic form of CPT, while the basic dianionic form of CPT has an emission maximum at 451 nm. However, in our spectra no shoulder or specific peak broadening was seen at this wavelength, but it must be kept in mind that the dianionic form of CPT accounts for 9-28.5% of the emission spectrum, depending on the pH of the solution (for more details see SI). Regular control measurements of pure water were effectuated and spectra are background corrected.

III.2.4 Chemical analysis

500 µL of each sample was diluted in 500 µL of a 1:1, v:v, water:acetonitrile mixture. Besides, 200 µL of each sample was diluted in 800 µL of a 1 mg mL^{-1} PFBHA solution (daily prepared, dissolved in a 1:1,v:v, water:acetonitrile mixture) and left at room temperature for 24 hours in order to complete the selective derivatization of the carbonyl groups. These two dilutions were performed in triplicates for each sample (two samples by experiment, before and after irradiation). For each experiment, solvent and PFBHA impurities were checked diluting 500 µL of water in 500 µL of a 1:1, v:v, water:acetonitrile mixture and 200 µL of water in 800 µL of the daily PFBHA solution.

All the diluted samples were analyzed by ultraperformance liquid chromatography coupled with heated electrospray ionization (positive and negative modes) and high resolution mass spectrometry [UPLC/(±)HESI-HRMS]. The Dionex Ultimate 3000 ultraperformance liquid chromatograph (UPLC, Thermo Scientific, U.S.) was equipped with a HSS T3 Acquity UPLC column (1.8 µm, 2.1 × 100 mm). The mobile phase was (A) acidified water (+ 0.1%, v/v, formic acid) and (B) acidified acetonitrile (+ 0.1%, v/v, formic acid). A 22 min gradient was applied at a constant flow rate of 0.3 mL min^{-1}: eluent (B) was kept at 1% for 2 min, was then increased to 100% in 11 min and kept to 100% for 2 min; the system then returned to initial conditions, 1% of (B), in 0.1 min and was left to stabilize for 7 min. The injection volume of the non-derivatized diluted samples was 5 µL and the injection volume of PFBHA derivatized samples was 10 µL. HESI voltages of +3.7 kV and −3.0 kV were applied for the positive (+) and negative (−) ionization modes respectively. All the HRMS acquisitions were performed in full MS mode with a scan ranging from m/z 50 to m/z 750 and a resolution set to 140,000. Signal stability over time was checked using two standard solutions of adipic acid (2 µM) and levulinic acid (20 µM), this latter being daily diluted by a factor 5 in a 1mg mL^{-1} PFBHA solution and left at room temperature for 24 hours for carbonyl group derivatization.

III.3. Results and discussion

III.3.1 Singlet state reactivity:

III.3.1.a. Fluorescence quenching in presence of halides and acids.

The reactivity of ^{1}CPT with the different halides and 5 different organics was measured by steady state fluorescence through its quenching properties. In fact, if a reaction between the ^{1}CPT and the quencher occurs, a part of the ^{1}CPT will be deactivated by the interaction with the quencher and thus the relative intensity of the fluorescence will decrease. For each quencher, UV-Vis spectra were first taken of a non-irradiated solution to assure that the quenching observed was not due to changes in the absorption spectrum of the ground state. The absorption spectrum and emission spectrum of a solution of CPT at pH 7 is shown figure III-1. At this pH, the UV-Vis absorption spectrum of CPT shows two maxima, around 285 nm and 347 nm, and the maximum fluorescence emission wavelength is 440 nm.

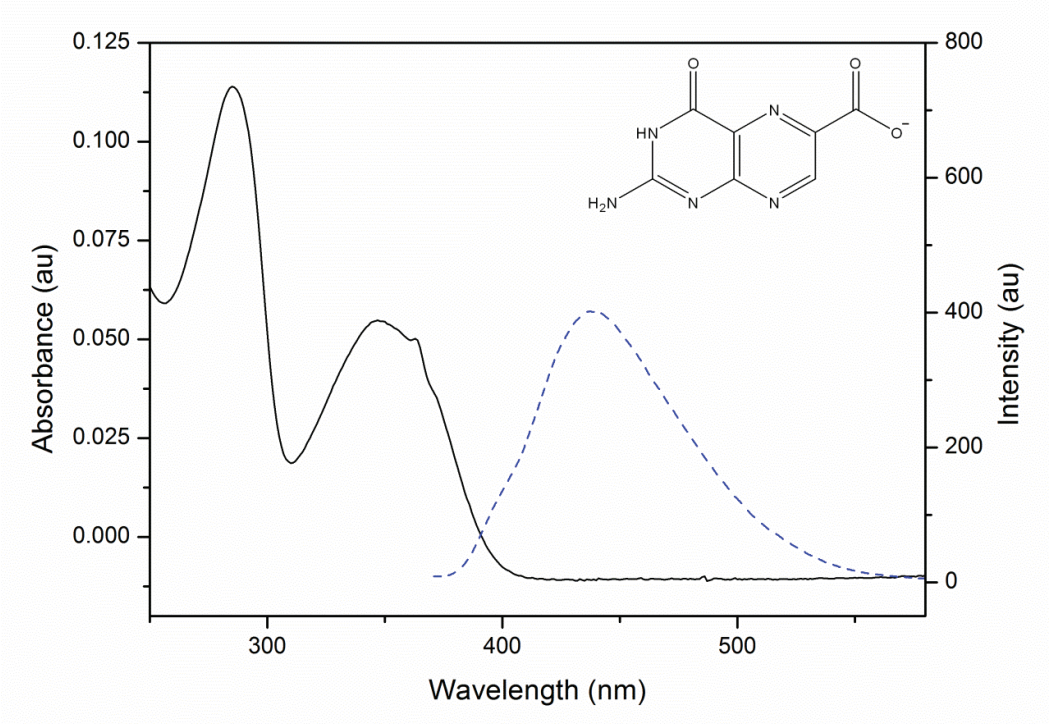

Figure III-1: Absorption (solid line) and fluorescence emission (dashed line) spectrum of aqueous solutions of CPT at respectively 0.1 mM, pH 7.0 and 0.1 µM, pH 7.1

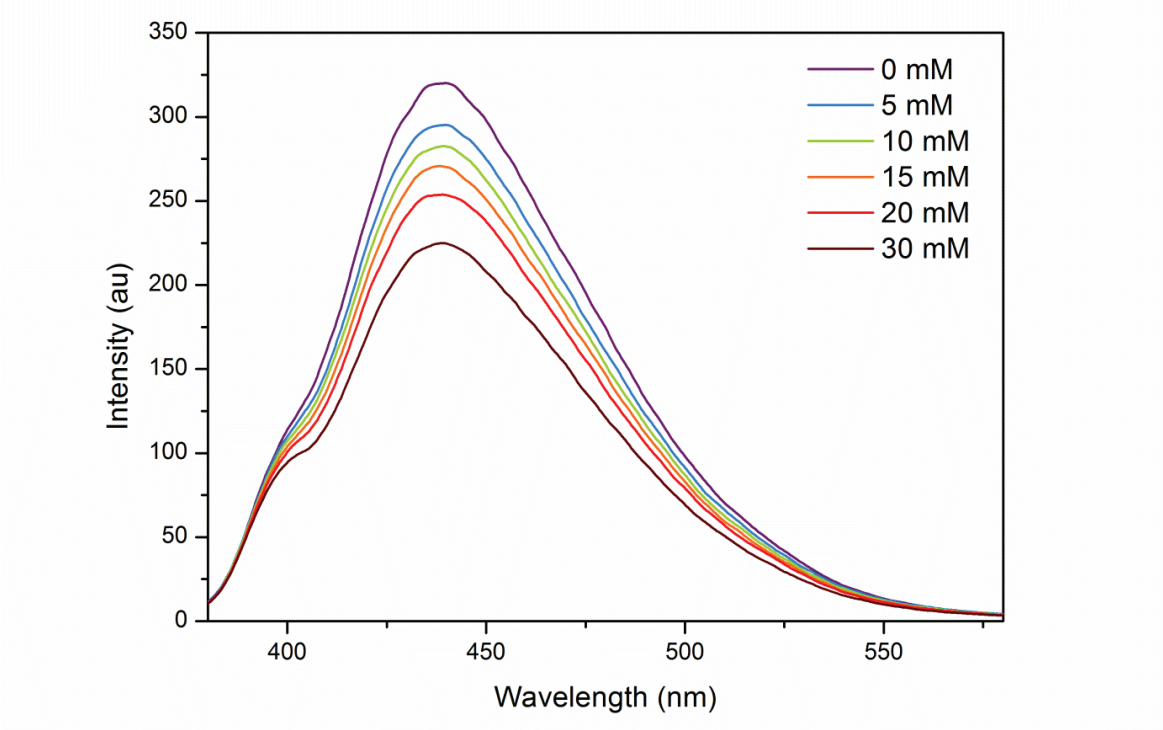

Figure III-2: Fluorescence emission spectrum of CPT in presence of different concentrations of NaBr (λ_{ex}=350 nm, pH=7.1)

Figure III-2 shows an example of the fluorescence emission spectra obtained of a solution of CPT in presence of bromide anions at different concentrations as a quencher. Similar spectra were obtained for the other tested quenchers, except for chloride and limonene (figures III-S2, a-g, section III.6. Supplementary Information). An increase in the concentrations of chloride did not lead to a clear decrease in fluorescence intensity, demonstrating that Cl^- does not chemically interact with ^{1}CPT. The case of quenching with limonene will be discussed in more detail in the next section.

The dynamic quenching rates were then determined for each quencher with the Stern-Volmer equation (Eq. III-1):

$$I_0/I = 1 + k_Q \tau_F [Q] \qquad \textit{(equation III-1)}$$

Where I_0 is the fluorescence intensity without quencher present, I the intensity in presence of the quencher, k_Q the bimolecular rate coefficient (M^{-1} L^{-1}), τ_F the fluorescence lifetime in absence of a quencher and [Q] the concentration of the quencher in M^{-1}. The fluorescence lifetime of CPT has been determined using the laser-flash photolysis set-up used for the transient study of triplet state reactivity. By exciting an aqueous solution of CPT at pH 7.3

with a laser pulse (355 nm) a transient fluorescent signal was measured. From the fit of this signal with a simple mono-exponential function:

$$y = a + be^{-tk} \qquad \textit{(equation III-2)}$$

The lifetime of the singlet state can be calculated as τ_F = 1/k. From our measurements, the fluorescence lifetime determined is: $\tau_F = 4.9 \times 10^{-9}$ s. This is in good agreement with the lifetime of 4.6×10^{-9} s reported by Swarna and co-workers for ^{1}CPT in a buffered solution at pH= 7.3 (Swarna et al., 2012).

From the Stern-Volmer plots for the different quenchers, figures III-3a-b, it can be seen that all quenchers, except chloride, exhibit a linear behavior, indicating a dynamic quenching reaction. For clarity reasons, limonene is not included in the plots (*vide infra*). Iodide is the most efficient quencher of all quenchers tested while citric acid and malonic acid are the most efficient organic quenchers. In presence of chloride, no change in the fluorescence intensity has been observed. It can therefore be concluded that no reaction occurs between ^{1}CPT and Cl^-. The bi-molecular rate coefficients have been determined by linearly fitting equation III-1 to our data and are listed in table III-1. The reported uncertainties arised from the fitting procedure and were derived as three times the standard deviation on the slope. The adjusted linear determination coefficient R^2 is also given as an indication for the goodness of fit.

Table III-1. Bimolecular rate coefficients k_Q for the efficient quenchers of singlet state CPT at neutral pH

Quencher	R^2	k_Q (M^{-1} s^{-1})	k_Q/nb acidities (M^{-1} s^{-1})	ΔG (eV)
I^-	0.98	$(4.06 \pm 0.06) \times 10^9$ 6.3×10^9 [a]	-	-0.94/-0.81
Br^-	0.99	$(3.13 \pm 0.09) \times 10^9$	-	-0.34/-0.21
Citric acid	0.95	$(2.89 \pm 0.03) \times 10^9$	9.62×10^8	
Malonic acid	0.99	$(2.71 \pm 0.03) \times 10^9$	1.36×10^9	
Propionic acid	0.96	$(1.23 \pm 0.06) \times 10^9$	1.23×10^9	
Lactic acid	0.91	$(9.90 \pm 0.06) \times 10^8$	9.90×10^8	

[a] (Swarna et al., 2012)

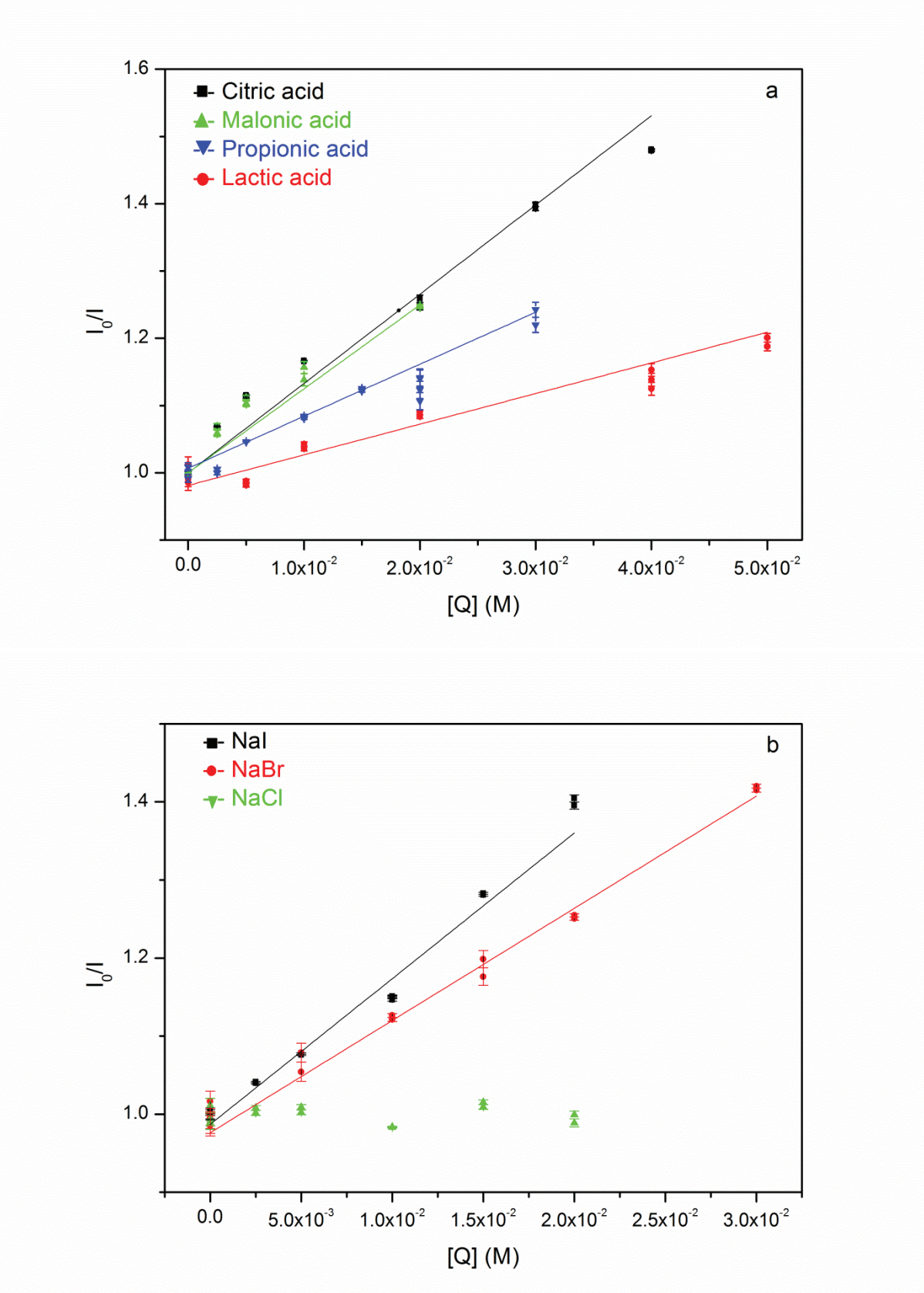

Figure III-3: Stern-Volmer plots of the quenching of the fluorescence of CPT with (a) the organic acids and (b) the halides as quenchers.

It finally appears that all reported bi-molecular rate coefficients are quite similar, and close to the diffusion controlled limit for aqueous solutions. As indicated in table III-1, the bimolecular rate coefficient for iodide obtained in this study is somewhat smaller than the one reported in literature before at pH= 7.3, but quite comparable.

The most efficient quenchers are the two halides, i.e., iodide and bromide. The quenching reaction by an electron transfer from these halides towards the excited photosensitizer is very efficient, but logically for chloride no quenching was observed. This is confirmed by the free energy calculated using the Rehm-Weller equation, which allows the estimation of the free energy change for electron transfer in polar solvents:

$$\Delta G\ (eV) = [E_{ox}(D) - E_{red}(A) - C] - \Delta E_{0,0} \qquad \textit{(equation III-3)}$$

where $E_{ox}(D)$ and $E_{red}(A)$ are the redox potentials of the electron donor (D) and acceptor (A) respectively. The values for the oxidation potential of CPT were taken as $E_{ox}(D)$=-0.6 V (Rembold, 1964) and $E_{ox}(D)$=-0.73 V (Song and Hwang, 2007). Both were used and the results given as an upper and under limit for ΔG. C is the Coulomb term expressing the solvation energy of an ion pair D^+A^-, but can be neglected in polar solvents. $E_{0,0}$ is the energy for the lowest singlet energy level of CPT which can be derived from the absorption and fluorescence emission spectra. Values obtained for the singlet state lowest energy level are estimated as 2.87eV (Thomas et al., 2003). Indeed, for chloride the free energy calculated with equation III-3 was 0.33/0.46 eV, which indicates that the electron transfer is thermodynamically unfavorable. As shown table 1, the free energies ΔG for an electron transfer from iodide and bromide are slightly negative, which confirms that an electron transfer in this case is thermodynamically favorable.

The reactivity of the deprotonated carboxylic acids is highest for malonic and citric acid, both bearing more than one acid function, and thus more than one negative charge at this pH. This strongly indicates that also in this case an electron transfer takes place as quenching reaction with ^{1}CPT. If a hydrogen transfer would take place, then one would expect the conjugated acids to be the most reactive species. Indeed, as the C-H bond strength of conjugated carbons is less energetic, the reaction would be favored by the presence of hydroxyl groups on the carbon chain, as is the case for citric and lactic acid. Although citric acid is the most reactive organic quencher, lactic acid shows the lowest

reactivity, which does not fit with an eventual hydrogen transfer mechanism. If the quenching rate coefficients are divided by the number of acid functions, and thus the number of easily available electrons, as shown in the third column table 1, all carboxylic acids exhibit very similar rate coefficients, i.e., ca. 1 x 10^9 M^{-1} s^{-1}, indirectly validating the assumption of quenching through an electron transfer from the carboxylate groups towards ^{1}CPT.

III.3.1.b. Fluorescence quenching in presence of limonene

In the case of limonene, no clear trend in the fluorescence intensity has been observed (figure III-S2-g). This can be explained by the fact that in this case, in order to solubilize the solutions containing limonene, a mixture of acetonitrile and water (50:50, v/v) was used. The absorption spectrum of CPT in presence of 30mM limonene does not provide evidence for any ground state changes, although the overall absorption is somewhat higher (±10%). However, in the acetonitrile-water mixture, the fluorescence is around 60% lower than in case of the pure water solvent, as illustrated figure III-S1(g). This effect can be attributed to the higher polarity of the acetonitrile-water mixture, leading to a larger solvent relaxation effect (Aaron et al., 1991). As the energy of the excited state is lowered by the interaction with the solvent, the probability of a reaction with the quencher is also lowered. Besides, the use of the mixture acetonitrile-water did not resolve entirely the problem of dissolution as the solution introduced in the quartz cell spontaneously organized in different phases, with limonene between the aqueous and organic layer. Upon vigorously shaking the solution, a visually homogeneous solution was obtained which contained many air bubbles, making the fluorescence measurements poorly reproducible. Due to these experimental difficulties, no singlet state quenching in presence of limonene could be evidenced by steady state fluorescence, although some indirect evidence indicates that such quenching reaction should exist (*vide infra*).

III.3.2 Triplet state reactivity

III.3.2.a. CPT triplet state in water at neutral pH

Excited triplet excited states are often considered the most reactive excited state in photochemistry, due to their longer lifetime and their ability to form singlet oxygen in presence of molecular oxygen. Laser flash photolysis of CPT in deoxygenated aqueous solutions allowed the identification of an absorption of a rather long-lived transient species, attributed to the triplet state of CPT. Figure III-4 shows the absorption spectrum of the triplet state at different time intervals after the laser pulse. The absorption spectrum shows a peak maximum at 400-425 nm, a broad absorption band around 500-550 nm and a peak at 650 nm. The latter is probably exaggerated by the higher systematic errors at these wavelengths which are at the end of the spectral range of the PM. The wavelength for the absorption maxima correspond quite well with the maxima found for a ^{3}CPT absorption in DMSO, but the DMSO spectrum does not show a maximum at 650 nm (Song and Hwang, 2007). The spectra at 1µs and 8 µs after the laser pulse demonstrate the rather uniform decrease of the absorbance, without formation of any significant band. These spectra do not evidence the existence of transient species, as proposed for the increased absorption observed at 480 nm for pterin or at 390 nm for CPT in DMSO and attributed to the formation of a semireduced pterin radical (Chahidi et al., 1981; Song and Hwang, 2007).

For the determination of the lifetime and reactivity, the triplet state decay was monitored at two wavelengths in the first broad maximum absorption peak, at 400 nm and 425 nm, since our laser flash photolysis system is most accurate in that region. The ^{3}CPT lifetime can be determined from the decay curves of the triplet state absorption, by fitting these curves with an exponential function. For pterin, the non-substituted form of 6-carboxy-pterin, a bi-exponential decay of the triplet state has been evidenced and confirmed by dual phosphorescence and was explained by the co-existence of lactim and lactam tautomers in the triplet excited state (Chahidi et al., 1981; Ledbetter et al., 1995). Even though at ground state one tautomer, the lactam form, is expected to be the dominant form, upon excitation, a fast intramolecular proton transfer produces two tautomeric forms in the triplet state. However, recent calculations have shown that the most probable tautomers for pterin and 6-methyl-pterin in aqueous solutions were rather the lactam and

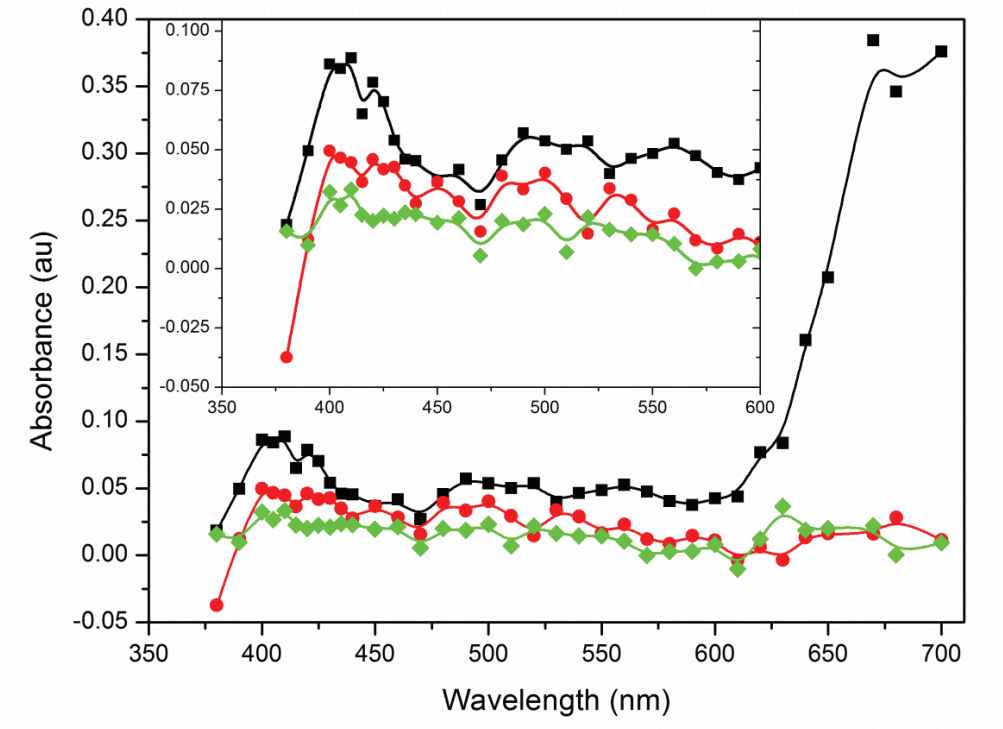

Figure III-4: LFP recorded transient absorption spectrum of the triplet state CPT (0.2mM) in deoxygenated water at pH = 7.4, recorded 450 ns (■), 1 µs (●) and 8 µs (◆) after the laser pulse. The insert shows a zoom on the 350-600 nm range.

1(*H*)-lactam tautomer than the lactim tautomer (Nekkanti and Martin, 2015; Soniat and Martin, 2008). By analogy and considering the very similar structures, the same tautomers, represented figure III-5, can be expected to be stable for excited CPT and hence a bi-exponential decay rate of the triplet state can be expected.

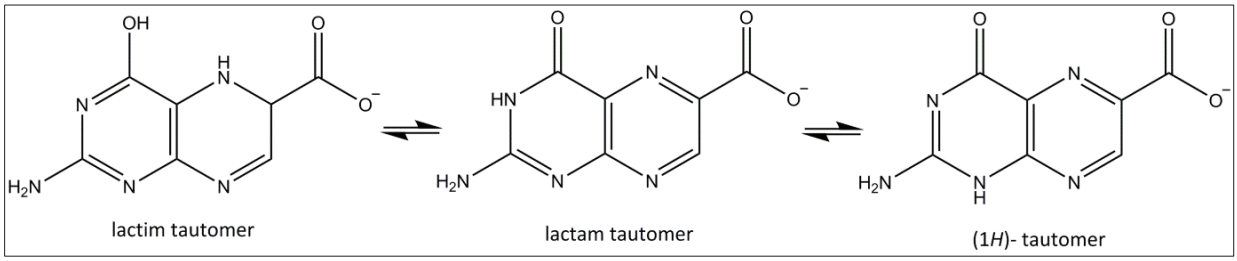

Figure III-5: Configuration of the most stable tautomers for CPT

The ^{3}CPT decay curve is indeed well fitted by the following bi-exponential function:

$$y = a + be^{-tk_1} + ce^{-tk_2} \qquad \textit{(equation III-4)}$$

The obtained decay rates, k_1 and k_2, for a triplet-triplet absorption curve monitored at 425 nm are (1.66 ± 0.27) x 10^6 s^{-1} and (3.70 ± 0.05) x 10^5 s^{-1} and corresponding triplet life-times of

0.6 µs and 2.7 µs. These lifetimes are quite shorter than the lifetime for ^{3}CPT in DMSO, 1.1 and 9.1 µs (Song and Hwang, 2007), but are comparable to the lifetimes obtained for aqueous solutions of triplet state biopterin, 0.3 and 2.0 µs (Ledbetter et al., 1995), and for triplet state pterin, 0.3 and 2.3 µs (Chahidi et al., 1981).

III.3.2.b Influence of pH on the triplet state absorption

The influence of the pH on the ground state CPT is clearly shown figure III-S1 and the influence of pH on fluorescence was already reported (Lorente and Thomas, 2006; Thomas et al., 2002). For pterin and pterin derivatives an influence of pH on the triplet state has also been seen (Chahidi et al., 1981; Thomas et al., 2003). The influence of pH on the triplet-triplet state absorption has thus been investigated and differential transient absorption spectra of ^{3}CPT absorption recorded by LFP at 4 different pHs (6.1, 7.3, 8.2 and 10.8) and compared in figure III-6. The absorption spectra of ^{3}CPT at different imes after the laser flash are shown for these different pHs figure III-S3a-e. It can clearly be seen from figure III-6 that ^{3}CPT absorbs more intensely at alkaline pH, with a maximum of absorption at pH = 8.2. All spectra show a broad absorption band around 550 nm, quite weakly defined, and another broad absorption band around 400-430 nm, composed of two peaks centered at 400-410 nm and 430-440 nm. Both peaks around 410 nm and 430 nm are present under all pH conditions and can thus not be attributed to the protonated mono- ionic CPT or deprotonated di-ionic CPT distinctively, since at pH = 6.1 only the mono-ionic CPT is present (pKa = 7.9) and at pH = 10.8 only the di-ionic form is present. This validates somehow the hypothesis that different tautomers of CPT contribute to the absorption in these bands, as described by a bi-exponential decay. In fact at all pHs, the decay rates are indeed best described by a bi-exponential equation at 440 nm, with lifetimes for pHs ranging from 6 to 9 of τ_{T1}= 0.45-0.60 x 10-6 s for the short-lived and τ_{T2} = 2.5-3.5 x 10-6 s for the long-lived components. Interestingly, a clear decrease of the triplet lifetime is seen at pH = 10.8, giving lifetimes of τ_{T1} = (0.81 ± 0.04) x 10-6 s and τ_{T2} = (0.29 ± 0.04) x 10-6 s, when fitting the decay rate of the absorption at 430 nm. In analogy to a similar feature observed for the triplet state of pterin, this can tentatively be explained by the deprotonation of the triplet state leading to a dissociation constant for the triplet state that is substantially higher, pKaT* > 9, than for ground state CPT (Chahidi et al., 1981). But contrary to the pterin absorption spectrum, CPT does not show very distinctive absorption

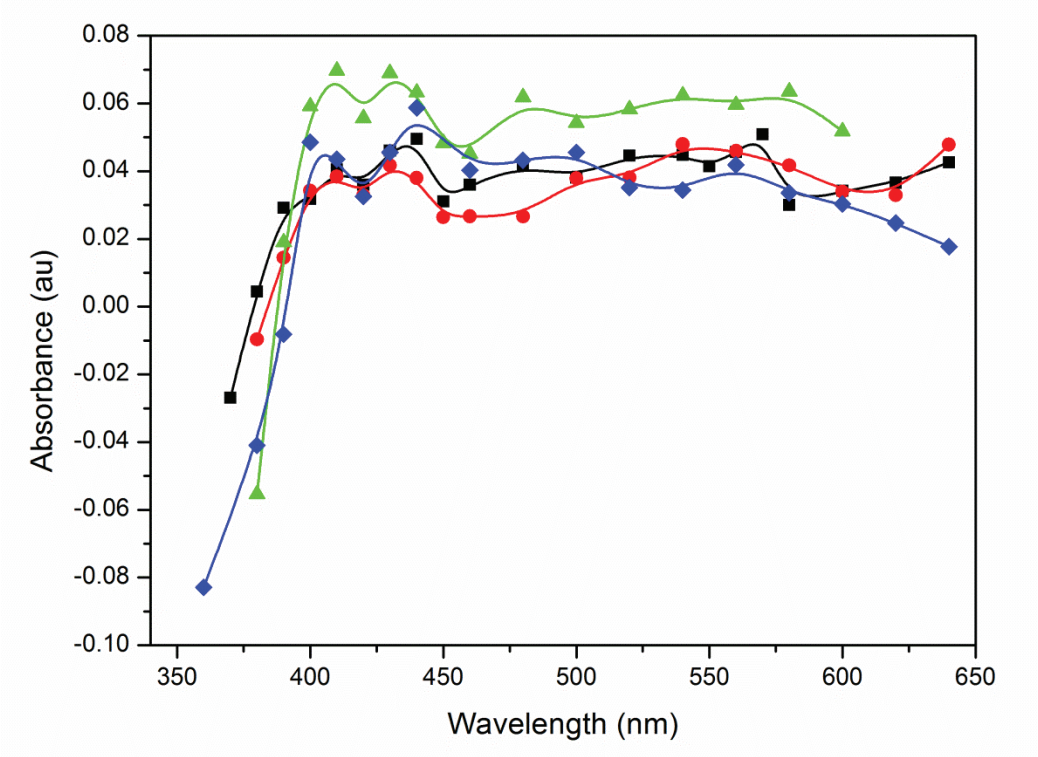

Figure III-6: Transient absorption spectra of deoxygenated aqueous solutions of 0.1 mM CPT at pH=6.1 (■), pH=7.3 (●), pH=8.2 (▲) et pH=10.8 (◆) registered 450 ns after the laser pulse.

for the deprotonated species at this pH, apart from a peak broadening around 440 nm. At this point, it remains difficult to attribute with certainty the higher triplet absorption decay rate at pH = 10.8 to the deprotonated triplet form. Other factors that could contribute tohigher decay rates are OH- quenching and the formation of different stable tautomers at pH > 9, but addressing these intriguing issues lays beyond the scope of this work.

III.3.2.c Quenching of the triplet state

The reactivity of ^{3}CPT with halides is interesting since the triplet state has a lifetime that is 3 orders of magnitude larger than the singlet state. As the reaction between singlet state CPT and some halides, namely I^- and Br^-, is not negligible, it is expected that the maximum ^{3}CPT absorption decreases in presence of increasing concentrations of halides, since part of the singlet state CPT will be deactivated by the reaction with the quencher present. But for constant concentrations of CPT under the same conditions, this should not influence the decay rate of the triplet state absorption. The reaction with halides was tested at neutral pH (7-7.5) by introducing increasing concentrations of a quencher in deoxygenated solutions of

CPT, with a large excess of the quencher in respect to CPT (> x 100) in order to maintain pseudo-first order conditions. The decay of the triplet state absorption was monitored at the maximum absorption wavelengths at this pH range, in the range of 400-430 nm. As discussed above, for the presence of tautomeric forms of the photosensitizer should lead to some bi-exponential decay of ^{3}CPT absorption at 400 nm. Surprisingly, the decay rate at 400 nm was best fitted with a mono-exponential function (figure III-7a, inset). This different behavior became even more evident upon the addition of halides. A clear difference can be seen in figure III-7 between the signals monitored at 400 nm (fig III-7a) and at 425 nm (fig III-7b) in presence of 10 mM of NaI. In the absence of a quencher, the decay rate obtained with the mono-exponential fits of the signals registered at 400 nm gave very similar decay rates as for the one component of the bi-exponential fits at 425 nm, namely the longer life-timed component. This leads to the conclusion that the tautomer absorbing at 400 nm, still shows some absorption at 425 nm at the same time as a second tautomer with a shorter life-time. As it becomes clear from figure III-7a, the tautomer absorbing at 400 nm shows no measurable reaction with I^- and the same is true for Br^- and Cl^-. Similar differences in the chemical kinetics for different tautomers of triplet state of a pterin derivative have been observed when reacting with an organic compound (Serrano et al., 2012). This decay rate can then be used to restrain the value of k_2 in equation 2 and to obtain the decay rate k_1 of the second tautomer in the decays recorded at 425 nm in presence of a quencher. The quenching rate quenching rate for the second tautomer can then be determined by the Stern-Volmer relation (equation III-4), using the k_1 decay rates obtained at 425 nm coefficients with different concentrations of the quencher:

$$-\frac{d[\,^3CPT]}{dt} = \left(k_{1,0} + k_{1,q}[Q]\right)[\,^3CPT] = k_{1,obs}[\,^3CPT] \qquad \textit{(equation III-5)}$$

where $k_{1,0}$ is the decay rate of the short lived component k_1 at 425 nm without quencher present and $k_{1,q}$ the bi-molecular rate coefficient for the quenching process in presence of a quencher *Q*. The slope of the linear fits of $k_{1,obs}$ in function of *[Q]* on the Stern-Volmer plot, gives the quenching rate coefficient $k_{1,q}$ for the short-lived tautomer.

By proceeding this way, the bi-molecular quenching coefficients for the three halides tested were determined, as shown on the plot figure III-7. For iodide, a clear quenching of the ^{3}CPT was evidenced, as expressed by the rather high reaction coefficient, (1.89 ± 0.22) x

10^8 m^{-1} s^{-1} (table III-2). The rate coefficient of ^{3}CPT with I^- is an order of magnitude lower than the reaction rate of 1CPT with iodide, but as the triplet lifetime is 3 orders of magnitude higher than the singlet state lifetime, triplet state reactivity will indeed play a prominent role in the reaction with iodide.

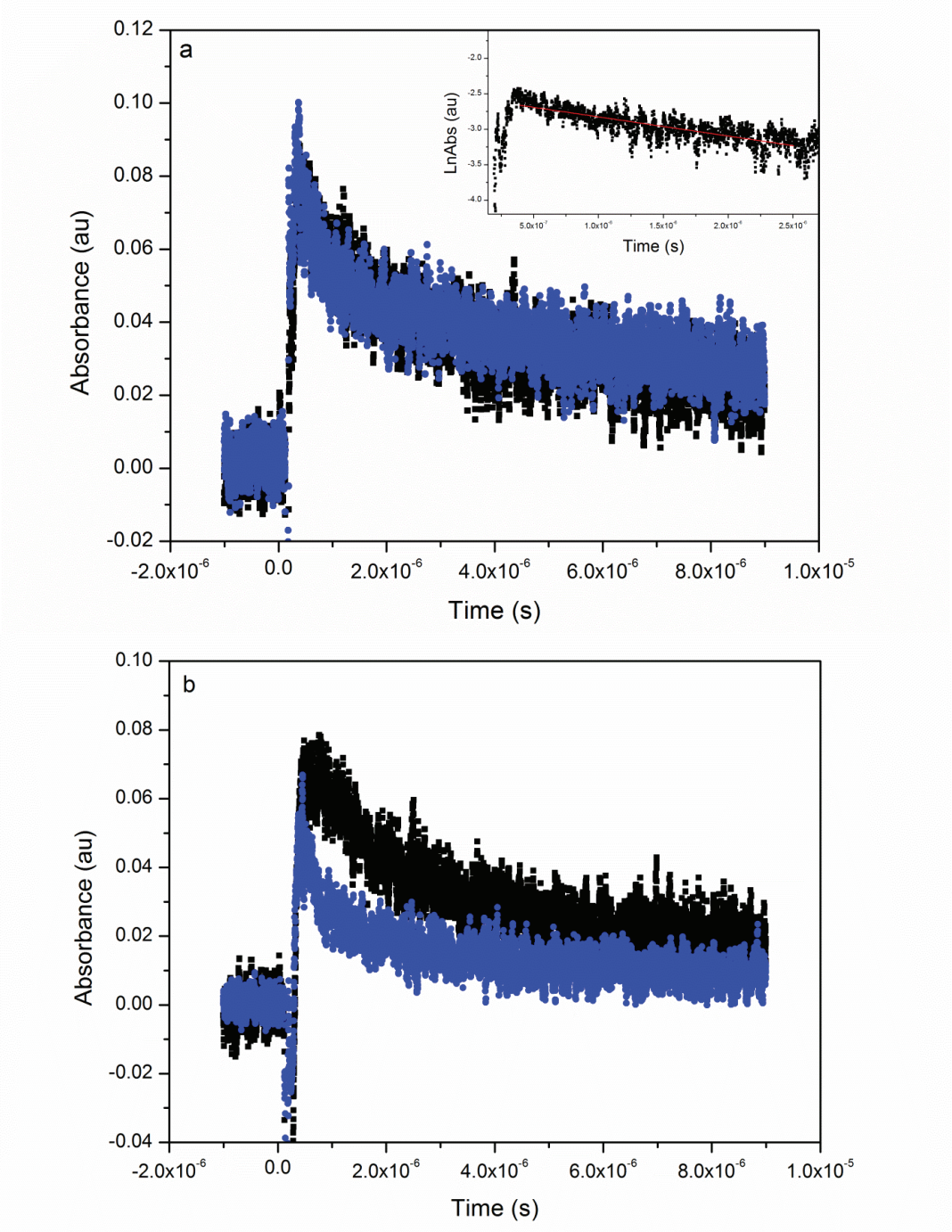

Figure III-7: Transient signal of triplet CPT absorption decay without quencher (■) and in presence of 10 mM NaI (●) monitored (a) at 400 nm and (b) at 425 nm. Inset on (a) shows the linear decay of the absorbance in log scale at 400 nm without quencher.

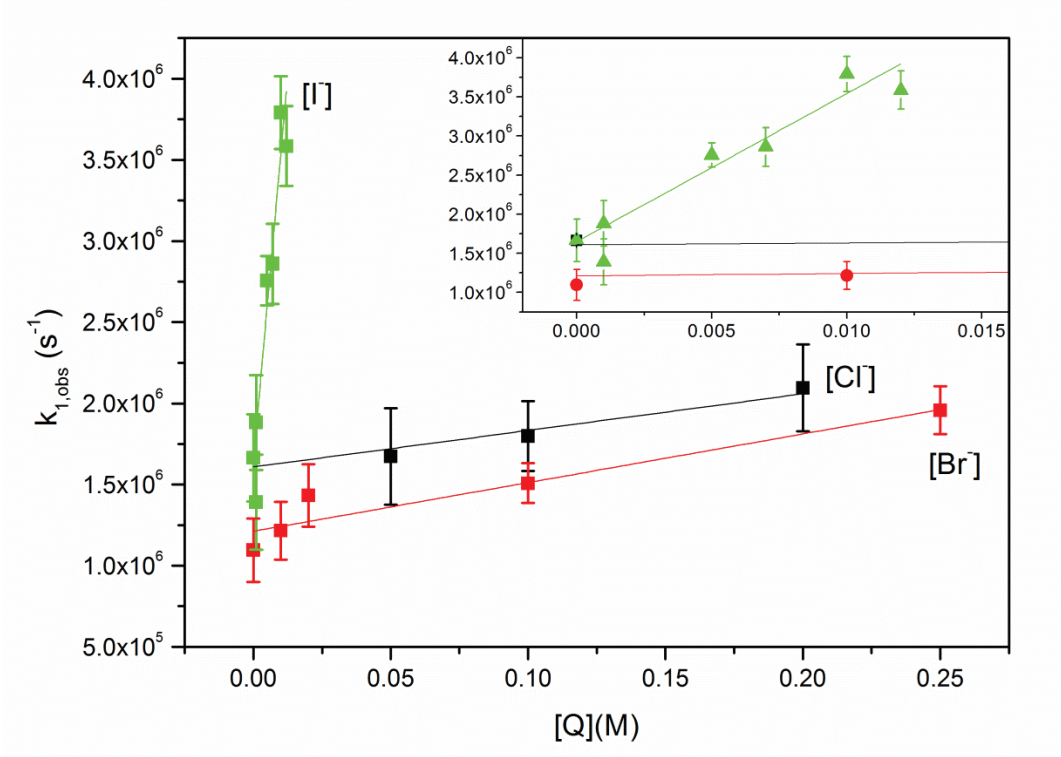

Figure III-8: Stern-Volmer plot of the pseudo-first order rate coefficients of $k_{1,obs}$ of ^{3}CPT quenching as a function of halide concentration

The quenching rate coefficients of ^{3}CPT with bromide and chloride are much lower, respectively (2.99 ± 0.76) x 10^6 and (2.25 ± 1.83) x 10^6 M^{-1} s^{-1} and almost no increase in decay rates was observed, even with concentrations of halides added up to 0.2 M. Higher concentrations of these halides (> 0.25M) even led to slightly longer lifetimes within the experimental error, which could be due to the change in ionic strength of the solution. These points were not taken into account in the Stern-Volmer plot, as they clearly did not show linear dependence.

Although almost no reaction was seen with bromide and chloride, the quenching with iodide was quite fast, pointing towards a quenching by electron transfer. Indeed, as iodide is the less electronegative anion of this serie, and thus the best electron donor, as shown table III-2, it is not surprising that it exhibits the highest rate coefficient. The electron transfer from bromide and chloride seems to be thermodynamically unfavorable, as reflected by the very low rate coefficients. This is confirmed by the free energy change of the associated electron-transfer reaction estimated by the Rehm-Weller equation (equation III-2), with $E_{0,0}$ in this case the energy for the lowest triplet energy level of CPT. This lowest triplet energy level can be obtained by the phosphorescence spectra and values reported in

literature are 2.52 eV (Song and Hwang, 2007) and 2.45 eV (Thomas et al., 2003). In table III-2 the calculated values for ΔG are given for each halide, with a upper and lower limit using the different values for $E_{T0,0}$ and $E_{ox}(D)$ reported.

Table III-2: Bi-molecular rate coefficients k_q obtained for the reaction of ^{3}CPT with halides

Quencher	$k_{1,q}$ (M^{-1} s^{-1})	R^2	Electronegativity	ΔG (eV)
NaCl	(2.25 ± 1.83) x 10^6	0.90	3.16	0.68/0.88
NaBr	(2.99 ± 0.76) x 10^6	0.91	2.96	0.01/0.21
NaI	(1.89 ± 0.22) x 10^8	0.90	2.66	-0.59/-0.39

As it becomes clear from the values of ΔG, the electron transfer is only thermodynamically favorable in the case of iodide. The positive values for the free energy in case of bromide and chloride indicates that the electron transfer from these halides towards the triplet state is not thermodynamically favorable and explains the very low reaction rates observed.

The quenching of ^{3}CPT by limonene was also investigated, as a proton transfer from the limonene towards the ^{3}CPT might occur, as shown for other photosensitizers (Rossignol et al., 2014). The solvent in this case was a mixture of acetonitrile and water, like for the fluorescence measurements, in order to solubilize limonene and the water was pH adjusted to reach an equivalent pH. At pH = 7.3 the transient absorbance signal obtained was too low to be exploited, while at pH = 10.6 the solution showed a higher absorbance and the deprontonated di-anionic form of CPT might also be a good hydrogen acceptor.

Accordingly, at pH = 10.6 the transient signals obtained using laser flash photolysis showed a clear absorbance of the triplet state with a clear mono-exponential behavior. The ^{3}CPT decay rate determined at 425 nm was (6.11 ± 0.04) x 10^5 s^{-1} meaning that the triplet state lifetime of 1.64 µs under these conditions is comparable but smaller to the longer-lived tautomer, τ_T = 2.7 µs in water at neutral pH. The mono-exponential decay indicates that in the acetonitrile-water mixture and at this equivalent pH no tautomerisation is taking place in the triplet state. The mechanisms suggested to explain the tautomerisation of pterins implies strong interactions with water, favoring the intramolecular proton shift as a solvent or directly implicated as reactant (Jaramillo et al., 2009). As acetonitrile is an aprotic solvent, this hydrogen bonding could be largely suppressed, explaining the monomeric form of CPT and hence the mono-exponential decay rate. Upon addition of limonene in the solution of

CPT, no quenching could be evidenced, demonstrated figure III-9, though a slight decrease in overall absorption could be noted in presence of 100 mM of limonene.

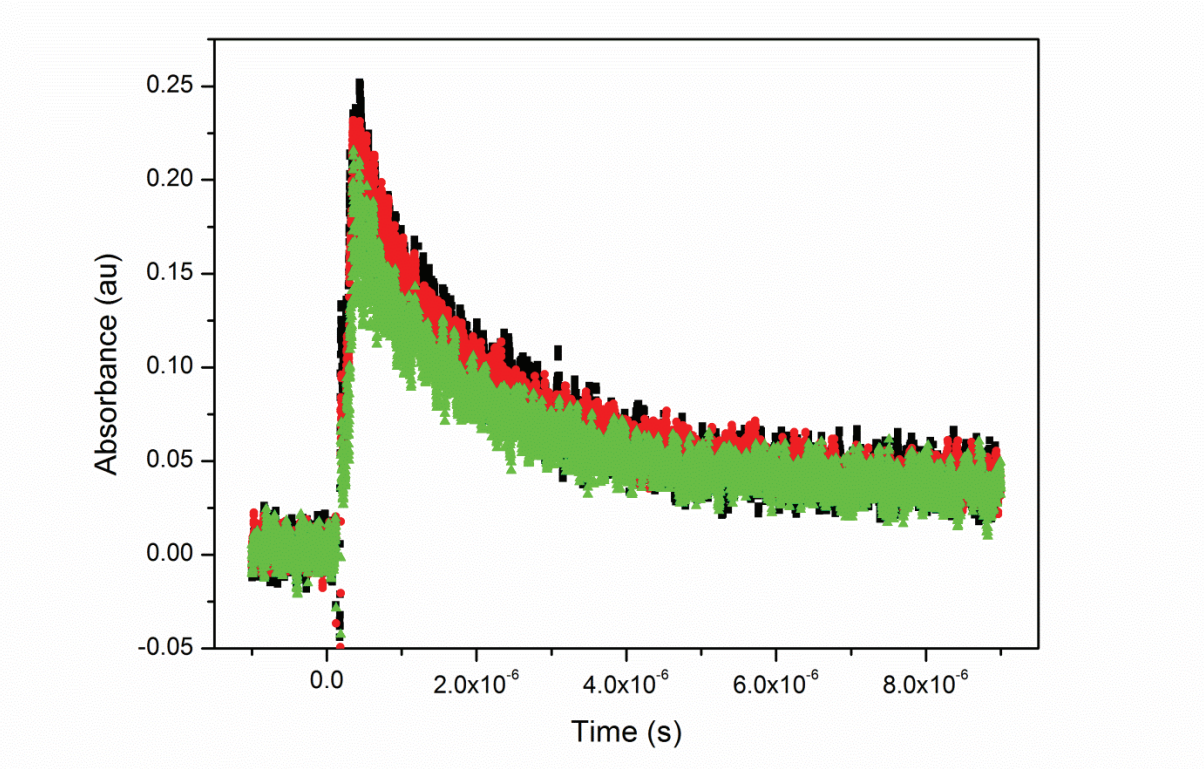

Figure III-9: Transient signal of absorption of triplet CPT (0.2 mM) in water-actonitrile at 425 nm without limonene (■) *and in presence of 50 mM* (●) *and 100 mM* (◆) *limonene*

III.3.3 Excited state reactivity: mechanism and product formation

III.3.3.a. General mechanism

The mechanism involved in all the quenching processes evidenced in this work is electron transfer between the quencher and the excited CPT. The electron transfer towards the singlet state is more efficient as the singlet state is more energetic but also because the quantum yield of a singlet state is higher than for the triplet state. The less energetic ^{3}CPT only shows an efficient quenching by electron transfer from iodide. The following general mechanism can thus be proposed for the evidenced photo-induced reactions between excited CPT and small carboxylic acids:

$^1CPT + Q \longrightarrow CPT^{\bullet -} + Q^{\bullet +}$ (R1)

$Q^{\bullet +} + CPT \longrightarrow$ products (R2)

$CPT^{\bullet -} + CPT \longrightarrow product$ (R3)

For the halides, these reactions give rise to the formation of atomic halogens ($X^{\bullet}$) who, in presence of an excess of the halide anion (X^-), can recombine and form radical anions ($X_2^{\bullet -}$), reaction 4 of the next mechanism. The reactions for triplet state CPT only take place with iodide.

$^1CPT + X^- \longrightarrow CPT^{\bullet -} + X^{\bullet}$ (R4)

$^1CPT \longrightarrow {}^3CPT$ (R5)

$^3CPT + X^- \longrightarrow CPT^{\bullet -} + X^{\bullet}$ (R6)

$^3CPT + X^- \longrightarrow CPT^{\bullet -} + X^{\bullet}$ (R7)

$X^{\bullet} + X^- \longrightarrow X_2^{\bullet -}$ (R8)

$X^{\bullet} + CPT \longrightarrow products$ (R9)

$X_2^{\bullet -} + CPT \longrightarrow products$ (R10)

$X_2^{\bullet -} + X_2^{\bullet -} \longrightarrow X_2 + 2X^-$ (R11)

$X_2 \rightleftarrows X_2\,(g)$ (R12)

Both the atomic halogen radical and the radical anion $X_2^{\bullet -}$ are strong oxidants and can react with the photosensitizer or other organic compounds present (R9-10). If sufficient radical anions $X_2^{\bullet -}$ are formed, the recombination of two radicals (R11) can lead to the release of molecular halogens in the gas phase (R12).

III.3.3.b. Chemical analysis of reaction products

In a different series of experiments, a solution containing CPT (0.1 mM, pH=7.0) and an organic compound, lactic acid or limonene (1mM), were introduced in a quartz reactor and irradiated with a 150 W Xenon lamp, equipped with a Pyrex filter to eliminate short wavelength exposure (λ < 280 nm), and a 1 cm water-filter to avoid excessive heating. During the entire irradiation time (360 minutes), samples were taken at regular time intervals. The samples were then analysed by UPLC-HRMS with and without PFBHA derivatization.

In presence of lactic acid, the formation of two products under irradiated conditions could be evidenced, as shown by the time traces for these products figure III-S4 (section III.6). The first product, as shown table III-3, corresponds to an addition of a hydroxyl group on the lactic acid, leading to the formation of a hydroxy-acid with formula $C_3H_6O_4$. The chemical mechanism leading to the formation of this hydroxyl-acid is detailed figure III-10 (A). After the initial electron transfer towards the singlet state CPT, an alkyl radical is formed which forms a peroxyl radical after the addition of molecular oxygen that can lead to a suite of products, amongst which the formation of a hydroxyl group (von Sonntag and Schuchmann, 1991). The addition of the hydroxyl function seems most probable on the β-carbon, as this carbon is not surrounded by electrophile oxygen atoms. The second product is $C_3H_4O_3$, and was detected as a derivatized compound, meaning this product bears a carbonyl function. This product could be formed through the loss of a hydroxyl function with a subsequent addition of molecular oxygen on the radical, but the proposition of a structure is rather speculative in this case.

Upon irradiation a strong decay in the concentration of CPT was observed, up to a factor of 20 after 150 min. of irradiation, mainly due to decarboxylation. This is in agreement with previous results where the decarboxylation of CPT under irradiation was observed in acidic solutions (pH range 4-7) as a main oxidation product of self-reactions (Suarez et al., 2000). In deoxygenated solutions, the observed decarboxylation yield was much lower. In our case, the decarboxylation was not the only loss path way for CPT. Indeed, a product with a mass corresponding to the chemical formula $C_{17}H_{21}O_3N_5$ was also detected in the irradiated solution of CPT in presence of limonene (Table III-3). This formula corresponds to a recombination product of limonene and CPT, evidencing that chemical reactions happen between the electronically excited CPT and this monoterpene, although this could not be measured with the spectroscopic methods here. As the overall absorbance of triplet state CPT, measured using laser flash photolysis, showed an overall lower signal in presence of limonene, this seems to point towards a singlet state reactivity of CPT with limonene. Indeed no quenching of the triplet state of CPT could be measured, but the overall lower absorption of the triplet state could tentatively be explained by a lower triplet yield due to singlet state quenching of the photosensitizer. This indirect evidence combined with the results of the mass spectrometry results, led us to propose a reaction mechanism of ^{1}CPT with limonene,

presented figure III-10(B). The reaction is started by an electron transfer from limonene towards ^{1}CPT, in analogy with the mechanism proposed for the other quenchers, followed by a proton transfer from limonene to ^{1}CPT. It was suggested by Rossignol et al. that the mechanism for electron transfer should preferentially lead to the formation of an allyl radical on the endocyclic double bond, as the radical cation formed would then be stabilized by the presence of secondary and tertiary carbons (Rossignol et al., 2014). But our available data does not permit to exclude the formation of an allyl radical on a secondary or tertiary allylic carbon and therefore both are represented figure III-10(B). The chromatogram showed several peaks for the mass of this recombination product, probably due to the presence of several isomers. Therefore, the two structures of these recombination products proposed in figure III-10(B) are suggestive and could not be established with certainty.

Table III-3: List of observed products of irradiated solutions of CPT in presence of lactic acid or limonene

Experiment	**m/z**	**Formula**
Lactic acid + CPT	105.019	$C_3H_6O_4$
	87.009	$C_3H_4O_3$
Limonene + CPT	342.157	$C_{17}H_{21}O_3N_5$
	151.113	$C_{10}H_{16}O$
	183.102	$C_{10}H_{16}O_3$
	181.087	$C_{10}H_{14}O_3$
	199.098	$C_{10}H_{16}O_4$
	197.082	$C_{10}H_{14}O_4$
	215.092	$C_{10}H_{16}O_5$
	213.077	$C_{10}H_{14}O_5$
	231.087	$C_{10}H_{16}O_6$
	229.072	$C_{10}H_{14}O_6$
	183.066	$C_9H_{12}O_4$
	169.087	$C_9H_{14}O_3$
	155.071	$C_8H_{12}O_3$

All other products detected in the irradiated solution of CPT with limonene are oxygenated compounds, as listed table III-3, with up to 6 additional oxygen atoms. Most compounds retain the C_{10} structure of limonene with addition of hydroxyl or carbonyl groups. An example of the time evolutions of two of these products, $C_{10}H_{16}O_5$ and $C_{10}H_{14}O_5$ is provided figure III-S5 (section III.6). Two C_9 compounds and one C_8 compound were also detected, but

proposing a chemical structure here would be purely speculative. These series of compounds detected is very similar to the products observed for the reaction of limonene with another photosensitizer, imidazole-2-carboxaldehyde (Rossignol et al., 2014). The formation of the products was explained by the initial formation of an allyl radical through an electron- or hydrogen-transfer form limonene to the triplet state excited photosensitizer, leading to a large range of oxidation products *via* the peroxyl-radical chemistry. This photochemical reaction caused the reactive uptake of limonene from the gaseous phase into the particulate phase, inducing particle growth. It is clearly shown that with CPT the same oxidation process is occurring in the bulk phase, leading to think that this photosensitized reaction between CPT and limonene could also occur through heterogeneous reactions. The environmental implications of this type of chemistry are discussed in the next section.

Figure III-10: Proposed reaction mechanism for the formation of some of the observed products for the reaction of (A) ^{1}CPT with lactic acid and (B) ^{1}CPT with limonene.

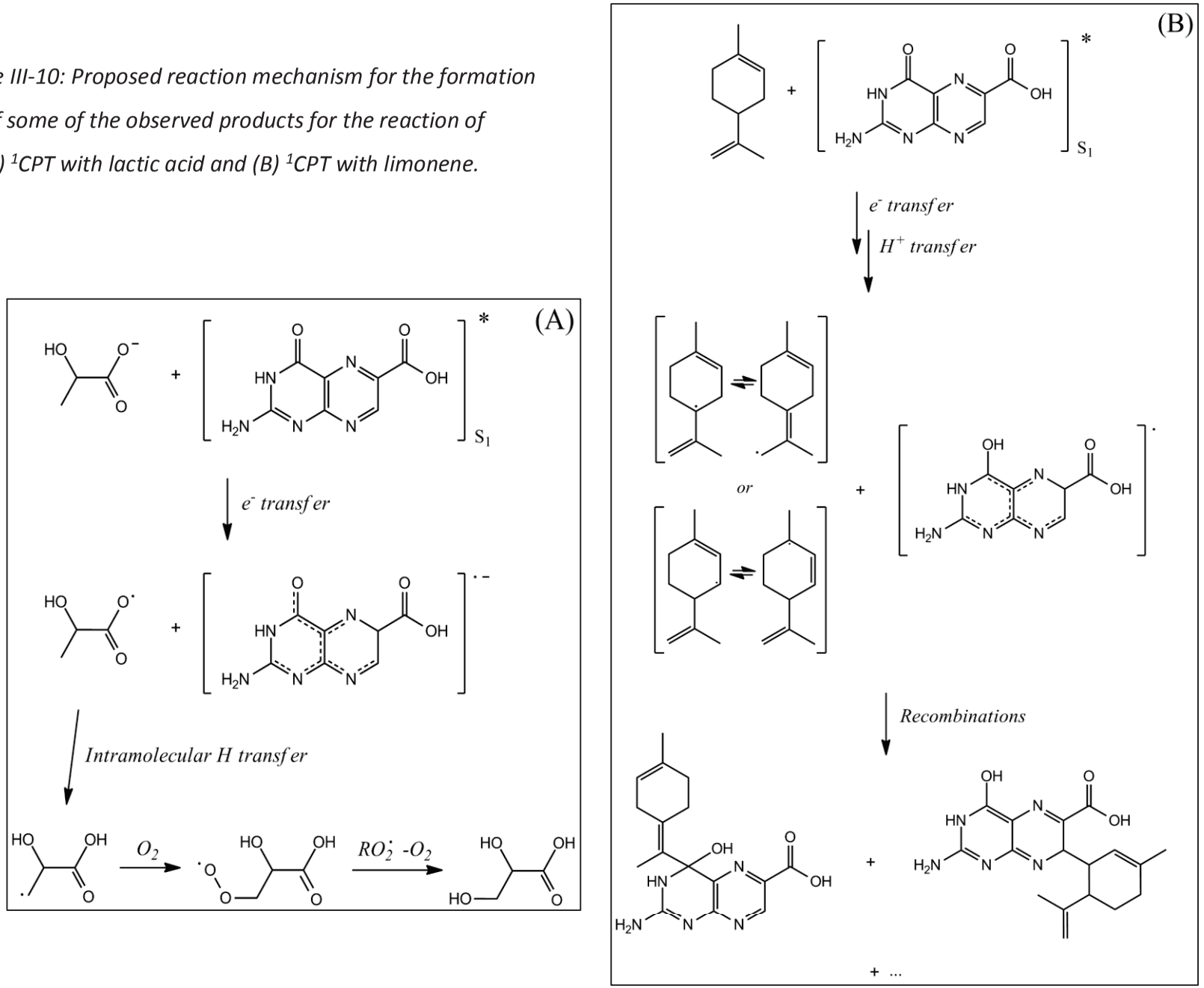

III.4. Conclusions:

6-carbxoy-pterin was demonstrated to be a photosensitizer inducing effective electron transfer in its singlet state in the presence of halides, notably bromide and iodide, and ubiquitous carboxylic acids. In its less energetic triplet state, CPT showed limited reactivity towards halides and an organic, limonene. Nonetheless, the very fast electron transfer reactions occurring in singlet state with halides and the somewhat slower reaction of ^{3}CPT with iodide can lead to the formation of very reactive species, as $I_2^{\bullet-}$ or I_2, in the bulk as well as in the gas-phase. Indeed, the impact of singlet state reactivity, although fast, is mostly limited by its short lifetime, whereas the triplet state reactivity measured with iodide, more than an order of magnitude smaller than singlet state reactivity, is expected to have a larger impact, since the lifetime of the reactive ^{3}CPT component is 2 orders of magnitude bigger than the singlet state lifetime. On the other hand, the marine concentrations of bromide is 3 orders of magnitude higher than the iodide concentration, 0.84 mM and 0.02-0.4 µM respectively (Chang et al., 2004; Kennish, 2000), which will make photo-oxidation of bromide by ^{1}CPT quantitatively more important than the ^{3}CPT oxidation of iodide. The species produced through this photo-oxidation process can have a very important influence for the emission of gas-species in the MBL and especially I_2 can influence directly the oxidative capacity of the marine boundary layer.

The observation of highly oxygenated products formed after the irradiation of a solution containing CPT and limonene indicates that a photochemical reaction between the photosensitizer and the monoterpene occurs, although the spectroscopic methods used here failed to evidence this reactivity. It is very interesting to see that the reaction between this rather moderately efficient photosensitizer leads to the formation of highly oxygenated products in the presence of a VOC as limonene. As it has been shown in presence of imidazole-2-carboxaldehyde, this type of oxygenated products show a low volatility and can lead to the growth of atmospheric aerosols (Rossignol et al., 2014). But also the oxidation of ubiquitous small carboxylic acids leads to the formation of more oxygenated and thus lower volatility products. This leads to think that this type of heterogeneous photochemical reactions at the surface of aerosols might be much larger spread than actually known.

This also points out that photochemistry in the SML might play an important, and quite unaccounted for, role in marine gas-phase chemistry and may contribute to the

unexplained I_2 concentrations measured. The pterins are biologically produced photosensitizers and all show interesting singlet and triplet properties, potentially leading to a non-negligible impact through photochemical reactions at the air/water interface. Importantly, the pterins are just one family of photosensitizers present at the air-sea interface and other photosensitizers can play the same role.

III.6. References:

Aaron, J.-J. et al., 1991. Solvent Effects upon the Electronic Absorption and Fluorescence Spectra of Pteridines and Riboflavin and Their Ground and First Excited Singlet State Dipole Moments

Pteridines, 3(3).

Abbatt, J.P.D. et al., 2012. Halogen activation via interactions with environmental ice and snow in the polar lower troposphere and other regions. Atmospheric Chemistry and Physics, 12(14): 6237-6271.

Aregahegn, K.Z., Noziere, B. and George, C., 2013. Organic aerosol formation photo-enhanced by the formation of secondary photosensitizers in aerosols. Faraday Discussions, 165: 123-134.

Brodhun, B. and Hader, D.P., 1990. Photoreceptor proteins and pigments in the paraflagellar body of the flagellate euglena-gracilis. Photochemistry and Photobiology, 52(4): 865-871.

Carpenter, L.J., 2003. Iodine in the marine boundary layer. Chemical Reviews, 103: 4953-4962.

Carpenter, L.J. and Nightingale, P.D., 2015. Chemistry and Release of Gases from the Surface Ocean. Chemical Reviews, 115(10): 4015-4034.

Chahidi, C., Aubailly, M., Momzikoff, A., Bazin, M. and Santus, R., 1981. Photophysical and photosensitizing properties of 2-amino-4 pteridinone - a natural pigment. Photochemistry and Photobiology, 33: 641-649.

Chang, W.N., Heikes, B.G. and Lee, M.H., 2004. Ozone deposition to the sea surface: chemical enhancement and wind speed dependence. Atmospheric Environment, 38(7): 1053-1059.

Chebbi, A. and Carlier, P., 1996. Carboxylic acids in the troposphere, occurrence, sources, and sinks: A review. Atmospheric Environment, 30(24): 4233-4249.

Clifford, D., Donaldson, D.J., Brigante, M., D'Anna, B. and George, C., 2008. Reactive uptake of ozone by chlorophyll at aqueous surfaces. Environmental Science & Technology, 42(4): 1138-1143.

D'Anna, B. et al., 2009. Light-induced ozone depletion by humic acid films and submicron aerosol particles. Journal of Geophysical Research-Atmospheres, 114.

Dixneuf, S., Ruth, A.A., Vaughan, S., Varma, R.M. and Orphal, J., 2009. The time dependence of molecular iodine emission from Laminaria digitata. Atmospheric Chemistry and Physics, 9(3): 823-829.

Donaldson, D.J. and Vaida, V., 2006. The influence of organic films at the air-aqueous boundary on atmospheric processes. Chemical Reviews, 106(4): 1445-1461.

Facchini, M.C. et al., 2008. Primary submicron marine aerosol dominated by insoluble organic colloids and aggregates. Geophysical Research Letters, 35(17).

Fairall, C.W., Helmig, D., Ganzeveld, L. and Hare, J., 2007. Water-side turbulence enhancement of ozone deposition to the ocean. Atmospheric Chemistry and Physics, 7: 443-451.

Gaill, F. and Momzikoff, A., 1975. Presence of riboflavin and 2 pterins in ascidians (tunicata) and their excretion into sea-water. Marine Biology, 29(4): 315-319.

Gallagher, M.W., Beswick, K.M. and Coe, H., 2001. Ozone deposition to coastal waters. Quarterly Journal of the Royal Meteorological Society, 127(572): 539-558.

Galland, P. and Senger, H., 1988. The role of pterins in the photoreception and metabolism of plants. Photochemistry and Photobiology, 48: 811-820.

Ganzeveld, L., Helmig, D., Fairall, C.W., Hare, J. and Pozzer, A., 2009. Atmosphere-ocean ozone exchange: A global modeling study of biogeochemical, atmospheric, and waterside turbulence dependencies. Global Biogeochemical Cycles, 23.

Hawkins, M.E., Pfleiderer, W., Jungmann, O. and Balis, F.M., 2001. Synthesis and fluorescence characterization of pteridine adenosine nucleoside analogs for DNA incorporation. Analytical Biochemistry, 298(2): 231-240.

Herbert, V. and Bertino, J.R., 1967. Chapter 8 - folic acid1a. In: P.G.N. Pearson (Editor), The Vitamins (Second Edition). Academic Press, pp. 243-276.

Hirakawa, K., Suzuki, H., Oikawa, S. and Kawanishi, S., 2003. Sequence-specific DNA damage induced by ultraviolet A-irradiated folic acid via its photolysis product. Archives of Biochemistry and Biophysics, 410: 261-268.

Hohl, N., Galland, P. and Senger, H., 1992. Altered pterin patterns in photobehavioral mutants of phycomyces-blakesleeanus. Photochemistry and Photobiology, 55(2): 239-245.

Jammoul, A., Dumas, S., D'Anna, B. and George, C., 2009. Photoinduced oxidation of sea salt halides by aromatic ketones: a source of halogenated radicals. Atmospheric Chemistry and Physics, 9: 4229-4237.

Jaramillo, P., Coutinho, K. and Canuto, S., 2009. Solvent Effects in Chemical Processes. Water-Assisted Proton Transfer Reaction of Pterin in Aqueous Environment. Journal of Physical Chemistry A, 113(45): 12485-12495.

Kennish, M.J., 2000. Practical handbook of marine science. crc press.

Ledbetter, J.W., Pfleiderer, W. and Freisheim, J.H., 1995. Photosensitized reduction of l-biopterin in the active ternary complex of dihydrofolate-reductase. Photochemistry and Photobiology, 62(1): 71-81.

Lorente, C., Capparelli, A.L., Thomas, A.H., Braun, A.M. and Oliveros, E., 2004. Quenching of the fluorescence of pterin derivatives by anions. Photochemical & Photobiological Sciences, 3: 167-173.

Lorente, C. and Thomas, A.H., 2006. Photophysics and photochemistry of pterins in aqueous solution. Accounts of Chemical Research, 39(6): 395-402.

Martino, M., Lézé, B., Baker, A.R. and Liss, P.S., 2012. Chemical controls on ozone deposition to water. Geophysical Research Letters, 39(5): L05809.

Martino, M., Mills, G.P., Woeltjen, J. and Liss, P.S., 2009. A new source of volatile organoiodine compounds in surface seawater. Geophysical Research Letters, 36: 5.

Miyazaki, Y., Sawano, M. and Kawamura, K., 2014. Low-molecular-weight hydroxyacids in marine atmospheric aerosol: evidence of a marine microbial origin. Biogeosciences, 11(16): 4407-4414.

Mmereki, B.T., Donaldson, D.J., Gilman, J.B., Eliason, T.L. and Vaida, V., 2004. Kinetics and products of the reaction of gas-phase ozone with anthracene adsorbed at the air-aqueous interface. Atmospheric Environment, 38: 6091-6103.

Momzikoff, A., Santus, R. and Giraud, M., 1983. A study of the photosensitizing properties of seawater. Marine Chemistry, 12: 1-14.

Monge, M.E. et al., 2012. Alternative pathway for atmospheric particles growth. Proceedings of the National Academy of Sciences of the United States of America, 109(18): 6840-6844.

Nekkanti, S. and Martin, C.B., 2015. Theoretical study on the relative energies of cationic pterin tautomers. Pteridines, 26(1): 13-22.

O'Dowd, C.D. and de Leeuw, G., 2007. Marine aerosol production: a review of the current knowledge. Philosophical Transactions of the Royal Society A: Mathematical, Physical and Engineering Sciences, 365: 1753-1774.

O'Dowd, C.D. et al., 2004. Biogenically driven organic contribution to marine aerosol. Nature, 431(7009): 676-680.

Peter S. Liss, R.A.D. (Editor), 1997. Sea Surface and Global Change. Cambridge University Press, Cambridge, 509 pp.

Pfleiderer, W., 1993. Natural pteridines: a chemical hobby. In: E.J. Ayling, M.G. Nair and M.C. Baugh (Editors), Chemistry and Biology of Pteridines and Folates. Springer, New York, pp. 1-17.

Putaud, J.P. et al., 2000. Chemical mass closure and assessment of the origin of the submicron aerosol in the marine boundary layer and the free troposphere at Tenerife during ACE-2. Tellus Series B-Chemical and Physical Meteorology, 52(2): 141-168.

Reeser, D.I. et al., 2009. Photoenhanced Reaction of Ozone with Chlorophyll at the Seawater Surface. Journal of Physical Chemistry C, 113: 2071-2077.

Rembold, H., 1964. Pteridine Chemistry. In: W. Pfleiderer and E.C. Taylor (Editors), Pteridine ChemistryPergamon Press, Oxford, pp. 465.

Rokos, H., Beazley, W.D. and Schallreuter, K.U., 2002. Oxidative stress in vitiligo: Photo-oxidation of pterins produces H2O2 and pterin-6-carboxylic acid. Biochemical and Biophysical Research Communications, 292: 805-811.

Rossignol, S. et al., 2014. Glyoxal Induced Atmospheric Photosensitized Chemistry Leading to Organic Aerosol Growth. Environmental Science & Technology, 48(6): 3218-3227.

Saiz-Lopez, A. and von Glasow, R., 2012, Reactive halogen chemistry in the troposphere. Chemical Society Reviews, 41: 6448-6472.

Schallreuter, K.U. et al., 2001. Epidermal H2O2 accumulation alters tetrahydrobiopterin (6BH(4)) recycling in vitiligo: Identification of a general mechanism in regulation of all 6BH(4)-dependent processes? Journal of Investigative Dermatology, 116(1): 167-174.

Schallreuter, K.U. et al., 1994. Regulation of melanin biosynthesis in the human epidermis by tetrahydrobiopterin. Science, 263(5152): 1444-1446.

Seibert, E. et al., 2002. Spectroscopy and theory of 6-methylisoxanthopterin, a fluorescent guanine analog. Biophysical Journal, 82(1): 432A-432A.

Serrano, M.P., Lorente, C., Vieyra, F.E.M., Borsarelli, C.D. and Thomas, A.H., 2012. Photosensitizing properties of biopterin and its photoproducts using 2 '-deoxyguanosine 5 '-monophosphate as an oxidizable target. Physical Chemistry Chemical Physics, 14(33): 11657-11665.

Shaw, M.D. and Carpenter, L.J., 2013. Modification of Ozone Deposition and I-2 Emissions at the Air-Aqueous Interface by Dissolved Organic Carbon of Marine Origin. Environmental Science & Technology, 47(19): 10947-10954.

Song, Q.H. and Hwang, K.C., 2007. Direct observation for photophysical and photochemical processes of folic acid in DMSO solution. Journal of Photochemistry and Photobiology a-Chemistry, 185: 51-56.

Soniat, M. and Martin, C.B., 2008. Theoretical Study on the Relative Energies of Neutral Pterin Tautomers. Pteridines, 19(4): 120-124.

Suarez, G., Cabrerizo, F.M., Lorente, C., Thomas, A.H. and Capparelli, A.L., 2000. Study of the photolysis of 6-carboxypterin in acid and alkaline aqueous solutions. Journal of Photochemistry and Photobiology a-Chemistry, 132(1-2): 53-57.

Swarna, S., Lorente, C., Thomas, A.H. and Martin, C.B., 2012. Rate constants of quenching of the fluorescence of pterins by the iodide anion in aqueous solution. Chemical Physics Letters, 542: 62-65.

Thomas, A.H. et al., 2003. Singlet oxygen ((1)Delta(g)) production by pterin derivatives in aqueous solutions. Photochemical & Photobiological Sciences, 2: 245-250.

Thomas, A.H. et al., 2002. Fluorescence of pterin, 6-formylpterin, 6-carboxypterin and folic acid in aqueous solution: pH effects. Photochemical & Photobiological Sciences, 1(6): 421-426.

Thomas, J.L., Jimenez-Aranda, A., Finlayson-Pitts, B.J. and Dabdub, D., 2006. Gas-phase molecular halogen formation from NaCl and NaBr aerosols: When are interface reactions important? Journal of Physical Chemistry A, 110: 1859-1867.

Tinel, L., Dumas, S. and George, C., 2014. A time-resolved study of the multiphase chemistry of excited carbonyls: Imidazole-2-carboxaldehyde and halides. Comptes Rendus Chimie, 17(7-8): 801-807.

von Glasow, R., Crutzen, P.J., Editors-in-Chief: Heinrich, D.H. and Karl, K.T., 2003. 4.02 - Tropospheric Halogen Chemistry, Treatise on Geochemistry. Pergamon, Oxford, pp. 1-67.

von Sonntag, C. and Schuchmann, H.-P., 1991. The Elucidation of Peroxyl Radical Reactions in Aqueous Solution with the Help of Radiation-Chemical Methods. Angewandte Chemie International Edition in English, 30(10): 1229-1253.

III.6. Supplementary information

Contribution of the dianionic (basic) form to the emission spectrum at pH=7.2:

At pH 7.2, CPT is for 18.8% under its dissociated dianionic form. Taking into account the reported fluorescence quantum yield of the acid and basic form, 0.26 and 0.18 respectively, the contribution of the acid and basic form to the total fluorescence emission spectrum would be 13.8% and 86.2% respectively (Thomas et al., 2002). But the dianionic form has a higher molar absorption coefficient, $\varepsilon_{\lambda 350nm}$, than the monoanionic form, which compensates almost for the lower quantum yield. Indeed the molar absorption coefficient measured at pH 4.6 ($\varepsilon_{\lambda 350nm}$ = 472.28 M-1 cm-1) is about 30% lower than the one obtained at pH 10.8 ($\varepsilon_{\lambda 350nm}$ = 663.98 M^{-1} cm^{-1}), while the quantum yield of the acid form is 44% higher. So the contribution of the basic dianionic form to the fluorescence emission spectrum will be around 16% of the total emission. Since our solutions have pH in the 7-7.3 range, containing 10-33.5% of dianionic CPT, the contribution of this form to the total fluorescent emission spectrum will be in the range of 9-28.5%.

Figure III S1:

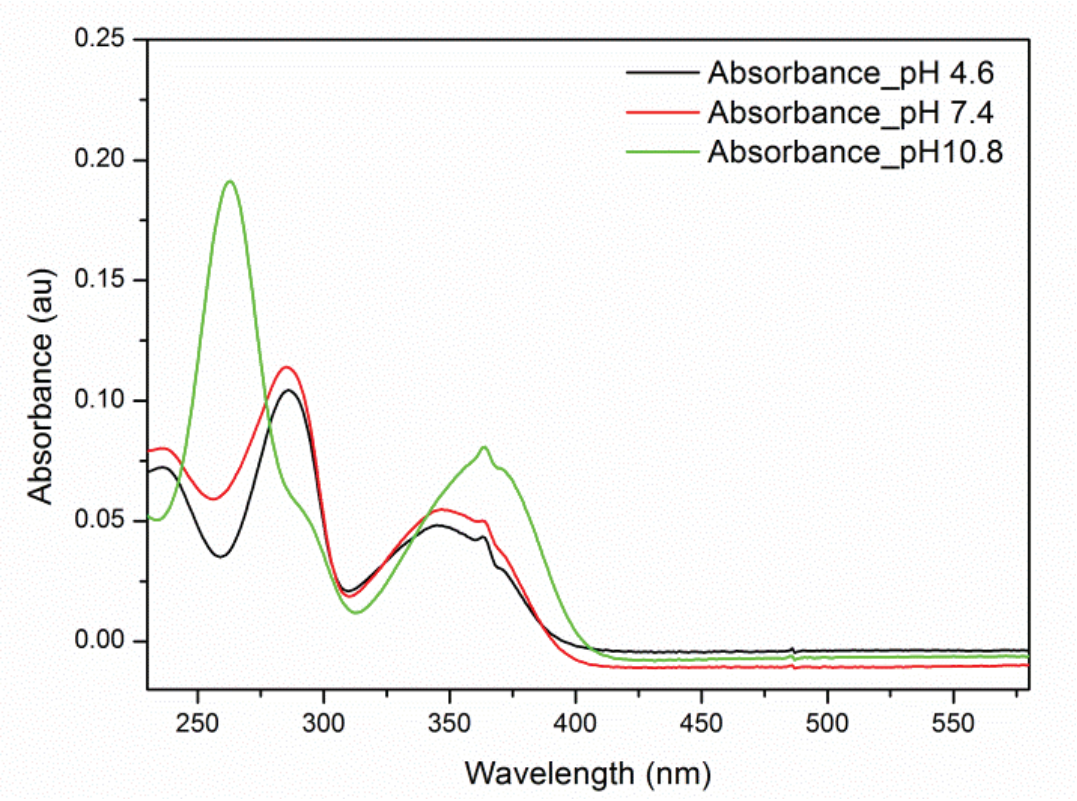

Figure III-S1: UV-Vis absorption spectrum of ground state CPT (0.1mM) at different pH: pH 4.6 (black), pH 7.4 (red) and pH 10.8 (green)

Figures III-S2:

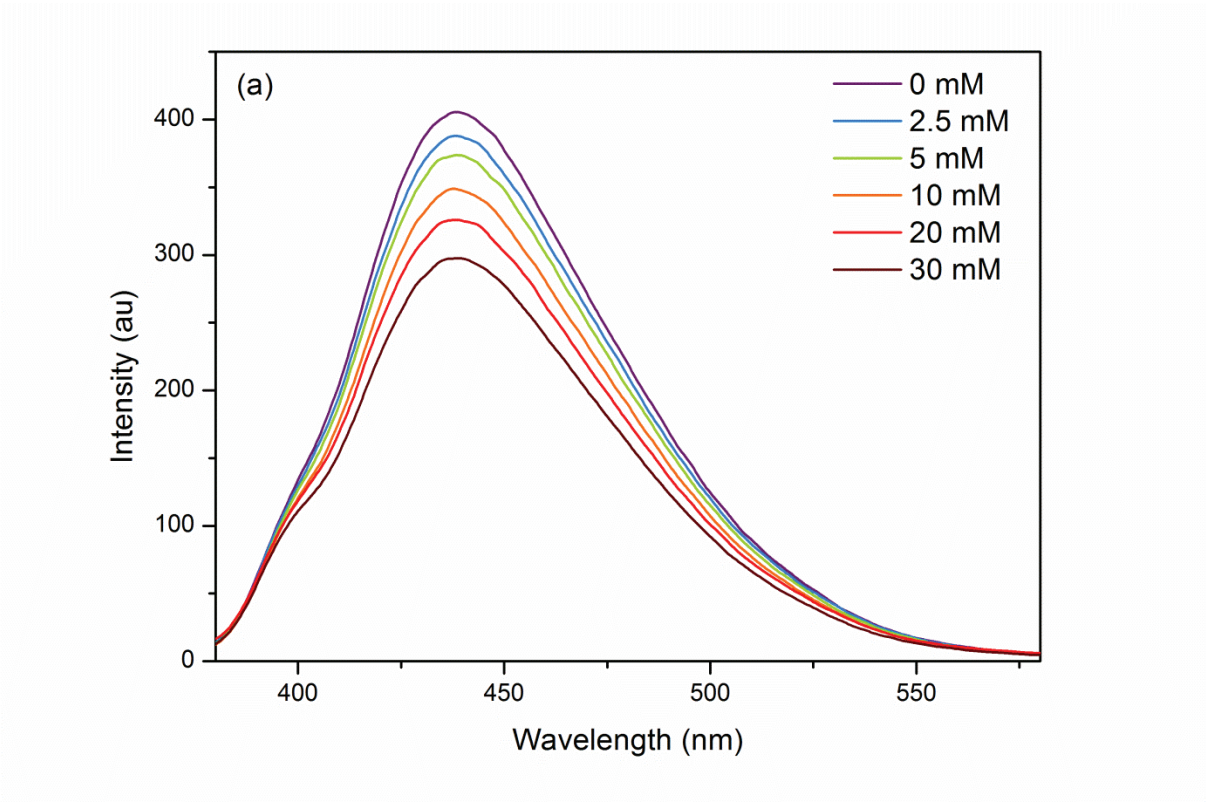

Fig III-S2 (a): iodide

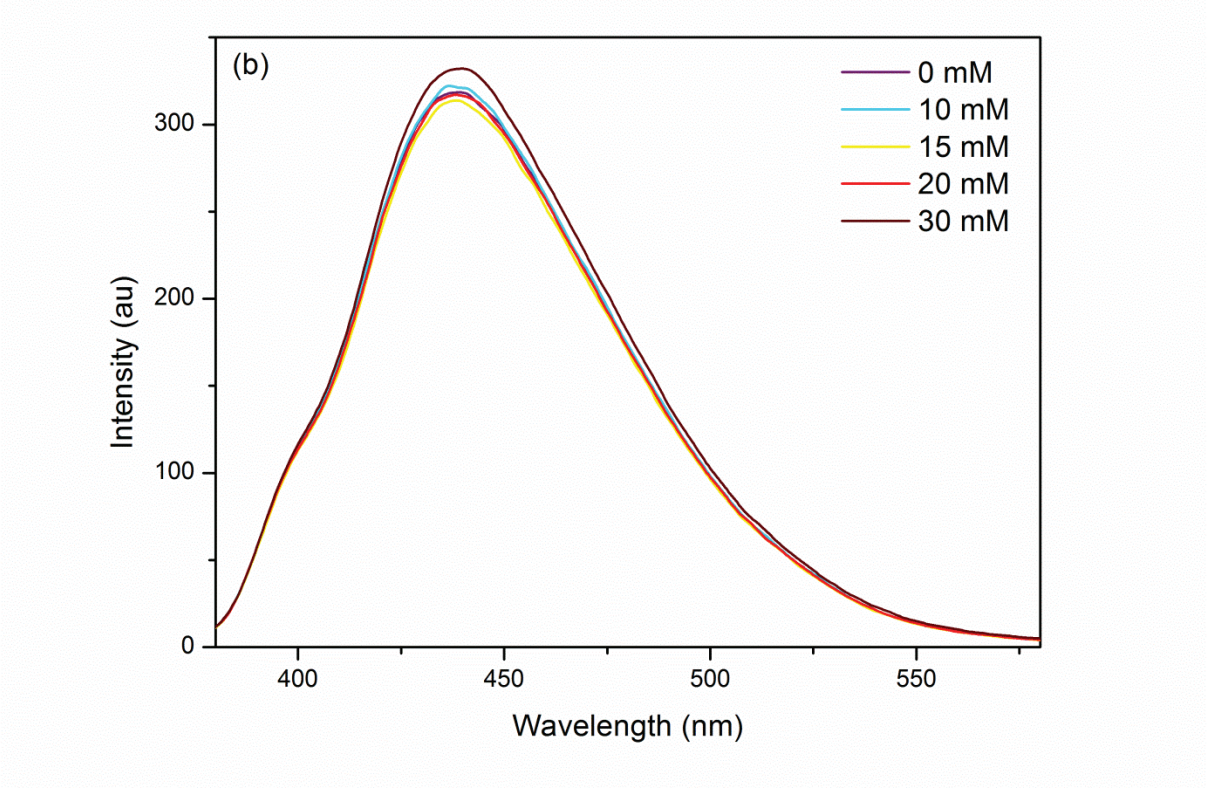

Fig III-S2 (b): chloride

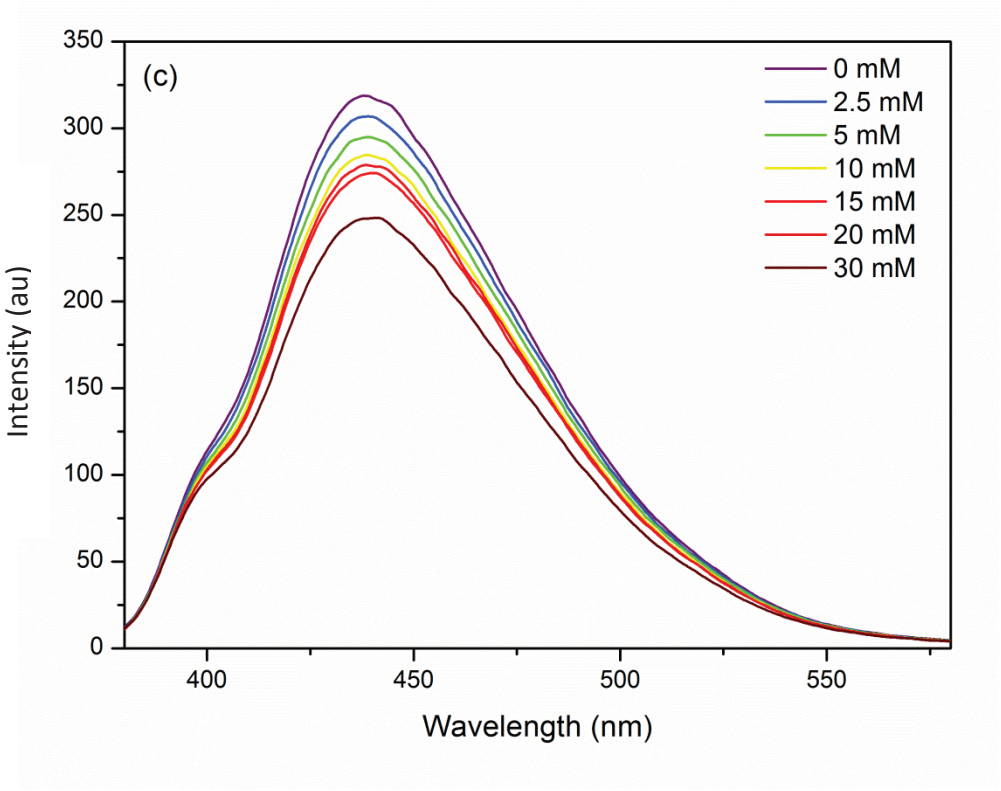

FigIII-S2(c): acide propionique

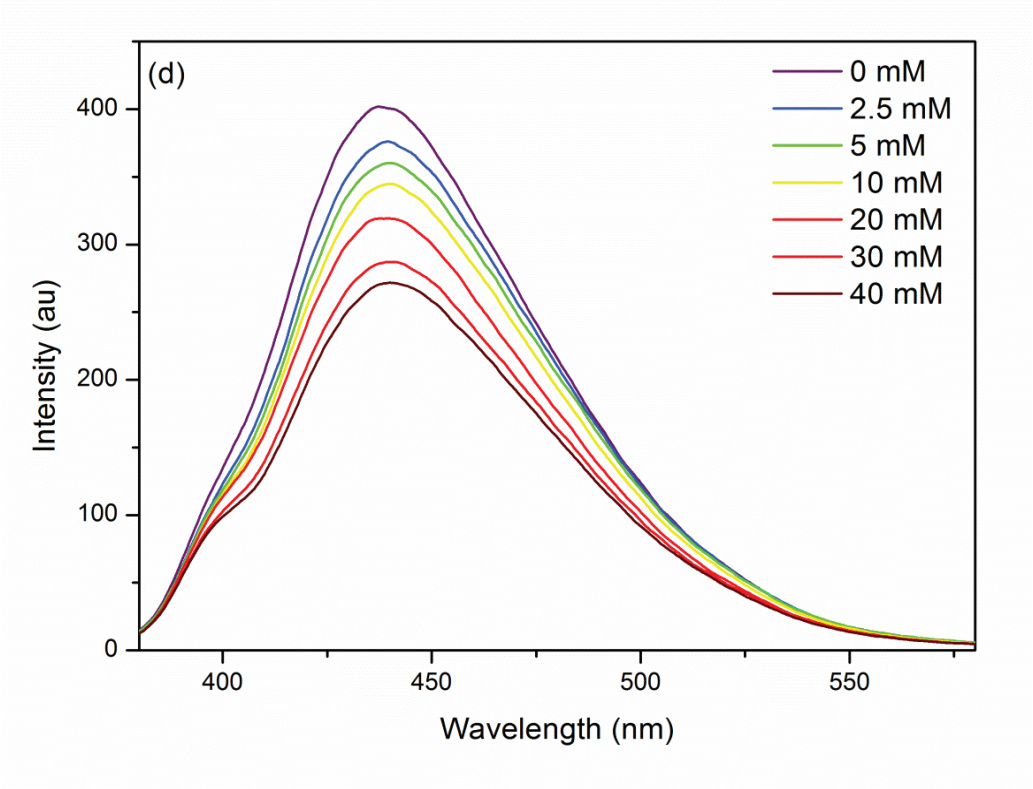

Figure III-S2 (d): citric acid

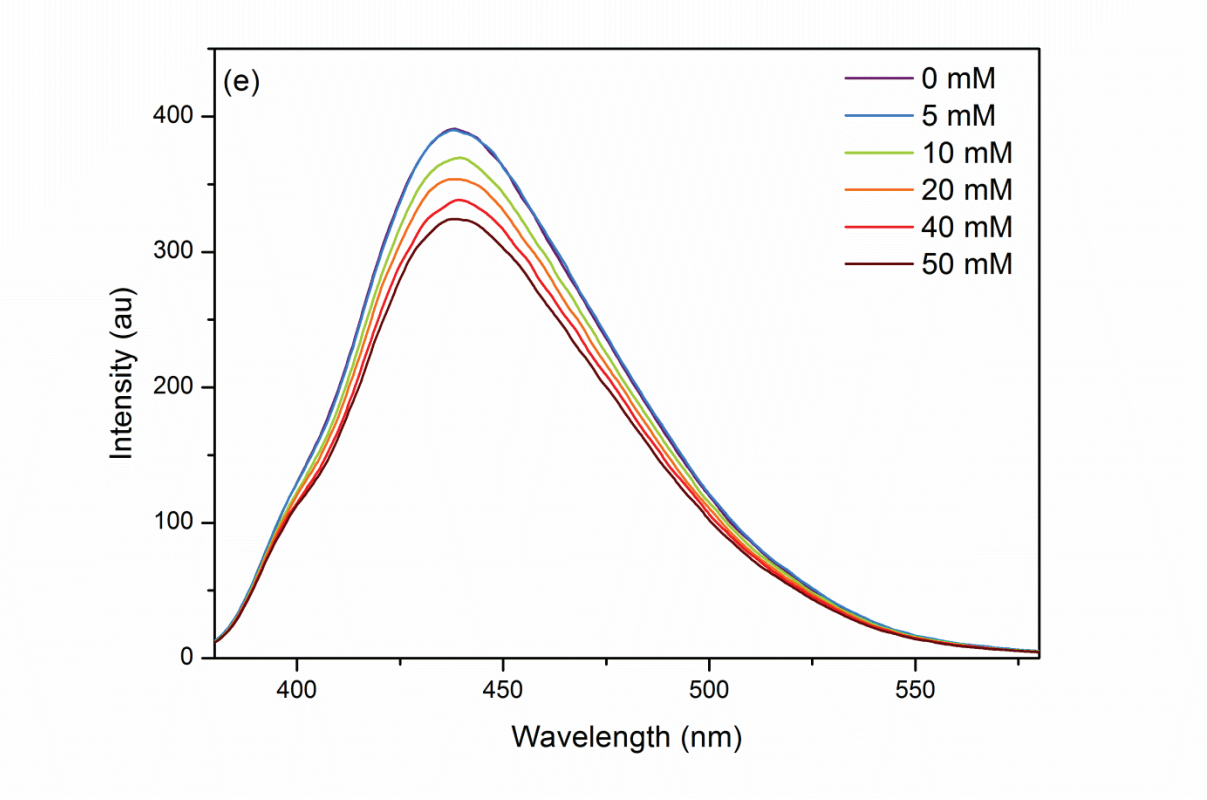

Figure III-S2 (e): lactic acid

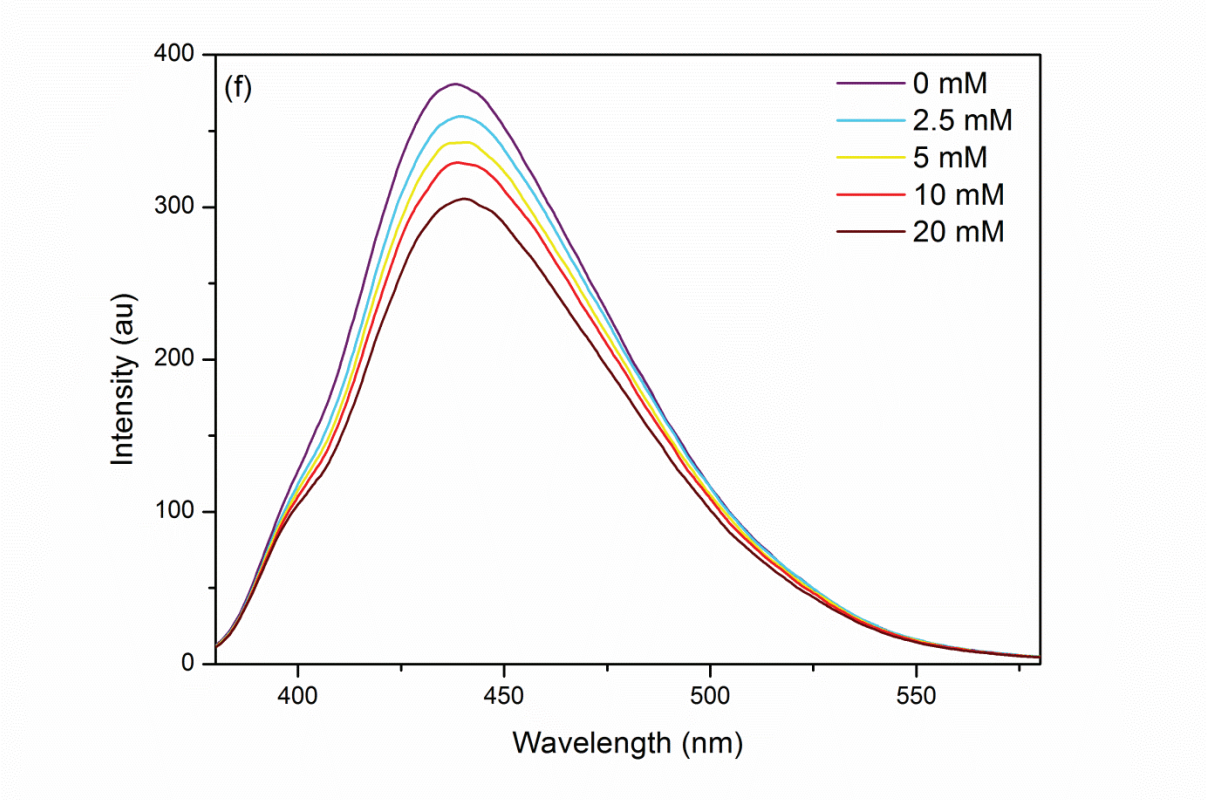

Figure III-S2 (f): malonic acid

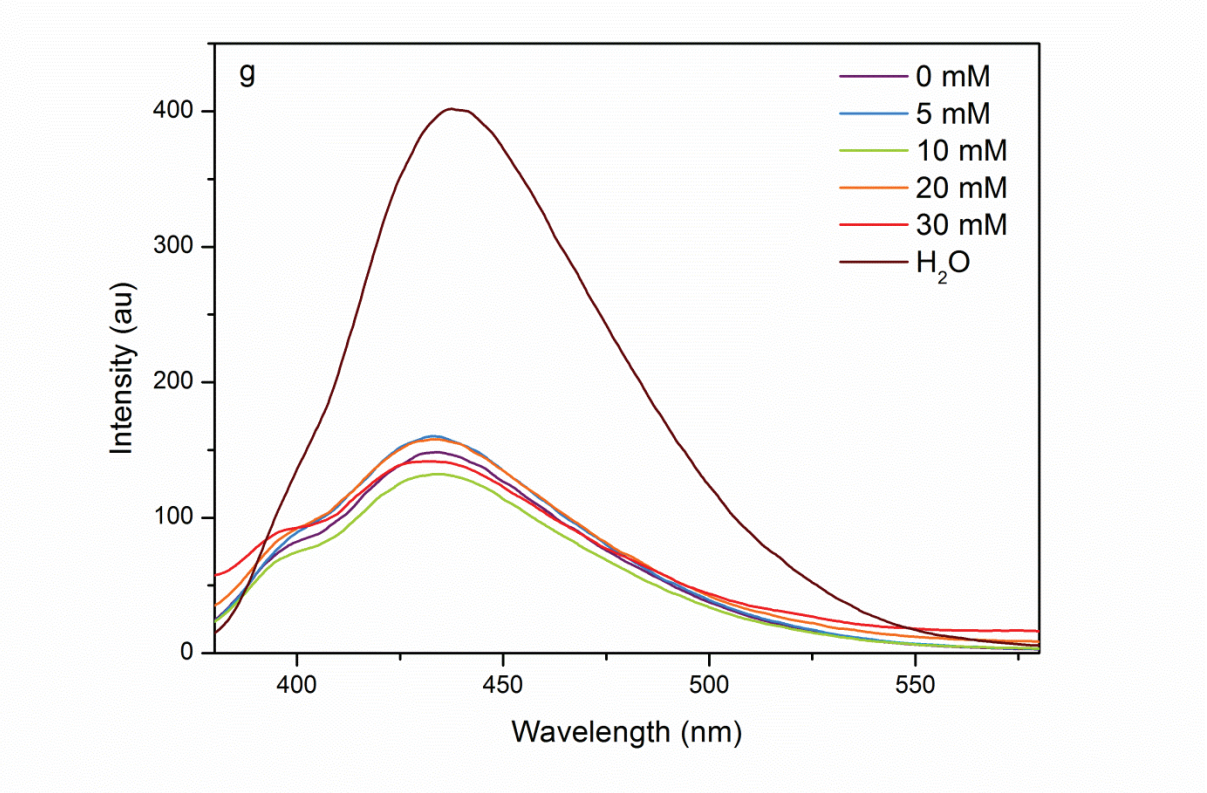

Figure III-S2: Fluorescence emission spectra of CPT with different concentrations of quenchers: (a) iodide, (b) chloride, (c) propionic acid, (d) citric acid, (e) lactic acid, (f) malonic acid and (g) limonene. The spectra in figure S2(g) were taken in a mixture acetonitrile-water, and the spectrum of an aqueous solution of CPT is shown for comparison.

Figure III-S3:

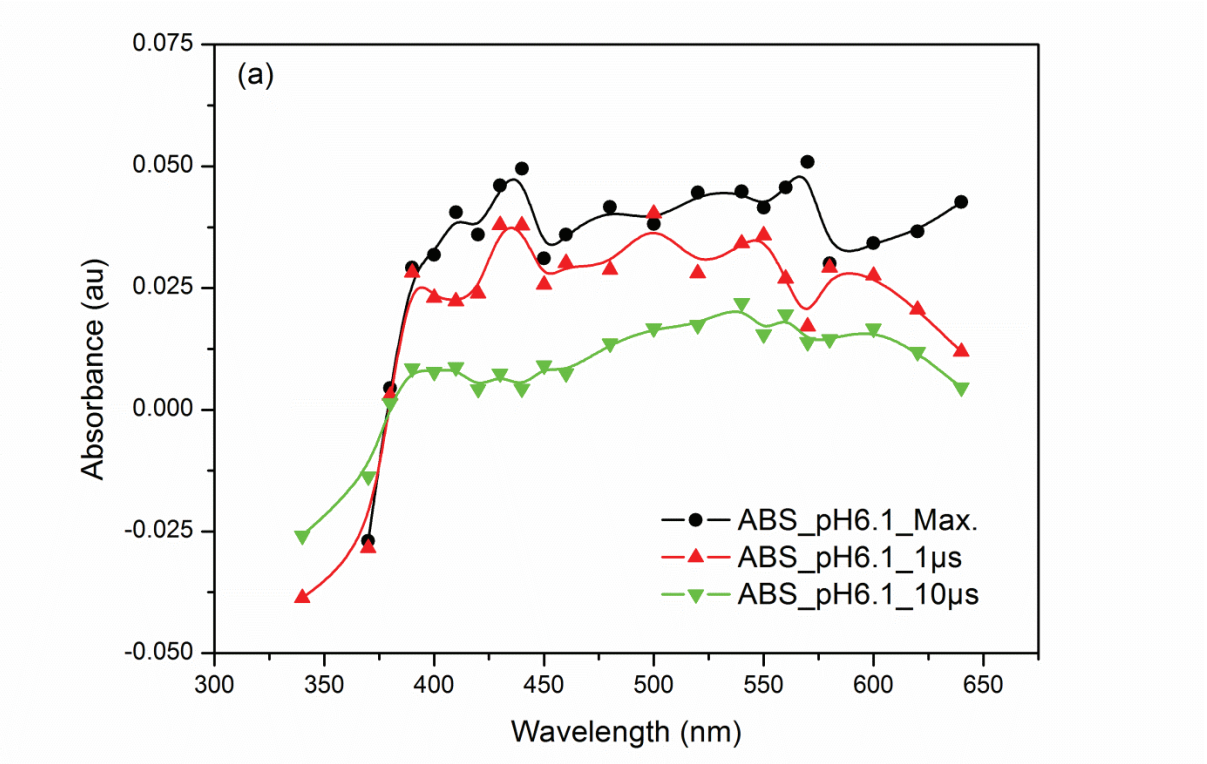

(a) pH=6.1

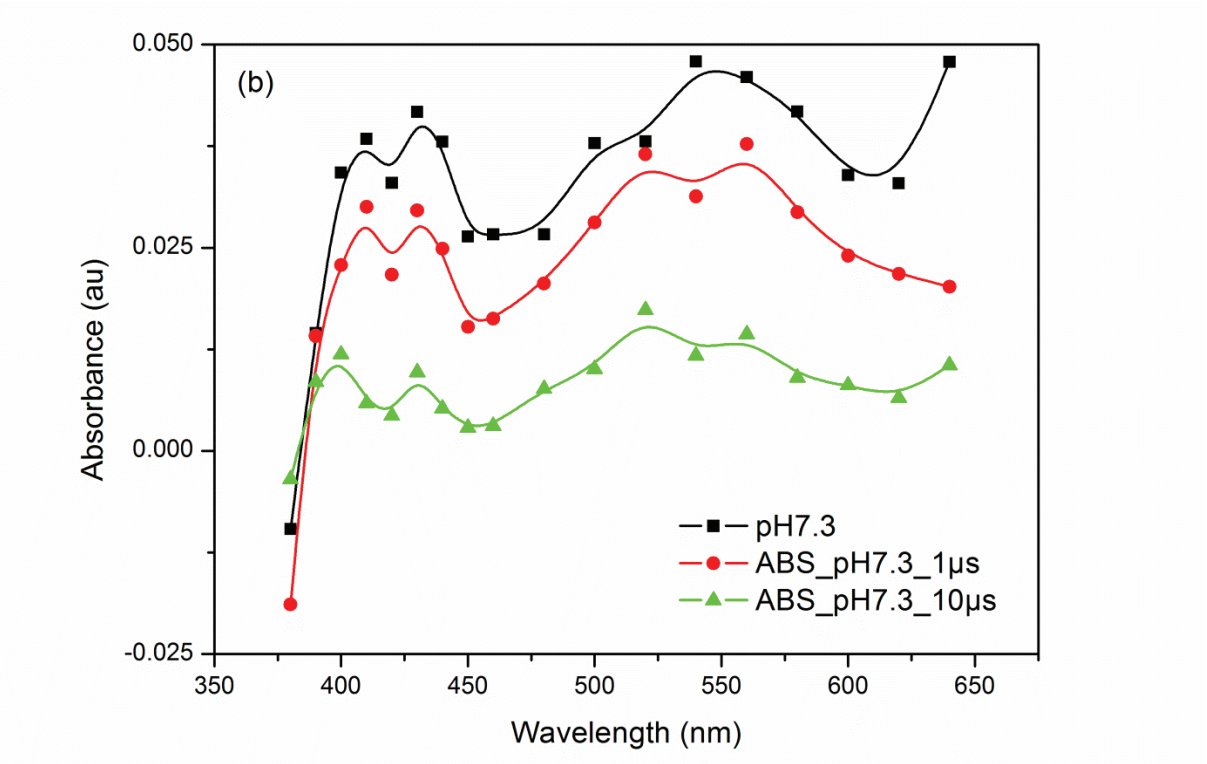

(b) pH=7.3

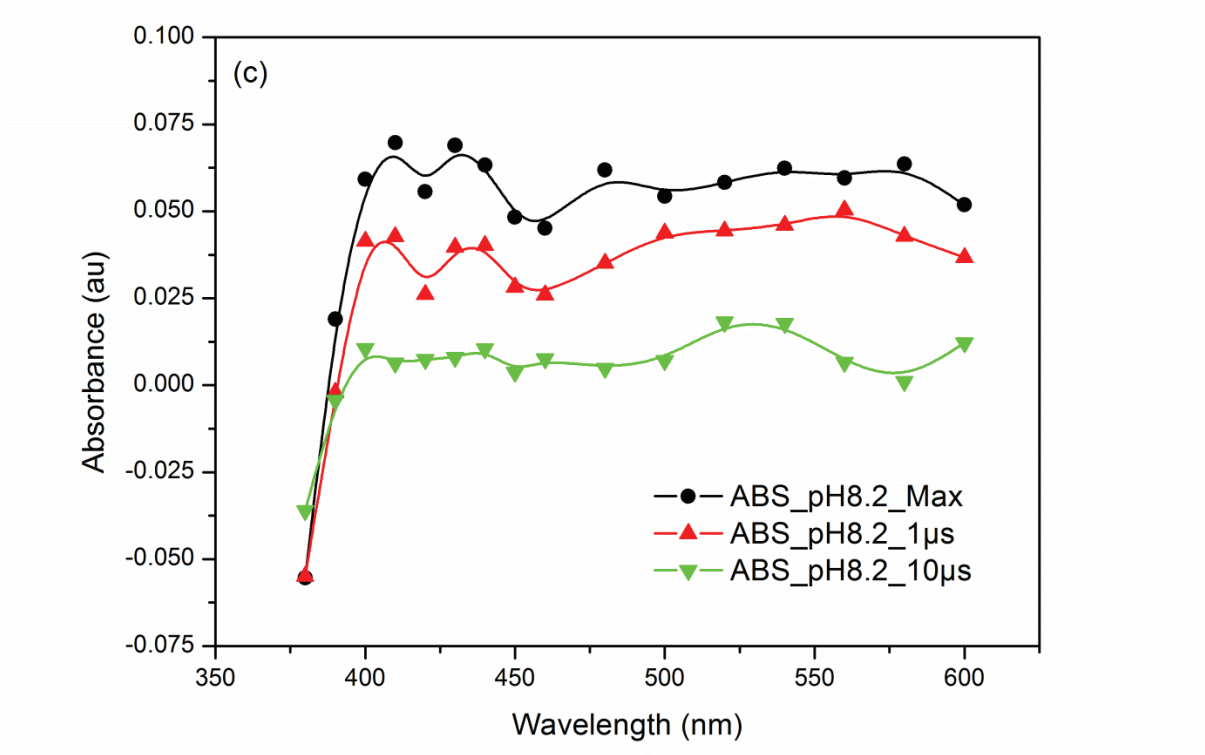
(c)
Absorbance (au)
Wavelength (nm)
ABS_pH8.2_Max
ABS_pH8.2_1µs
ABS_pH8.2_10µs

(c) pH=8.2

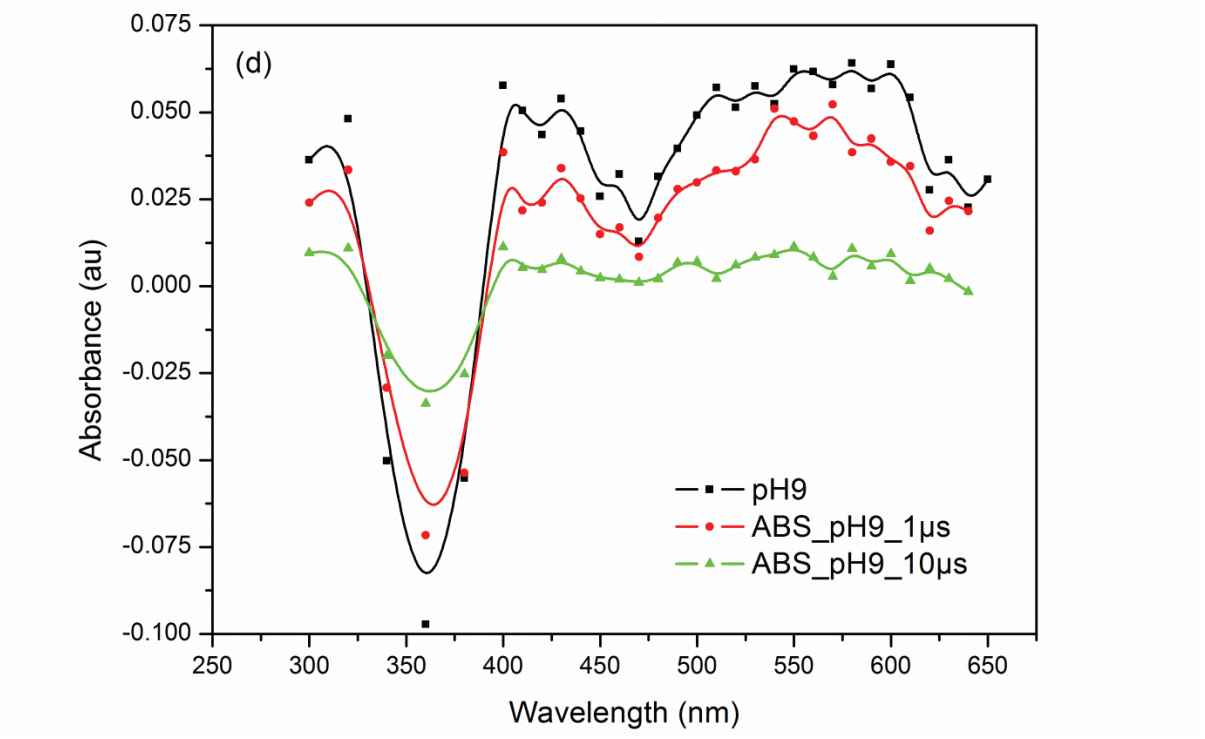
(d)
Absorbance (au)
Wavelength (nm)
pH9
ABS_pH9_1µs
ABS_pH9_10µs

(d) pH=9

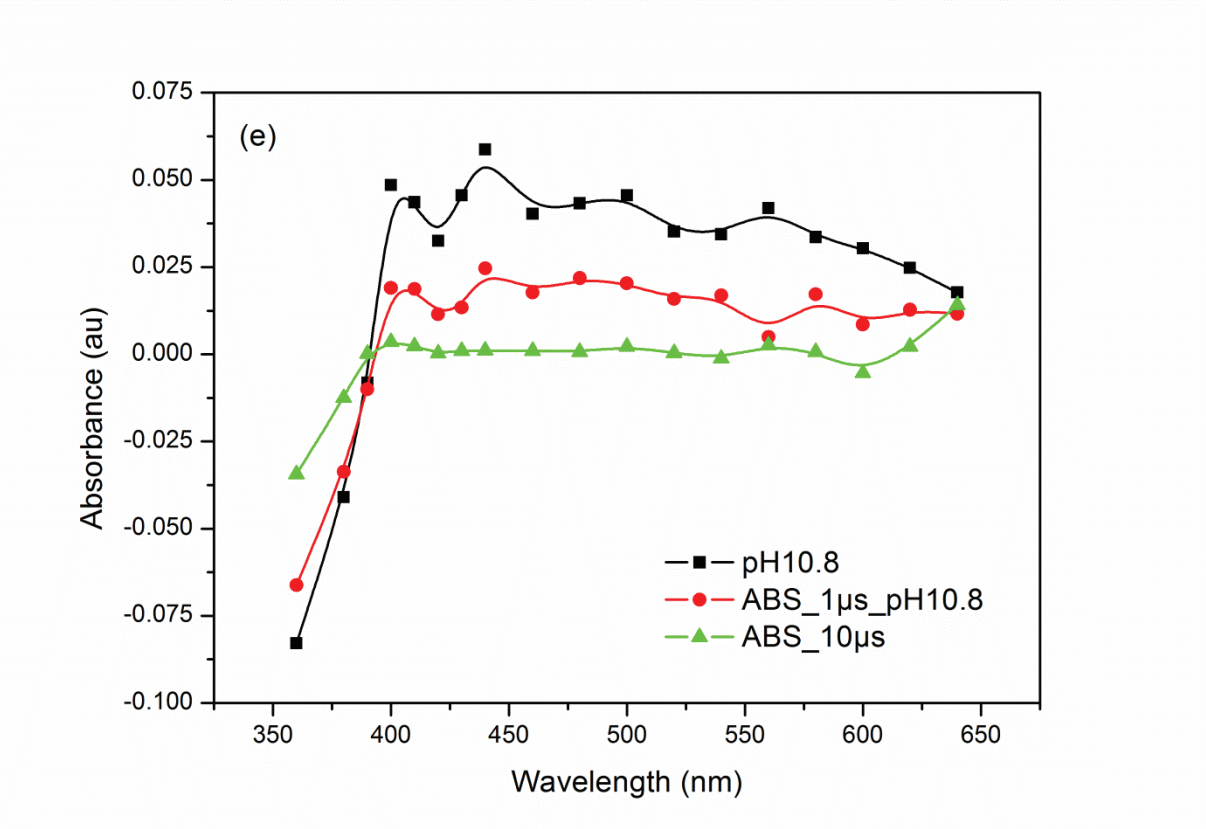

Figure III-S3: Transient absorption spectrum of triplet state CPT (0.1 mM) at different pH, recorded 450 ns, 1 µs and 10 µs after laser flash: (a) pH 6.1, (b) pH 7.3, (c) pH 8.2, (d) pH 9, (e) pH 10.8.

Figure III-S4

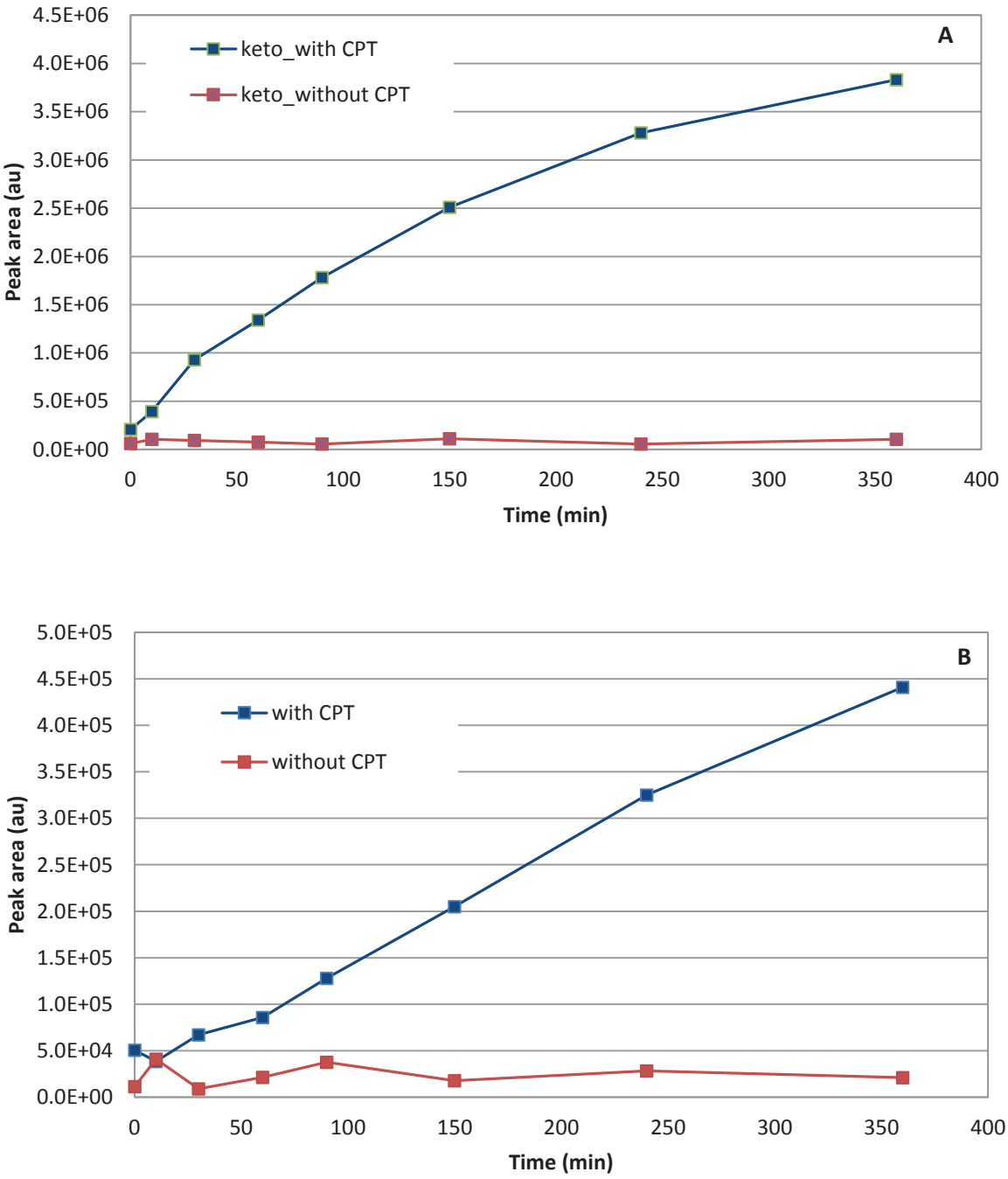

Figure III-S4: Time evolution of the HPLC-HRMS signal of two products in an irradiated solution of lactic acid with and without CPT, showing the formation of (A) a keto-acid and (B) a hydroxy-acid

Figure III-S5

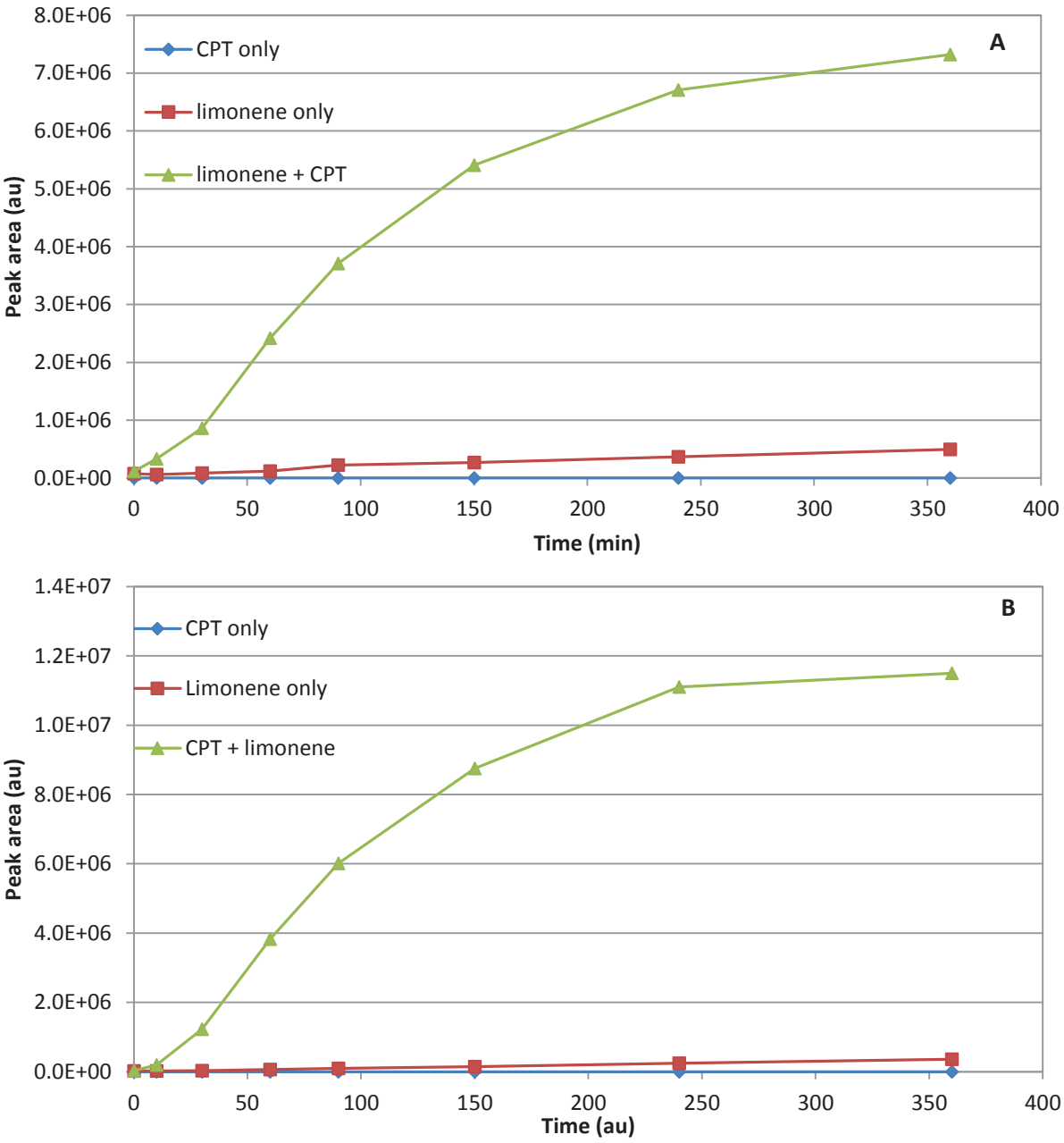

Figure III-S5: Time evolution of the HPLC-HRMS signal of products in an irradiated solution of limonene alone, CPT alone and limonene and CPT, showing the formation of (A) a $C_{10}H_{16}O_5$ and (B) a $C_{10}H_{14}O_5$ compounds.

Chapter IV: Photosensitized reactions induced by imidazole-2-carboxaldehyde at interfaces

IV.0. Motivations

This chapter treats the investigation of photochemical reactions induced by the triplet state of a new photosensitizer, imidazole-2-carboxaldehyde, in bulk aqueous phase and at the interface of aerosols. As presented in chapter II, imidazole-2-carboxaldehyde is one of the light absorbing products that can be formed in situ in aerosols in presence of ammonia and glyoxal. These imidazole-based products have a potential to act as photosensitizers and induce oxidative reactions with different types of compounds, such as VOC. The oxidation of VOC can lead to the formation of lower volatility oxidation products, who could contribute to particle formation or aerosol growth. Indeed, a recent study in our group observed light induced aerosol growth in presence of aerosol seeds containing glyoxal and ammonia, pointing towards a photosensitized mechanism, most efficiently initiated by imidazole-2-carboxaldehyde (Aregahegn et al., 2013). As these photosensitized reactions take very probably place at the interface of the particles, it is thought that this type of reaction can also take place at other interfaces where imidazole-2-carboxaldehyde is present, such as e.g. the sea surface microlayer.

The studies presented in this chapter in the form of 2 published articles investigate firstly the fundamental photophysical properties of this new photosensitizer by laser flash photolysis and its reactivity with 3 halides, iodide, bromide and chloride. It is shown that reactive halogen radicals are formed through photochemical oxidation of these halides and the environmental implications of such reactions are discussed. In the second article the mechanism behind the observed particle growth of aerosols containing IC is investigated by UPLC-HRMS analysis of grown aerosol samples. In presence of limonene as VOC, the photoinduced particle growth is explained by the reactive uptake of limonene in the particulate phase, leading to lower volatility oxidative products and the observed particle growth. A reaction mechanism initiated by a hydrogen abstraction on the VOC is proposed and environmental implications are discussed.

Chapter IV: Photosensitized reactions induced by imidazole-2-carboxaldehyde at interfaces

IV. 1. A time resolved study of the multiphase chemistry of excited carbonyls: imidazole-2-carboxaldehyde and halides

Authors : Liselotte Tinel, Stéphane Dumas, Christian George

Published in Compte Rendu de Chimie, 2014, volume 17, issue 7-8, pages 801-807.

IV.1.1. Introduction

A significant fraction of the carbon atoms present in dissolved natural organic material bears carbonyl groups (Averett et al., 1994). These carbonyls, and more particularly aromatic carbonyls, are thought to be important photooxidants for various phenols present in natural waters. Aromatic ketones absorb in the natural emission spectrum of the sun and their photoactivated states react with phenols at rates close to the diffusion-controlled limit (Foote and Pryor, 1976). Canonica and co-workers brought into evidence that this photooxidation involved proton or electron transfer from the triplet excited state of the carbonyl functionalities, which showed to be important oxidants despite their rather short lifetime (Canonica et al., 2000; Canonica et al., 1995a). Aromatic ketones, like benzophenone, also oxidize efficiently sea salt halides after absorption of actinic sunlight (Jammoul et al., 2009a). Photosensitized reactions of aromatic carbonyls are not only a known pathway for the formation of oxidants in natural waters, but showed also to be an important source of hydrogen peroxide in atmospheric aerosols (Vione et al., 2006).

Imidazole-2-carboxaldehyde (IC), bearing a carbonyl function, and other imidazoles get growing interest in atmospheric chemistry, since their presence in secondary organic aerosols (SOA) has been explained by a catalytic process *in situ* involving ammonium salts and glyoxal, an ubiquitous organic compound in the troposphere (Nozière et al., 2008; Yu et al., 2011). This catalytic product formation in aerosols explains part of the missing glyoxal in

the gas-phase through an uptake of glyoxal that was ignored for a long time (Galloway et al., 2009; Volkamer et al., 2009a). Recently, it has been shown that imidazole-2-carboxaldehyde, one of the products formed by the 'iminium-pathway', can efficiently photo-induce the growth of aerosols (Aregahegn et al., 2013). This compound is thus a secondary formed photosensitizer and can play an important role in SOA growth in the absence of gas-phase oxidants under light conditions. The presence of these nitrogen containing compounds in particles can also lead to changes in the optical properties of the aerosol, hence affecting the aerosols' radiative forcing and cloud properties (Kampf et al., 2012b; Trainic et al., 2012).

Imidazole compounds are also known to be present in the sea and at the sea surface microlayer (SML) (Forte et al., 2009; Lion and Leckie, 1981). Glyoxal has been measured in the marine boundary layer (MBL) (Sinreich et al., 2010) and amines are an important constituent of marine aerosols (Facchini et al., 2008), which comforts the hypothesis of formation of imidazoles in the marine environment. The SML shows also an enrichment of nitrogen content during periods of high biological activity (Liss and Duce, 1997). The organic-enriched SML, the thin interfacial zone between the atmosphere and the subsurface water, presents different chemical and physical features than the underlying water and plays an important role in the sea-air chemical interactions. Ozone loss from the marine boundary layer (MBL), for example, can occur through the reactive uptake of ozone by plant exudates such as chlorophyll present in the SML (Clifford et al., 2008; Martino et al., 2012; Reeser et al., 2009b). SML samples also feature higher absorption in UV-region than the bulk, implying that photochemical processes can be important in transformations in and between dissolved and particulate matter (Liss and Duce, 1997).

Photoactive compounds, found in a higher concentration in the SML than in the underlying water, can also produce active halogen species after oxidation of the halides present in the MBL, both as aerosols and in the sea water. Photo-activated aromatic carbonyls, like benzophenone, and other photoactive compounds like chlorophyll, can lead to the formation of the reactive radical anion ($X_2^{\bullet-}$) and molecular halogens, that can be released in the gas-phase (Jammoul et al., 2009a; Reeser et al., 2009a). This kind of direct photochemical reactions at the interface could account for a part of the halides observed over open oceans (O'Dowd and de Leeuw, 2007). Gas-phase halogen atoms, especially iodine and bromine, will set in catalytic cycles of ozone destruction in the MBL, thus changing locally the oxidizing capacities. Gas-phase iodine chemistry can also give rise to

particle formation (Carpenter, 2003; Jimenez et al., 2003), while chlorine will be incline to oxidize hydrocarbons (McFiggans et al., 2004). Other sources of such reactive halogen atoms in the MBL include photolysis of polyhalogenated compounds emitted by algae (Saiz-Lopez and von Glasow, 2012), heterogeneous chemistry of ozone or NO_y on snow or sea-salt particles (Abbatt et al., 2012) and particularly for chlorine, photochemical reactions at the air-sea interface (Oum et al., 1998). Halogen chemistry is thus profoundly entwined with the aerosol production and oxidizing strength of the MBL, affecting potentially the cloud condensation nuclei and hence climate change.

The aim of this work is to explore the photochemical properties of imidazole-2-carboxaldehyde (IC), a secondary photosensitizer potentially present in the marine environment and known to induce particle growth as a secondary formed photosensitizer and to examine the bimolecular rate coefficients of this compound in presence of halide anions, Cl^-, Br^- and I^- by means of laser flash photolysis.

IV.1.2. Experimental

IV.1.2.a. Laser flash photolysis:

The transient absorption spectrum of the excited IC was followed with a classical laser flash photolysis apparatus (Reeser et al., 2009b). The photolysis excitation source was the third harmonic (266 nm, pulse width ~7 ns) of a Nd:YAG laser (Surelite II 10, Continuum) operated in the single-shot mode. The choice of the wavelength is justified by the maximum of absorption of IC at 290 nm, as can be seen from the absorption spectrum shown on figure IV-1, even if it has been shown that at wavelengths > 290 nm, IC can induce a photosensitized reaction (Aregahegn et al., 2013).

During the experiments, the laser pulse energy was limited at 15 mJ per pulse (~39 mJ/cm²) to limit as much as possible photolysis of the photosensitizer and therefore the possible interferences of its products on the studied chemistry, but also two photons excitation. The laser output passed through the aperture in the short axis (4 mm path length) of a fully masked quartz flow cell, mounted at 13 cm of the laser output. The solution containing the photosensitizer was introduced in the flow cell of 450 µL by means of a peristaltic pump, with a flow of 1.6 mL/min, ensuring a complete purge of the exposed volume every 17 seconds. This limited the exposition of the introduced solution to 3-4 laser

shots and maintained a constant temperature in the flow cell. All connections where made from either glass or PTFE tubing, ensuring a clean liquid flow.

Transient species produced by the pulsed laser beam were monitored by means of time-resolved absorption spectroscopy. The analyzing light, provided by a 75 W high-pressure Xenon arc lamp (LOT-Oriel), passed through the two apertures of long axis of the flow cell (1 cm path length). The light was then collected by a ¼ m monochromator (Spectral Products DK240) equipped with a 2400 grooves/mm grating and detected by a photomultiplier (Hamamatsu H7732-01). The PMT signal was passed through a high-speed current amplifier/discriminator (Femto) and the AC component recorded on a 300 MHz oscilloscope (Tektronix TDS3032c). The digitalized signal was then transferred to a computer for further processing. Typically, 16 measurements were averaged at each wavelength to obtain a transient absorption spectrum, with an accuracy of 3%. The full transient absorption spectrum was then reconstructed from the steady and transient signals. For construction of an absorption spectrum, measurements were repeated every 10-20 nm between 320 nm and 720 nm, limits determined by the measuring system; for the kinetics, the probe wavelengths for the transient absorption decay of triplet state of IC were 330 nm and 350 nm.

For the analysis of triplet state decays of IC in pure water, linear regression on a logarithmic plot of the data and a mono-exponential decay model fits were performed on the same data sets. As the results of both fitting methods were comparable, we will here only present the results obtained by non-linear fits.

IV.1.2.b. Materials and solutions:

All the experiments were performed at room temperature in the range 295-300 K. Aqueous solutions containing 0.25mM of IC were deoxygenated with nitrogen for 20 minutes prior to analysis and kept under a continuous stream of nitrogen during the experiment. All solutions were freshly prepared using 18MΩ ultra pure water (ELGA) and were put in an ultrasonic bath for 10 min. to promote solubility. The chemicals used in this study - imidazole-2-carboxaldehyde (Aldrich, 97%), sodium chloride (>99% Sigma-Aldrich), sodium iodide (>99% Sigma-Aldrich), sodium bromide (>99% Sigma-Aldrich) – were all used without further purification. The known impurity of bi-imidazole in the commercial imidazole-2-carboxaldehyde did not notably interfere, since no absorption for triplet state bi-imidazole

was detected. In our conditions, aqueous solutions of pH 6.5, IC is expected to be in its aldehyde form (Lázaro Martínez et al., 2010).

IV.1.3.Results

IV.1.3.a. Characteristics of the triplet state imidazole-2-carboxaldehyde

Laser flash photolysis of N_2-saturated solutions of 0.25 mM IC in pure water showed strong transient absorptions, as shown in figure IV-1. The transient absorption of excited IC also shows intense fluorescence in the first nanoseconds after the laser pulse. Figure IV-1 shows recorded transient absorption spectra at different time intervals after the laser pulse, demonstrating the uniform decrease of the absorbance without formation of any significant band. The absorption spectrum can thus be attributed to the triplet-triplet absorption of ^{3}IC* and was recorded for the first time, since very little is known about the photochemistry of IC. The transient absorption spectrum recorded after the laser pulse is characterized by a strong absorption peak with a maximum absorption wavelength around 330 nm and a weaker broad absorption band around 650 nm. For the determination of lifetimes and quenching rate coefficients, the decay of the triplet state was monitored at 330 nm.

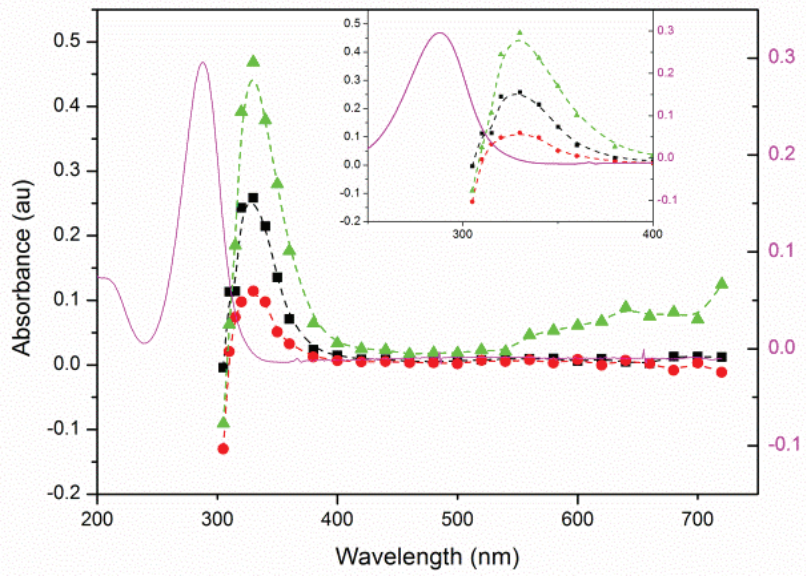

Figure IV-1: Absorption spectrum of aqueous solution of IC (0.25 mM) recorded 330 ns (▲), 1 µs (■) and 2 µs (●)after the laser pulse. The pink solid line (–) shows the absorption spectrum of a solution of 0.25 mM IC (right Y scale). The insert is a zoom of the spectrum from 250 nm to 400 nm.

The absorption decay trace of excited ^{3}IC* at 330 nm fitted well a single exponential process of the form:

$$y = a + be^{-tk_1} \qquad \textit{(equation IV-1)}$$

over the 0-10 µs region with k_1= (8.87 ±0.11) × 10^5 s^{-1}. The lifetime of the triplet state of IC, defined as

$$\tau = \frac{1}{k_1} \qquad \textit{(equation IV-2)}$$

could thus be determined and was found to be τ =1.21 µs in a deoxygenated solution. This lifetime seems to be in accordance with a triplet state excitation, for which lifetimes are expected to be in the range of 10^{-7} to 1s (Braun et al., 1986). Other photosensitizers like pterin have a reported triplet state lifetime of the same order (2.3 ± 0.2 µs) (Chahidi et al., 1981).

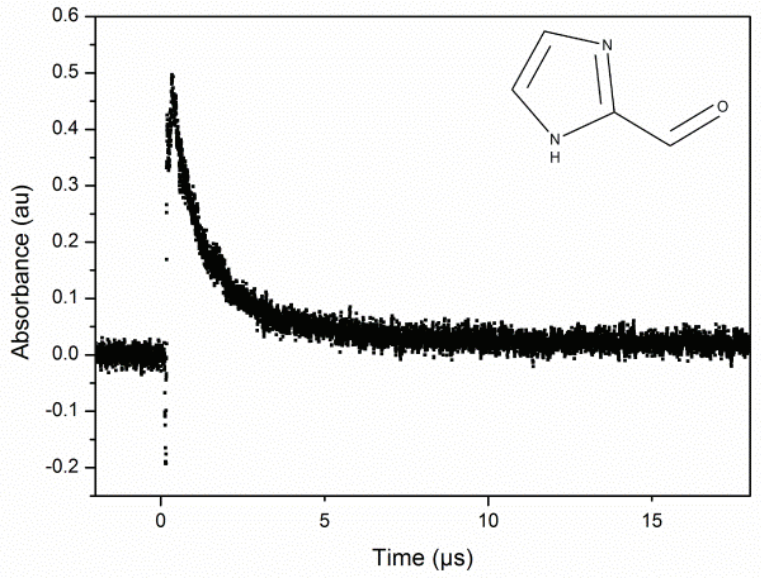

Figure IV-2: Transient absorption decay obtained at 330 nm of the IC triplet state in a deoxygenated aqueous solution of 0.25 mM IC

In presence of oxygen, the lifetime of the triplet state decreased in an oxygen saturated solution, which indicates that an energy transfer to oxygen is possible. In an air saturated solution the quenching constant for the reaction with oxygen was estimated at 3.9 x 10^9 $M^{-1}s^{-1}$, assuming that the concentration of oxygen is described by Henry's law. This fast energy transfer could generate reactive oxygen species such as singlet oxygen or superoxide anions.

VI.1.3.b. Quenching

The reaction of ^{3}IC* with 3 sea salt halides i.e. chloride, bromide and iodide was investigated. These salts are present in different and varying concentrations in the seawater (and aerosols); the average chloride concentration is around 0.54 M, bromide concentration around 0.84 mM and iodide varying between 0.02 µM and 0.4 µM (Chang et al., 2004; Kennish, 2000). Previous studies have shown that sea salts, like phenols, can act as electron donors towards the excited carbonyls forming reactive halide radicals (Canonica et al., 2000; Jammoul et al., 2009a). The reaction mechanism for the growth of aerosols containing traces of IC, proposed by Aregahegn (Aregahegn et al., 2013), suggests that the excited state ^{3}IC* can act through a proton or an electron transfer from limonene towards IC. In this study, photoactivated IC is expected to interact with the halide anions by electron transfer to produce atomic halogens (Jammoul et al., 2009a):

$$^3IC^* + X^- \rightarrow IC^{\bullet -} + X^{\bullet} \qquad (1)$$

The reactivity of the three quenchers was investigated by introducing NaI, NaBr or NaCl in different concentrations in deoxygenated aqueous solutions of IC, with a large excess of the quencher towards the photosensitizer, respecting pseudo-first order conditions. The quenching rates coefficients for ^{3}IC* in presence of the halides were determined by the Stern-Volmer equation (equation IV-3):

$$-\frac{d[\,^3IC^*]}{dt} = \left(k_0 + k_q[X^-]\right)[\,^3IC^*] = k_{obs}[\,^3IC^*] \qquad \textit{(equation VI-3)}$$

where k_0 is the rate coefficient of the triplet state decay in the absence of oxygen and k_q the rate coefficient for the quenching process by the halide X^- (Braun et al., 1986). A Stern-Volmer plot of the observed rate coefficient k_{obs} in function of the concentration of the quencher X^- permits to obtain the quenching rate coefficient k_q from the slope of the curve.

Iodide

The decay of the triplet-triplet absorption monitored at 330 nm in the presence of NaI showed still a mono-exponential decay, but decreased much faster in presence of increasing concentration of I^- (figure IV-3). The quenching rate coefficient $k_q(I^-)$ obtained for ^{3}IC* by I^- from the slope of the Stern-Volmer plot shown figure IV-4, is $k_q(I^-) = (5.33 \pm 0.25) \times 10^9$ M^{-1} s^-

[1]. The high rate coefficient obtained is close to the diffusion controlled limit and shows that the quenching by the iodide anion is highly efficient.

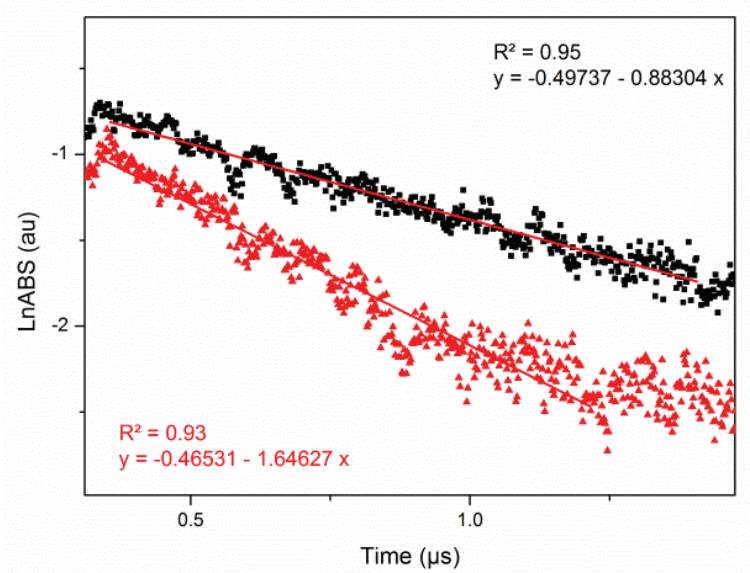

Figure IV-3: Log plot of a transient absorption decay obtained at 330 nm of the IC triplet state in a deoxygenated aqueous solution of 0.25 mM IC alone (■) and in presence of 0.25 mM NaI (▲) and the linear fits showing a greater slope in presence of NaI

Bromide

Triplet-triplet absorption decay of IC was also faster in presence of increasing concentrations of NaBr, remaining mono-exponential at 330 nm for concentrations of bromide < 200 mM. From the Stern-Volmer plot (figure IV-4), the quenching rate coefficient determined was $k_q(Br^-) = (6.27 \pm 0.53) \times 10^6\ M^{-1}\ s^{-1}$ for bromide. The quenching rate coefficient is orders of magnitude lower than the quenching rate for iodide and also quite slow compared to the rates obtained with other photosensitizers, such as benzophenone, where values for quenching rates for bromide are comprised between 2.2 - 3.5 $\times 10^8\ M^{-1}\ s^{-1}$ (Jammoul et al., 2009a; Murov et al., 1993).

Chloride

In the presence of chloride, the absorbance of ^{3}IC* showed only small decreased lifetimes, even with chloride concentrations up to 1 M (figure IV-4). The quenching rate coefficient determined is $k_q(Cl^-) = (1.31 \pm 0.16) \times 10^5\ M^{-1}\ s^{-1}$ and in view of the coefficients obtained for the other halides, we can conclude that the quenching of triplet state IC by chloride is not efficient.

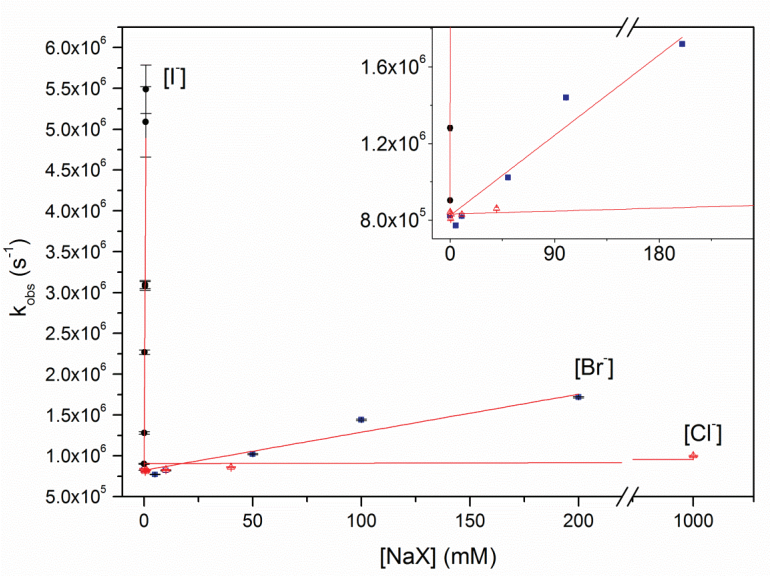

Figure IV-4: Stern-Volmer plot of the pseudo-first order rate coefficients k_{obs} of IC triplet state quenching in function of the halide concentrations.

Comparison of the three quenchers

When considering the three quenching rate coefficients, it comes into evidence that the quenching rate coefficients are linked to the oxidation potentials of the used halides. Table 1 lists the quenching rate coefficients and the oxidation potentials for each halide. For the halide with the lowest oxidation potential, iodide, the quenching rate coefficient obtained is four orders of magnitude higher than the quenching rate coefficient obtained for chloride. It seems thus probable that the excited triplet state of IC is quenched by these halides by an electron transfer towards ^{3}IC*. Electron transfer from a halide (X^-) to the excited triplet state of a carbonyl compound yields a halide radical and a ketyl radical.

Such an intramolecular electron transfer is usually described by a mechanism, schematized in reaction (2), involving the formation of a contact complex, after which the electron transfer takes place and a charge complex is formed. Finally, the charge complex breaks up and oxidized donor and reduced acceptor are separated.

$$^3(IC)^* + X^- \rightleftarrows [\,^3(IC)^* \bullet\bullet\bullet X^-] \rightleftarrows [\,IC^{\bullet-} \bullet\bullet\bullet X^{\bullet}] \rightarrow IC^{\bullet-} + X^{\bullet} \qquad (2)$$

This mechanism requires the free enthalpy of the electron transfer (ΔG_{ET}) to be negative or close to zero for the electron transfer to become thermodynamically favorable (Jammoul et al., 2009a; Murov et al., 1993) . It could be interesting to compare the free enthalpy of the

Table IV-1: The oxidation potential $E(X^-/X)$ of each halide and their quenching rate coefficients K_q obtained for $^3IC^*$. Oxidation potentials were taken from (Hurley et al., 1988)

Quencher	$E(X/X^-)$ (V)	k_q (M^{-1} s^{-1})
Cl^-	2.6	$(1.31 \pm 0.19) \times 10^5$
Br^-	1.93	$(6.27 \pm 0.53) \times 10^6$
I^-	1.33	$(5.33 \pm 0.25) \times 10^9$

electron transfer for each quencher, if the reduction potential of IC and the energy of the triplet state of the photosensitizer were known. It seems that iodide, the halide with the lowest electronegativity, will be the best electron donor and consequently the most efficient quencher, hence the highest rate coefficient determined. Chloride on the other hand displays the highest electronegativity and oxidation potential and is a poor electron donor. The rate coefficient of the quenching with chloride was, as expected, lower than for bromide and iodide. The energy of triplet state IC is thus expected to be higher than the oxidation energy of iodide and lower than the oxidation energy of bromide, since the rate for the electron transfer from iodide is close to the diffusion limited rate but substantially lower for bromide. The electron transfer from chloride is thermodynamically unfavorable as is reflected by the very low rate coefficient.

IV.1.4. Discussion

In the mechanism (reaction 2) proposed above, there is formation of halogen atom radicals. These radicals are very reactive, can form secondary products and give rise to transient product absorption. By establishing transient absorption spectra at different times after the laser pulse and for different concentrations of halogens, transient absorption products could be detected in presence of iodide and bromide. No radical product formation was observed following the excitation of IC in presence of chloride, since the quenching reaction with chloride was shown to be much slower.

IV.1.4.a. Iodide

As mentioned in the previous section, the decays of absorption of ^{3}IC* in presence of iodide could be fitted by a mono-exponential function at wavelengths around 330 nm, the maximum absorption of ^{3}IC*. At longer wavelengths, particularly at 380 nm, as illustrated by figure IV-5, the decays fitted a bi-exponential decay of the form:

$$y = a + b_1 e^{-tk_1} + b_2 e^{-tk_2} \qquad \textit{(equation IV- 4)}$$

providing evidence for the existence of a species with a short lifetime and a species with a longer lifetime absorbing at this wavelength. The short lifetime could be attributed to the absorption of ^{3}IC*, since the lifetime of this species increased with decreasing NaI

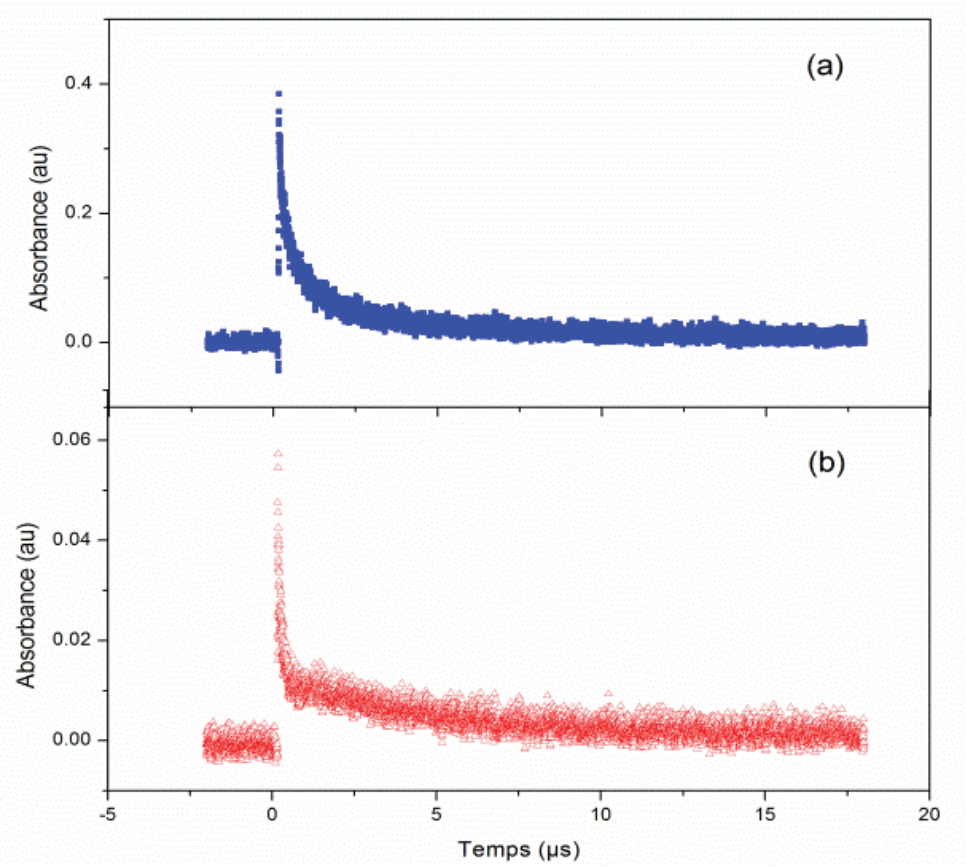

Figure VI-5: Transient absorption decay of ^{3}IC (a) in presence of 300 mM NaBr (■) monitored at 355 nm and (b) in presence of 0.4 mM NaI (Δ) monitored at 380 nm, showing a bi-exponential decay.*

concentration, leading to a decay similar to the decay of ^{3}IC* in pure water at that wavelength, and tending to be mono-exponential at low NaI concentrations (0.1 mM).

After comparison of absorption spectra at different times after the laser pulse, the absorption at 380 nm of the species with the longer lifetime could be observed several µs after the laser pulse and was stronger, though still low, than the absorption of a solution of IC in pure water (figure IV-6). The comparison of the absorption spectrum of ^{3}IC* in pure water with the absorption spectrum of ^{3}IC* in presence of 0.4 mM of NaI after shorter time intervals after the laser pulse, illustrated by the insert of figure IV-6, does not feature this enhanced absorption around 380 nm. This indicates clearly a secondary formation for the species absorbing at 380 nm.

One of the products that are possibly formed by the atom radical I$^\bullet$ is the radical anion $I_2^{\bullet-}$, formed by the combination of the anion with the oxidized halide radical. This well known transient species is relatively stable and shows absorption maxima at 385 nm and at 725 nm, hence showing a long lifetime (Devonshire and Weiss, 1968; Ershov and Janata, 2003; Hug, 1981). Our system did not permit to detect the second absorption peak of $I_2^{\bullet-}$ at 725 nm, which intensity is expected to be 3.5 times lower than the intensity of the peak

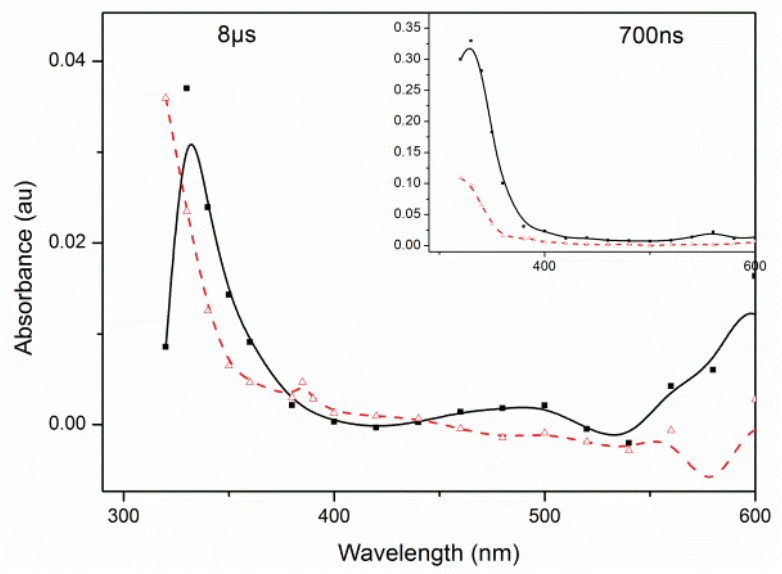

Figure IV-6: Absorption spectrum of IC (0.25 mM) in presence of NaI (0.4mM) registered at 8 µs after the laser pulse, showed as ---Δ, featuring a peak around 385 nm, not observed in the absorption spectrum of IC alone (-■). At shorter times after the laser pulse (700 ns, insert), the spectrum of IC in presence of NaI (---Δ) is less intense at all wavelengths than the spectrum of IC only (-■).

around 385 nm. The peak of $I_2^{\bullet-}$ is low, despite the rather high molar absorption of this transient species (9600 cm^{-1} mol^{-1}) (Hug, 1981). This could be explained by rapid I_2 formation (Mulazzani and Buxton, 2006) or by fast scavenging reactions of $I^{\bullet}$ and $I_2^{\bullet-}$, limiting the amount of $I_2^{\bullet-}$ detected, as has been showed in the case of chloride (Buxton et al., 2000). These radical reactions are possible with the solvent or with the photosensitizer (Bũchler and Bũhler, 1976; Jammoul et al., 2009a), which could explain the high absorption, even 8 µs after the laser pulse at wavelengths < 330 nm (figure IV-6). The radical $I_2^{\bullet-}$ is the only species expected to absorb at 380 nm and the peak can thus distinctively be attributed to this transient species. The absorption at shorter wavelengths cannot be completely monitored with our system and would not be characteristic for one expected transient species.

IV.1.4.b. Bromide

The transient species formed after the photooxidation of bromide by ^{3}IC* were more difficult to follow, since the absorbance of one the expected products, $Br_2^{\bullet-}$, was overlapping with the absorbance of triplet state IC. Nonetheless, the fitted curves at the maximum absorption, 330 nm, of the triplet state IC, showed a mono-exponential decay in presence of bromide concentrations in the range of 1 – 200 mM. The decay became bi-exponential for wavelengths around 354 nm, the maximum absorption of $Br_2^{\bullet-}$ in water (Lampre et al., 2013), indicating secondary product formation. As in the case of iodide, two species with distinct lifetimes could be distinguished, the short lived ascribed to the decay of ^{3}IC*. On the absorption spectrum (figure IV-7) taken 10 µs after the laser pulse, the absorption around 360 nm is higher in presence of bromide than the absorption obtained with IC alone. This could be due to the formation of $Br_2^{-\bullet}$, a strong absorbing radical species (ε_{max} = 9900 M^{-1} cm^{-1} (Mulazzani and Buxton, 2006)) formed from the reaction of $Br^{\bullet}$ with Br^-.

Figure IV-7 also shows increased absorption for wavelengths shorter than 355 nm, even at long times after the laser pulse, absorption not explained by the triplet state IC absorption. This absorption, detected only partially with our apparatus, shows a large peak with a rather long lifetime. Products contributing to this absorption could be recombination products of IC with $Br^{\bullet}$ or the very strong absorbing Br_3^- (ε_{max} = 40 900 M-1 cm-1, λ_{max} = 266 nm (Mirdamadi-Esfahani et al., 2009)).

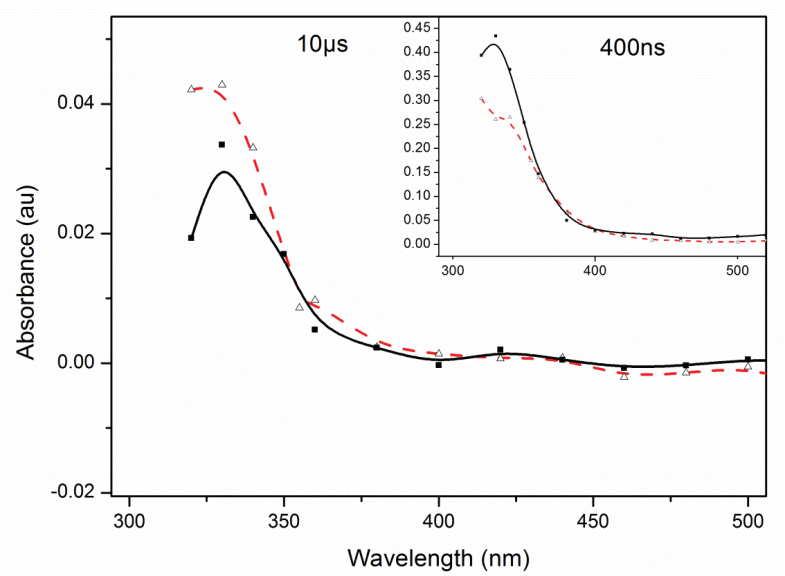

Figure IV-7: Absorption spectrum of IC (0.25 mM) in presence of NaBr (300 mM) showing higher absorption around 360 nm (---Δ) than the absorption spectrum of IC alone (-■), registered at 10 µs after the laser impuls. At shorter times after the laser impuls (400 ns, insert), the spectrum of IC in presence of NaBr (---Δ) is less intense at all wavelengths than the spectrum of IC only (-■).

The absorption of $Br_2^{\bullet-}$ seems rather low, indicating that $Br_2^{\bullet-}$ is not a major product of this photooxidative process. This could be due to Br_2 formation or scavenging reactions of $Br^{\bullet}$ and $Br_2^{\bullet-}$ by the solvent or the photosensitizer (Ershov, 2004). One of the products possibly formed from the reaction of $Br^{\bullet}$ with water is $BrOH^{\bullet-}$ (Ershov, 2004). This radical shows a maximum absorption at 352 nm, very similar, but less intense, to the absorption $Br_2^{\bullet-}$ (Lampre et al., 2013), but the reaction of $Br^{\bullet}$ with water is very slow ($k = 1.4\ s^{-1}$, in (Ershov, 2004)). Even if the absorption at this wavelength cannot be unambiguously ascribed to $Br_2^{\bullet-}$ the formation of $BrOH^{\bullet-}$ can thus be considered negligeable.

IV.1.4.c. Proposed mechanism

To resume the reactions and the formation of the products detected, the proposed mechanism involves the following reactions:

$$IC^* + X^- \rightarrow IC^{\bullet-} + X^{\bullet} \quad (3)$$

$$X^{\bullet} + IC \rightarrow \text{products} \quad (4)$$

$$X^{\bullet} + X^- \rightleftarrows X_2^{\bullet-} \quad (5)$$

$$X_2^{\bullet-} + IC \rightarrow \text{products} \quad (6)$$

$$X_2^{\bullet-} + X_2^{\bullet-} \rightleftarrows X_3^- + X^- \quad (7)$$

$$X_3^- \rightleftarrows X_2 + X^- \quad (8)$$

$$X^{\bullet} + X^{\bullet} \rightarrow X_2 \quad (9)$$

$$X_2^{\bullet-} + X_2^{\bullet-} \rightarrow X_2 + 2X^- \quad (10)$$

$$X_2 \rightleftarrows X_2\,(g) \quad (11)$$

This mechanism explains the formation of reactive radicals and can lead to the formation of halogen molecules in the gas phase.

IV.1.5. Conclusions and atmospheric implications

Our results confirm the role of IC as photosensitizer proposed by Aregahegn (Aregahegn et al., 2013), for the first time evidencing the existence of a triplet state for this compound. The lifetime of $^3IC^*$ is estimated at 1.21 µs in a deoxygenated aqueous solution and the maximum absorbance was measured at 330 nm.

The triplet state of IC was efficiently quenched by iodide, $k_q(I^-) = (5.33 \pm 0.25) \times 10^9\ M^{-1}\ s^{-1}$, and much less by bromide, $k_q(Br^-) = (6.27 \pm 0.53) \times 10^6\ M^{-1}\ s^{-1}$. Chloride showed a slow quenching rate, $kq(Cl^-) = (1.31 \pm 0.16) \times 10^5\ M^{-1}\ s^{-1}$ and reactions with chloride might thus be negligible. Reactions with these halides form atomic halogens, some of which could be detected by increased transient absorption. Also, the quenching rate constants show the same trends as the oxidation potential of each sea salt anion, suggesting an electron transfer is the mechanism behind the photooxidation of the halides.

Imidazole-2-carboxaldehyde showed to be a quite efficient photosensitizer and, as IC can also be formed in aerosols in presence of glyoxal and ammonia, its presence, even in traces, could have an important influence on the particle phase chemistry at the interface of aerosols. Its photosensitized reactions can lead to an uptake of gas-phase VOCs and lead to particle growth, as demonstrated by the works in (Aregahegn et al., 2013). The photochemical radical production mechanism initiated by carbonyl compounds proposed in this study is potentially important in the SML, not only in reactions with sea salts but also for the oxidation of other organic compounds with a one electron oxidation potential. Indirectly, photochemistry evidenced for IC and other carbonyl compounds may also influence the chemistry of the SML by the radicals and secondary products formed during this process and the MBL by the release of reactive (halogenated) species, such as Br_2, $Br_2^{\bullet-}$, I_2 and $I_2^{\bullet-}$ in the gas-phase (Aregahegn et al., 2013; Jammoul et al., 2009a).

IV.1.6. Affiliations of the authors

All authors :

Université de Lyon 1, Lyon, F-69626, France, CNRS, UMR5256, IRCELYON, Institut de Recherches Sur la Catalyse et l'Environnement de Lyon, Villeurbanne, F-69626, France

IV.1.7. References

Abbatt, J.P.D. et al., 2012. Halogen activation via interactions with environmental ice and snow in the polar lower troposphere and other regions. Atmospheric Chemistry and Physics, 12(14): 6237-6271.

Aregahegn, K.Z., Noziere, B. and George, C., 2013. Organic aerosol formation photo-enhanced by the formation of secondary photosensitizers in aerosols. Faraday Discussions, 165: 123-134.

Averett, R.C., Leenheer, J.A., McKnight, D.M. and Thorn, K.A., 1994. Humic substances in the Suwannee River, Georgia; interactions, properties, and proposed structures. 2373.

Braun, A.M., Maurette, M.-T. and Oliveros, E., 1986. Technologie photochimique. Presses polytechniques romandes.

Būchler, H. and Bühler, R., 1976. The radical ion complex IOH−: Spectrum and reactions studied by pulse radiolysis of aqueous iodide solutions. Chemical Physics, 16(1): 9-18.

Buxton, G.V., Bydder, M., Salmon, G.A. and Williams, J.E., 2000. The reactivity of chlorine atoms in aqueous solution. Part III. The reactions of Cl-center dot with solutes. Physical Chemistry Chemical Physics, 2: 237-245.

Canonica, S., Hellrung, B. and Wirz, J., 2000. Oxidation of Phenols by Triplet Aromatic Ketones in Aqueous Solution. The Journal of Physical Chemistry A, 104: 1226-1232.

Canonica, S., Jans, U., Stemmler, K. and Hoigne, J., 1995. Transformation Kinetics of Phenols in Water: Photosensitization by Dissolved Natural Organic Material and Aromatic Ketones. Environmental Science & Technology, 29: 1822-1831.

Carpenter, L.J., 2003. Iodine in the marine boundary layer. Chemical Reviews, 103: 4953-4962.

Chahidi, C., Aubailly, M., Momzikoff, A., Bazin, M. and Santus, R., 1981. photophysical and photosensitizing properties of 2-amino-4 pteridinone - a natural pigment. Photochemistry and Photobiology, 33: 641-649.

Chang, W.N., Heikes, B.G. and Lee, M.H., 2004. Ozone deposition to the sea surface: chemical enhancement and wind speed dependence. Atmospheric Environment, 38(7): 1053-1059.

Clifford, D., Donaldson, D.J., Brigante, M., D'Anna, B. and George, C., 2008. Reactive uptake of ozone by chlorophyll at aqueous surfaces. Environmental Science & Technology, 42(4): 1138-1143.

Devonshire, R. and Weiss, J.J., 1968. Nature of the transient species in the photochemistry of negative ions in aqueous solution. The Journal of physical chemistry, 72(11): 3815-3820.

Ershov, B.G., 2004. Kinetics, mechanism and intermediates of some radiation-induced reactions in aqueous solutions. Uspekhi Khimii, 73: 107-120.

Ershov, B.G. and Janata, E., 2003. The reduction of I-2 by 1-hydroxyalkyl radicals in aqueous solution. A pulse radiolysis study. Chemical Physics Letters, 372: 195-198.

Facchini, M.C. et al., 2008. Important Source of Marine Secondary Organic Aerosol from Biogenic Amines. Environmental Science & Technology, 42: 9116-9121.

Foote, C. and Pryor, W.A., 1976. Free radicals in biology. by WA Pryor, Academic Press, New York, 2: 85.

Forte, B. et al., 2009. A Submarine Journey: The Pyrrole-Imidazole Alkaloids. Marine Drugs, 7(4): 705-753.

Galloway, M.M. et al., 2009. Glyoxal uptake on ammonium sulphate seed aerosol: reaction products and reversibility of uptake under dark and irradiated conditions. Atmospheric Chemistry and Physics, 9(10): 3331-3345.

Hug, G.L., 1981. Optical spectra of nonmetallic inorganic transient species in aqueous solution, DTIC Document.

Hurley, J.K., Linschitz, H. and Treinin, A., 1988. interaction of halide and pseudohalide ions with triplet benzophenone-4-carboxylate - kinetics and radical yields. Journal of Physical Chemistry, 92: 5151-5159.

Jammoul, A., Dumas, S., D'Anna, B. and George, C., 2009. Photoinduced oxidation of sea salt halides by aromatic ketones: a source of halogenated radicals. Atmospheric Chemistry and Physics, 9: 4229-4237.

Jimenez, J.L. et al., 2003. Ambient aerosol sampling using the Aerodyne Aerosol Mass Spectrometer. Journal of Geophysical Research: Atmospheres, 108: 8425.

Kampf, C.J., Jakob, R. and Hoffmann, T., 2012. Identification and characterization of aging products in the glyoxal/ammonium sulfate system – implications for light-absorbing material in atmospheric aerosols. Atmospheric Chemistry and Physics, 12(14): 6323-6333.

Kennish, M.J., 2000. Practical handbook of marine science. crc press.

Lampre, I. et al., 2013. Oxidation of Bromide Ions by Hydroxyl Radicals: Spectral Characterization of the Intermediate BrOH•–. The Journal of Physical Chemistry A, 117(5): 877-887.

Lázaro Martínez, J.M., Romasanta, P.N., Chattah, A.K. and Buldain, G.Y., 2010. NMR characterization of hydrate and aldehyde forms of imidazole-2-carboxaldehyde and derivatives. The Journal of organic chemistry, 75(10): 3208-3213.

Lion, L.W. and Leckie, J.O., 1981. The biogeochemistry of the air-sea interface. Annual Review of Earth and Planetary Sciences, 9: 449-486.

Liss, P.S. and Duce, R.A. (Editors), 1997. Sea Surface and Global Change. Cambridge University Press, Cambridge, 509 pp.

Martino, M., Lézé, B., Baker, A.R. and Liss, P.S., 2012. Chemical controls on ozone deposition to water. Geophysical Research Letters, 39(5): L05809.

McFiggans, G. et al., 2004. Direct evidence for coastal iodine particles from Laminaria macroalgae–linkage to emissions of molecular iodine. Atmospheric Chemistry and Physics, 4(3): 701-713.

Mirdamadi-Esfahani, M., Lampre, I., Marignier, J.-L., de Waele, V. and Mostafavi, M., 2009. Radiolytic formation of tribromine ion Br 3− in aqueous solutions, a system for steady-state dosimetry. Radiation Physics and Chemistry, 78(2): 106-111.

Mulazzani, Q.G. and Buxton, G.V., 2006. On the kinetics and mechanism of the oxidation of I- by (OH)-O-center dot/O center dot- in alkaline aqueous solution. Chemical Physics Letters, 421(1-3): 261-265.

Murov, S.L., Carmichael, I. and Hug, G.L., 1993. Handbook of photochemistry. CRC Press.

Nozière, B., Dziedzic, P. and Córdova, A., 2008. Products and Kinetics of the Liquid-Phase Reaction of Glyoxal Catalyzed by Ammonium Ions (NH4+). The Journal of Physical Chemistry A, 113(1): 231-237.

O'Dowd, C.D. and de Leeuw, G., 2007. Marine aerosol production: a review of the current knowledge. Philosophical Transactions of the Royal Society A: Mathematical, Physical and Engineering Sciences, 365: 1753-1774.

Oum, K.W., Lakin, M.J., DeHaan, D.O., Brauers, T. and Finlayson-Pitts, B.J., 1998. Formation of molecular chlorine from the photolysis of ozone and aqueous sea-salt particles. Science, 279: 74-77.

Reeser, D.I., George, C. and Donaldson, D.J., 2009a. Photooxidation of Halides by Chlorophyll at the Air-Salt Water Interface. Journal of Physical Chemistry A, 113: 8591-8595.

Reeser, D.I. et al., 2009b. Photoenhanced Reaction of Ozone with Chlorophyll at the Seawater Surface. Journal of Physical Chemistry C, 113: 2071-2077.

Saiz-Lopez, A. and von Glasow, R., 2012. Reactive halogen chemistry in the troposphere. Chemical Society Reviews, 41(19): 6448-6472.

Sinreich, R., Coburn, S., Dix, B. and Volkamer, R., 2010. Ship-based detection of glyoxal over the remote tropical Pacific Ocean. Atmospheric Chemistry and Physics, 10(23): 11359-11371.

Trainic, M., Riziq, A.A., Lavi, A. and Rudich, Y., 2012. Role of Interfacial Water in the Heterogeneous Uptake of Glyoxal by Mixed Glycine and Ammonium Sulfate Aerosols. Journal of Physical Chemistry A, 116(24): 5948-5957.

Vione, D. et al., 2006. Photochemical reactions in the tropospheric aqueous phase and on particulate matter. Chemical Society Reviews, 35(5): 441-453.

Volkamer, R., Ziemann, P.J. and Molina, M.J., 2009. Secondary Organic Aerosol Formation from Acetylene (C2H2): seed effect on SOA yields due to organic photochemistry in the aerosol aqueous phase. Atmospheric Chemistry and Physics, 9: 1907-1928.

Yu, G. et al., 2011. Glyoxal in Aqueous Ammonium Sulfate Solutions: Products, Kinetics and Hydration Effects. Environmental Science & Technology, 45(15): 6336-6342.

VI.2. Glyoxal induced atmospheric photosensitized chemistry leading to organic aerosol growth

Authors: Stéphanie Rossignol, Kifle Z. Aregahegn, Liselotte Tinel, Ludovic Fine, Barbara Nozière and Christian George

Published in Environmental Science & Technology, 2014, volume 48, issue 6, pages: 3218-3227

VI.2.1.Introduction

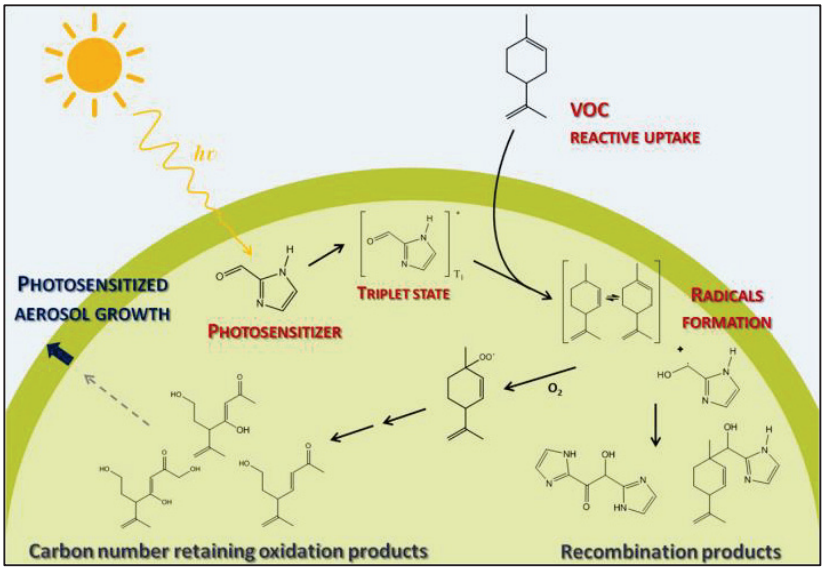

Organic aerosol (OA) represents an important fraction (20 to 90% in mass) of the total budget of atmospheric aerosols, and its oxygenated fraction, considered as mainly of secondary origin, is significant in many locations (Hallquist et al., 2009; Jimenez et al., 2009). A detailed knowledge of the formation and aging pathways of secondary organic aerosol (SOA) is thus critical to accurately assess their impact on visibility, health and climate. Traditionally, SOA formation has been described as proceeding only through gas phase oxidation of volatile organic compounds (VOC) forming low volatility products, which then partition between gas and particulate phases. However, in recent years it has become increasingly apparent that this simple model was not sufficient to accurately reproduce the OA mass observed and its oxidation state (Hallquist et al., 2009; Hodzic et al., 2009). Important efforts were thus made to explain and close the gap between observations and modeling. The classical approach including only anthropogenic and biogenic VOCs (aromatic compounds, isoprene, limonene, pinene, etc.) has been widened to include semi- and low-volatile precursors, thus bringing the calculated SOA masses closer to observations (Dzepina et al., 2009; Robinson et al., 2007; Shrivastava et al., 2011; Shrivastava et al., 2006).

However, in addition to these condensation processes, it has also been pointed out that very volatile compounds such as glyoxal can significantly contribute to SOA mass through multiphase chemistry. As glyoxal and other small di-carbonyl species are emitted in large amounts during oxidation of VOCs (Fu et al., 2008), the existence of condensed phase sinks for these gases is indeed able to explain an important part of the missing SOA mass in models (Volkamer et al., 2006; Volkamer et al., 2007; Volkamer et al., 2009b; Waxman et al., 2013) for example, at least 15% of the SOA mass in the specific case of glyoxal uptake in Mexico city (MCMA-2003 campaign) (Volkamer et al., 2007).

It was shown that glyoxal uptake into droplet and water containing aerosol particles leads to the formation of low volatility species, and thus to SOA formation, through three main processes: (1) oligomer formation, (2) photochemical radical oxidation and (3) condensation with ammonium cations (NH_4^+) and amines leading to nitrogen-containing products (Ervens and Volkamer, 2010; Lim et al., 2010). Oligomer formation occurs via acetal formation (C-O-C bond formation) (Hastings et al., 2005; Lim et al., 2010; Loeffler et al., 2006; Nozière et al., 2009). Photochemical oxidation of glyoxal is initiated by hydrogen abstraction by OH radical and leads to the formation of small organic acids, such as glyoxylic acid or formic acid, but also to the formation of larger oxygenated products through organic radical recombination in concentrated solutions (Lim et al., 2010). These two pathways (oligomerization and photochemical oxidation), are particularly interesting as they form low volatility products that can match with the high oxygen to carbon ratio (O/C) detected in ambient aerosols, not yet well reproduced in models. Although this condensation pathway is certainly minor relative to SOA mass formation (Kampf et al., 2012a), glyoxal reactivity towards ammonium cations and amines has gained interest in recent years due to the fact that it leads to the formation of compounds absorbing in the UV-visible region (Bones et al., 2010; Nozière et al., 2009; Shapiro et al., 2009). Nozière and co-workers (Nozière et al., 2009) showed that the reaction of glyoxal with NH_4^+ ions indeed forms light-absorbing nitrogen-containing species. Among these nitrogen-containing products, Galloway and co-authors have identified 1H-imidazole-2-carboxaldehyde (IC), which absorbs UV radiation at λ = 290 nm (Galloway et al., 2009). A number of laboratory studies have further confirmed the formation of products bearing an imidazole ring (De Haan et al., 2011; Trainic et al., 2011), including IC (Kampf et al., 2012a; Yu et al., 2011). It was also shown that these minor

products were nevertheless able to impact optical and radiative properties of ambient aerosols (Trainic et al., 2011).

However, the formation of such light absorbing species can also induce new photochemical processes within the aerosol particles and/or at the gas/particle interfaces. Monge and co-workers found experimental evidence of a photoinduced pathway for organic aerosol growth (Monge et al., 2012). The growth was observed when seeds containing light absorbing material [e.g., humic acid or 4-(benzoyl)benzoic acid] were exposed to light and gaseous VOCs, suggesting a reactive uptake for the latter under irradiation. Interestingly, a similar observation was made with IC-containing seeds by Aregahegn and co-authors who, based on the works of Canonica, suggested a photosensitized mechanism where radical chemistry is initiated by the reaction of a VOC with the triplet state of IC (Aregahegn et al., 2013; Canonica et al., 1995b).

Given of the potential importance of this new photosensitized pathway for SOA production and ageing, we aimed to understand the reaction mechanism leading to the aerosol growth as reported by Aregahegn et al. (Aregahegn et al., 2013). A first series of experiments investigated the reactivity of the IC triplet state toward limonene, chosen as a key VOC compound, using laser flash photolysis. Bulk experiments were then carried out to identify the products of the reaction between the IC triplet state and limonene, using direct electrospray ionization (positive and negative modes) coupled to high resolution mass spectrometry [(+/-)ESI-HRMS] and ultra-performance liquid chromatography coupled with heated (+/-)ESI-HRMS [UPLC/(+/-)HESI-HRMS]. Finally, aerosols produced in flow tube experiments, similar to those of Aregahegn et al. (Aregahegn et al., 2013) were analyzed by UPLC/(+/-)HESI-HRMS and compared with the bulk experiments to identify the organic products responsible for SOA growth.

VI.2.2. Experimental

VI.2.2.a. Laser flash photolysis experiment.

The reactivity of excited IC toward limonene was investigated using a classical laser flash photolysis apparatus (Jammoul et al., 2009b). IC triplet state was produced upon excitation under UV irradiation and its deactivation over time was followed by monitoring its absorption in the presence or absence of limonene. The photolysis excitation source was the third harmonic (266 nm, pulse width ~7 ns) of an Nd:YAG laser (Surelite II 10, Continuum,

USA) operated in a single-shot mode. During these experiments, the laser pulse energy was limited at 20 mJ per pulse to reduce photolysis of the photosensitizer. It was experimentally observed that under this energy threshold the upper limit of the fraction of IC depleted by each pulse was negligible (< 0.14 µM). Ground state IC extinction coefficient was calculated as ε_{266nm} = 4698.59 M^{-1} cm^{-1}. The laser output passed through the aperture in the short axis (4 mm path length) of a fully masked quartz flow cell. The working water-acetonitrile (1:1) solutions containing IC (0.25 mM, 97%, Sigma-Aldrich, USA) and various amounts of limonene (0 mM, 4 mM, 8 mM and 12 mM, (R)-(+)-limonene 97%, Sigma-Aldrich, USA) were deoxygenated for at least 1 hour. They were introduced into the flow cell (volume of 450 µL) by means of a peristaltic pump, with a flow rate of 1.6 mL min^{-1}, ensuring a complete purge of the exposed volume every 17 sec. This limited the exposure of the introduced solution to 3-4 laser shots and maintained a constant temperature in the flow cell. All connections on the apparatus were made from either glass or PTFE tubing, ensuring a clean liquid flow. The transient absorption of the excited IC produced upon 266 nm excitation was followed by means of time-resolved absorption spectroscopy at 330 nm in the absence and presence of limonene. The analyzing light, provided by a 75 W high-pressure Xenon arc lamp (LOT-Oriel, Germany), passed through the two apertures of the long axis of the flow cell (1 cm path length). The light was then collected by a ¼ m monochromator (DK240, Spectral Products, USA) equipped with a 2400 grooves/mm grating and detected by a photomultiplier (PMT, H7732-10, Hamamatsu, Japan). The PMT signal was passed through a high-speed current amplifier/discriminator (Femto, Germany) and the AC and DC component recorded on a 300 MHz oscilloscope (TDS3032c, Tektronix, USA). The digitalized signal was then transferred to a computer for further processing. The analysis of transient absorbance decays as well as the fitting was performed on OriginPro (version 8.5).

VI.2.2.b. Bulk experiments.

A water-acetonitrile solution (1:1, v:v, Elga ultrapure water, France/Fischer Chemical, UK) containing IC (1 mM, 97%, Sigma-Aldrich, USA) and limonene (10 mM, (R)-(+)-limonene 97%, Sigma-Aldrich, USA) was placed in a small cylindrical quartz reactor (volume of 15 ml) and exposed to light in a box equipped with 7 UV-lamps (Cleo 20 W, emission range 280-400 nm, Philips, Netherlands) for 23 h. At different intervals, two 400 µL samples were diluted by a

factor 25, in a water-acetonitrile solution (1:1, v:v) or pure water for direct analysis in (+/-) ESI-HRMS and analysis by UPLC/(+/-)HESI-HRMS respectively.

VI.2.2.c. Flow tube experiments

Photosensitized growth of aerosols was carried out using a horizontal double wall aerosol flow tube made of Pyrex (13 cm id × 152 cm of length) kept at 293±1 K by means of a circulating water bath. The carrier gas was dry air (purity 99.9990%, Air Liquide, France), introduced at a total flow rate of 0.4 L min^{-1} allowing an aerosol residence time of 50 min. The flow tube was surrounded by 7 UV-lamps (Cleo, Philips, Netherlands) with a continuous emission spectrum over 300 – 420 nm and a total irradiance of 3.7×10^{16} photon cm^{-2} s^{-1}. A complete description of this aerosol flow tube setup is given elsewhere (Monge et al., 2012).

For physical characterization of the aerosol growth, a monodispersed aerosol ("seed particles") was generated from an aqueous solution containing IC (1.3 mM, 97%, Sigma-Aldrich, USA) and ammonium sulfate (0.95 mM, 99.0%, Sigma-Aldrich, USA). The atomized solution (atomizer 3076, TSI, USA) was then dried using a Silica gel 20 diffusion drier and an initial seed particles diameter of 50 nm was selected using a Differential Mobility Analyzer (DMA 3081, TSI, USA, impactor size 0.0588 cm, aerosol flow=0.3 L min^{-1}, sheath flow=3 L min^{-1}). This monodispersed aerosol contained typically 5000 particles cm^{-3} and corresponded to a total mass of a few µg m^{-3}. It was flown into the reactor where it was exposed to gaseous limonene and, when required, to UV light. A limonene concentration of around 0.9 ppm was generated using a permeation tube placed in a temperature controlled oven (Dynacal, Valco Instruments Co. Inc., USA, using VICI Metronics, USA, Dynacalibrator, model 150). The particle size distribution and concentration obtained at the outlet of the flow tube were monitored using a Scanning Mobility Particle Sizer (SMPS 3080, TSI, USA), consisting of a DMA (TSI 3081) and a Condensation Particle Counter (CPC, TSI 3776).

For the aerosol sampling and subsequent chemical analysis, we decided to increase the seed particles concentration in order to improve the signal-to-noise ratio of the ESI-HRMS. At the flow tube inlet, the DMA was removed to generate a polydispersed dry aerosol. Particles were then collected at the flow tube outlet on a Teflon filter (47 mm Fluoropore™ membrane filters, 0.45 µm FH, Merk Millipore, USA) using a stainless steel filter holder (Aerosol standard filter holder, 47 mm, Merk Millipore, USA). Two experiments of 16 h were systematically and consecutively performed; first, a "blank" consisting of

introducing both seed particles and gaseous limonene but without light, and second, a "sample" was collected with the light on. The filters were subsequently solvent extracted under ultrasonication (40 min) in 7 ml of a water-acetonitrile solution (4:6, v:v) in an Erlenmeyer, maintained at low temperature in an ice bath. Extracts were then concentrated to 1 mL under a gentle stream of nitrogen and were subsequently analyzed by UPLC/(+/-) HESI-HRMS.

VI.2.2.d. ESI-(+/-)HRMS and UPLC/(+/-)HESI-HRMS analysis

The UPLC/(+/-)HESI-HRMS system comprised a Dionex Ultimate 3000 ultra-performance liquid chromatograph (UPLC, Thermo Scientific, USA) coupled to a Q-Exactive high resolution mass spectrometer (HRMS, Thermo Scientific, USA) equipped with a heated electrospray ionization (HESI) source. Half of the bulk samples (diluted in water-acetonitrile mixture) were analyzed by direct infusion of the diluted solutions into the non-heated electrospray source (ESI-(+/-)HRMS analysis) at a flow rate of 30 µL min^{-1}. Source voltages of +3.5 kV and -2.6 kV were applied for the positive (+) and negative (-) ionization modes respectively. The remaining bulk fraction and the flow tube samples were analyzed by means of UPLC/(+/-) HESI-HRMS. The chromatograph was equipped with a HSS T3 Acquity UPLC column (1.8 µm, 2.1 × 100 mm). The mobile phase was (A) acidified water (Fischer Chemical, UK, + 0.1%, v:v, formic acid, Sigma-Aldrich, USA) and (B) acidified acetonitrile (Fischer Chemical, UK, + 0.1%, v:v, formic acid, Sigma-Aldrich, USA). A 16 min gradient was applied: eluent (B) was kept at 1% for 2 min and was then increased to 90% in 10 min, this ratio was maintained for 2 min before returning to the initial condition for 2 min. The flow rate was 0.3 ml min^{-1}. Source voltages of 3.7 kV and 3.0 kV were applied for the positive (+) and negative (-) ionization modes respectively. All acquisitions were performed in full MS mode with a scan ranging from m/z 50 to m/z 750 and a resolution set to 140,000. Specific MS^2 spectra were acquired in direct infusion mode applying a normalized collision energy level of 35%. The data were processed using Xcalibur 2.2 software. The Q-Exactive mass spectrometer was mass calibrated using commercial Calmix solutions (Thermo Scientific, USA). To achieve good accuracy for low masses (< 4 ppm) commercially used mass lists were completed with mass 74.09643 for the positive mode and masses 59.01385 and 514.28440 for the negative mode. All the exact mass assignments to chemical formula were done considering carbon, hydrogen, oxygen, nitrogen, sodium and potassium as potential elements and with a mass

accuracy below 4 ppm. All the proposed chemical formulas comply with the octet rule (i.e., an integer double bond equivalent) for the related neutral compounds.

VI.2.3. Results and discussion

VI.2.3.a. Triplet state chemistry of IC

This first series of experiments was performed to verify the hypothesis proposed by Aregahegn that the excited triplet state of IC could react with limonene (Aregahegn et al., 2013). The formation of an IC triplet state under UV-irradiation was demonstrated elsewhere by Tinel and co-authors (Tinel et al., 2013). The triplet-triplet IC absorption

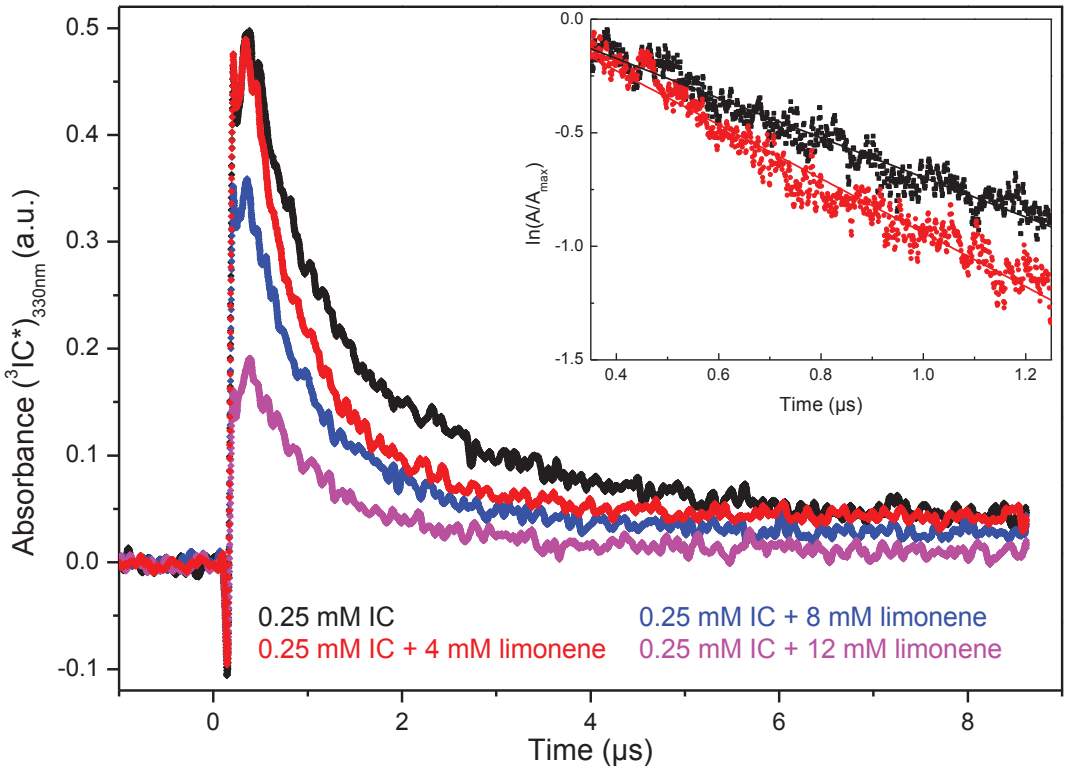

Figure VI-8: Transient triplet-triplet absorption of the excited IC followed at 330 nm in a water-acetonitrile (1:1) mixture in the absence of limonene as a quencher (black), in the presence of 4 mM of limonene (red), 8 mM of limonene (blue) and 12 mM of limonene (pink). Inset: linear fitting of corresponding ln(A/A$_{max}$)=f(t). A$_{max}$: maximum absorbance observed for each data series.

monitored at 330 nm showed a mono-exponential decay. By adding increasing amounts of limonene to the IC containing solution, the decay of the transient absorption was observed to be faster (figure VI-8). These results confirmed that limonene quenches the IC triplet

state, i.e., introducing a reaction that may proceed *via* electron or hydrogen transfer in agreement with the previous study (Aregahegn et al., 2013).

VI.2.3.b. Photosensitized aerosol growth

In order to produce SOA from photosensitization for chemical analysis, flow tube experiments similar to those presented by Aregahegn and co-authors were performed (Aregahegn et al., 2013). Monodisperse IC/ammonium sulfate aerosol seeds and gaseous limonene were first injected and irradiated. A typical profile for the evolution of the median diameter of the particles at the flow tube outlet is shown in Figure VI-9. As expected, a significant particle growth was observed when seed particles were exposed to both limonene and UV light. In the dark (from initial time to A on Figure VI-9), the median diameter was constant and very close to the seed particle diameter selected at the inlet of the flow tube (50 nm). Under irradiation, this diameter increased during a period corresponding to the residence time of the aerosol in the flow tube (50 min, from A to B on Figure VI-9), to reach a value of 68 nm, corresponding to a diameter growth factor of around 25 % (calculated as the ratio of the difference between the final and the initial and final diameters). When the lamps were subsequently turned off (from C on Figure VI-9), the median diameter decreased, during a period corresponding to the residence time, returning to its initial value, confirming the key role of light in the growth of IC containing particles exposed to gaseous limonene. The observed growth was consistent with that obtained by Aregahegn and co-workers (Aregahegn et al., 2013). The experimental parameters (seed composition, limonene concentration, irradiation and residence time) were consequently chosen to explore the composition of the grown aerosols from an initial polydisperse seed aerosol. This grown aerosol was collected and extracted by the method described in the experimental section for chemical analysis.

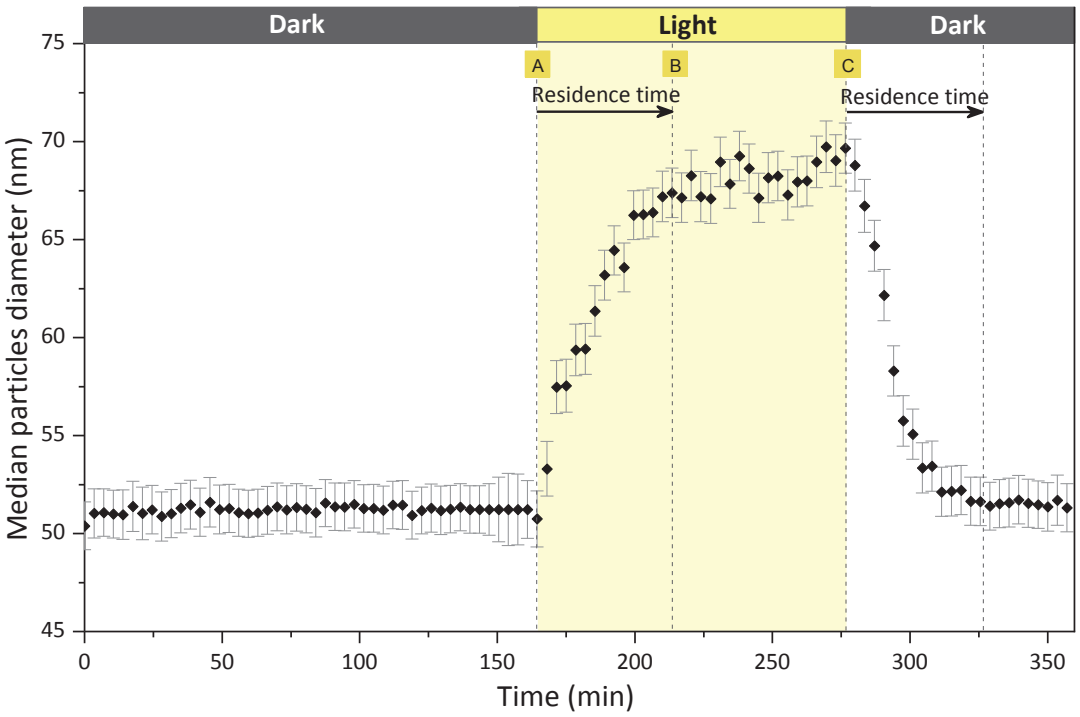

Figure VI-9: *Temporal evolution of the median diameter of particles during a flow tube experiment. Monodisperse seed particles (IC/ammonium sulfate) were exposed to gaseous limonene continuously (0.9 ppmv) and to UV light between 165 and 277 min. Error bars correspond to 2 times the geometrical standard deviation. Arrows and doted vertical lines mark the theoretical aerosol residence time at two critical points: when the lamps were switched on (A) and off (C).*

VI.2.3.c. Photosensitized radical formation from $^3IC^*$

Bulk and flow tube experiments were performed to identify the major products of the reaction between the IC triplet state and limonene. In the bulk experiments, direct (+/-)ESI-HRMS analysis showed the formation of nitrogen-containing products as well as a range of oxygenated species. Among them, the formation of a major product at m/z 233.1643 ± 0.0001 was observed in the positive ionization mode (figure VI-10). The signal intensity for this ion rose faster during the first 2 h of the experiment than during the last 21 h, however still increasing with time (figure VI-10 inset).

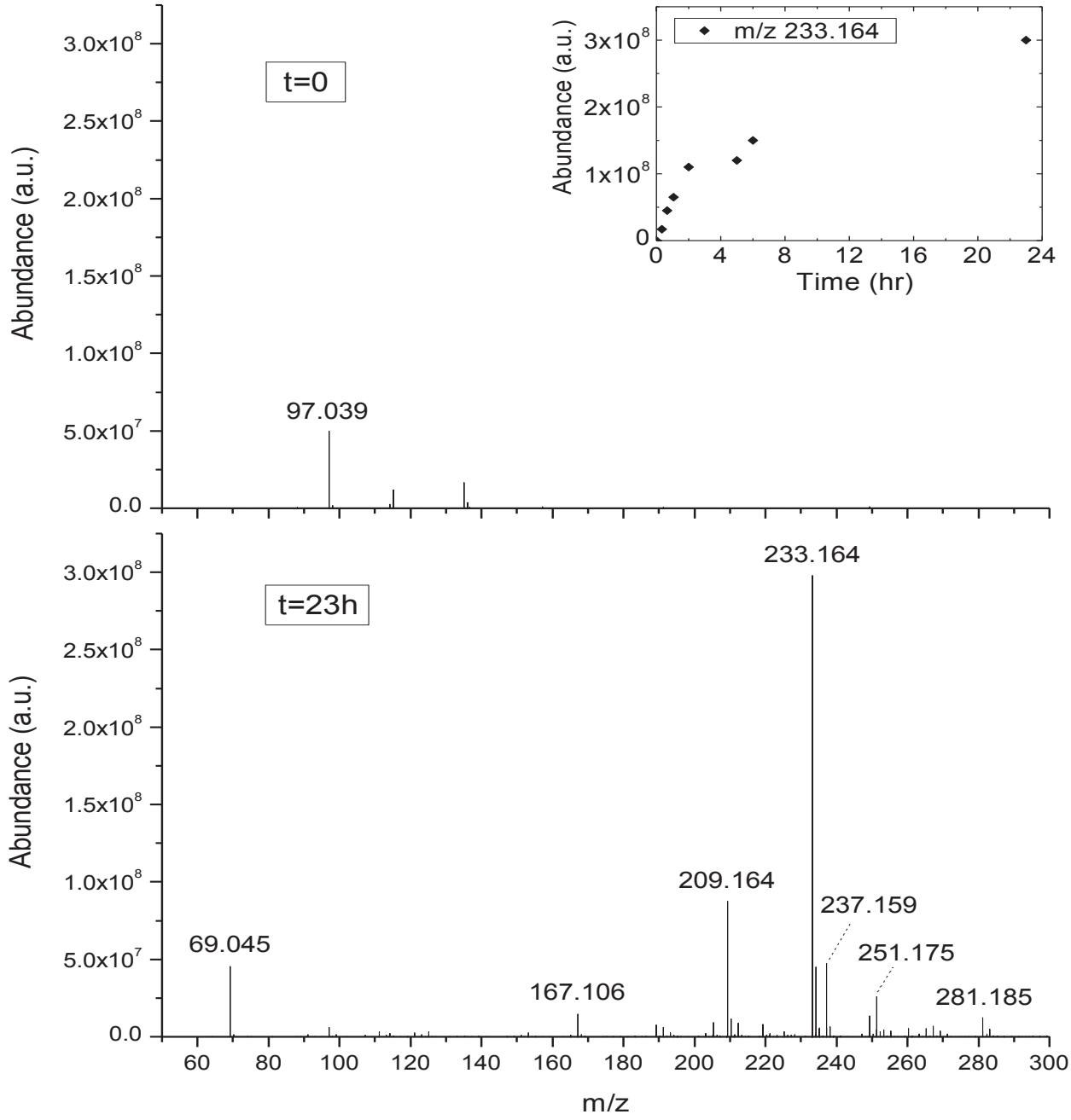

Figure VI-10: Average mass spectra obtained in (+)ESI-HRMS for bulk experiment at initial time and after 23 h of irradiation (average on ~70 spectra on 1 min acquisition time in direct infusion). Inset: time evolution of m/z 233.164 abundance.

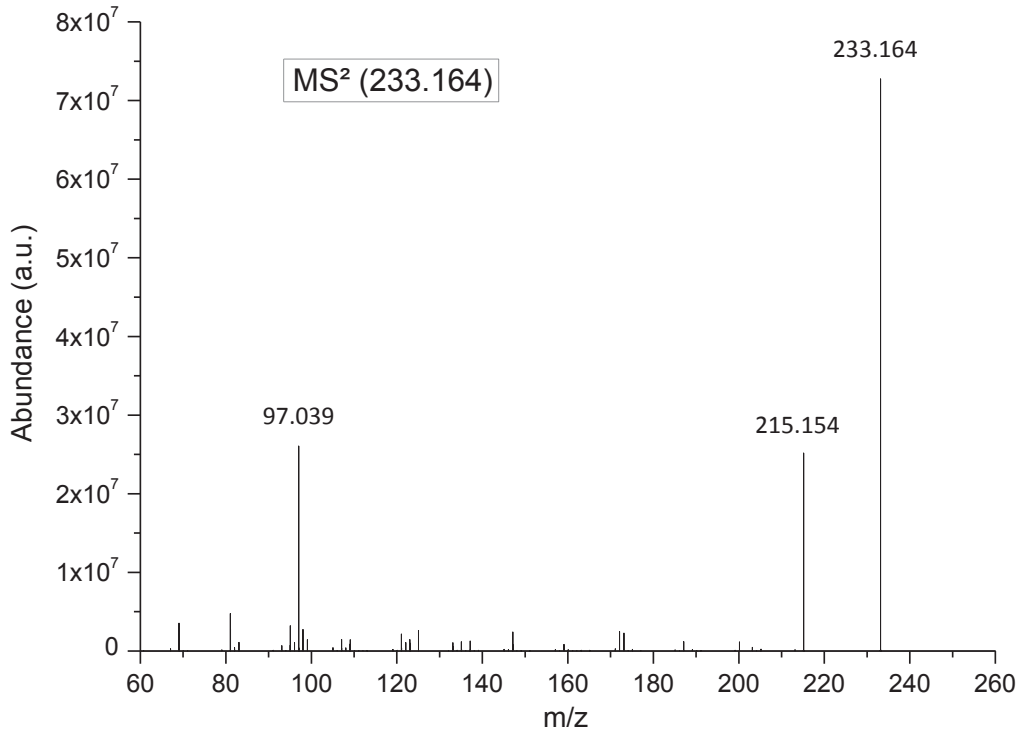

Figure VI-11: MS² mass spectrum of m/z 233.164 in (+)ESI-HRMS.

The high resolution of the instrument coupled with a mass accuracy estimated to be below 4 ppm under our experimental conditions allowed us to identify $C_{14}H_{21}ON_2^+$ (exact mass 233.1648, Δppm = -2.3) as the unique matching positive ion, which corresponds to a $C_{14}H_{20}ON_2$ neutral compound. A MS² mass spectrum of m/z 233.164 was acquired (figure VI-11) and its fragmentation pattern reveals the formation of a major fragment at m/z 97.0394 ± 0.0001. This fragment corresponds to a $C_4H_5ON_2^+$ chemical formula (exact mass 97.0396, Δppm = -2.5) and can consequently be attributed to an IC fragment ($C_4H_4ON_2$). The compound detected at the exact mass m/z 233.164 might thus be a radical-radical recombination product of IC ($C_4H_4ON_2$) and limonene ($C_{10}H_{16}$). This would be consistent with the expected reactivity of the IC triplet state, proceeding most probably *via* a hydrogen transfer leading to the formation of alkyl radicals (Aregahegn et al., 2013). This hydrogen transfer can be either a direct transfer or proceed via an electron transfer followed by a proton transfer.

To account for these results, formation mechanisms proceeding *via* the photosensitized formation of two radicals, an IC and limonene radical, are hereby suggested as shown figure VI-12. The position of the transferred hydrogen on the limonene structure could be mechanism dependent. In principle, the weaker C-H bond in the limonene molecule

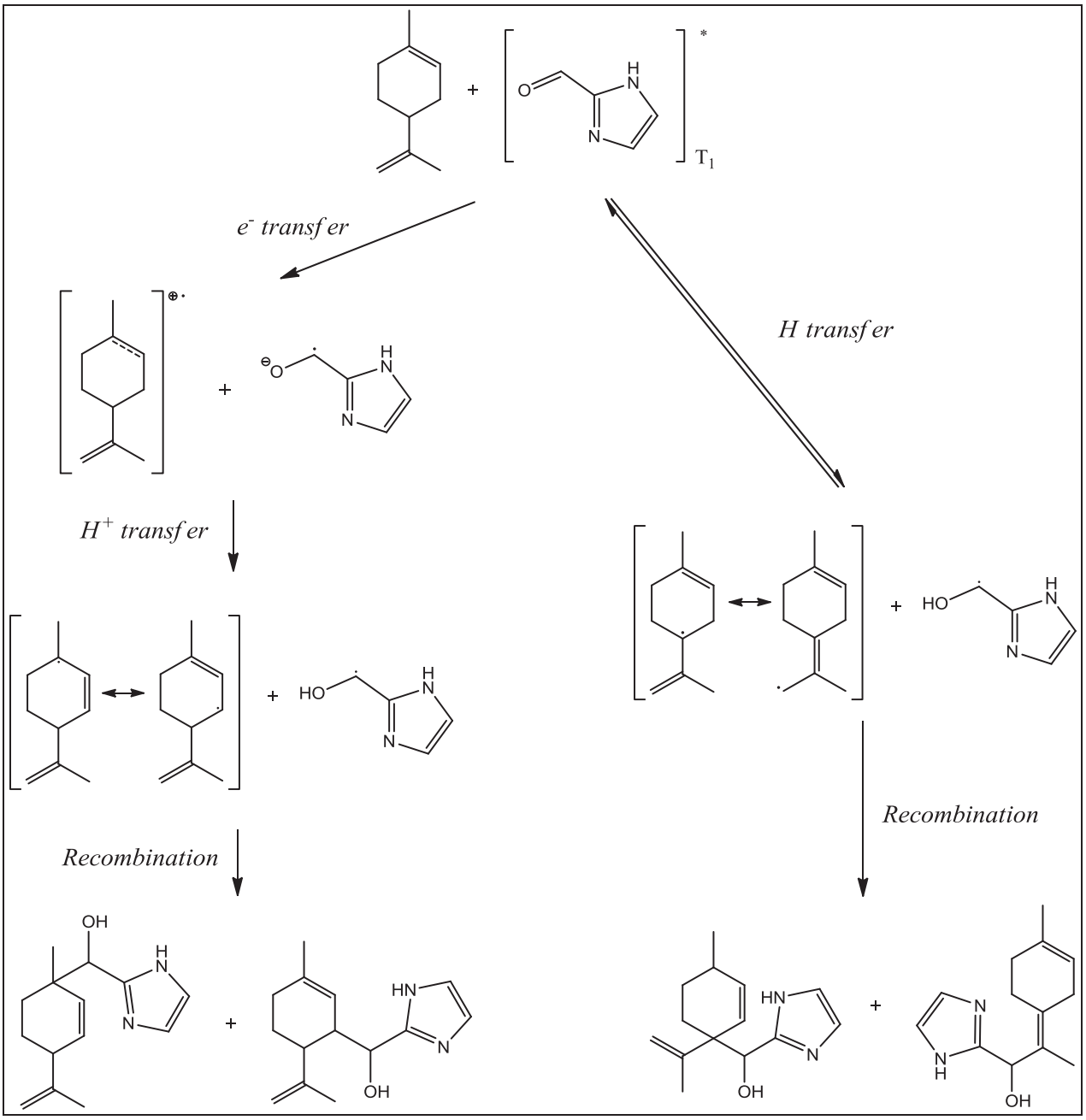

Figure VI-12: Potential formation mechanisms of the recombination product of IC and limonene detected at mass m/z 233.164 in the bulk experiments from molecular limonene and IC triplet state.

should be on the secondary allylic carbons or on the tertiary allylic carbon (Blanksby and Ellison, 2003). Accordingly, these hydrogen atoms will be preferentially transferred in case of a direct transfer. If the mechanism proceeds firstly *via* an electron transfer, the abstracted electron will preferentially be located on the endocyclic double bond as the corresponding radical cation is stabilized by both tertiary and secondary carbons. Using the available data it

remains difficult to suggest which of the proposed pathways is most dominant. Furthermore, the chromatographic peak obtained for m/z 233.164 by UPLC/(+)HESI-HRMS analysis of bulk samples was broad and bore shoulders that could correspond to the formation of several isomers. In any case, the detection of such recombination product(s) highlights the photosensitized formation of radicals from limonene and IC the bulk solutions.

Table 1. Detected exact masses in the grown aerosols coming from a flow tube experiment by UPLC/(+/-)HESI-MS.

Ionization mode	Detected mass (m/z)	Chemical formula [1]	R_t (min)	Area[2] (×10^5 a.u.)	Light/Dark ratio [3]
(+)	233.164	$C_{14}H_{20}ON_2$	7.53	26	459
(+)	193.072	$C_8H_8O_2N_4$	6.61	1100	101
(+)	191.056	$C_8H_6O_2N_4$	5.27	820	380
(-)	151.113	$C_{10}H_{16}O$	8.99 - 9.41	1.7 (9.41)	344
(-)	167.108	$C_{10}H_{16}O_2$	7.06 - 7.31 - 7.60	7.6 (7.31)	89
(-)	183.102	$C_{10}H_{16}O_3$	8.05 - 8.14	36 (8.05)	97
(-)	181.087	$C_{10}H_{14}O_3$	8.35	10 × 10^6	40
(-)	199.098	$C_{10}H_{16}O_4$	6.88	280	14
(-)	197.082	$C_{10}H_{14}O_4$	6.64	26	73
(-)	215.092	$C_{10}H_{16}O_5$	5.80 - 6.15	86 (6.15)	203
(-)	213.077	$C_{10}H_{14}O_5$	6.10 - 6.46 - 6.65	19(6.65)	37
(-)	231.087	$C_{10}H_{16}O_6$	4.91 - 5.14	49 (4.91)	1245
(-)	229.072	$C_{10}H_{14}O_6$	5.89	11	106
(-)	185.082	$C_9H_{14}O_4$	7.26	330	130
(-)	183.066	$C_9H_{12}O_4$	5.19 - 5.31- 5.84	15 (5.19)	333
(-)	169.087	$C_9H_{14}O_3$	7.73	26	40
(-)	155.071	$C_8H_{12}O_3$	6.33	23	9
(-)	187.061	$C_8H_{12}O_5$	5.53	220	340

[1]: Neutral chemical formula corresponding to the positively or negatively charged chemical formula determined form detected exact mass.

[2]: In case of several retention times, the area of the main peak is given (peak retention time in brackets).

[3]: Ratio of the peak area detected in the irradiated sample on the peak (or the noise) area detected at the same retention time in the non-irradiated sample.

In the flow tube aerosol samples, the mass at m/z 233.164 was also observed by means of UPLC/(+)HESI-HRMS analysis, but at a lower level, which precluded a direct quantitative comparison with the bulk experiments. However, two additional masses were also detected i.e., at m/z 193.072 and m/z 191.056 (Table VI-2). These masses only match with neutral compounds having as chemical formulas $C_8H_8O_2N_4$ and $C_8H_6O_2N_4$ respectively and could

therefore correspond to recombination products of IC ($C_4H_4ON_2$) with itself via a pathway depicted in Figure VI-13. The high IC concentration in the seed particles in the flow tube experiments, results in a high probability of the IC triplet state reacting with another IC molecule leading to hydrogen transfer from the fundamental state to the triplet state.

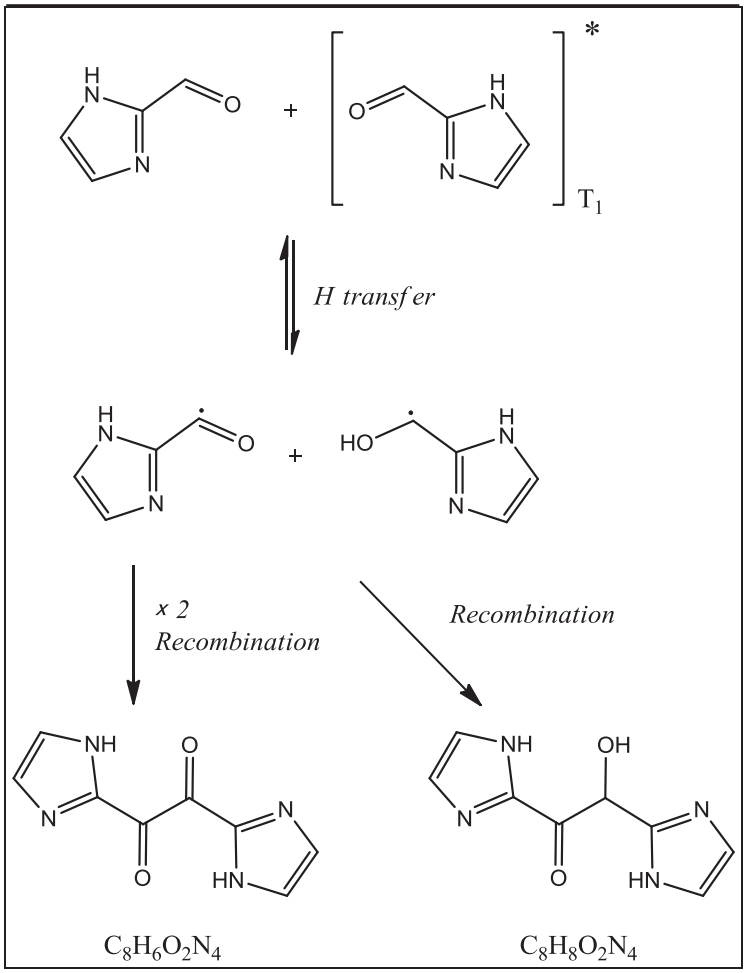

Figure VI-13: Potential formation mechanisms of the recombination products of IC with itself detected in flow tube sample.

This hydrogen transfer likely involves the carbonyl hydrogen as the corresponding C-H bond dissociation energy is in the same order of magnitude as an allylic transfer (Blanksby and Ellison, 2003). This hydrogen transfer subsequently leads either directly to the recombination of the two just formed radicals to give the recombination product detected at m/z 193.072, or to the recombination of two radicals having undergone hydrogen abstraction to give the compound detected at m/z 191.056. These two recombination products of IC with itself were not detected in bulk experiments. A simple concentration effect can be invoked here, as in the bulk experiments, IC was 10 times less concentrated

than limonene. On the contrary, in flow tube experiments, seed particles were only composed of dry IC and ammonium sulfate exposed to 0.9 ppm of gaseous limonene leading to the predominance of IC-IC recombination products over IC-limonene ones.

It is difficult to infer from these experiments if the formation of IC-limonene and IC-IC recombination products is atmospherically relevant as the IC and limonene concentrations used here are high compared to expected atmospheric concentrations. However, the presence of these recombination products both in the bulk and in the flow tube samples indicates that the photosensitized chemistry of IC initiates radical chemistry in the aerosol phase and/or at the gas/particle interface under realistic irradiation conditions. In addition, the results of the bulk experiments showed explicitly that the IC triplet state is able to react with limonene through hydrogen abstraction.

VI.2.3.d. Highly oxygenated limonene oxidation products

Both bulk and flow tube experiments provided evidence of radical formation from the IC triplet state. Here, results of the flow tube experiments will be preferentially discussed to explain the observed aerosol growth. In addition to the recombination products, the SOA analysis by means of UPLC/(-)HESI-HRMS revealed the formation of a range of highly oxygenated products with a majority of compounds bearing between C_8 and C_{10} carbon chains and up to 6 oxygen atoms (Table VI-2). No attempt was made here to elucidate their chemical structure nor to quantify them. However, the fact that these oxygenated products were formed in only 50 min without any gas phase oxidant is noteworthy.

Of particular interest are the compounds that kept the C_{10} carbon chain of limonene and contained 4 to 6 oxygen atoms, which are remarkable in that they cannot be explained by classical gas-phase ozonolysis or photooxidation chemistry; the terminal double bond of limonene implying necessarily some fragmentation reducing the carbon number (Chacon-Madrid and Donahue, 2011; Jaoui et al., 2006; Leungsakul et al., 2005). The presence of such compounds clearly shows that limonene reacts in the particle upon uptake and not in the gas phase. The formation of similar oxygenated products was confirmed in the analysis of bulk experiments, with corresponding ion intensities increasing with time. Because of their expected low volatility, due to the presence of up to 6 oxygen atoms on the limonene structure, these oxygenated products are expected to participate to the observed SOA growth.

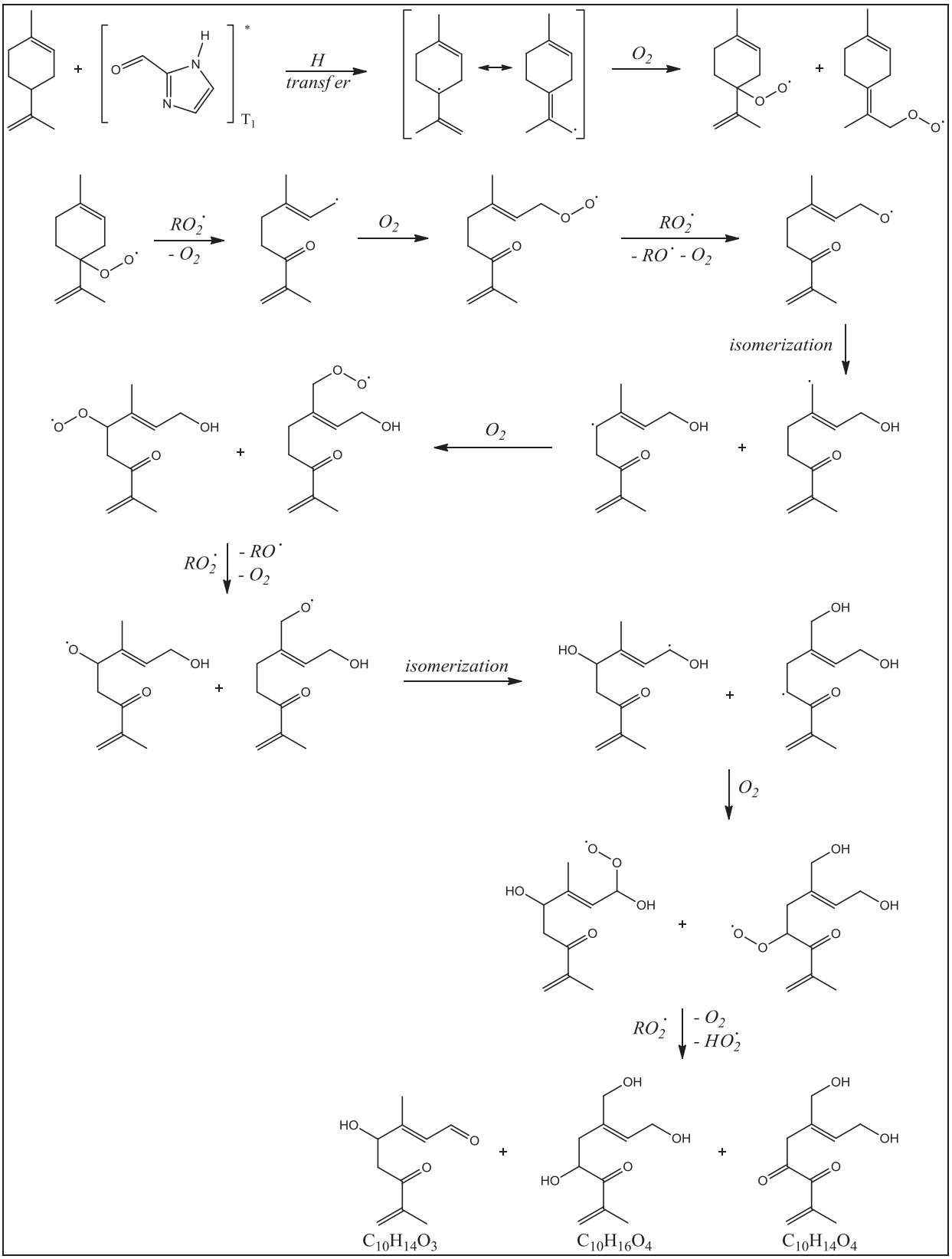

Figure VI-14: Limonene photosensitized oxidation mechanism initiated by hydrogen abstraction on limonene molecule through reaction with IC triplet state and based on the peroxy radical chemistry. Example for the formation of three compounds keeping the C_{10} limonene skeleton by two steps of isomerization.

Based on the IC radical chemistry evidenced in this work and the previous observation that molecular oxygen is necessary for SOA growth (Aregahegn et al., 2013), a mechanism explaining the formation of such compounds and based on peroxy radical chemistry is suggested. This mechanism is initiated by the direct abstraction of a hydrogen atom on limonene by the IC triplet state leading to the formation of a stable allylic radical. The addition of molecular oxygen leads to a peroxy radical that can evolve toward a large range of oxidation products (von Sonntag and Schuchmann, 1991), including compounds retaining the same number of carbons as limonene. As an illustration, the formation mechanism of the three compounds $C_{10}H_{16}O_4$, $C_{10}H_{14}O_4$ and $C_{10}H_{14}O_3$, detected at m/z 199.098, m/z 197.082 and m/z 181.087 respectively is presented in Figure VI-14. This mechanism underlines that the observed products are the result, after ring opening, of intramolecular isomerization (1,5 hydrogen shift, (Atkinson, 1997)) which are particularly favored in the case of limonene. The number of possible 1,5 hydrogen shifts is indeed numerous in the limonene structure because of the chain of 7 carbons and the isopropene side chain. Furthermore, the first step of the mechanism is controlled by the formation of an allylic radical, especially stable in the case of limonene and any other VOC bearing unsaturated tertiary carbon. This mechanism would thus be consistent with the previous observations of Aregahegn et al. that aerosol growth was mostly observed with this type of compounds (Aregahegn et al., 2013).

VI.2.4. Atmospheric implications.

Light-induced reactive uptake of VOCs was previously observed and presented as a potentially important atmospheric pathway, but still unaccounted for in SOA mass budget, by Monge et al. (Monge et al., 2012) and Aregahegn et al. (Aregahegn et al., 2013). However, the data reported here is, to our knowledge, the first proposed photosensitized mechanism based on actual reaction products. In this work the identification of various recombination products has clearly shown that the presence of IC in the aerosol phase can initiate radical chemistry under near-UV irradiation. The IC triplet state is able to abstract hydrogen from limonene molecules leading to their reactive uptake with subsequent oxidation, and similar mechanisms can be inferred for the other unsaturated and branched VOCs studied by Aregahegn et al.(Aregahegn et al., 2013). Such VOCs (i.e., bearing a branched allylic or a branched aromatic structure) are emitted in large amounts by biogenic and anthropogenic

sources (Guenther et al., 2006; Seinfeld and Pankow, 2003; Tsigaridis and Kanakidou, 2003). Their direct uptake into the particulate phase without the need of previous gas phase oxidation and partitioning steps and the subsequent fast formation of highly oxygenated products, could lead to significant SOA formation even if other reactants are present in the particulate phase or if photosensitizers are present at trace quantities (Aregahegn et al., 2013). Recent studies have shown that IC can indeed be formed within a timescale relevant for atmospheric processes (1 to 2 h), even if the reaction may not be complete and depends on involved reactant concentrations (Aregahegn et al., 2013; Galloway et al., 2009; Yu et al., 2011). Furthermore, one may suppose that the recently evidenced near UV light-absorbing material formation *via* particulate phase chemistry of carbonyls with ammonium ions and amines, potentially involves a variety of additional still unknown photosensitizers (Bones et al., 2010; De Haan et al., 2011; Kampf et al., 2012a; Nozière et al., 2009; Shapiro et al., 2009; Updyke et al., 2012).

Beyond the reactive uptake of VOCs (or even SVOCs bearing hydrogen available for abstraction), *in situ* photosensitizer formation could also efficiently impact the chemistry of the particulate phase. Until now, the only source of radicals considered for the particulate phase was the transfer of oxidants from the gas phase (OH, O_3, NO_3 and halogens), photo-Fenton chemistry and nitrate photolysis (Chevallier et al., 2004; Nguyen et al., 2013). The photoinduced processes studied in this work could represent a previously unaccounted for *in situ* particulate phase source of radicals. Furthermore, previous works reported experimental evidences potentially supporting such photosensitized processes (Galloway et al., 2009). In the SOA produced by glyoxal uptake in the presence of ammonium sulfate seeds, Galloway and co-workers observed the formation of IC and, only in the presence of light, the co-formation of highly oxidized organic species (e.g. glyoxylic, glycolic, formic acid) (Galloway et al., 2009). As no oxidant was added, no clear origin of these products, OH or some other radical mechanisms, has been evidenced. Formation of IC could thus be involved. In these experiments, as glyoxal was the only VOC to be added, the reaction of the IC triplet state would have to be with glyoxal. Moreover, this reaction is expected to be as efficient as with limonene because C-H bond dissociation energy on an aldehydic carbon is of the same order of magnitude as on an allylic carbon (Blanksby and Ellison, 2003). In that case, the *in situ* IC formation *via* glyoxal reactivity could interestingly be able to influence daytime fate of glyoxal within the particulate phase, enhancing its irreversible loss.

The results of this work suggest that, generally speaking, the presence of photosensitizers in ambient aerosol might influence (1) the daytime SOA growth *via* the reactive uptake of VOCs and (2) the O/C ratio and volatility of the organic fraction of the aerosol *via* the fast formation of highly oxidized products. As these two points are critical to assess SOA budget and properties, further research is now required to estimate the magnitude of these processes in real environments. In particular, it would be interesting to compare the rate of light-induced uptake of VOCs due to these processes and those of their gas phase oxidation processes. The comparison between these different pathways in the atmosphere could also be based on the identification of different tracers. The identification of other potential photosensitizers is also necessary.

IV.2.5. Affiliations of the authors

All authors :

Université de Lyon 1, Lyon, F-69626, France, CNRS, UMR5256, IRCELYON, Institut de Recherches Sur la Catalyse et l'Environnement de Lyon, Villeurbanne, F-69626, France

IV.2.6. References.

Abbatt, J.P.D. et al., 2012. Halogen activation via interactions with environmental ice and snow in the polar lower troposphere and other regions. Atmospheric Chemistry and Physics, 12(14): 6237-6271.

Aregahegn, K.Z., Noziere, B. and George, C., 2013. Organic aerosol formation photo-enhanced by the formation of secondary photosensitizers in aerosols. Faraday Discussions, 165: 123-134.

Atkinson, R., 1997. Gas-phase tropospheric chemistry of volatile organic compounds .1. Alkanes and alkenes. Journal of Physical and Chemical Reference Data, 26(2): 215-290.

Averett, R.C., Leenheer, J.A., McKnight, D.M. and Thorn, K.A., 1994. Humic substances in the Suwannee River, Georgia; interactions, properties, and proposed structures. 2373.

Blanksby, S.J. and Ellison, G.B., 2003. Bond dissociation energies of organic molecules. Accounts of Chemical Research, 36(4): 255-263.

Bones, D.L. et al., 2010. Appearance of strong absorbers and fluorophores in limonene-O_3 secondary organic aerosol due to NH_4^+-mediated chemical aging over long time scales. Journal of Geophysical Research-Atmospheres, 115: D05203.

Braun, A.M., Maurette, M.-T. and Oliveros, E., 1986. Technologie photochimique. Presses polytechniques romandes.

Būchler, H. and Būhler, R., 1976. The radical ion complex IOH−: Spectrum and reactions studied by pulse radiolysis of aqueous iodide solutions. Chemical Physics, 16(1): 9-18.

Buxton, G.V., Bydder, M., Salmon, G.A. and Williams, J.E., 2000. The reactivity of chlorine atoms in aqueous solution. Part III. The reactions of Cl-center dot with solutes. Physical Chemistry Chemical Physics, 2: 237-245.

Canonica, S., Hellrung, B. and Wirz, J., 2000. Oxidation of Phenols by Triplet Aromatic Ketones in Aqueous Solution. The Journal of Physical Chemistry A, 104: 1226-1232.

Canonica, S., Jans, U., Stemmler, K. and Hoigne, J., 1995a. Transformation Kinetics of Phenols in Water: Photosensitization by Dissolved Natural Organic Material and Aromatic Ketones. Environmental Science & Technology, 29: 1822-1831.

Canonica, S., Jans, U., Stemmler, K. and Hoigne, J., 1995b. Transformation Kinetics of Phenols in Water: Photosensitization by Dissolved Natural Organic Material and Aromatic Ketones. Environmental Science & Technology, 29(7): 1822-1831.

Carpenter, L.J., 2003. Iodine in the marine boundary layer. Chemical Reviews, 103: 4953-4962.

Chacon-Madrid, H.J. and Donahue, N.M., 2011. Fragmentation vs. functionalization: Chemical aging and organic aerosol formation. Atmospheric Chemistry and Physics, 11(20): 10553-10563.

Chahidi, C., Aubailly, M., Momzikoff, A., Bazin, M. and Santus, R., 1981. Photophysical and photosensitizing properties of 2-amino-4 pteridinone - a natural pigment. Photochemistry and Photobiology, 33: 641-649.

Chang, W.N., Heikes, B.G. and Lee, M.H., 2004. Ozone deposition to the sea surface: chemical enhancement and wind speed dependence. Atmospheric Environment, 38(7): 1053-1059.

Chevallier, E., Jolibois, R.D., Meunier, N., Carlier, P. and Monod, A., 2004. "Fenton-like" reactions of methylhydroperoxide and ethylhydroperoxide with Fe2+ in liquid aerosols under tropospheric conditions. Atmospheric Environment, 38(6): 921-933.

Clifford, D., Donaldson, D.J., Brigante, M., D'Anna, B. and George, C., 2008. Reactive uptake of ozone by chlorophyll at aqueous surfaces. Environmental Science & Technology, 42(4): 1138-1143.

De Haan, D.O. et al., 2011. Formation of nitrogen-containing oligomers by methylglyoxal and amines in simulated evaporating cloud droplets. Environmental Science & Technology, 45(3): 984-991.

Devonshire, R. and Weiss, J.J., 1968. Nature of the transient species in the photochemistry of negative ions in aqueous solution. The Journal of physical chemistry, 72(11): 3815-3820.

Dzepina, K. et al., 2009. Evaluation of recently-proposed secondary organic aerosol models for a case study in Mexico City. Atmospheric Chemistry and Physics, 9(15): 5681-5709.

Ershov, B.G., 2004. Kinetics, mechanism and intermediates of some radiation-induced reactions in aqueous solutions. Uspekhi Khimii, 73: 107-120.

Ershov, B.G. and Janata, E., 2003. The reduction of I-2 by 1-hydroxyalkyl radicals in aqueous solution. A pulse radiolysis study. Chemical Physics Letters, 372: 195-198.

Ervens, B. and Volkamer, R., 2010. Glyoxal processing by aerosol multiphase chemistry: Towards a kinetic modeling framework of secondary organic aerosol formation in aqueous particles. Atmospheric Chemistry and Physics, 10(17): 8219-8244.

Facchini, M.C. et al., 2008. Important Source of Marine Secondary Organic Aerosol from Biogenic Amines. Environmental Science & Technology, 42: 9116-9121.

Foote, C. and Pryor, W.A., 1976. Free radicals in biology. by WA Pryor, Academic Press, New York, 2: 85.

Forte, B. et al., 2009. A Submarine Journey: The Pyrrole-Imidazole Alkaloids. Marine Drugs, 7(4): 705-753.

Fu, T.M. et al., 2008. Global budgets of atmospheric glyoxal and methylglyoxal, and implications for formation of secondary organic aerosols. Journal of Geophysical Research-Atmospheres, 113(D15): D15303.

Galloway, M.M. et al., 2009. Glyoxal uptake on ammonium sulphate seed aerosol: reaction products and reversibility of uptake under dark and irradiated conditions. Atmospheric Chemistry and Physics, 9(10): 3331-3345.

Guenther, A. et al., 2006. Estimates of global terrestrial isoprene emissions using MEGAN (Model of Emissions of Gases and Aerosols from Nature). Atmospheric Chemistry and Physics, 6: 3181-3210.

Hallquist, M. et al., 2009. The formation, properties and impact of secondary organic aerosol: Current and emerging issues. Atmospheric Chemistry and Physics, 9(14): 5155-5236.

Hastings, W.P., Koehler, C.A., Bailey, E.L. and De Haan, D.O., 2005. Secondary organic aerosol formation by glyoxal hydration and oligomer formation: Humidity effects and equilibrium shifts during analysis. Environmental Science & Technology, 39(22): 8728-8735.

Hodzic, A. et al., 2009. Modeling organic aerosols during MILAGRO: Importance of biogenic secondary organic aerosols. Atmos. Chem. Phys., 9(18): 6949-6981.

Hug, G.L., 1981. Optical spectra of nonmetallic inorganic transient species in aqueous solution, DTIC Document.

Hurley, J.K., Linschitz, H. and Treinin, A., 1988. Interaction of halide and pseudohalide ions with triplet benzophenone-4-carboxylate - kinetics and radical yields. Journal of Physical Chemistry, 92: 5151-5159.

Jammoul, A., Dumas, S., D'Anna, B. and George, C., 2009a. Photoinduced oxidation of sea salt halides by aromatic ketones: a source of halogenated radicals. Atmospheric Chemistry and Physics, 9: 4229-4237.

Jammoul, A., Dumas, S., D'Anna, B. and George, C., 2009b. Photoinduced oxidation of sea salt halides by aromatic ketones: A source of halogenated radicals. Atmos. Chem. Phys., 9(13): 4229-4237.

Jaoui, M. et al., 2006. Analysis of secondary organic aerosol compounds from the photooxidation of d-limonene in the oresence of NO_x and their detection in ambient $PM_{2.5}$. Environmental Science & Technology, 40(12): 3819-3828.

Jimenez, J.L. et al., 2009. Evolution of organic aerosols in the atmosphere. Science, 326(5959): 1525-1529.

Jimenez, J.L. et al., 2003. Ambient aerosol sampling using the Aerodyne Aerosol Mass Spectrometer. Journal of Geophysical Research: Atmospheres, 108: 8425.

Kampf, C.J., Jakob, R. and Hoffmann, T., 2012a. Identification and characterization of aging products in the glyoxal/ammonium sulfate system - implications for light-absorbing material in atmospheric aerosols. Atmospheric Chemistry and Physics, 12(14): 6323-6333.

Kampf, C.J., Jakob, R. and Hoffmann, T., 2012b. Identification and characterization of aging products in the glyoxal/ammonium sulfate system – implications for light-absorbing material in atmospheric aerosols. Atmospheric Chemistry and Physics, 12(14): 6323-6333.

Kennish, M.J., 2000. Practical handbook of marine science. crc press.

Lampre, I. et al., 2013. Oxidation of Bromide Ions by Hydroxyl Radicals: Spectral Characterization of the Intermediate BrOH•–. The Journal of Physical Chemistry A, 117(5): 877-887.

Lázaro Martínez, J.M., Romasanta, P.N., Chattah, A.K. and Buldain, G.Y., 2010. NMR characterization of hydrate and aldehyde forms of imidazole-2-carboxaldehyde and derivatives. The Journal of organic chemistry, 75(10): 3208-3213.

Leungsakul, S., Jeffries, H.E. and Kamens, R.M., 2005. A kinetic mechanism for predicting secondary aerosol formation from the reactions of d-limonene in the presence of oxides of nitrogen and natural sunlight. Atmospheric Environment, 39(37): 7063-7082.

Lim, Y.B., Tan, Y., Perri, M.J., Seitzinger, S.P. and Turpin, B.J., 2010. Aqueous chemistry and its role in Secondary Organic Aerosol (SOA) formation. Atmospheric Chemistry and Physics, 10(21): 10521-10539.

Lion, L.W. and Leckie, J.O., 1981. The biogeochemistry of the air-sea interface. Annual Review of Earth and Planetary Sciences, 9: 449-486.

Liss, P.S. and Duce, R.A. (Editors), 1997. Sea Surface and Global Change. Cambridge University Press, Cambridge, 509 pp.

Loeffler, K.W., Koehler, C.A., Paul, N.M. and De Haan, D.O., 2006. Oligomer formation in evaporating aqueous glyoxal and methyl glyoxal solutions. Environmental Science & Technology, 40(20): 6318-6323.

Martino, M., Lézé, B., Baker, A.R. and Liss, P.S., 2012. Chemical controls on ozone deposition to water. Geophysical Research Letters, 39(5): L05809.

McFiggans, G. et al., 2004. Direct evidence for coastal iodine particles from Laminaria macroalgae–linkage to emissions of molecular iodine. Atmospheric Chemistry and Physics, 4(3): 701-713.

Mirdamadi-Esfahani, M., Lampre, I., Marignier, J.-L., de Waele, V. and Mostafavi, M., 2009. Radiolytic formation of tribromine ion Br 3− in aqueous solutions, a system for steady-state dosimetry. Radiation Physics and Chemistry, 78(2): 106-111.

Monge, M.E. et al., 2012. Alternative pathway for atmospheric particles growth. Proceedings of the National Academy of Sciences, 109(18): 6840-6844.

Mulazzani, Q.G. and Buxton, G.V., 2006. On the kinetics and mechanism of the oxidation of I- by (OH)-O-center dot/O center dot- in alkaline aqueous solution. Chemical Physics Letters, 421(1-3): 261-265.

Murov, S.L., Carmichael, I. and Hug, G.L., 1993. Handbook of photochemistry. CRC Press.

Nguyen, T.B., Coggon, M.M., Flagan, R.C. and Seinfeld, J.H., 2013. Reactive Uptake and Photo-Fenton Oxidation of Glycolaldehyde in Aerosol Liquid Water. Environmental Science & Technology, 47(9): 4307-4316.

Nozière, B., Dziedzic, P. and Córdova, A., 2008. Products and Kinetics of the Liquid-Phase Reaction of Glyoxal Catalyzed by Ammonium Ions (NH4+). The Journal of Physical Chemistry A, 113(1): 231-237.

Nozière, B., Dziedzic, P. and Córdova, A., 2009. Products and kinetics of the liquid-phase reaction of glyoxal catalyzed by ammonium ions (NH_4^+). Journal of Physical Chemistry A, 113(1): 231-237.

O'Dowd, C.D. and de Leeuw, G., 2007. Marine aerosol production: a review of the current knowledge. Philosophical Transactions of the Royal Society A: Mathematical, Physical and Engineering Sciences, 365: 1753-1774.

Oum, K.W., Lakin, M.J., DeHaan, D.O., Brauers, T. and Finlayson-Pitts, B.J., 1998. Formation of molecular chlorine from the photolysis of ozone and aqueous sea-salt particles. Science, 279: 74-77.

Reeser, D.I., George, C. and Donaldson, D.J., 2009a. Photooxidation of Halides by Chlorophyll at the Air-Salt Water Interface. Journal of Physical Chemistry A, 113: 8591-8595.

Reeser, D.I. et al., 2009b. Photoenhanced Reaction of Ozone with Chlorophyll at the Seawater Surface. Journal of Physical Chemistry C, 113: 2071-2077.

Robinson, A.L. et al., 2007. Rethinking organic aerosols: Semivolatile emissions and photochemical aging. Science, 315(5816): 1259-1262.

Saiz-Lopez, A. and von Glasow, R., 2012. Reactive halogen chemistry in the troposphere. Chemical Society Reviews, 41(19): 6448-6472.

Seinfeld, J.H. and Pankow, J.F., 2003. Organic atmospheric particulate material. Annual Review of Physical Chemistry, 54: 121-140.

Shapiro, E.L. et al., 2009. Light-absorbing secondary organic material formed by glyoxal in aqueous aerosol mimics. Atmospheric Chemistry and Physics, 9(7): 2289-2300.

Shrivastava, M. et al., 2011. Modeling organic aerosols in a megacity: Comparison of simple and complex representations of the volatility basis set approach. Atmospheric Chemistry and Physics, 11(13): 6639-6662.

Shrivastava, M., Lipsky, E.M., Stanier, C.O. and Robinson, A.L., 2006. Modeling semivolatile organic aerosol mass emissions from combustion systems. Environmental Science & Technology, 40(8): 2671-2677.

Sinreich, R., Coburn, S., Dix, B. and Volkamer, R., 2010. Ship-based detection of glyoxal over the remote tropical Pacific Ocean. Atmospheric Chemistry and Physics, 10(23): 11359-11371.

Tinel, L., Dumas, S. and George, C., 2013. A time resolved study of the multiphase chemistry of excited carbonyls: Imidazole-2-carboxaldehyde and halides. Comptes Rendus Chimie.

Trainic, M., Riziq, A.A., Lavi, A., Flores, J.M. and Rudich, Y., 2011. The optical, physical and chemical properties of the products of glyoxal uptake on ammonium sulfate seed aerosols. Atmospheric Chemistry and Physics, 11(18): 9697-9707.

Trainic, M., Riziq, A.A., Lavi, A. and Rudich, Y., 2012. Role of Interfacial Water in the Heterogeneous Uptake of Glyoxal by Mixed Glycine and Ammonium Sulfate Aerosols. Journal of Physical Chemistry A, 116(24): 5948-5957.

Tsigaridis, K. and Kanakidou, M., 2003. Global modelling of secondary organic aerosol in the troposphere: A sensitivity analysis. Atmospheric Chemistry and Physics, 3(5): 1849-1869.

Updyke, K.M., Nguyen, T.B. and Nizkorodov, S.A., 2012. Formation of brown carbon via reactions of ammonia with secondary organic aerosols from biogenic and anthropogenic precursors. Atmospheric Environment, 63(0): 22-31.

Vione, D. et al., 2006. Photochemical reactions in the tropospheric aqueous phase and on particulate matter. Chemical Society Reviews, 35(5): 441-453.

Volkamer, R. et al., 2006. Secondary organic aerosol formation from anthropogenic air pollution: Rapid and higher than expected. Geophysical Research Letters, 33(17): L17811.

Volkamer, R. et al., 2007. A missing sink for gas-phase glyoxal in Mexico City: Formation of secondary organic aerosol. Geophysical Research Letters, 34(19): L19807.

Volkamer, R., Ziemann, P.J. and Molina, M.J., 2009a. Secondary Organic Aerosol Formation from Acetylene (C2H2): seed effect on SOA yields due to organic photochemistry in the aerosol aqueous phase. Atmospheric Chemistry and Physics, 9: 1907-1928.

Volkamer, R., Ziemann, P.J. and Molina, M.J., 2009b. Secondary Organic Aerosol Formation from Acetylene (C2H2): seed effect on SOA yields due to organic photochemistry in the aerosol aqueous phase. Atmospheric Chemistry and Physics, 9(6): 1907-1928.

von Sonntag, C. and Schuchmann, H.-P., 1991. The Elucidation of Peroxyl Radical Reactions in Aqueous Solution with the Help of Radiation-Chemical Methods. Angewandte Chemie International Edition in English, 30(10): 1229-1253.

Waxman, E.M. et al., 2013. Secondary organic aerosol formation from semi- and intermediate-volatility organic compounds and glyoxal: Relevance of O/C as a tracer for aqueous multiphase chemistry. Geophysical Research Letters, 40(5): 978-982.

Yu, G. et al., 2011. Glyoxal in Aqueous Ammonium Sulfate Solutions: Products, Kinetics and Hydration Effects. Environmental Science & Technology, 45(15): 6336-6342.

Chapter V: Photosensitized production of atmospherically reactive organic compounds at the air-aqueous interface

V.0. Motivations

In this chapter, in the form of a published article, the specificities of photochemistry at the air-water interface are investigated. The interfacial region is a region that does not just connect the two phases, but displays its own specific chemistry. Here, we follow reactions of octanol, a proxy for environmentally relevant soluble surfactants, initiated by an attack by triplet state carbonyl compounds, amongst which IC, imidazole-2-carboxaldehyde, already presented in the in the previous chapter. These carbonyl compounds are concentrated at this interface by the presence of the surfactant. The gas phase products are determined using PTR-Tof-MS and those remaining in solution by ATR-FTIR spectroscopy and HPLC-HRMS. The photosensitized production of carboxylic acids is observed, as well as unsaturated and branched-chain oxygenated products. A mechanism which is consistent with the observations is detailed here and the energetics of several key reactions are calculated using quantum chemical methods. The results suggest that the concentrating nature of the interface leads to its being a favorable venue for radical reactions yielding complex and functionalized products which themselves could initiate further secondary chemistry and new particle formation in the atmospheric environment.

Chapter V: Photosensitized production of atmospherically reactive organic compounds at the air-aqueous interface

Authors: Hongbo Fu*, Raluca Ciuraru, Yoan Dupart, Monica Passananti, Liselotte Tinel, Stéphanie Rossignol, Sebastien Perrier, D. James Donaldson[$], Jianmin Chen*, Christian George

Article published in the Journal of the American Chemical Society, 2015, volume 137, n° 16, pp. 8348-8351

V.1. Introduction

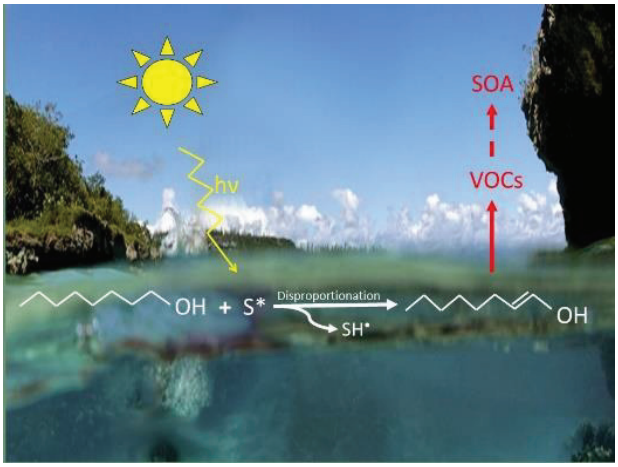

Air-water interfaces are ubiquitous in the environment, with the air-sea interface being among the most obvious (Donaldson and Vaida, 2006). The air-water interface represents an unique environment for chemical reactions, because the high surface energy of water means that many organic species are surface active, having surface mole fractions greater than those in the bulk (Donaldson and Vaida, 2006; Griffith et al., 2014). This surface activity gives rise to a concentrating effect at the interface: reagents may be present there at much greater effective concentrations than in either the underlying water or overlying air bulk phases. Moreover, this concentrating effect may be enhanced if the presence of one compound at the interface increases the propensity of other compounds to reside there as well (Donaldson and Vaida, 2006). This effect is seen, for example, in the increased surface partitioning of polycyclic aromatic hydrocarbons (PAHs) compounds to the water surface when there is a near monolayer coating of 1-octanol present there (Henderson and Donaldson, 2012; Mmereki et al., 2003; Wick et al., 2010). Organic coatings at the surface of aerosols, lakes, and oceans have been proposed to impact both atmospheric and prebiotic chemistries (Buch et al., 2007; Donaldson and Vaida, 2006; Griffith and Vaida, 2013).

Such surface coatings, potentially as thin as a monolayer, may also provide a different reaction medium compared to bulk water, thus modifying reaction mechanisms, rates, and products (Cosman and Bertram, 2008; Donaldson and George, 2012; Donaldson and Vaida, 2006; Laskin et al., 2003), as shown for peptide bond formation (Griffith and Vaida, 2012). Furthermore, specific chromophores concentrated within organic surface films could absorb actinic radiation and initiate photochemistry at the interface (Canonica et al., 1995; Gerecke et al., 2001). This led to the investigation of photoenhanced uptake of NO_2 and O_3 at surfaces containing photoactive compounds such as simple aromatic ketones or chlorophyll present at the air/sea interface (Jammoul et al., 2009; Reeser et al., 2009). There is also a growing body of evidence that some aerosols contain strong light-absorbing compounds, such as humic-like substances (Dinar et al., 2008), aromatic carbonyls or in situ produced N-derivatized imidazoles (Yu et al., 2011), which can photosensitize reactions that give rise to secondary organic aerosol (SOA) formation and aging (Rossignol et al., 2014).

In general, however, photochemistry at interfaces remains very poorly characterized, giving rise to potentially large uncertainties in our ability to simulate and predict both atmosphere processes and sea surface chemistry (George et al., 2015). In particular, there has been no attention paid to the impact of such specific chemistry on the photosensitized production of gaseous volatile organic compounds from aqueous surfaces, nor to the chemical signatures of the VOCs thus released. Although ozonolysis at (marine) environmental surfaces has been shown to produce a series of gaseous carbonyls and some unsaturated compounds, these carry only unsaturations present in their parent molecules (Zhou et al., 2014). For the most part, the production of unsaturated compounds in the marine environment has been attributed solely to biological activity.

In the following, we challenge this viewpoint and show that trace amounts of photoactive agents, concentrated at the air/water interface, can give rise to a distinct interfacial chemistry producing unsaturated products from linear alkyl chains.

V.2. Results and discussion

We probed photochemistry by measuring the gas phase products obtained from a radical reaction initiated at the octanol-coated air-water interface, and compared these to those from a reaction initiated in the same way, but taking place in a bulk octanol environment. Trace quantities of a photosensitizer present at the interface (either imidazole carboxaldehyde (IC) or 4-benzoylbenzoic acid (4-BBA)) when excited to the triplet state, initiated radical reactions by abstracting a hydrogen atom from 1-octanol molecules present in monolayer amounts, creating a C_8 alcohol radical. The ultimate gas phase reaction products - which surprisingly include atmospherically reactive unsaturated and carbonyl-containing compounds - were detected using Proton-Transfer-Reaction Time of Flight Mass Spectrometry (PTR-ToF-MS). These products are compared to those obtained from the reaction initiated by either IC or 4-BBA in a thin film of 1-octanol spread on a ZnSe crystal, measured by Attenuated Total Reflection Fourier Transform Infrared Spectroscopy (ATR-FTIR) and High Performance Liquid Chromatography coupled with Heated ElectroSpray Ionisation and High Resolution Mass Spectrometry (HPLC-HESI/HRMS). Quantum chemical calculations are used to confirm the proposed reaction mechanisms.

To demonstrate the concentrating effect of an organic monolayer on the photosensitizers used here, figure V-1 displays adsorption isotherms of IC at the air-aqueous interface, obtained from glancing-angle laser-induced fluorescence spectra. Although the bulk fluorescence of IC in octanol is about 5 times less intense than in pure water, a clearly enhanced fluorescence of IC is observed at the surface of a 1 mM solution of 1-octanol, an aqueous concentration giving rise to near monolayer coverage at the surface (Mmereki et al., 2003). It is clear that the surface concentration of the photosensitizer is enhanced in the presence of a 1-octanol coating, indicating an increased propensity to partition to the organic-coated interface. An enhanced presence of photosensitizer at the coated interface strongly suggests that photosensitized reactions may also be enhanced there.

To test this hypothesis, we measured the gas phase products evolved following illumination of a cell containing an octanol-coated aqueous solution of 4-BBA, which is also expected to show an enhanced concentration at an organic-coated aqueous interface. A quartz cell (2 cm diameter and 5 cm length) was half-filled with 7 ml of 18 MΩ deionized

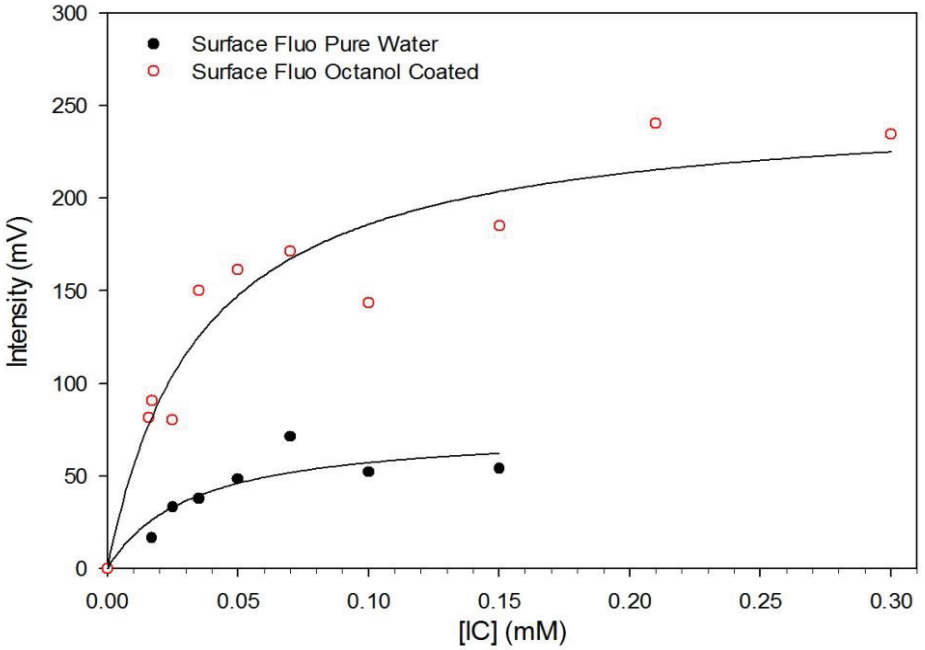

Figure V-1: Fluorescence intensity of IC at the air-aqueous interface, measured at its max. Emission wavelength of 335 nm as a function of the concentration of photosensitizer (IC) in the bulk, measured at a pure water surface (•) and at an octanol (1 mM) coated surface (○). The solid lines show fits to a Langmuir adsorption isotherm.

water, containing 0.1 mM 4-BBA and 2.5 mM 1-octanol; this solution was continuously purged with 100 sccm of purified air. After a stabilization time, the cell was illuminated by a 150 W xenon lamp, simulating actinic solar radiation. As soon as the continuous illumination started, a series of gas-phase compounds, containing double bonds and/or carbonyl functions are rapidly produced and reach a steady state level after ~25 min. As soon as the light is switched off, the gas phase concentrations of these compounds decrease swiftly and return to background levels after 20 min. The detected unsaturated species include hexenal (*m*/*z*, 99.080), octenal (*m*/*z*, 127.112), hexenoic acid (*m*/*z*, 115.075), octenoic acid (*m*/*z*, 143.107), and heptene (*m*/*z*, 99.117), as illustrated for octenal figure V-2. These unsaturated compounds were about 14 times more plentiful in the gas phase than the C_6 and C_8 acids. Long carbon chain products (C_{15},C_{16}) were also detected (listed in table V-S1). Control experiments indicated no formation of any gas phase organic compounds in the dark or in the absence of the photosensitizer.

Because the gas phase products seen with illumination (and reported in table V-S1) appear to derive from 1-octanol, we carried out further experiments in which thin films of 1-

octanol containing either IC or 4-BBA, were deposited on top of a ZnSe ATR crystal, then irradiated with a UV lamp (20 W, emission range 280-400 nm). The photochemical reaction was followed in time by monitoring changes in the FTIR spectrum. The reactions initiated by both photosensitizers show similar behavior. Net changes in the absorption spectra are shown in figure V-3 with peak assignments given in table V-S2. Peaks assigned to 1-octanol diminished in intensity, as indicated by the negative-going peaks in the figure, appearing at 2958 cm^{-1} (-CH_3 asymmetric stretching), 2926 cm^{-1} (-CH_2 symmetric stretching), 2852 cm^{-1}

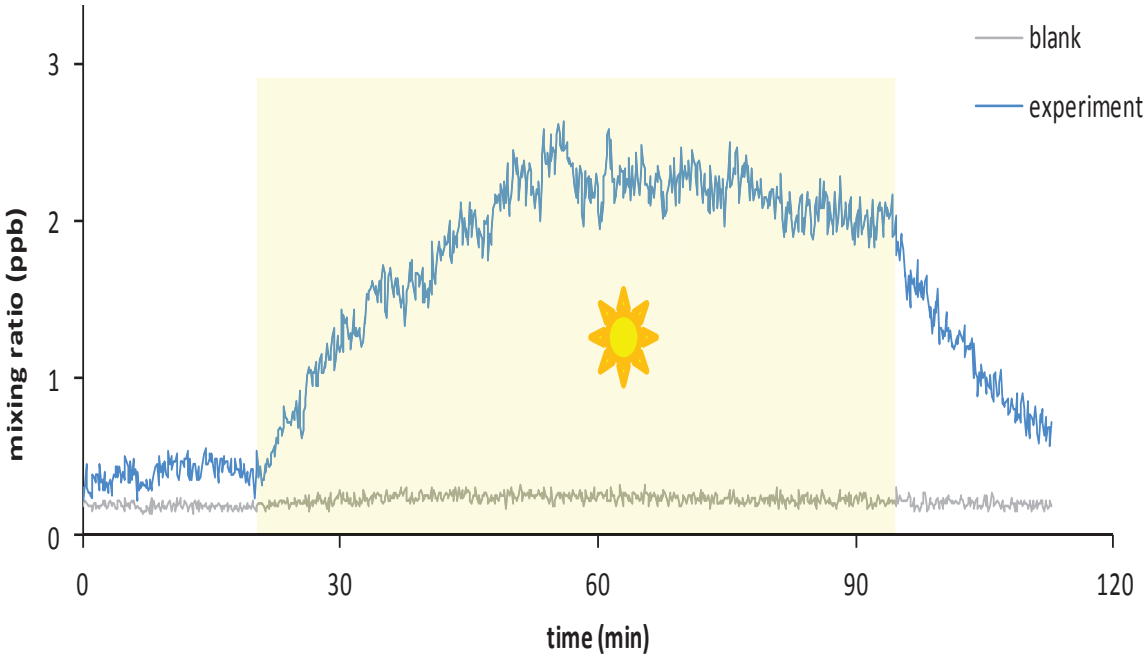

Figure V-2: PTR-Tof-MS results from a typical irradiation experiment. The gas phase concentration of 1-octenal is shown as a function of time following illumination (highlighted in yellow). The grey line shows the result from a blank experiment, in which no 4-BBA was present. The blue line displays the results seen when a solution containing water, 1-octanol and 4-BBA is irradiated.

(-CH_2 asymmetric stretching), 1461 cm-1 (-CH_3 bending mode), and 1061 cm^{-1} (C-O stretching vibration) (Tremblay et al., 2011). At the same time, product peaks appeared, indicative of branched aliphatic hydrocarbon components, for instance, the peak seen at 1108 cm^{-1}, corresponding to the bending vibration of a branched carbon backbone. The wide band appearing around 1380 cm^{-1} splits into a doublet with peaks at 1388 and 1368 cm^{-1}, assigned to the C-H bending from tertiary carbon (Nieto-Gligorovski et al., 2008). A broad product peak was also observed in the region of 1600-1750 cm^{-1}, which could be separated into four

independent peaks centered at 1713, 1671, 1642, and 1611 cm^{-1} using Gaussian fitting (OMNIC8.2, Thermo Scientific). The resulting fits are shown in figure V-S1. The shoulder peak at 1713 cm^{-1} is assigned to an absorption band from C=O groups of carboxylic acids, supported by the observation of weak absorption bands at ~2680 and ~2558 cm^{-1}, assigned as the O-H stretching vibration of carboxylic acids (Fu et al., 2007; Sax et al., 2005). The peak at 1671 cm^{-1} was assigned to the C=O vibrations of unsaturated aldehyde structures, and the sharp peak at 1642 cm^{-1} to the C=C stretching of the same structure.

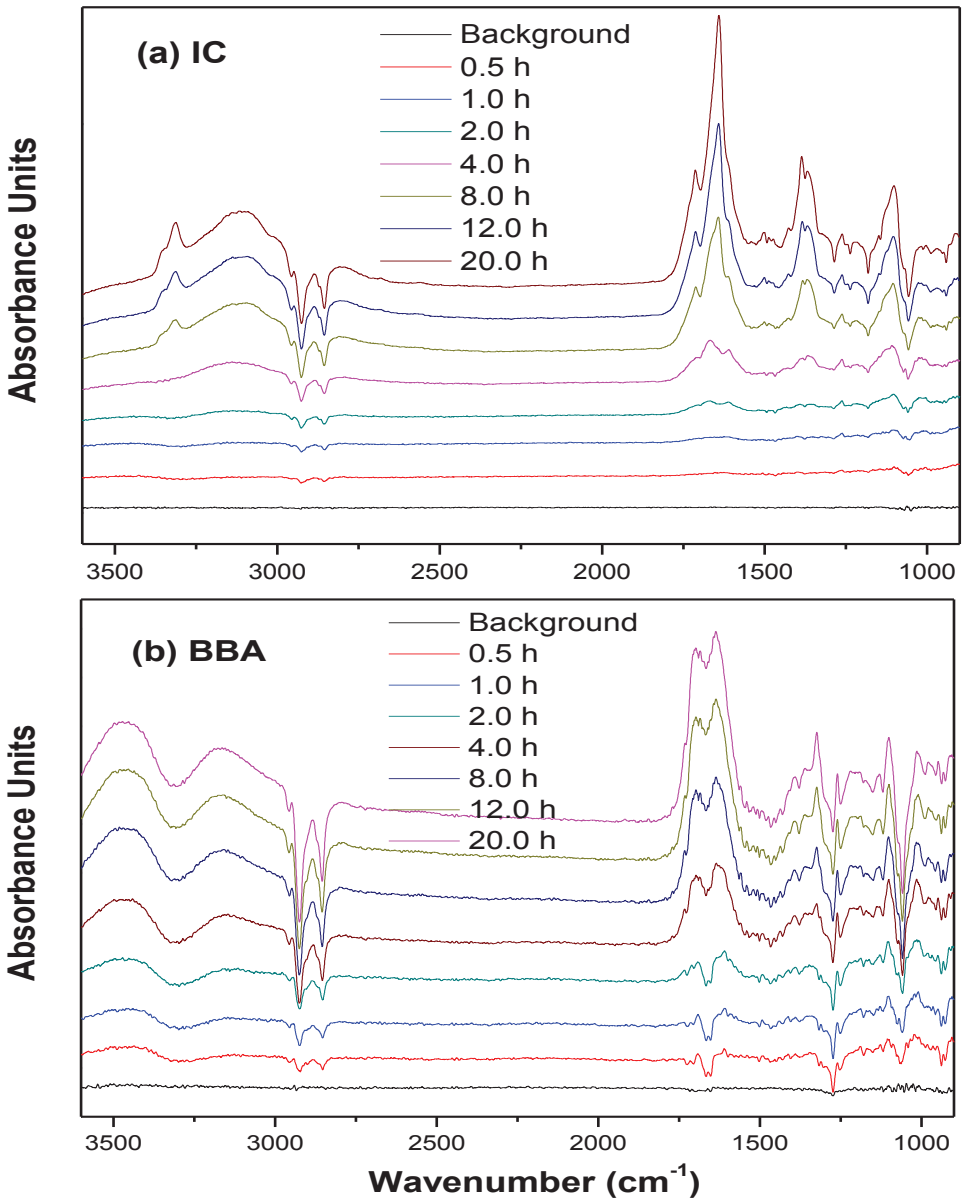

Figure V-3: Time-resolved ATR-IR absorbance spectra: phototransformation of 1-octanol in the presence of IC (a) and 4-BBA (b) under the irradiation.

The FTIR results described above are consistent with the general picture obtained from the PTR-MS measurements: formation of branched and unsaturated functionalized compounds from the 1-octanol following illumination. After the FTIR experiments, the products in the illuminated sample were identified using HPLC-(-)HESI/HRMS. The major product seen was $C_8H_{16}O_3$ (*m/z* 159.103), attributed to hydroxyl-octanoic acid. Five chromatographic peaks at this mass were observed (shown in figure V-S2), probably due to 5 different positions of the hydroxyl function on the carbon chain. This is in good agreement with the FTIR spectra (figure V-3) showing a new peak around 1700 cm^{-1}, which could be assigned to the carbonyl region of the –COOH groups. Generally, the condensed phase products detected here represent longer carbon chains (~C_{22}) compared to those identified by PTR-MS (~C_{16}). This points to different partitioning of the products: those with higher solubility or lower vapor pressure are trapped in the condensed phase, while those with significant volatility are more readily observed in the gas phase (Ziemann and Atkinson, 2012).

From this global picture of the products formed during the irradiation of an octanol layer in the presence of a photosensitizer, a general mechanism can be proposed, as illustrated in figure V-4 and confirmed by the results of quantum chemical calculations, reported in tables V-S3 and V-S4. The first step is the known formation of the photosensitizer triplet state under irradiation (Alvarez et al., 2012; Canonica et al., 1995). This energetic species can then abstract a hydrogen from 1-octanol to form a hydroxyoctil radical, a process that is quite exothermic, as estimated by the quantum calculations. This step could be kinetically enhanced at the interface because of the enhanced concentration of the photosensitizer there. Regeneration of the IC molecule is possible in the presence of O_2 via hydrogen abstraction to form HO_2, another very exothermic process. Formation of condensed phase HO_2/O_2^- was indeed observed by means of ESR, as shown in figure V-S3. Characteristic peaks of HO_2/O_2^- were observed for 1-octanol mixed with 4-BBA (Chen et al., 2006; Fu et al., 2006) and the signal intensity increased markedly with irradiation time. No such signals were observed in the dark.

The C_8 alcohol radical formed in the first reaction can suffer one of two probable fates: disproportionation or dimerization in the presence of another such radical, and addition of O_2, forming a peroxy-alcohol radical. Although both are strongly exothermic, one expects that the likelihood of the disproportionation will increase as the local concentration

of radicals becomes large, e.g., under our conditions of continuous illumination with constant regeneration of the photosensitizer. The ready availability of oxygen molecules from the gas phase will certainly help to promote the O_2 addition reaction at the air interface, giving a ready source of peroxy-alcohol radicals there. The disproportionation of the hydroxyoctil radical will yield as products an unsaturated product and the original alcohol. The location of the unsaturation will depend upon the location from which the hydrogen abstraction occurs. The formation of octanal from the α/β unsaturated alcohol is energetically favorable, providing a route to aldehyde products. Although elimination of HO_2 from the peroxy-alcohol could also give unsaturated or aldehyde products, this process is calculated to be quite endothermic, so is likely to be very slow at room temperature. A more likely fate for α-peroxy-alcohol is carboxylic acid formation via elimination of OH, which is calculated to be exothermic. Although such four-membered ring reactions typically exhibit high activation barriers, the presence of a bridging water molecule has been shown in similar cases to lower considerably the transition state energy (Vaida et al., 2003). The ready availability of water molecules at the air-water interface thus is likely to play an important role in the acid formation reaction.

Following the production of these first-generation products, similar radical reactions involving these daughter compounds may take place. For example, a disproportionation type reaction involving an octanoic acid radical could yield the octenoic acid observed here. Likewise, radical recombination without reaction will give branched compounds containing C_{16} backbones, also as observed here.

The similarity in the products observed from the 1-octanol film and the water surface experiments suggests that the latter take place in an octanol-rich region of the aqueous system. The strong partitioning of IC to the 1-octanol-coated interface that we observe here, in conjunction with the known surface partitioning behavior of the alcohol, suggests that the initial radical formation takes place in the interface region, where both reagents are concentrated. Indeed, to be competitive with quenching of ^{3}IC* by water, the first order reaction rate of ^{3}IC* with 1-octanol in bulk aqueous solution must exceed 6×10^5 s^{-1}; with the concentration of 1-octanol used here, this implies a near diffusion-limited reaction rate constant of 2.4×10^8 M^{-1} s^{-1} for the H-abstraction reaction (Tinel et al., 2014). Although conceivable, this seems unphysically high for an atom transfer reaction between neutral

species. The formation of acidic products requires the availability of O_2; it may be that the presence of water is also critical to lower the OH elimination barrier. The concentrations of both of these are high in the interface region.

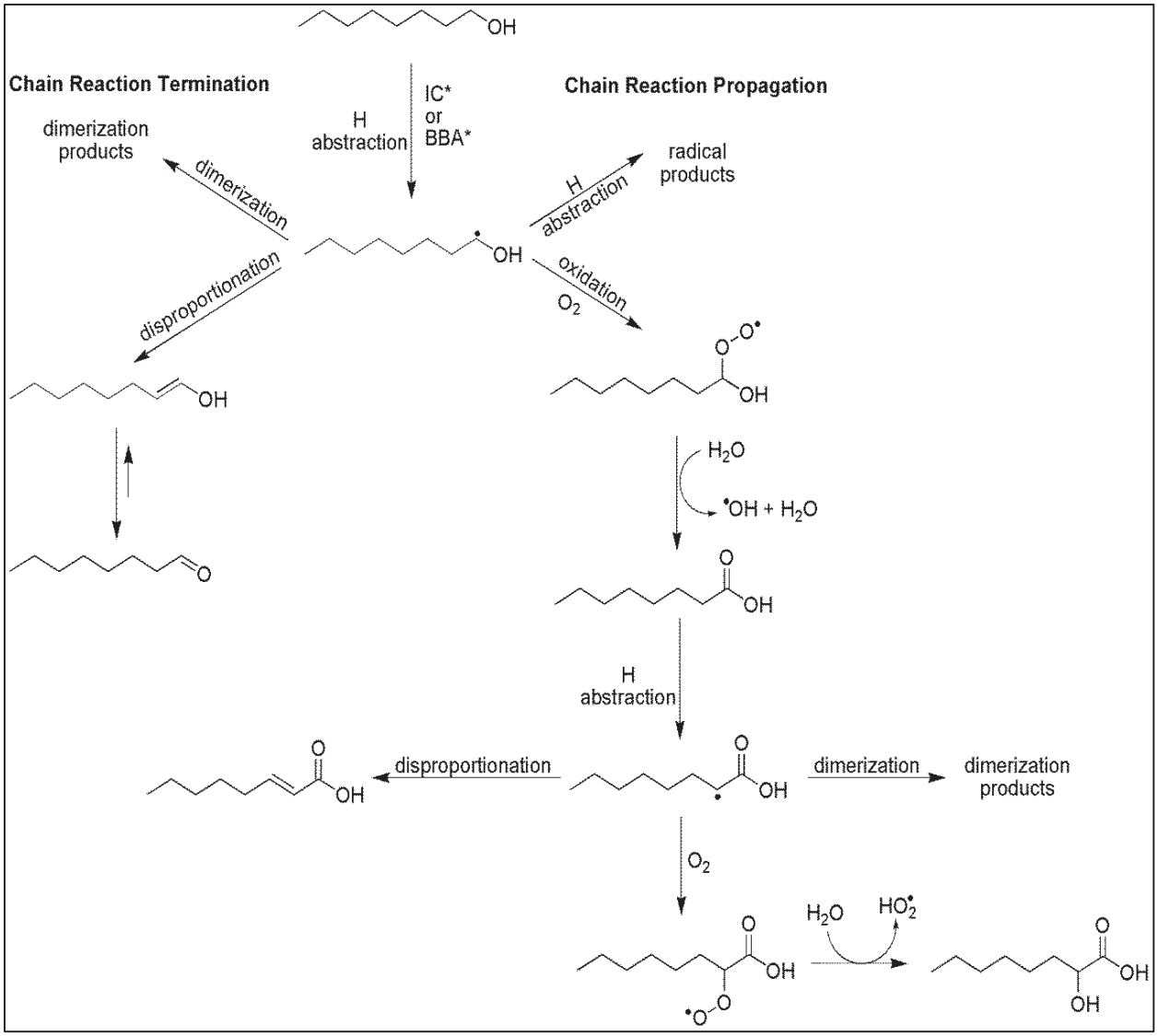

Figure V-4: Proposed mechanisms for photochemical reactions at the interface in the presence of octanol and a photosensitizer.

V.3. Conclusions and environmental implications

In summary, the irradiation of an organic film in the presence of photosensitizers at the water surface clearly leads to a release of VOCs to the gas phase, without any gas phase oxidants, except O_2, playing a role. The advantageous venue provided by the organic-coated water surface region can help promote photoinitiated radical chain reactions, including radical-radical, radical-molecule, or intramolecular rearrangement, to produce either another radical or molecule. The surface activity of the organic compounds involved in the interfacial photochemistry allows for their local concentrations to be greater than their bulk concentrations, increasing the probability of contact between reactive species. The presence at the interface of both gas phase O_2 and aqueous phase water allows these species to participate as well in the reaction in a facile manner. The work presented here demonstrates that an organic film, at the top of an aqueous phase, represents a favorable venue for photoinduced chemistry. As aqueous surfaces coated with organic films are potentially widespread in the environment (oceans, lakes, wet aerosols, cloud droplets, …), it seems clear that such photochemistry has the potential to increase abiotic VOC emissions, including unsaturated VOC emissions, that can contribute to secondary organic aerosol (SOA) formation. This process could be one of the missing sources of SOA in current modeling and could be consistent with a number of previously unexplained field study observations (George et al., 2015; Ziemann and Atkinson, 2012)

V.4. Experimental Methods

V.4.1. Reagents

All chemicals were reagent grade or better and used as received: 1-octanol (Sigma Aldrich, 99%); 4-benzoylbenzoic acid (4-BBA, Sigma Aldrich; 99%); imidazole-2-carboxaldehyde (IC, Sigma Aldrich, 99%); methanol for ESR experiments (Fisher, 99%); the spin trap 5, 5-dimethyl-1-pyrroline-*N*-oxide (DMPO) (Sigma Aldrich, 99%); ethanol (Sigma Aldrich, 99.5%); ethanol for cleaning purposes (VWR Co., 96%). Aqueous solutions were freshly prepared using 18MΩ ultra-pure water (ELGA).

V.4.2. Glancing-Angle Laser Induced Fluorescence (GALIF)

Fluorescence at the air-aqueous interface of the samples of interest was induced using the unfocussed output of an Nd:YAG-pumped optical parametric oscillator (OPO) fixed at 285 nm, using the glancing-angle LIF method which has been reported previously in detail (Kahan et al., 2007; Mmereki and Donaldson, 2002). The ~5 ns pulses from the laser operating at 10 Hz repetition rate had energies of ~2 mJ/pulse, with a pulse-to-pulse variability of about 15%. The laser beam impinged the liquid sample surface at an angle >85° from the surface normal. The aqueous sample (100 mL) was held in a modified three-neck round bottom flask with two quartz windows for laser beam entry and exit. Fluorescence was collected using a 7 mm diameter liquid light guide suspended ~8 mm above the sample surface, directly above the place where the incoming laser beam impinged on the surface. The collected light was imaged onto the entrance slit (200 μm) of a grating monochromator; the transmitted intensity was detected by a photomultiplier tube and sent to a digital oscilloscope which averaged the intensity vs. time signal over 16 laser shots. A time slice of 50 ns of the fluorescence decay captured by the oscilloscope, starting at 10 ns after the laser pulse, was averaged and output to a computer. This was registered as the fluorescence intensity observed at the detection wavelength.

For each concentration of IC, a full emission spectrum was recorded between 300 – 380 nm, at 5 nm intervals. Adsorption isotherms are constructed from the average of the 4 maximum points for each individual spectrum at a particular IC concentration, using the intensity obtained at 335 nm, the maximum emission wavelength for the system. Aqueous

solutions containing 0.3 mM of IC with and without 1 mM octanol were freshly prepared and introduced into the round-bottomed flask at least 20 minutes before each measurement to stabilize the surface layer. The procedure for obtaining each isotherm was as follows: starting with the most concentrated solution of IC in either pure water or in water containing 1 mM of 1-octanol, a complete spectrum was recorded. Then 10.0 mL of the solution were removed and replaced with 10.0 mL of a solution that was identical, except with no IC present. The solution was allowed to sit for 20 minutes, then a full spectrum recorded at this lower concentration. This process was repeated many times until the fluorescence signal level dropped to be too low to measure.

V.4.3. PTR-Tof-MS Measurements

The photochemical reactions of octanol at the water surface were performed using a Quartz cell (2 cm diameter and 5 cm length) filled with 7 ml of 18 MΩ deionized water, a photosensitizer (4-BBA) and an organic surfactant (1-octanol), present at a concentration of 2.5 mM. These solutions were irradiated using a 150 W Xenon lamp (an IR filter was used to prevent heating). 100 sccm of purified air was continuously flowed through the quartz cell. Gas-phase products were investigated using proton transfer reaction mass spectrometry (PTR-Tof-MS) with H_3O^+ as reagent ion. PTR-Tof-MS measurements were carried out using a commercial SRI-PTR-Tof-MS 8000 instrument from Ionicon Analytik GmbH (Innsbruck, Austria) (Lindinger et al., 1998). The PTR-MS continuously samples 80 sccm from the emission stream through 1.5 m of 6 mm (i.d.) heated polyetheretherketone (PEEK) tubing. No particle filter was placed at the inlet to avoid possible artifacts from any deposition of organics onto the filter. Internal calibration of the TOF data and peak extraction were performed according to the procedure described in detail by Lindinger et al. (Lindinger et al., 1998). PTR-Tof-MS spectra were collected at a time resolution of 8 s, using a drift voltage of 600 V, drift temperature of 60°C and a drift pressure of 2.25 mbar, resulting in an E/N of about 130 Td (1 Td = 10^{-17} cm^2 V^{-1}). The VOC concentrations are expressed in ppbv and were calculated according to the formula described previously (Cappellin et al., 2012).

V.4.4. FTIR Experiments.

A Bruker (VERTEX 70) FTIR spectrometer equipped with a horizontal ZnSe attenuated total reflectance (ATR) cell (Korth Kristalle, Altenholz) was used. The entire horizontal ATR cell was placed inside the internal compartment of the FTIR spectrometer that contains optics for the ATR cell. A 20 W UV lamp (λ, 300-420 nm) was used as the irradiation light source. All of liquid-phase measurements were carried in the ATR cell at ambient temperature. The penetration depth of the evanescent wave is approximately 6 μm for the ZnSe crystal. The collected spectra are, therefore, sensitive only to the condensed-phase reaction products and not to any volatilized reaction products.

For ATR-FTIR experiments, a solid powder of 4-BBA or IC with known mass (100 mg) was first dissolved in 50 mL of ethanol. Then 0.5 mL of the solution was dripped onto the ZnSe crystal and dried with a nitrogen flow for about 3 h. This process left behind a thin layer of sensitizer. Then 0.5 mL of 1-octanol was deposited onto the crystal, and the cell was sealed quickly with a quartz mask to prevent evaporation. After each solution was added to the cell, spectral scans were collected at 15 min intervals for up to 1.0 h until no change in the spectra was observed, suggesting the system had stabilized. A spectrum was taken at this point to act as a reference spectrum prior to the irradiation. After that, the UV lamp was turned on and spectra were collected automatically in the range of 600-4000 cm^{-1} at time intervals of 10 min or 1 h under irradiation. Each spectrum averaged 128 scans and had resolution of 4 cm^{-1} unless otherwise noted. Using the initial spectrum as a reference, any losses of species during photochemical reactions show negative bands, whereas those of the products show positive ones.

All of the measurements were repeated at least twice. The blank runs in the dark or in the absence of the photosensitizers were performed under the same conditions. Before each measurement, the ZnSe ATR crystal was subjected to various consecutive cleaning procedures, using acetone, ultra-pure water and ethanol, until there were no visible impurities left. Small particles originating from cleansing tissues used in the first cleaning steps were blown off by compressed air before taking background spectra.

V.4.5. HPLC-HESI/HRMS Analyses

HPLC-HESI/HRMS analysis was carried out on a Dionex UltiMate 3000 U-HPLC system equipped with a photodiode array detector and coupled with an high mass resolution Q-Exactive Hybrid Quadrupole-Orbitrap mass spectrometer (Thermo Scientific, USA) equipped with a Heated Electrospray Ionization source (H-ESI). The samples, irradiated (and non-irradiated) by UV lamp during FTIR experiments, were analyzed after solubilization in H_2O/CH_3CN (1:1 v/v) (octanol concentration 1 mM), injection volume 5 µL. The chromatographic separation was performed on a C_{18} Acquity UPLC HSS T3 column (1.8µm, 2.1 mm x 100 mm, Waters) with a flow rate of 0.3 mL min^{-1}. The mobile phase was: (A) water with 0.1% formic acid and (B) acetonitrile with 0.1% formic acid (chemicals' grade Optima® LC-MS, Fischer Scientific, USA). The following elution gradient was used: at initial time (B) was kept at 1% for 2 min and was then linearly increased to 100% within 11 min; this ratio was maintained constant for 2 min before returning to initial conditions (B at 1%) in 0.1 min for 6.9 min. Electrospray ionization was performed in negative mode using the following conditions: spray voltage -3.0 kV, capillary temperature 350 °C, sheath gas (N_2) flow rate 40 (arbitrary units), auxiliary gas (N_2) flow rate 25 (arbitrary units), heater temperature 250 °C, S-lens RF level 50. The mass spectrometer was operated in full MS mode with a scanning range from 50 to 750 m/z and a resolution of 140 000.

V.4.6. Electron Spin Resonance (ESR)

Measurements. ESR spectra of spin-trapping radicals by DMPO were recorded at room temperature on a Bruker EPR ELEXSYS 500 spectrometer equipped with an in situ irradiation source (a Quanta-Ray ND:YAG laser system. λ = 355 nm). TEMPO (*g*) 2.0051) was chosen as a standard for determination of *g* factors as recommended elsewhere (Che et al., 2005). Typical instrumental conditions were as follows: center field, 316 G; sweep width, 100 G; resolution, 1024 pts; microwave frequency, ~9.77 GHz; microwave power, 12.68 mW; modulation frequency, 100 kHz. To minimize experimental errors, the same quartz capillary was used for all the measurements. The simulations of ESR spectra were obtained with the use of WinSim EPR simulation software.

V.4.7. Quantum Chemical Calculation

Quantum chemical calculations were performed to calculate the energies of all species involved in the first steps of the proposed mechanism. The calculations were carried out using the Spartan 14 set of programs for the Mac OS-X operating system (Shao et al., 2006; Spartan, '14). Geometries were optimized at the B3LYP/6-31G* level and zero-point energies were calculated from the vibrational frequencies predicted during this stage. Energies for each compound were then calculated at these optimized geometries, at the B3LYP/6-311+ G (2df, 2p) level. Table V-S3 reports the energies and zero-point energies used here. The reaction energetics were calculated from these higher-level results, with a zero-point correction applied using the unscaled vibrational frequencies calculated at the lower level. These results are reported in table V-S4.

The accuracy of the calculated energetics at the level of theory used here (i.e. B3LYP/6-311+G(2df, 2p)) was estimated by comparison to experimental energies for these or similar systems. First, we estimate the uncertainty in the calculated singlet-triplet energy difference for IC be calculating this difference for several other systems. The singlet-triplet energy splitting for O_2 (between the ground $^3\Sigma$ and second excited $^1\Sigma$ states) is calculated to be 13,450 cm^{-1} (161 kJ/mol) compared to the experimental value of 13,195 cm^{-1} (158 kJ/mol) (Huber and Herzberg, 1979). The energy difference between the vibrationless levels of the ground and lowest triplet states of acetone is calculated to be 297 kJ/mol; this value is experimentally estimated to be between 332 and 342 kJ/mol from unresolved phosphorescence measurements at 77K in an *i*-propyl alcohol - ether matrix (Borkman and Kearns, 1966; Montalti et al., 2006). Finally, naphthalene's lowest triplet is calculated to be 242 kJ/mol above the ground state (zero-point corrected); experimentally this difference is reported to be 253 kJ/mol (Montalti et al., 2006). We conclude that the IC triplet excitation energy calculated at the B3LYP/6-311+G(2df, 2p) level is probably accurate to better than 20 kJ/mol. Since reaction A1a is calculated to be exothermic by about twice that amount, we are confident that errors in the calculated triplet energy are not causing an unfavorable reaction to seem favorable.

We estimate an uncertainty on the calculated overall reaction energies in a similar manner, by comparison to several experimentally known systems. Like reaction A1a, the well-studied reaction $O(^3P) + H_2$ --> OH + H features an overall reaction taking place on a

triplet surface, but with triplet and singlet state reagents evolving into two doublet state products. We calculate a reaction energy of + 9.6 kJ/mol, compared to +11.3 kJ/mol experimental value. From table V-S3, we obtain an energy for the reaction: OH + 1-propanol --> H_2O + CH_3CH_2CHOH of -102.4 kJ/mol, compared to -98.6 kJ/mol experimental (Afeefy et al., 2005; Finlayson-Pitts and Pitts Jr, 1999). From these we estimate that the reaction energetics are probably accurate to within ca. 10 kJ/mol.

V.5. Affiliations of the authors

All authors :

Université de Lyon 1, Lyon, F-69626, France, CNRS, UMR5256, IRCELYON, Institut de Recherches Sur la Catalyse et l'Environnement de Lyon, Villeurbanne, F-69626, France

Except:

*Shanghai Key Laboratory of Atmospheric Particle Pollution and Prevention, Department of Environmental Science and Engineering, Fudan University, Shanghai China; Collaborative Innovation Center of Atmospheric Environment and Equipment Technology (CICAEET), Nanjing, China

[$]Department of Chemistry, University of Toronto, 80 St. George St. Toronto, ON Canada M5S 3H6

V.6. Supplementary information

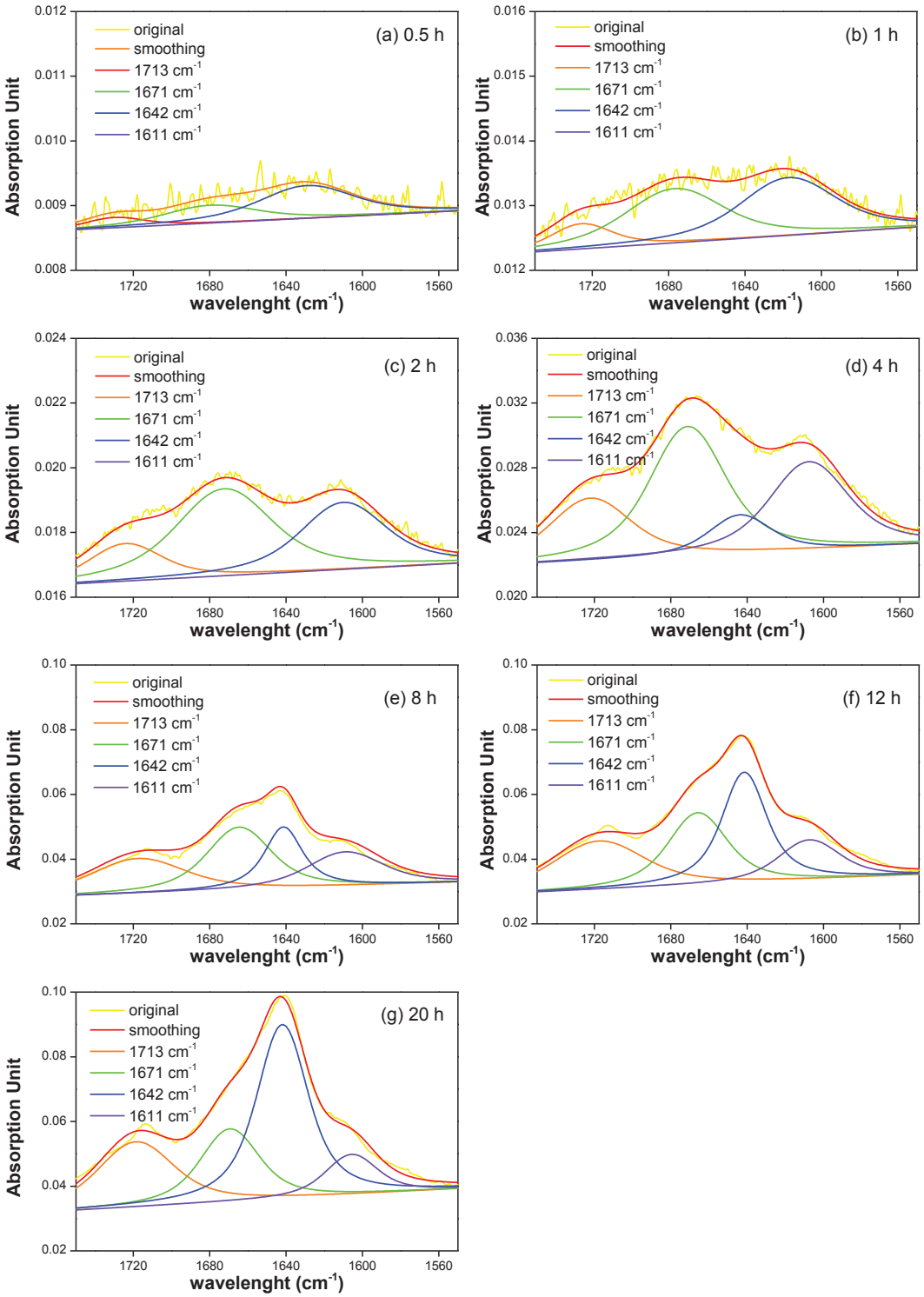

Figure V-S1: Time-resolved FTIR spectra (from 1600 cm-1 to 1750 cm-1) of octanol phototransformation in the presence of IC under the UV irradiation. The wide peak in this region was fitted using four Gaussian curve fits (OMNIC 8.2, Thermo Scientific).

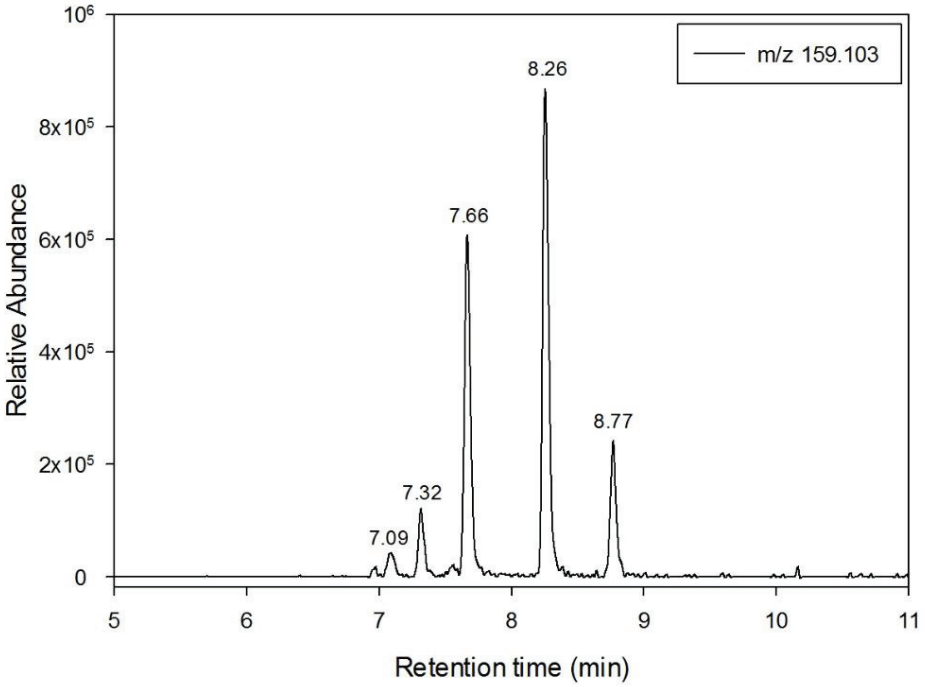

Figure V-S2: Extracted ion chromatogram of m/z 159.103 (corresponding neutral formula: $C_8H_{16}O_3$) obtained by UHPLC-(-)HESI/HRMS analysis of a mixture of 4-BBA solubilized in octanol irradiated during ATR-FTIR experiment.

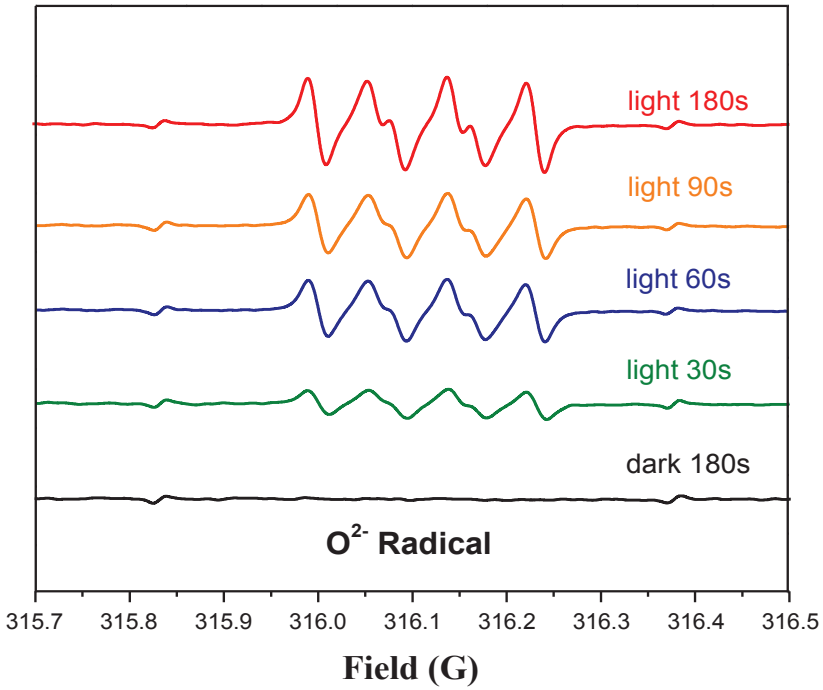

Figure V-S3: DMPO spin-trapping ESR spectra of the octanol solution in the presence of 4-BBA under UV irradiation. 4-BBA concentration, 0.5 g L^{-1}; DMPO concentration, 1.6 × 10^{-2} M.

Table V-S1. Detected compounds by PTR-Tof-MS and HPLC-(-)HESI/HRMS during octanol coated water and octanol film experiments respectively.

Compound	PTR-Tof-MS	HPLC-(-)HESI/HRMS
C_7H_{14}	x	-
$C_7H_{16}O$	x	-
C_6H_{14}	x	-
$C_6H_{10}O$	x	-
$C_6H_{12}O_2$	x	-
$C_6H_{10}O_2$	x	-
$C_8H_{14}O$	x	-
$C_8H_{16}O_2$	x	x (low intensity)
$C_8H_{14}O_2$	x	-
$C_8H_{14}O_4$	x	x
$C_8H_{16}O_4$	-	x
$C_8H_{16}O_3$	x	x
$C_8H_{18}O_2$	x	x (low intensity)
Dimerization products:		
$C_{15}H_{30}O_2$	x	-
$C_{16}H_{34}O_2$	x	-
$C_{16}H_{30}O_3$	x	Trace
$C_{16}H_{30}O_4$	x	Trace
$C_{16}H_{12}O_4$	x	x
$C_{22}H_{28}O_4$	-	x
$C_{22}H_{26}O_5$	-	x
$C_{22}H_{26}O_4$	-	x
$C_{22}H_{24}O_4$	-	x
$C_{14}H_{10}O_4$	x	x
$C_8H_6O_4$	x	x

Table V-S2. Peak assignments of the FTIR spectra (ν, stretching vibration; σ, bending vibration)

Absorption Bands (cm^{-1})		Assignment	Functional Group
IC	**4-BBA**		
2958	2956	ν_{as} (C-H)	$-CH_3$
2926	2926	ν_s (C-H)	$-CH_2-$
2852	2852	ν_{as} (C-H)	
2680/2558		σ (O-H)	-COOH
1461	1466	σ (C-H)	$-CH_3$
1061	1059	ν (C-O)	$-C-OH$
1388	1390	σ (C-H)	$-\overset{\vert}{\underset{\vert}{C}}H-$
1368	1363		
1108	1105	σ (C-C-C)	$-C-\overset{\vert}{\underset{\vert}{C}}-C-$
1713	1736	ν (C=O)	$-C(=O)-OH$
3113	3162	ν (O-H)	
1671	1693	ν (unsaturated C=O)	$-C=C-C(=O)-H$
1642	1636	ν (C=C)	
1611	1616	ν (C=O)	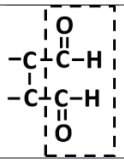

Table V-S3: Energies of species calculated at B3LYP/6-311+G(2df2p) level

species	E (hartree)	ZPE (hartree)
1-octanol	-391.05988	0.25267
IC	-339.667208	
^{3}IC	-339.553321	0.07717
1-octanol α-radical	-390.400436	0.23905
1-octanol γ-radical	-390.394728	0.2379
IC-OH	-340.233052	0.09014
$O_2(^3\Sigma)$	-150.378479	0.00373
HO_2	-150.966708	0.01418
OH	-75.7650576	0.00846
$O_2(^1\Sigma)$	-150.317170	
1-octanol α-peroxy	-540.833455	0.24858
octanoic acid	-465.124832	0.2347
1-octanol β-peroxy	-540.828799	0.2487
octanal	-389.847798	0.22859
oct-1-en-1-ol	-389.833952	0.22861
(E)-2-octenol	-389.830744	0.22871
octanoic acid α-radical	-464.470752	0.21928
octanoic acid α-peroxy	-614.889697	0.23061
(E)-2-octenoic acid	-463.909588	0.21097
1-propanol	-194.430251	0.10928
1-propanol α-radical	-193.770594	0.09522
acetone	-193.218264	0.08313
^{3}acetone	-193.101056	0.07912
naphthalene	-386.014780	0.147796
^{3}naphthalene	-385.915150	0.142399

Table V-S4: Quantum chemical calculations for the photosensitized reactions proposed in the present study.

Reaction	ΔE_o^o (kJ/mol)
A. Radical formation/ IC regeneration	
A1a) 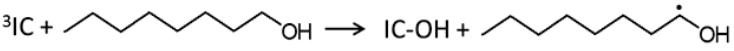	-54.7
A1b) 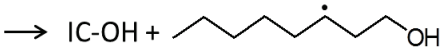	-42.6
A2) $IC\text{-}OH + O_2 \rightarrow IC + HO_2$	-267.5
B. Carbonyl formation	
B1) 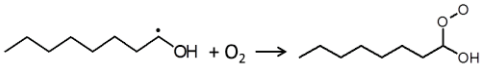	-127.9
B2a) 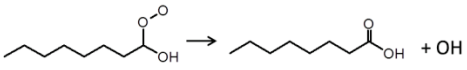	-162.2
B2b) 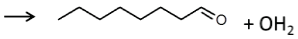	+34.3
B3) 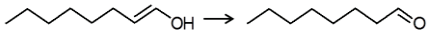	-36.4
C. Olefin formation	
C1) 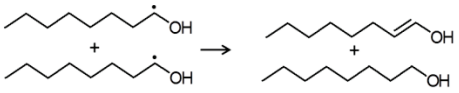	-235.3
C2) 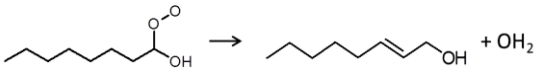	+66.9
C3) 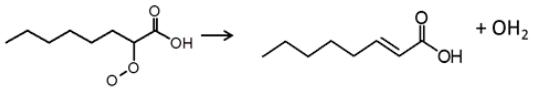	+20.9

V.7. References

Afeefy, H., Liebman, J. and Stein, S., 2005. Neutral thermochemical data. NIST chemistry webbook, NIST standard reference database, 69.

Alvarez, E.G., Wortham, H., Strekowski, R., Zetzsch, C. and Gligorovski, S., 2012. Atmospheric Photosensitized Heterogeneous and Multiphase Reactions: From Outdoors to Indoors. Environmental Science & Technology, 46(4): 1955-1963.

Borkman, R.F. and Kearns, D.R., 1966. ELECTRONIC-RELAXATION PROCESSES IN ACETONE. Journal of Chemical Physics, 44(3): 945-&.

Buch, V., Milet, A., Vácha, R., Jungwirth, P. and Devlin, J.P., 2007. Water surface is acidic. Proceedings of the National Academy of Sciences, 104(18): 7342-7347.

Canonica, S., Jans, U., Stemmler, K. and Hoigne, J., 1995. Transformation Kinetics of Phenols in Water: Photosensitization by Dissolved Natural Organic Material and Aromatic Ketones. Environmental Science & Technology, 29(7): 1822-1831.

Cappellin, L. et al., 2012. On quantitative determination of volatile organic compound concentrations using proton transfer reaction time-of-flight mass spectrometry. Environmental Science & Technology, 46(4): 2283-2290.

Che, Y.K. et al., 2005. Photooxidation of dibenzothiophene and 4,6-dimethyldibenzothiophene sensitized by N-methylquinolinium tetrafluoborate: Mechanism and intermediates investigation. Journal of Physical Chemistry B, 109(16): 8270-8276.

Chen, C.C. et al., 2006. Photodegradation of dye pollutants catalyzed by porous K3PW12O40 under visible irradiation. Environmental Science & Technology, 40(12): 3965-3970.

Cosman, L.M. and Bertram, A.K., 2008. Reactive uptake of N2O5 on aqueous H2SO4 solutions coated with 1-component and 2-component monolayers. Journal of Physical Chemistry A, 112(20): 4625-4635.

Dinar, E. et al., 2008. The complex refractive index of atmospheric and model humic-like substances (HULIS) retrieved by a cavity ring down aerosol spectrometer (CRD-AS). Faraday Discussions, 137: 279-295.

Donaldson, D.J. and George, C., 2012. Sea-Surface Chemistry and Its Impact on the Marine Boundary Layer. Environmental Science & Technology, 46(19): 10385-10389.

Donaldson, D.J. and Vaida, V., 2006. The influence of organic films at the air-aqueous boundary on atmospheric processes. Chemical Reviews, 106(4): 1445-1461.

Finlayson-Pitts, B.J. and Pitts Jr, J.N., 1999. Chemistry of the upper and lower atmosphere: theory, experiments, and applications. Academic press.

Fu, H., Wang, X., Wu, H., Yin, Y. and Chen, J., 2007. Heterogeneous uptake and oxidation of SO2 on iron oxides. Journal of Physical Chemistry C, 111(16): 6077-6085.

Fu, H.B., Zhang, L.W., Zhang, S.C., Zhu, Y.F. and Zhao, J.C., 2006. Electron spin resonance spin-trapping detection of radical intermediates in N-doped TiO2-assisted photodegradation of 4-chlorophenol. Journal of Physical Chemistry B, 110(7): 3061-3065.

George, C., Ammann, M., D'Anna, B., Donaldson, D.J. and Nizkorodov, S.A., 2015. Heterogeneous Photochemistry in the Atmosphere. Chemical Reviews, 115(10): 4218-4258.

Gerecke, A.C., Canonica, S., Muller, S.R., Scharer, M. and Schwarzenbach, R.P., 2001. Quantification of dissolved natural organic matter (DOM) mediated

phototransformation of phenylurea herbicides in lakes. Environmental Science & Technology, 35(19): 3915-3923.

Griffith, E.C., Rapf, R.J., Shoemaker, R.K., Carpenter, B.K. and Vaida, V., 2014. Photoinitiated Synthesis of Self-Assembled Vesicles. Journal of the American Chemical Society, 136(10): 3784-3787.

Griffith, E.C. and Vaida, V., 2012. In situ observation of peptide bond formation at the water–air interface. Proceedings of the National Academy of Sciences, 109(39): 15697-15701.

Griffith, E.C. and Vaida, V., 2013. Ionization state of L-Phenylalanine at the Air-Water Interface. Journal of the American Chemical Society, 135(2): 710-716.

Henderson, E.A. and Donaldson, D.J., 2012. Influence of Organic Coatings on Pyrene Ozonolysis at the Air–Aqueous Interface. The Journal of Physical Chemistry A, 116(1): 423-429.

Huber, K.-P. and Herzberg, G., 1979. Molecular spectra and molecular structure, Vol. 4. Constants of diatomic moleculesVan Nostrand Reinhold, New York: 534.

Jammoul, A., Dumas, S., D'Anna, B. and George, C., 2009. Photoinduced oxidation of sea salt halides by aromatic ketones: a source of halogenated radicals. Atmospheric Chemistry and Physics, 9(13): 4229-4237.

Kahan, T.F., Reid, J.P. and Donaldson, D.J., 2007. Spectroscopic probes of the quasi-liquid layer on ice. Journal of Physical Chemistry A, 111(43): 11006-11012.

Laskin, A. et al., 2003. Reactions at interfaces as a source of sulfate formation in sea-salt particles. Science, 301(5631): 340-344.

Lindinger, W., Hansel, A. and Jordan, A., 1998. On-line monitoring of volatile organic compounds at pptv levels by means of proton-transfer-reaction mass spectrometry (PTR-MS) - Medical applications, food control and environmental research. International Journal of Mass Spectrometry, 173(3): 191-241.

Mmereki, B.T., Chaudhuri, S.R. and Donaldson, D.J., 2003. Enhanced uptake of PAHs by organic-coated aqueous surfaces. Journal of Physical Chemistry A, 107(13): 2264-2269.

Mmereki, B.T. and Donaldson, D.J., 2002. Laser induced fluorescence of pyrene at an organic coated air-water interface. Physical Chemistry Chemical Physics, 4(17): 4186-4191.

Montalti, M., Credi, A., Prodi, L. and Gandolfi, M.T., 2006. Handbook of photochemistry. CRC press.

Nieto-Gligorovski, L. et al., 2008. Interactions of ozone with organic surface films in the presence of simulated sunlight: impact on wettability of aerosols. Physical Chemistry Chemical Physics, 10(20): 2964-2971.

Reeser, D.I. et al., 2009. Photoenhanced Reaction of Ozone with Chlorophyll at the Seawater Surface. Journal of Physical Chemistry C, 113(6): 2071-2077.

Rossignol, S. et al., 2014. Glyoxal Induced Atmospheric Photosensitized Chemistry Leading to Organic Aerosol Growth. Environmental Science & Technology, 48(6): 3218-3227.

Sax, M., Zenobi, R., Baltensperger, U. and Kalberer, M., 2005. Time resolved infrared spectroscopic analysis of aerosol formed by photo-oxidation of 1,3,5-trimethylbenzene and alpha-pinene. Aerosol Science and Technology, 39(9): 822-830.

Shao, Y. et al., 2006. Advances in methods and algorithms in a modern quantum chemistry program package. Physical Chemistry Chemical Physics, 8(27): 3172-3191.

Spartan, '14. Spartan '14, Wavefunction, Irvine, CA.

Tinel, L., Dumas, S. and George, C., 2014. A time-resolved study of the multiphase chemistry of excited carbonyls: Imidazole-2-carboxaldehyde and halides. Comptes Rendus Chimie, 17(7-8): 801-807.

Tremblay, L., Alaoui, G. and Leger, M.N., 2011. Characterization of Aquatic Particles by Direct FTIR Analysis of Filters and Quantification of Elemental and Molecular Compositions. Environmental Science & Technology, 45(22): 9671-9679.

Vaida, V., Kjaergaard, H.G., Hintze, P.E. and Donaldson, D.J., 2003. Photolysis of sulfuric acid vapor by visible solar radiation. Science, 299(5612): 1566-1568.

Wick, C.D., Chen, B. and Valsaraj, K.T., 2010. Computational Investigation of the Influence of Surfactants on the Air-Water Interfacial Behavior of Polycylic Aromatic Hydrocarbons. Journal of Physical Chemistry C, 114(34): 14520-14527.

Yu, G. et al., 2011. Glyoxal in Aqueous Ammonium Sulfate Solutions: Products, Kinetics and Hydration Effects. Environmental Science & Technology, 45(15): 6336-6342.

Zhou, S. et al., 2014. Formation of gas-phase carbonyls from heterogeneous oxidation of polyunsaturated fatty acids at the air-water interface and of the sea surface microlayer. Atmospheric Chemistry and Physics, 14(3): 1371-1384.

Ziemann, P.J. and Atkinson, R., 2012. Kinetics, products, and mechanisms of secondary organic aerosol formation. Chemical Society Reviews, 41(19): 6582-6605.

Chapter VI: Photochemical chemistry of nonanoic acid at the air-water interface.

VI.0. Motivation

This chapter reports the findings of experiments conducted at the air-water interface coated with a carboxylic acid, namely nonanoic acid. By irradiating a carboxylic acid coated aqueous solutions containing a photosensitizer, saturated and unsaturated functionalized compounds are photochemically produced and released in the gas-phase and in the condensed phase. It is shown that photosensitizers have a propensity to partition to the organic layer, in this case the carboxylic acid surface layer, and therefore different chemical routes for the formation of products can be considered. The analysis of both phases, gas and bulk condensed phase, by high resolution mass spectrometry provides important insights in the mechanism leading to the formation of these compounds and the role of oxygen in the formation process is discussed.

The experiments conducted for this study also revealed another very interesting process. Indeed, analysis of irradiated solutions containing only the carboxylic acid also showed the formation of series of functionalized compounds in the gas phase as well as in the condensed bulk phase. Further investigations showed a weak absorption band of concentrated nonanoic acid, which can probably trigger this chemistry at the air-water interface, favored by the high concentrations of carboxylic acid encountered there. A mechanism for the formation of the observed compounds is proposed.

The production of functionalized saturated and unsaturated compounds produced solely by the absorption of actinic sunlight by a photosensitizer or a carboxylic acid at the interface can have very important impacts for the marine environment, for the condensed phase as well as for the gas-phase and not in the least for the role these compounds could play in the formation of new particles.

Chapter VI: Photochemistry of nonanoic acid at the air-water interface.

Authors: Liselotte Tinel*, Stéphanie Rossignol*, Angelica Bianco[$], Monica Passananti, James Donaldson[£], Marcello Brigante[$], Christian George

(*) These authors contributed equally to this work.

Article soon to be submitted.

VI.1.Introduction

During the last decades, increased interest in climate has led to a better understanding of the global atmosphere and underlined the key role played by oceans. Despite a growing body of knowledge on atmospheric and oceanic chemistries, large uncertainties remain concerning the air-sea interactions. Notably, the role of the sea surface microlayer(SML) in the regulation of emissions and uptake of volatile organic compounds (VOCs) and aerosols seems to be relatively unknown (Carpenter and Nightingale, 2015). The sea surface microlayer which is operationally defined as the upper 1 µm to 1 mm of the surface water has a chemical composition which depends on location and season, and is still far from being well characterized (Cunliffe et al., 2013). However, It seems clear that the SML is enriched in hydrocarbons, proteinaceous matter and fatty acids, which, as hydrophobic material, will have an important effect even at low concentrations on the mass exchange at the air-water interface (Carpenter and Nightingale, 2015). Dry deposition of ozone on organic coated water surfaces for example could constitute an important sink for ozone in the marine boundary layer, both through its reactivity with the components of the SML and through increased solubility in this more organic layer (Donaldson and Vaida, 2006; Zhou et al., 2014). Contrary to what was previously thought, the SML is widespread over the sea surface and stable under wind speeds up to 6.6 m s^{-1} (Wurl et al., 2011). Evidence also shows rapid reformation, within minutes, of the perturbed SML (Cunliffe et al., 2013).

Moreover, the concentration of dissolved organic matter at the air-water interface brings along an increased concentration of light absorbing species. These can participate in heterogeneous light induced reactions with gases at the interface, as has been shown for NO_2 when reacting with humic acids (Stemmler et al., 2006) or ozone and chlorophyll

(Reeser et al., 2009b). These photochemical reactions can also be a source of gaseous reactive species, as demonstrated for the light induced release of volatile halogen radicals above organic films (Jammoul et al., 2009; Reeser et al., 2009a).

The chemical composition of the SML also influences the composition of marine atmospheric aerosols through processes such as bubble bursting, which entrains the organics from the water surface to the particles (de Leeuw et al., 2011). Through their hydrophobic nature, the organics entrained from the SML can have important consequences on the particles ability to act as cloud condensation nuclei (Ovadnevaite et al., 2011). The optical properties of the aerosols can also be impacted, as well as their chemistry e.g. through heterogeneous reactions with the atmospheric traces gases (George et al., 2015).

Although it is believed that the surface microlayer could be a very favorable venue for photochemical reactions to take place, still very little is known about the light induced processes taking place there (Liss and Duce, 1997). In a study by Gever and co-workers (1996), the microlayer sampled in a commercial rice field and highly enriched in pesticides, with concentrations up to 10^5 times higher than in the subsurface waters, showed an enhanced degradation for the pesticide thiobencarb compared to the sampled subsurface water. The composition of the identified fraction of the microlayer in this study was dominated by $C_{>14}$ fatty acids, but relatively large amounts of smaller fatty acids (C_8-C_{13}) were measured as well.

The main obstacles for a better chemical characterization of the natural SML is the sampling of this thin (submicron) surface layer and its highly complex composition. By design, laboratory studies overcome these difficulties and can be a helpful approach in understanding the fundamental photochemical processes in the SML. Recently, laboratory studies by means of mass spectrometric measurements of the gas phase above an irradiated real SML sample or synthetic microlayer enriched with humic acids, our group identified the formation of a wide variety of functionalized VOCs (Ciuraru et al., 2015a; Ciuraru et al., 2015b). A different set of experiments showed the photosensitized formation of unsaturated compounds in a synthetic interfacial layer composed of a well-known surfactant, 1-octanol (Fu et al., 2015).

This work presents the study of photochemical reactions in a synthetic surface microlayer, composed of a saturated carboxylic acid, nonanoic acid (NA), and focuses on the fundamental processes leading to the formation of functionalized and unsaturated

compounds in the gas- and condensed bulk phase, observed in parallel with SRI-ToF-MS and UPLC-HRMS techniques. Experiments were performed with and without photosensitizers. Hydrogen peroxide (H_2O_2) was also used as photo-initiator for comparison purpose. UV-visible spectroscopy and surface fluorescence experiments were additionally performed to help understanding the observations. Possible mechanisms explaining these observations are discussed.

VI.2. Material and methods

VI.2.1. Materials

Hydrogen peroxide (35 wt.-% solution in water, Sigma Aldrich), imidazole-2-carboxaldehyde (97%) and 4-benzoylbenzoic acid (4-BBA, 95%) were purchased from Sigma Aldrich and used without further purification. The solutions of 4-BBA were prepared using ultrasonication to promote complete dissolution. All solutions were freshly prepared using pure water (Elga Purelab Classic, 18.2 MΩ). Two purity grades were used for nonanoic acid, 97% (Alfa Aesar) and 99.5 % (Sigma Aldrich), the purity used is specified for each experiment. For the chromatographic analysis, acetonitrile, water and formic acid were purchased from Fisher Scientific, all three Optima® LC/MS grade. O-(2,3,4,5,6-pentafluorophenyl) methylhydroxyl amine hydrochloride (PFBHA, ≥ 99.0%) provided by Fluka.

VI.2.2. UV-visible absorption spectroscopy

UV-visible absorption spectra of diluted and neat nonanoic acid were recorded using a Cary 60 UV-Vis spectrometer (Agilent Technologies) and 1 cm quartz cuvettes. Transfer of 4-BBA from an aqueous phase to a pure nonanoic acid phase were studied using UV-vis spectrometry. Absorption spectra of nonanoic acid and 4-BBA solutions in water were first recorded at pH 2.0 and 7.0 in quartz cuvettes with 1 cm or 5 cm optical pathways in order to determine corresponding molar absorption coefficients. For the incompletely dissolved solution of 4-BBA at pH 2, a filtered saturated solution (24 µM) was used to determine the molar absorption coefficient. Molar absorption coefficient of 4-BBA was also determined in neat NA using a 1 cm cuvette. Spectra of the organic phase, i.e., neat NA, and spectra of the aqueous phases of an equilibrated air-NA solution were recorded for two different pH of the

aqueous phase, pH 2.0 and 7.0 and used as reference. Before recording the spectra, the two phases were shaken, left to equilibrate for a few minutes and then separated by centrifugation at 4500 rpm for 2 minutes. Transfer of 4-BBA from an aqueous phase to a neat NA phase was studied with aqueous 4-BBA solutions at pH 2.0 and pH 7.0 in the same way.

VI.2.3. Glancing angle laser induced fluorescence

Fluorescence of imidazole-2-carboxaldehyde at the air-water interface has been studied by glancing angle laser-induced fluorescence (GALIF). Detailed description of the set-up and principles have been given elsewhere (Mmereki and Donaldson, 2002; Mmereki and Donaldson, 2003) and therefore only a brief description will be given here. Fluorescence at the air-aqueous interface of the samples of interest was induced using the unfocussed output of an Nd:YAG-pumped optical parametric oscillator (OPO) fixed at 285 nm. The ~ 5 ns pulses from the laser operating at 10 Hz repetition rate had energies of ~ 2 mJ/pulse, with a pulse-to-pulse variability of about 15%. The laser beam impinged the liquid sample surface at an angle >85° from the surface normal. The aqueous sample (100 mL) was held in a modified three-neck round bottom flask with two quartz windows for laser beam entry and exit. Fluorescence was collected using a 7 mm diameter liquid light guide suspended ~8 mm above the sample surface, directly above the place where the incoming laser beam impinged on the surface. The collected light was imaged onto the entrance slit (200 µm) of a grating monochromator; the transmitted intensity was detected by a photomultiplier tube and sent to a digital oscilloscope which averaged the intensity vs. time signal over 16 laser shots. A time slice of 50 ns of the fluorescence decay captured by the oscilloscope, starting at 10 ns after the laser pulse, was averaged and output to a computer. This was registered as the fluorescence intensity observed at the detection wavelength.

For each concentration of IC, a full emission spectrum was recorded between 300 - 380 nm, at 5 nm intervals. Adsorption isotherms are constructed from the average of the 4 maximum points for each individual spectrum at a particular IC concentration, using the intensity obtained at 335 nm, the maximum emission wavelength for the system. Aqueous solutions containing 0.3 mM of IC with and without 1.5 mM nonanoic acid were freshly prepared and introduced into the round-bottomed flask at least 20 minutes before each measurement to

stabilize the surface layer. The procedure for obtaining each isotherm was as follows: starting with the most concentrated solution of IC in either pure water or in water containing 1.5 mM of nonanoic acid, a complete spectrum was recorded. Then 10.0 mL of the solution were removed and replaced with 10.0 mL of a solution that was identical, except with no IC present. The solution was allowed to sit for 20 minutes, and then a full spectrum recorded at this lower concentration. This process was repeated many times until the fluorescence signal level dropped to be too low to measure.

VI.2.2. Quartz cell experiments – Gas phase analysis

The experiments were performed using a 14 mL cylindrical quartz cell with two inlets (5 cm path length, 2 cm id; Starna, UK) maintained at 13 cm of a Xenon lamp (150 W Xe, LOT-QuantumDesign, France). The lamp was equipped with a 1 cm water filter to avoid excessive heating of the quartz cell. The cell was half-filled - in order to maximize the surface to volume ratio (1.4 cm^2 cm^{-3}) - with 7 mL of the aqueous phase under study, either pure water or an aqueous solution of 10 mM hydrogen peroxide, 0.1 mM 4-BBA or 0.1 mM IC. For the experiments with nonanoic acid the cell was filled only with 6.988 mL of solution after which 2mM of nonanoic acid (2.46 µL) was added and slightly stirred, to promote the spreading of the acid over the surface. Then it was left to sit for over 20 minutes before the start of the experiment. An incoming gas flow with a flow rate of 200 sccm, controlled by a mass flow controller (750 sccm; El-Flow Bronkhorst, Netherlands) was continuously introduced in the cell. 80 sccm of the outgoing gas flow were sampled for analysis at the outlet of the cell through a system of PTFE connections (BOLA, Bohlender, Germany) and PTFA tubing of less than 5 cm, connected directly to the polyetheretherketone (PEEK) inlet (1.5 m of 6 mm i.d.) of the Switchable Reagent Ion-Time of Flight-Mass Spectrometer (SRI-ToF-MS). The gasses used were purified compressed dry air (DF Ultrafilter, Donaldson, USA) and dry nitrogen. No particle filter was used at the outlet of the cell to avoid artefacts of any organics deposited on the filter. The sample inlet was constantly heated to 60°C to minimize adsorption and condensation.

The analysis of the gas phase products was performed using an Ionicon Analytik GmbH (Innsbruck, Austria) type 8000 SRI-ToF-MS using both H_3O^+ and NO^+ ionization modes. The combined use of two reagent ions can provide complementary information about the structure of the molecules detected, since the product ions formed with both ions are not

the same (Jordan et al., 2009; Karl et al., 2012; Knighton et al., 2009; Smith and Spanel, 2005). The reagent ions are generated by a hollow cathode discharge ion source, as described elsewhere (Blake et al., 2006; Hansel et al., 1995), using water vapor in the case of H_3O^+ ionization mode and a mixture of N_2 and O_2 in the case of NO^+ ionization mode. The settings of the source were optimized for each ionization mode in order to obtain less than 5 % impurities in the primary ion signal. In the H_3O^+ mode, the settings used were: source current 4 mA; source voltage: 100 V; source outlet voltage: 80 V and source valve opening at 37 % with a flow of 5.8 sccm of water vapor. With these settings the main impurity ions were at relative levels (ratio impurity/H_3O^+) of 0.02-4.5% and 0.05-0.15 % for O_2^+ and NO^+ respectively. In the NO^+ ionization mode, the source settings were the following: source current 5.5; source voltage: 25 V; source outlet voltage: 69 V and source opening valve at 36 % with flows of 5.4 sccm and 2.8 sccm for O_2 and N_2 respectively. The main source impurities in this ionization mode are H_3O^+, O_2 and NO_2 which were detected at relative levels of 0.2-0.3 %, 0.6-1.2 %, 1.5-2.5 % respectively. For both ionization modes, the cleanest signals were obtained when a flow of nitrogen was used in the reactor, as very little oxygen could then diffuse backwards to the source.

For both ionization modes, the pressure in the drift tube was held at 2.24 mbar at a temperature of 60°C with an overall applied voltage of 600 V, which led to an E/N ratio of approximately 135 Td (Townsend, 1 Td = 10-17 $cm^2\ V^{-1}$). This rather high E/N ratio was chosen to minimize the formation of water clusters occurring in our high humidity sample environment. Water clusters can interfere through proton transfer and ligand switching and make precise quantification difficult (Cappellin et al., 2012; de Gouw et al., 2003). Under our experimental conditions, the water clusters represented between 0.06 and 16.5 % of the primary ion signal and were generally much lower in NO^+ mode. Spectra were acquired between 1 and 350 m/z at a sampling frequency of 35 kHz and were registered by co-adding single TOF-extractions for a time of 1-10 s. The resolution of the spectra was approximately 4300 at m/z 100. The data treatment was done with the PTR Viewer 3 software (Ionicon Analytik, Innsbruck, Austria), using isotopes m/z 21 and m/z 31 to calculate the primary ions H_3O^+ and NO^+ respectively. Fragmentation patterns for the main products under our experimental conditions was carefully assessed for using liquid standards diluted in 7 mL of water in the reactor and analyzed under the same conditions as the samples. As no quantitative calibration could be done and reaction rates for most of the products with NO^+

are unknown, only phenomenological results and normalized signals will be discussed for the NO^+ reagent mode. Concentrations were theoretically determined for the spectra taken in H_3O^+ ionization mode and corrected for the branching ratios where these were known, but due to many approximations within this method, the global uncertainty on the absolute concentrations can be estimated to be up to 40 % (Herndon et al., 2006). Background spectra were taken before each experiment above the pure water, before adding the surfactant or photosensitizer.

VI.2.3. Quartz cell experiments – Aqueous phase analysis

The condensed phase experiments were performed in a second but similar set-up, consisting of a second 14 mL cylindrical quartz cell and a second 150 W Xenon lamp. The cell was first filled with 11 mL of the aqueous phase that was either pure water or a solution containing 0.1 mM 4-BBA, a 10 mM hydrogen peroxide or 0.1 mM IC. 3.83 µL of nonanoic acid was then added to achieve a theoretical concentration of 2 mM. The solution was stirred for a few minutes and then left aside for a few minutes. Before irradiation, 4 mL of the bulk solution were sampled and left at room temperature in the dark until dilution and analysis. The remaining 7 mL filled the cell half way. A fixed irradiation time of 1 hour was used for all the experiments. After irradiation, the solution was stirred again for a few minutes before the sampling. Then, 4 mL of the bulk solution were sampled and left in the dark until dilution and analysis. For the experiments performed under ambient air, the cell was opened at the beginning and at the end of the experiment and hermetically closed during irradiation. No bubbling of the aqueous phase was performed for these ambient air experiments. For the experiments performed under purified air and under nitrogen, trace gases and/or oxygen were removed from the aqueous phase by bubbling the corresponding gas for 25 min, prior to the nonanoic acid introduction. The empty volume of the cell was purged with the corresponding gas before hermetical closing. Samples were taken before and after irradiation through a septum.

500 µL of each sample were diluted in 500 µL of a 1:1, v:v, water:acetonitrile mixture. Next to that, 200 µL of each sample were diluted in 800 µL of a 1 mg mL^{-1} PFBHA solution (daily prepared from PFBHA dissolved in 1:1,v:v, water:acetonitrile mixture) and were left at room temperature for 24 hours in order to complete the selective derivatization of the carbonyl groups. These two dilutions were performed in triplicates for each sample (two

samples by experiment, before and after irradiation). For each experiment, solvent and PFBHA impurities were checked diluting 500 µL of water in 500 µL of a 1:1, v:v, water:acetonitrile mixture and 200 µL of water in 800 µL of the daily PFBHA solution.

All the diluted samples were analyzed by ultrahigh performance liquid chromatography coupled with heated electrospray ionization (positive and negative modes) and high resolution mass spectrometry [UPLC/(±)HESI-HRMS]. The Dionex Ultimate 3000 ultrahigh performance liquid chromatograph (UPLC, Thermo Scientific, U.S.) was equipped with a HSS T3 Acquity UPLC column (1.8 µm, 2.1 × 100 mm). The mobile phases were (A) acidified water (+ 0.1%, v/v, formic acid) and (B) acidified acetonitrile (+ 0.1%, v/v, formic acid). A 22 min gradient was applied at a constant flow rate of 0.3 mL min^{-1}: eluent (B) was kept at 1% for 2 min, was then increased to 100% in 11 min and kept to 100% for 2 min; the system then returned to initial conditions, 1% of (B), in 0.1 min and was left to stabilize for 7 min. The injection volume of the non-derivatized diluted samples was 5 µL and the injection volume of PFBHA derivatized samples was 10 µL. HESI voltages of +3.7 kV and −3.0 kV were applied for the positive (+) and negative (−) ionization modes respectively. All the HRMS acquisitions were performed in full MS mode with a scan ranging from m/z 50 to m/z 750 and a resolution set to 140,000. Signal stability over time was checked using two standard solutions of adipic acid (2 µM) and levulinic acid (20 µM), this latter being daily diluted by a factor 5 in a 1mg mL^{-1} PFBHA solution and left at room temperature for 24 hours for carbonyl group derivatization.

VI.3. Results and discussion

VI.3.1. Neat nonanoic acid and photosensitizer enrichment at the surface

VI.3.1.a. Absorption spectrum of neat nonanoic acid

The neat nonanoic acid corresponds to a 5.67 M liquid. Nonanoic acid was diluted in protic (ethanol, fig. VI-1 A) and aprotic (acetonitrile, fig. VI-1 B) polar solvents. The corresponding

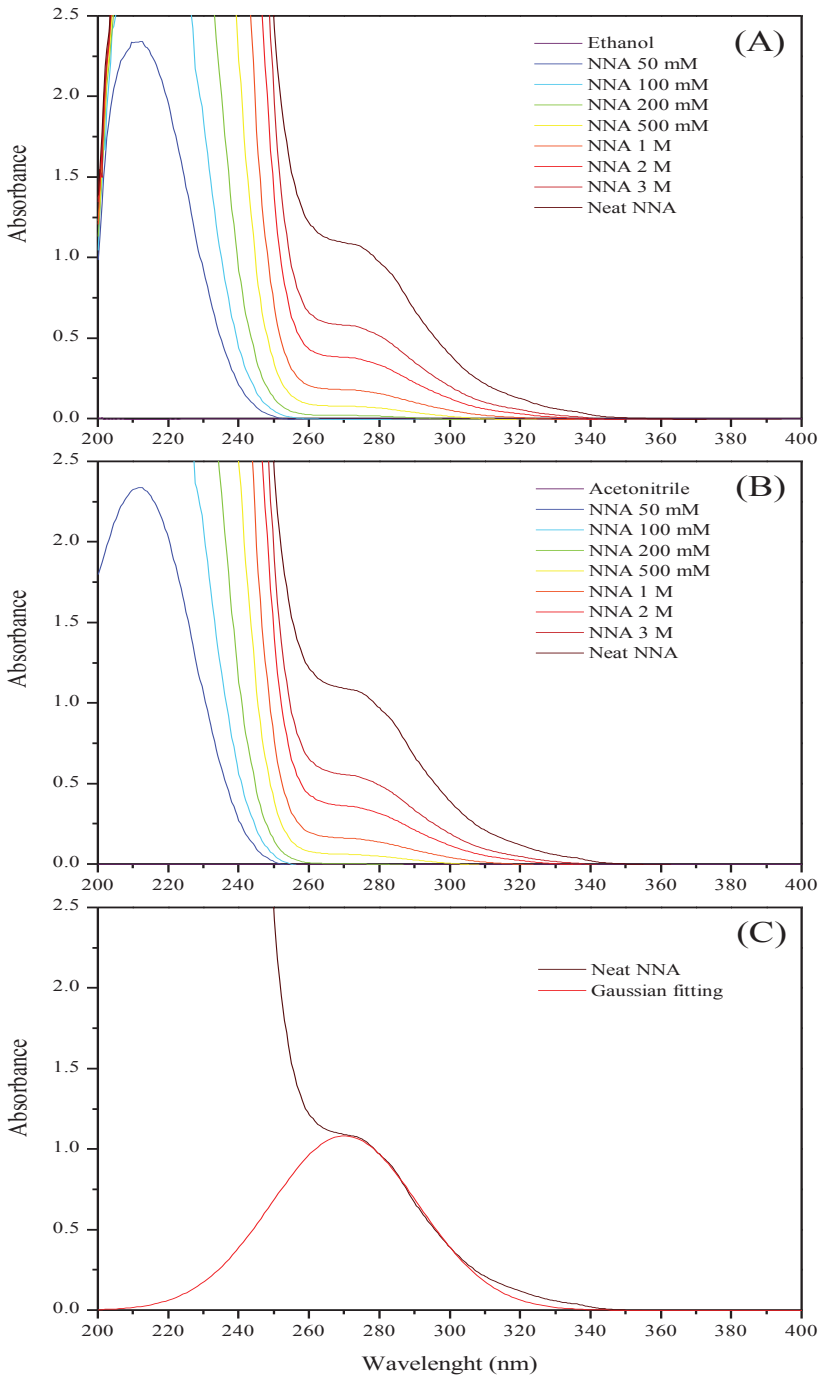

Figure VI-1: UV-absorption spectra of nonanoic acid diluted in (A) ethanol and (B) acetonitrile. (C) Gaussian fit of the absorption band centered at 270 nm.

absorption spectra are shown figure VI-1 A and B. No influence of the solvent on the absorption spectrum was noted. The main absorption band is centered at 212 nm and widens with increasing concentration. In a carboxylic acid, group the n ⟶ π* transition is blue shifted compared to a carbonyl function, due to interactions of the π-symmetry orbitals of the C=O group with the doubly occupied non-bonding orbital of the OH group. As a consequence, aliphatic acids usually exhibit such an absorption maximum below 220 nm (Coyle, 1978). However, for solutions with NA concentrations higher than 0.2 M, a second absorption band appears as a shoulder of the first one. This band is centered at 270 nm and is broad enough to induce absorption until about 330-340 nm (figure VI-C). The sunlight UV cut-off at the earth surface being about 290 nm (as illustrated by the solar spectrum on figure VI-S1 in section VI.7.Supplementory Information) this absorption band could induce environmentally relevant photochemistry. The related absorption coefficient ε_{270} is equal to 0.19 M^{-1} cm^{-1}.

Such weak absorption bands centered at ca. 270 nm ($\varepsilon_{max} \sim 0.04$ M^{-1} cm^{-1}) were previously observed for a series of neat small aliphatic carboxylic acids (Caswell et al., 1976). For acetic acid, a red shift of the absorption maximum was observed with increasing aqueous concentration up to 2 M (Ruderman et al., 1998). This shift from 195 to 236 nm comes with an increasing complexity of the acetic acid UV-absorption spectrum. At the highest concentration, the last appearing band was assumed to be related to the formation of cyclic dimers involving two hydrogen bonds between two acetic acid molecules. Here, such cyclic dimers of NA involving O-H···O=C hydrogen bonds, are expected to exist in concentrated solutions and could explain the appearance of the absorption band centered at 270 nm. Other types of hydrogen bonding might be invoked, even if much more speculative, such as weak C-H···O=C hydrogen bonds, since the hydrogen in alpha position on the nonanoic acid molecule is slightly acidic (Desiraju, 1991; Desiraju, 1996; Nakabayashi et al., 1999). Examples of possible hydrogen bonded structures are given figure VI-2.

Despite a quite low related absorption coefficient, the presence of such an absorbance band centered at 270 nm for concentrated and neat aliphatic acids could be of importance. Indeed, aliphatic acids can be found in abundance at interfaces, as the air-sea interface, forming a concentrated environment largely exposed to sunlight. Environmental implications will be discussed below.

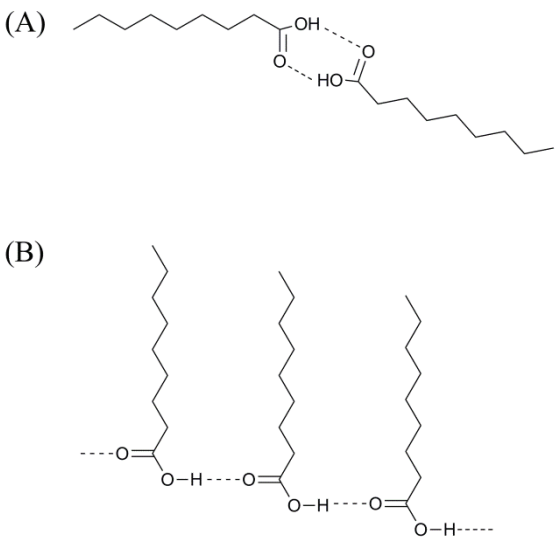

Figure VI-2: Examples of possible hydrogen bonded structures in concentrated solution of nonanoic acid: (A) cyclic dimers and (B) open chain polymer.

VI.3.1.b. Photosensitizer enrichment at the surface

The ability of 4-BBA present in an aqueous phase to migrate toward an organic nonanoic acid phase was investigated at pH 2.0 and 7.0. UV-absorption spectra showing this transfer are presented in figure VI-3. At pH 7.0, figure VI-3 A, just after shaking and centrifugation, 4-BBA is almost quantitatively transferred to the nonanoic phase (98 %). At pH 2.0, this transfer is lower but still very significant (70% effectively removed from the aqueous phase). One hour later without any supplementary shaking, the percentage of 4-BBA transferred from the aqueous phase to the nonanoic phase had increased (98.1% at pH 7.0 and 76% at pH 2.0, data not shown), suggesting that even without any mechanical assistance, the migration of 4-BBA or similar compounds from an aqueous phase to an organic layer present above occurs.

These results are in agreement with those obtained by Fu et al. showing the enrichment of imidazole-2-carboxaldehyde (IC) at an 1-octanol coated water surface (Fu et al., 2015). The presence of IC at the surface was probed with glancing-angle laser-induced fluorescence with and without organic coating. In presence of a near monolayer of 1-octanol at the water surface, the surface fluorescence was enhanced by a factor of about 4, meaning that IC is more concentrated at the surface when an organic monolayer is present.

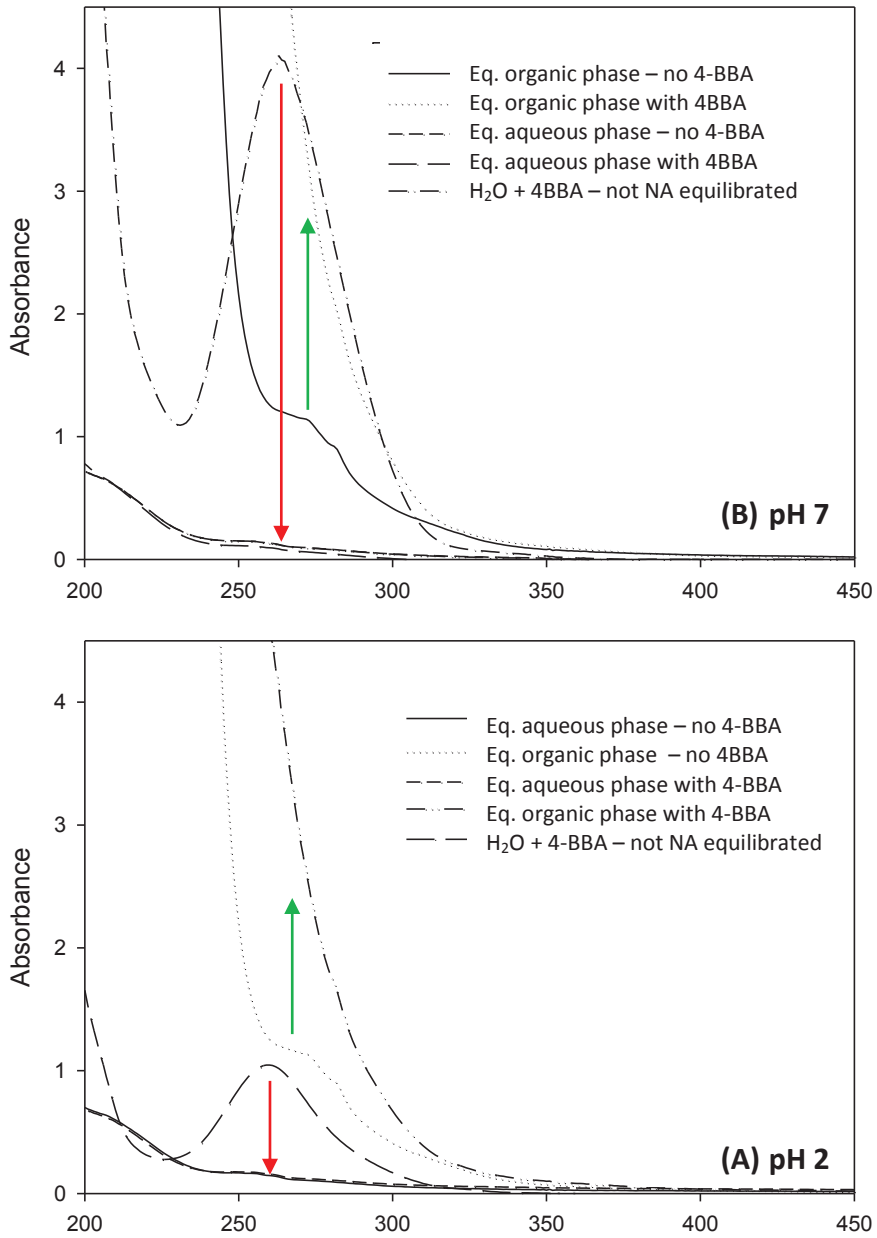

Figure VI-3: UV-absorption spectra showing neat nonanoic acid enrichment in 4-BBA (green arrows) when equilibrated with 4-BBA aqueous solution (red arrows). Aqueous phase at (A) pH 7.0 and (B) pH 2.0. Initial concentrations of 4-BBA in the aqueous phase: 2.0 x 10^{-4} M at pH 7.0 and 2.4 x 10^{-5} M at pH 2.0

The enhancement of IC in presence of an organic layer of nonanoic acid is demonstrated here using the same technique. Figure VI-4 shows the enhancement of surface fluorescence intensity of a NA coated solution compared to a pure water solution. It can clearly be seen that the fluorescence is largely enhanced (x 50) in the presence of a nonanoic acid coating, although in bulk fluorescence measurements of IC in pure NA no

fluorescence of IC could be measured. As for 1-octanol coated aqueous surfaces, the strongly enhanced fluorescence in presence of near monolayer of NA indicates the migration of the photosensitizer to this organic surface layer, leading very probably to an enhanced and specific photochemistry there.

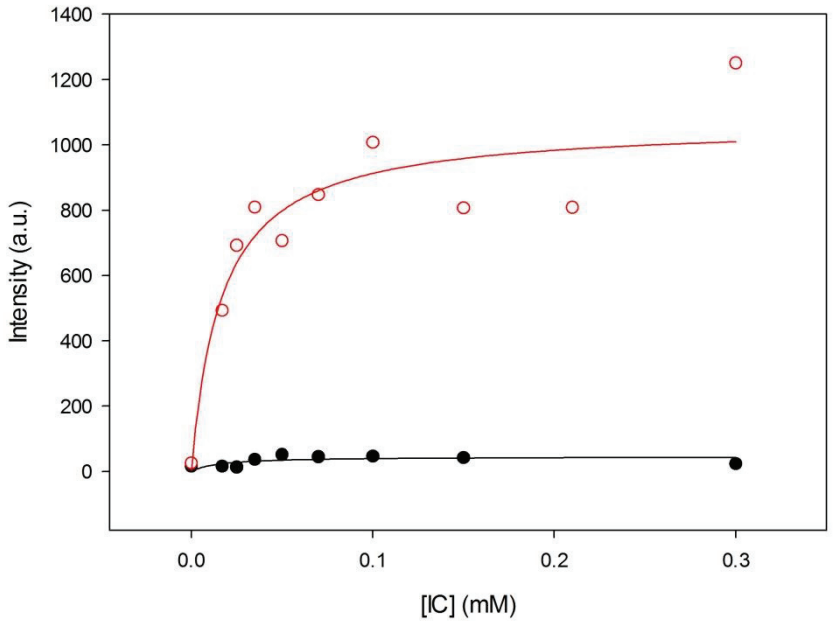

Figure VI-4: Fluorescence intensity of IC at the air-water interface. Emission wavelength 335 nm as a function of the bulk concentration of IC, measured at a pure water surface (●) and at a 1.5 mM nonanoic acid coated surface (○) The solid lines show the fits to a Langmuir adsorption isotherm.

The presence of a nonanoic acid monolayer at the top of a 4-BBA aqueous solution is thus expected to concentrate 4-BBA at the surface compared to the bulk, even if it seems impossible at this point to provide an absolute surface concentration for 4-BBA. In the environment, such enrichment is expected for all organic species with relatively low water solubility, and among them many species bearing chromophores such as carbonyl groups.

VI.3.2. Gas phases products

A series of experiments were performed to identify the gas phase products formed by photochemistry at the air-water interface in a system containing nonanoic acid as surfactant, with and without photo-initiator. The results of these experiments are presented hereafter. Similar series of experiments were conducted for the analysis of bulk condensed phase products and will be discussed in the next section.

Each experiment was repeated using NO^+ and H_3O^+ ionization modes. In order to attribute a certain functional structure to the ions, both results were compared and the ions considered for the different types of VOCs in each ionization mode are listed table VI-S1. As can be seen from table VI-S1, aldehydes and ketones can easily be distinguished in NO^+ ionization mode as ketones will mainly be detected as NO^+ adducts (Mochalski et al., 2014). In the NO^+ mode interferences in the signal for acids and alkenes can be ruled out by using the minor NO^+ adduct ion, although unsaturated acids can probably not be distinguished from dicarbonyls, as both might form NO^+ adducts. In what follows these adduct ions - unsaturated acids or dicarbonyls- will be designated by the term dicarbonyls. In comparison with the results obtained in the aqueous phase, it seems more likely that these compounds are dicarbonyl compounds, but the presence of unsaturated acids in the gas phase cannot be ruled out. Alcohols are quite difficult to identify undoubtedly by SRI-ToF-MS, as they easily loose the hydroxyl group in both ionization modes to give product ions that can be confounded with the ions of other compounds (alkenes notably) (Fiches et al., 2013; Karl et al., 2012; Smith and Spanel, 2005). Although in NO^+ mode alcohols also give an $(M-H)^+$ product ion, this ion interferes with the major product ion of alkanes (not considered here). Therefore, the formation of alcohols will not be discussed here, as their ascertained identification in the gas phase is difficult under our experimental conditions. As hydroxyl groups in both ionization methods easily fragment, they can cause interferences not only for alcohols but also for other groups of compounds: (1) Hydroxyl groups on carbonyl compounds or in hydroxy-acids will probably also readily fragment and lead to ions confounded with the corresponding protonated unsaturated carbonyl or acid in H_3O^+ mode or the $(M-H)^+$ ion of carbonyls in NO^+ mode. As said previously, the eventual interference with acids and ketones in the NO^+ mode can be overcome by the use of the NO^+ adduct ion. But in the H_3O^+ mode contributions of fragmented alcohols in the signals of unsaturated

aldehydes and alkenes cannot be discarded. (2) In both ionization modes the loss a hydroxyl group of the carboxylic function of occurs but as a minor fragmentation pathway. The so formed ions can contribute to the signal of unsaturated aldehydes in the H_3O^+ mode and of aldehydes in NO^+ mode. In what follows, it has to be kept in mind that interferences for these hydroxyl bearing compounds exist and are not accounted for. The products presented are identified by the product ions noted in bold table VI-S1.

VI.3.2. Experiments without photo-initiator

During the experiments using only nonanoic acid and pure water, considered firstly as blanks, it became clear that even without presence of photo-initiator, net production of series of compounds could be observed upon irradiation. To rule out the influence of eventual impurities in the nonanoic acid, the results of irradiation of an aqueous solution of NA with 97% purity were compared to the results obtained with a higher purity NA (99.5%). Also the presence of trace metals was ruled out by ICP analysis.

Indeed, as illustrated figure VI-5, upon irradiation, highlighted in yellow, of an NA coated aqueous solution and nitrogen as carrier gas, a rapid formation of gas-phase products is observed. The traces show a rapid stabilization corresponding to a steady state production in less than 7 seconds, in agreement with the calculated dilution rate for the reactor using a gas flow rate of 200 mL min^{-1}. Figure VI-5 shows the time traces for two major products measured in H_3O^+ ionization mode. An overview of the main gas phase products formed with both purity grades is shown in figures VI-6 et VI-7. As can be seen, the measured concentrations are generally somewhat lower when the highest purity NA is used, but for most compounds the variation lays within the experimental uncertainty. For some compounds the differences are more marked, but in both cases products are formed upon irradiation of the coated aqueous solution

This nonanoic acid photochemistry was not expected but is in agreement with the assumption made from the UV-absorption spectra of nonanoic acid, showing absorption until 340 nm, that photo-induced processes could happen under environmentally relevant conditions.

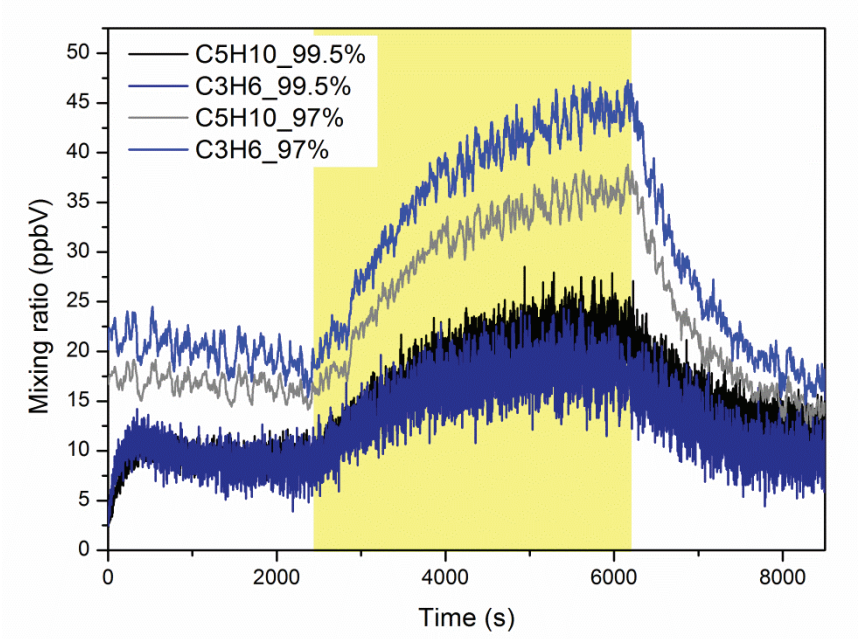

Figure VI-5: Time traces of two major compounds measured in the H_3O^+ ionization mode above an irradiated (1h) aqueous solution of 2 mM NA of 97% purity (brighter colors) and 99.5% purity (darker colors) with N_2 as carrier gas. The given concentrations are background corrected.

The influence of the carrier gas on the chemistry was investigated by using a nitrogen flow in the reactor and by deoxygenation of the aqueous phase prior to the start of the experiment. The results of these experiments, conducted with NA of 97% purity, are resumed in figure VI-6 for the H_3O^+ mode and in figure VI-7 for the NO^+ mode. In an oxygen poor environment, alkenes are clearly favored and the formation of acids, even the unsaturated ones, hindered. The only C_9 compound detected, $C_9H_{15}O_3^+$, could correspond to nonanoic acid with a hydroxyl and carbonyl group added ($C_9H_{16}O_4$), which would very probably lose H_2O after protonation in the H_3O^+ mode and has also been observed in the aqueous phase. More unlikely, this ion could also correspond to the protonated ion of the triple unsaturated C_9 compound $C_9H_{14}O$. This C_9 compound seems to be inhibited by the absence of oxygen.

The formation of aldehydes and ketones seems to be enhanced in a low oxygen environment, although the results obtained in the NO^+ mode are less uniformly pointing this out (figure 7). The most abundant oxygenated products formed are unsaturated (or cyclic)

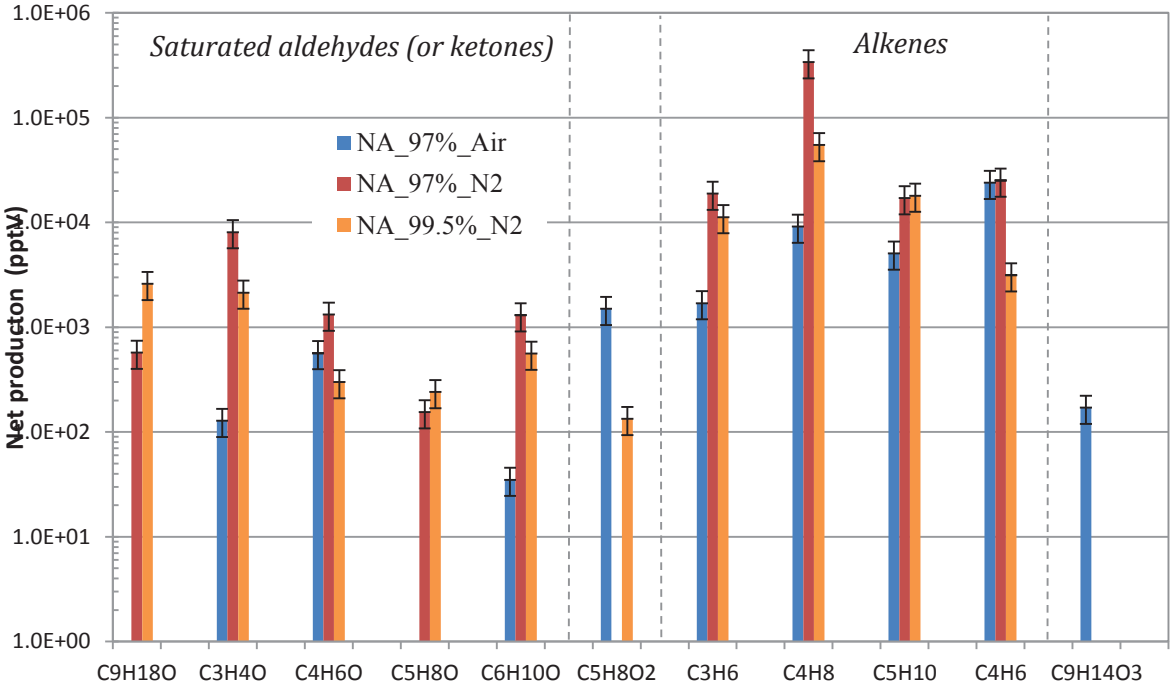

Figure VI-6: Overview of different products detected using H_3O^+ ionization in the gas phase above an aqueous solution using purified air as carrier gas and NA of 97% purity (■) and using N_2 as carrier gas with NA of 97% (■) and 99.5% (■) purity (log_{10} scale). The concentrations (in pptV) correspond to the net productions of the ions considered. The error bars reflect the repeatability between experiments.

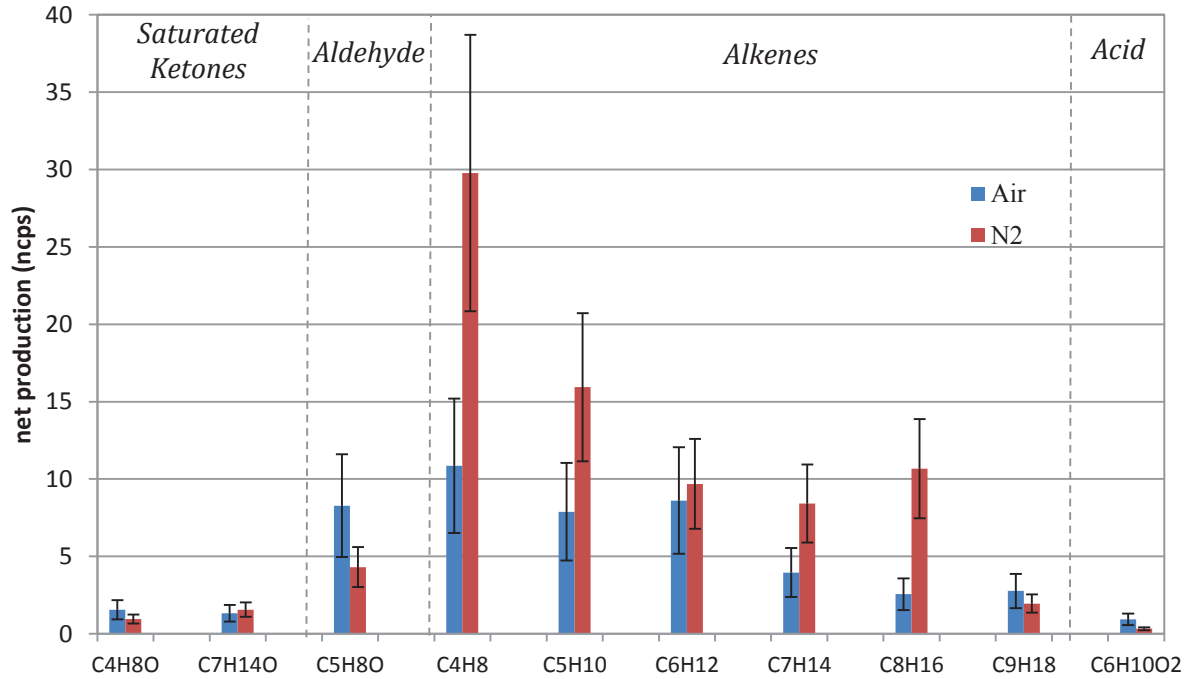

Figure VI-7: Net gas phase production of selected compounds observed for three experiments with NO^+ ionization in the gas phase above an aqueous solution containing NA (2 mM, 97% purity) using purified air (■) and N_2 (■) as carrier gas. The error bars reflect the repeatability between experiments.

aldehydes (or ketones), as illustrated by the C_3-C_6 compounds figure VI-9. The signals for these compounds are rather low, especially in NO^+ mode. This could be due to the addition of both aldehydes and ketones to H_3O^+ signal, whereas in the NO^+ mode these species are detected separately and therefore possibly stay below detection limit. The positive influence of a low oxygen environment on the formation of unsaturated oxygenated compounds could point towards enhanced radical-radical reactions in absence of oxygen leading to the formation of these unsaturated compounds. This point will be further discussed below.

For the experiments using only nonanoic acid in an aqueous solution, the full spectrum of a Xenon lamp was used. This type of short arc lamps mimics the actinic sunlight, but provides a much larger photon flux, particularly in the lower UV-region (as illustrated figure VI-S1, section VI.7. Supplementary Information). Therefore, experiments were also conducted using a Pyrex filter, cutting off the UV irradiation under 280 nm. Contrary to the experiments conducted for aqueous phase analysis, which were done in a closed reactor, the flow-system used for the gas-phase experiments did not allow any accumulation of the eventual products formed and no products were observed. However, in a second experiment with a closed reactor using the Pyrex filter and an irradiation time of 2 h, traces of products could be observed. Considering the absorption spectrum of pure NA (figure VI-1), this outcome is not surprising, as the second absorption peak has its maximum around 270 nm and the absorption at wavelengths greater than 280 nm will thus be very weak.

VI.3.2.a. Experiments with photo-initiators

The gas products of photochemical processes induced between NA and two different types of photo-initiators were also analyzed, namely hydrogen peroxide and 4-benzoyl benzoic acid. 4-BBA is a well-known photosensitizer (Murov et al., 1993) and used here as a proxy for carbonyl functions found in humic substances in the natural surface waters. 4-BBA shows a large absorption peak in the near UV region with a maximum at 262 nm (figure VI-3) and can be considered as an efficient photosensitizer since its triplet excited state is produced with a high quantum yield.

Indeed, as illustrated figure VI-8, upon irradiation of an NA coated aqueous solution containing 2 mM of 4-BBA and air as carrier gas, a rapid formation of gas-phase products is observed. The main gas phase products formed upon irradiation of an aqueous solution

containing 4-BBA coated with NA are oxygenated products, such as octanal shown in red on figure VI-8. Other types of oxygenated species detected during the irradiation of the reactor,

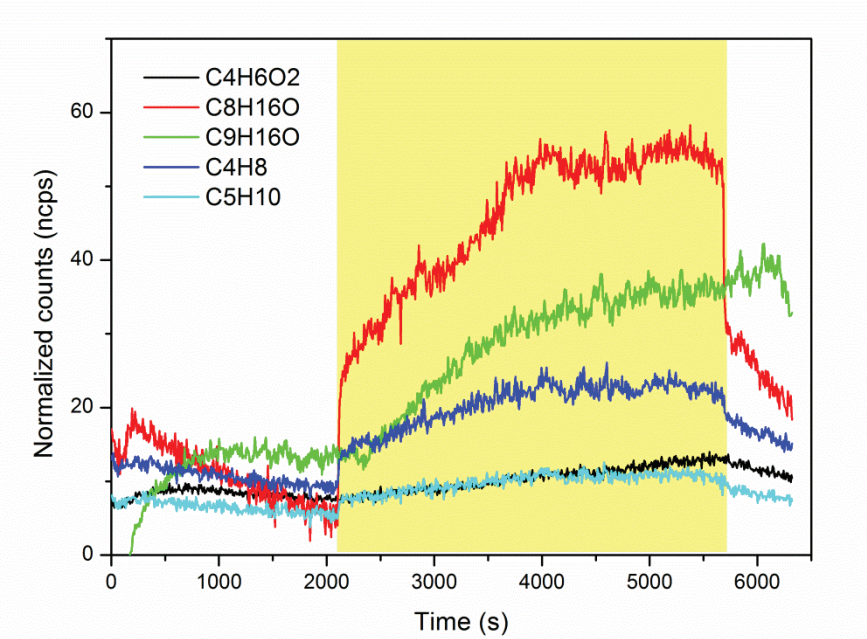

Figure VI-8: Time traces of the main gas phase products measured in NO^+ mode above an aqueous solution of 4-BBA (0.1 mM) and NA (97%, 2 mM) irradiated for 1h under air flow.

but to a lesser extent, are dicarbonyls, as for example $C_4H_6O_2$ shown figure VI-8. Acids were only detected as traces in the gas phase, both in NO^+ and H_3O^+ mode, probably due to their low volatility and their propensity to partition to underlying aqueous phase. As is shown in the next section, acids are indeed detected in the aqueous phase, but not as major products.

More surprisingly, species bearing unsaturations on the carbon chain (or cyclic structures) were also detected in the gas phase. Figure VI-8 shows the traces of three such unsaturated species, the two alkenes in C_4 and C_5, and also an unsaturated aldehyde, nonenal ($C_9H_{16}O$). This is in agreement with the results obtained in a previous study by our group, using humic acids as photochemical active compound and points towards the importance of a interfacial organic layer in the formation of these unsaturated products (Ciuraru et al., 2015a; Ciuraru et al., 2015b). In the bulk condensed phase chemistry, unsaturated products are not expected to be formed significantly by the photochemistry with 4-BBA since this system will be governed by oxidative reactions, leading to more oxygenated products and fragmentation forming alcohols, aldehydes and smaller carboxylic acids as end products, although the formation of alkenes as byproducts of photochemical

oxidation of alkanes has been reported by several authors (Ehrhardt and Petrick, 1985; Guiliano et al., 1997). But at the interface, constituting a highly concentrated environment, radical-radical reactions such as disproportionation reactions could favor the formation of unsaturated compounds, as has been proposed by Fu and co-workers. They report the formation of unsaturated compounds above and inside an irradiated 1-octanol coated aqueous solution containing a photosensiziter (Fu et al., 2015). The gas phase release of such unsaturated compounds is particularly interesting from an atmospheric chemistry point of view as this would be a potential source of reactive species in the atmosphere.

Saturated aldehydes, in particular octanal, and alkenes, butene and pentene, are the major products in the gas phase, with concentrations estimated at 10-15 ppb for octanal and 7-10 ppb for pentene as determined in H_3O^+ ionization mode for these experimental conditions (taking fragmentation branching ratios into account for octanal).

The influence of the carrier gas on the chemistry was investigated by using a nitrogen flow in the reactor and by deoxygenation of the aqueous phase prior to the start of the experiment. In this oxygen poor environment, the product distribution is slightly different, but the main products remain aldehydes and alkenes. A comparison of the results of two experiments in the NO^+ mode, one using purified air and one using nitrogen as carrier gas, are shown figure VI-9. The irradiation of a solution of pure water containing 0.1 mM of 4-BBA under the same conditions did not lead to the detectable production of any of these compounds (results not shown, all below detection limit).

Globally, the use of nitrogen as carrier gas induces a slight reduction in the production of saturated aldehydes, ketones and acids. For the unsaturated compounds, a different trend can be seen, which becomes especially clear when we consider the formation of alkenes. In a low oxygen environment, the formation of unsaturated compounds seems to be favored, though this trend is less clear when only the oxygenated unsaturated compounds (unsaturated aldehydes and dicarbonyls) are considered. This points towards the role oxygen plays in the initial steps of the mechanism, and the competition between oxygen addition and radical-radical reactions. The mechanistic insights will be discussed more in detail in section VI.3.4.

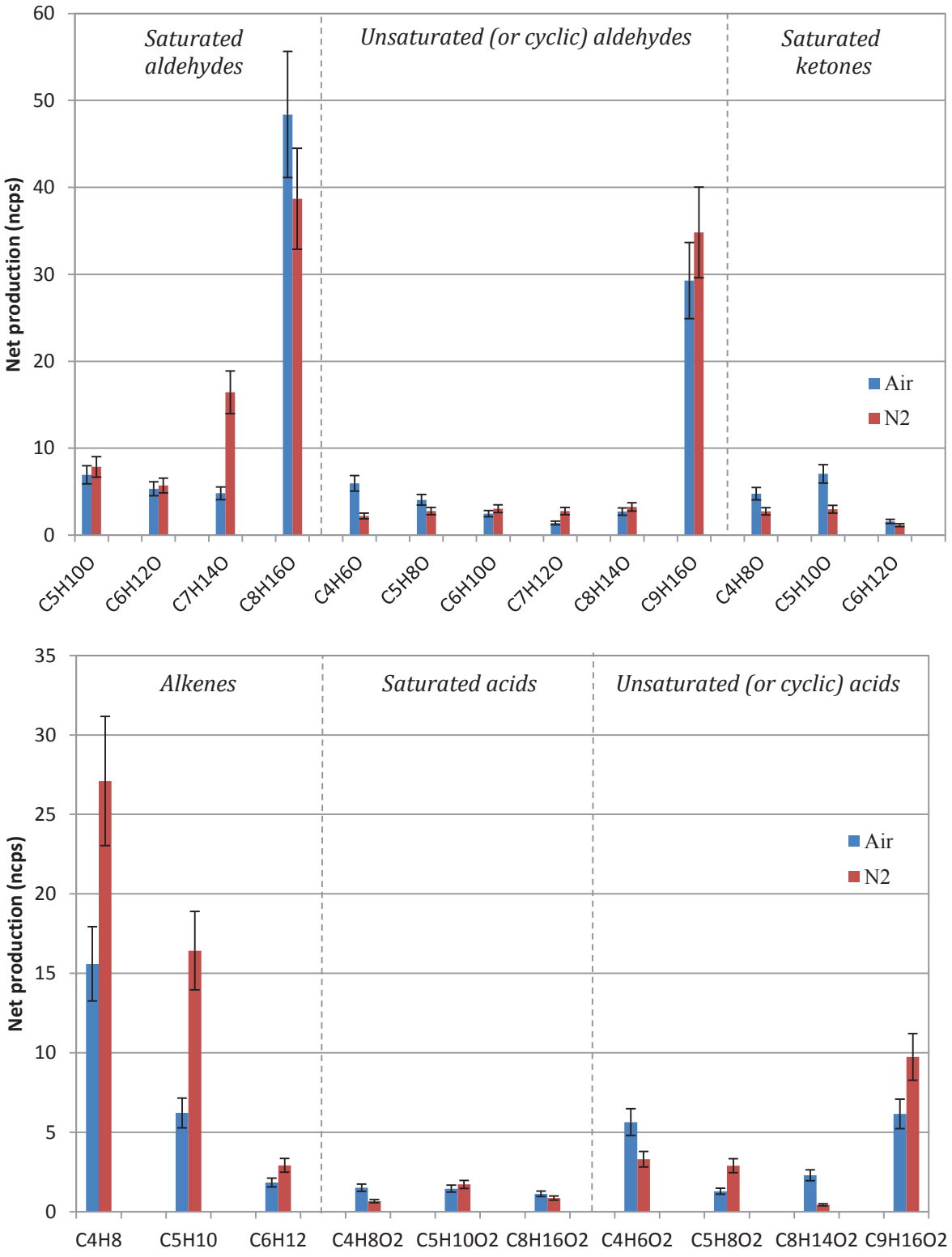

Figure VI-9: Net production observed for selected compounds in the gas phase detected in NO^+ mode, in presence of purified air (■) and nitrogen (■) above an irradiated solution (1h) containing 2 mM NA (97%) and 0.1 mM 4-BBA. Errors reflect the repeatability based on the peaks of NA between 4 experiments.

In view of these results, it becomes clear that the triplet state of an excited photosensitizer as 4-BBA can react with a carboxylic acid at the interface to form a large variety of functionalized compounds and even unsaturated reactive gas species. A second photosensitizer, imidazole-2-carboxaldehyde, has been tested in this system, producing similar results, but with lower overall intensities, partially due to lower concentrations used (0.1 mM IC and 1 mM of AN, results not shown). The role of singlet oxygen as initiator cannot totally be ruled out from these experiments, but seems at least not so important, seen the results obtained using nitrogen.

To further investigate the mechanism initiating this chemistry, a second initiator, H_2O_2, was used. Hydrogen peroxide, will readily photolyze under UV irradiation to form OH radicals, which can then trigger the chemistry at the interface by a hydrogen abstraction on the carboxylic acid. Hydrogen peroxide is not a photosensitizer and is expected to be depleted quickly, justifying the use of a rather high initial concentration of H_2O_2 (10 mM). It has to be noted here that the repeatability for these experiments was rather poor (more than 40% variability between the different experiments under the same conditions), but clear trends can still be seen, as illustrated by the figures VI-S2 and VI-S3 (Section VI. 7, supplementary information) showing the net productions under N_2 and air in both ionization modes.

The time traces of three major products formed during typical experiments with H_2O_2 using air or nitrogen as carrier gas, using both ionization modes, are presented figure VI-10. As can be seen from the traces figure VI-10, the intensities of the products formed are much higher than with 4-BBA (at least x 3). As expected, no steady state is reached as H_2O_2 will be quickly depleted. It has to be mentioned here that the excess of H_2O_2 in the system can lead to the formation of O_2, inducing some molecular oxygen in oxygen-poor experiments, but this effect is expected to be limited under our experimental conditions. Under nitrogen the formation of C_8 aldehydes, saturated and unsaturated, is favored, compared to the experiment under air. This can tentatively be explained by rapid molecular oxygen additions on the C_8 alkyl radical and more terminal radical-radical reactions under nitrogen, whereas under air, oxygen would not be limiting and further oxidation and fragmentation would then lead to smaller products and the higher amount of acids observed (figure VI-S3). The time traces of the experiments with H_2O_2 seem to indicate indeed a rapid production of these C_8 compounds.

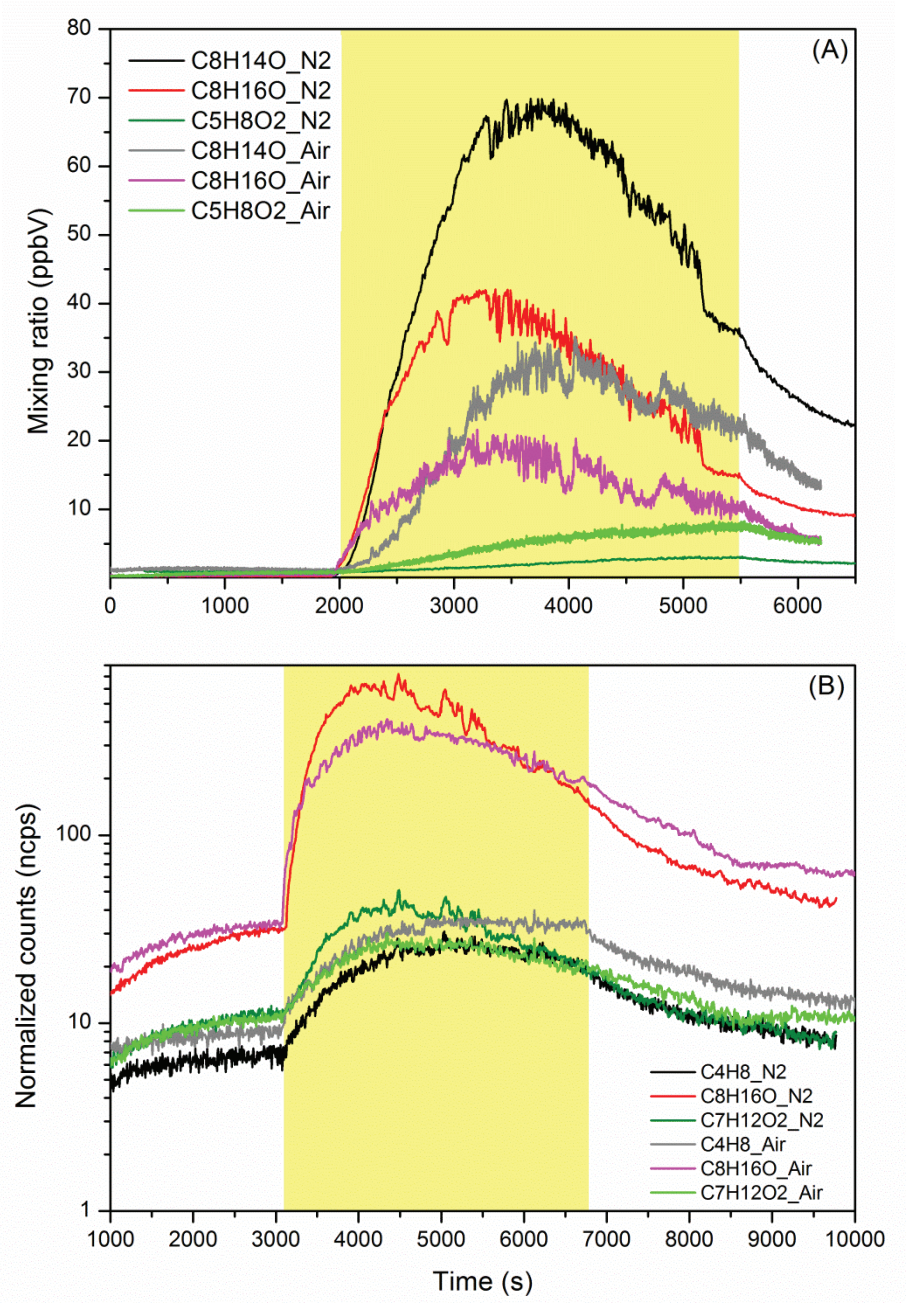

Figure VI-10: Time traces of selected compounds measured in (A) the H_3O^+ ionization mode and (B) the NO^+ ionization mode (log_{10} scale) above an aqueous solution of NA (97%, 2 mM) and H_2O_2 (10 mM) comparing the influence of nitrogen (darker colors) or air (lighter colors) as carrier gas.

The positive influence of oxygen on the formation of dicarbonyls seems quite straightforward when considering the trace of the C_5 compound ($C_5H_8O_2$) observed with H_3O^+ ionization (fig. VI-10 A) and the time trace seems to suggest that these are secondary products. For the C_7 compound ($C_7H_{12}O_2$) shown in NO^+ ionization mode though, the

presence of oxygen seems rather to inhibit its formation. In general, the influence of oxygen on the formation of dicarbonyls seems positive for smaller ($C_{n<7}$) dicarbonyls (fig. VI-S2). For the $C_{n>7}$ dicarbonyls, the formation seems to be favored under nitrogen, in the absence of oxygen and is consistent with the observations for the C_8 aldehyde. No clear trend can be seen in the influence of oxygen on the formation of the alkenes in these experiments.

The experiments using H_2O_2 as initiator of the chemistry at the air-water interface show globally the formation of the same products, including saturated and unsaturated aldehydes and alkenes, as for 4-BBA as photosensitizer. This appears to confirm that the initiation step to form these products from the 4-BBA triplet state is an H-abstraction on the NA molecule and that singlet oxygen is not intervening. The variety of products formed by this photo-induced process is reflected by the list of all products observed during the experiments with photo-initiators, provided table VI-S2 of section VI.7. The influence of oxygen provides some indications in the complex mechanisms leading to the varied functionalized products that will be further discussed below.

VI.3.3. Aqueous phase products

Similarly as for the study of the products released in the gas phase, a series of experiments were performed to identify the photo-products remaining into the aqueous phase during the irradiation of an aqueous solution (eventually doped with 4-BBA or H_2O_2) coated with a nonanoic acid near monolayer.

VI.3.3.a. Experiments without photo-initiator

The experiments performed with pure water as the aqueous phase, nonanoic acid at a purity of 97% and under laboratory air, firstly considered as "blank" experiments, showed, similarly as in the gas phase, the net formation of a series of photo-products in the aqueous phase after one hour of irradiation. To check the eventuality of a photochemistry initiated either by reactive species present in the laboratory air or by impurities in the NA used, the results of these experiments were compared (1) to those obtained under filtered air with no NA and (2) to those obtained using NA of higher purity (99.5%) and under filtered air (figure VI-S4). Globally, the series of photo-products detected in each case is similar and includes mainly, on the one hand, C_9 products bearing three or more O atoms that could correspond to NA oxidation products with additional hydroxyl or carbonyl functions and on the other hand, C_5 to C_9 saturated and mono-unsaturated mono-carbonyl compounds and C_4 to C_6 saturated di-carbonyls. Similarly to the observations made in the gas-phase, the nonanoic acid purity does not seem to significantly impact formation of the products. The experiment performed under ambient air shows nevertheless slightly higher signal intensities for most of the compounds. A contribution of gas phase produced radicals reacting at the interface with nonanoic acid could be invoked but this clearly does not drive the observed chemistry here.

Anyhow, this first series of experiments shows that, even under the cleanest environment (filtered air and highest purity of NA), photo-products of NA are formed after only one hour of irradiation with a Xenon lamp, without the need of any photosensitizer.

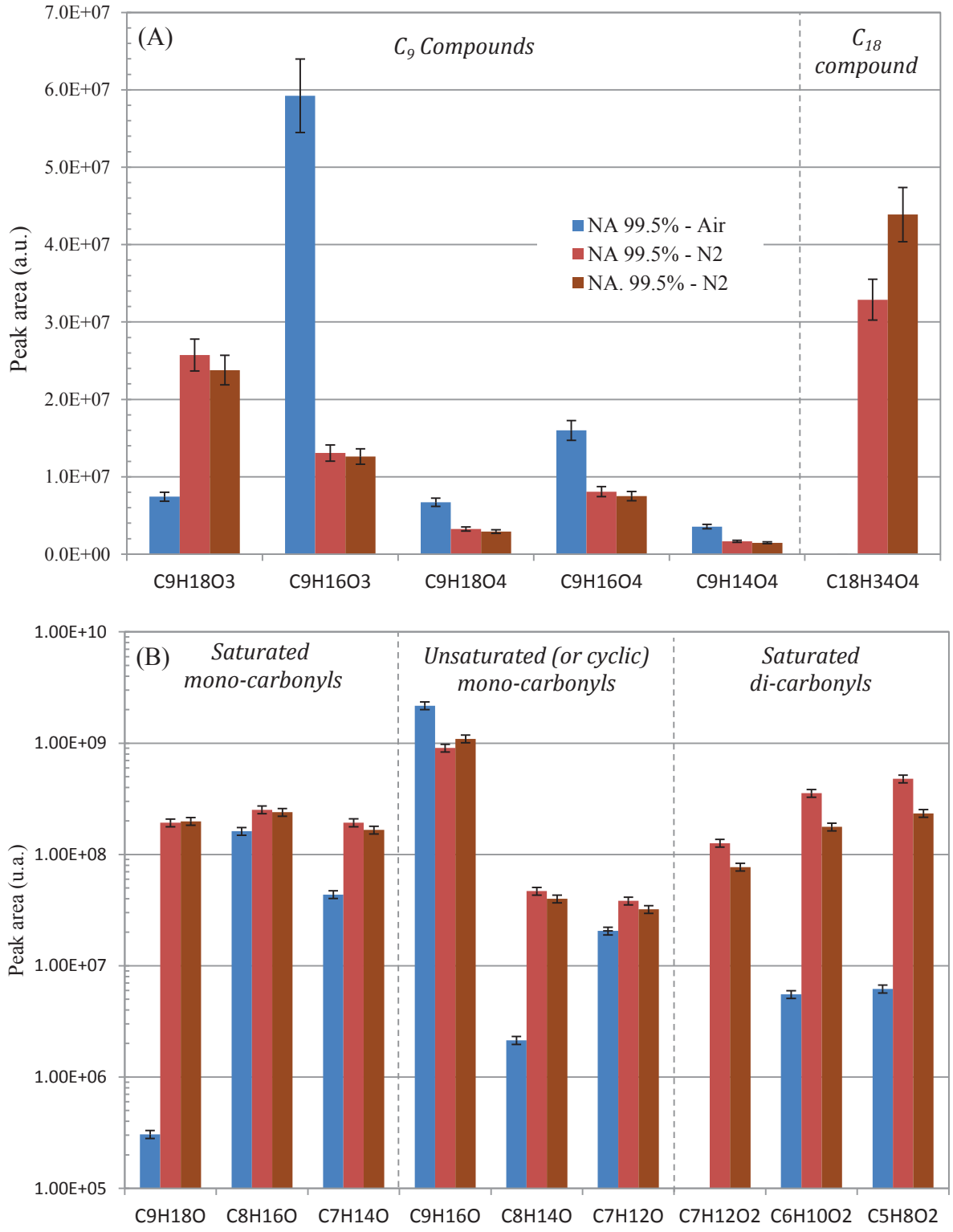

Figure VI-11: Signals obtained for selected condensed phase compounds after irradiating (1h) an aqueous solution of NA alone (99.5% purity) under filtered air (■) and under nitrogen (■). (A) C9 oxidation products and C18 recombination products detected in negative (-) ionization mode and (B) carbonyl species detected after PFBHA derivatization in positive (+) ionization mode (log_{10} scale). Error bars correspond to the estimated analytical uncertainties.

Complementary experiments were performed to gain insights into this new process. Figure VI-11 shows the comparison between the experiment conducted under filtered air and two similar experiments performed under nitrogen with a deoxygenated aqueous phase. These three experiments were carried out with the 99.5% purity NA. Except for the $C_9O_3H_{18}$ species, formation of C_9 products with more than two O atoms, expected to be NA oxidation products, appear favored under air. This could be consistent with a mechanism involving the addition of molecular oxygen after a radical H abstraction on the nonanoic acid molecule. The extracted ion chromatograms for the $C_9O_3H_{18}$ species show that one isomer, at a retention time of 9.53 min, is systematically favored under nitrogen compared to air experiments (figure VI-S5, section VI.7). This isomer could possibly not correspond to the addition of one hydroxyl group on the NA carbon chain. The higher retention time of this isomer points toward a compound of higher hydrophobicity, consistent with the fact that is favored under nitrogen, but the proposition of any structure would be here purely speculative.

The $C_{18}O_4H_{34}$ products presented on figure VI-11 are interestingly only formed under nitrogen. The related extraction ion chromatograms show that at least four isomers are formed (figure VI-S6, section VI.7). Given their molecular formula, these C_{18} products could correspond to the recombination of two NA molecules ($C_9O_2H_{18}$) after H-abstraction on each molecule. Such a mechanism is consistent with the fact that these compounds are not formed under air, as in this case the recombination of the two nonanoic acid radicals would be in competition with molecular oxygen addition.

The PFBHA derivatization of the samples (figure VI-11 B) clearly shows the formation of a series of C_4 to C_9 mono and dicarbonyl species. Some of them present equivalent double bond values equal to 2, i.e., bear one unsaturation or one cycle in addition to the carbonyl function for compounds with only one O atom. This is consistent with the measurements in the gas phase, and could be explained, as mentioned before, by radical-radical reactions such as disproportionation. Besides, among all the carbonyl species, the formation of the C_9 ones is particularly challenging as it requires the loss of the carboxylic function without fragmentation of the nonanoic acid carbon chain. In condensed phase as in gas phase, the use of air has an apparent negative impact compared to nitrogen on the formation of most carbonyls. Further discussion on this point from a mechanistic point of view is provided below.

To better understand the role of the gas-water interface in the photo-chemistry of NA, a series of experiments was conducted where the bulk produced products and the bulk plus surface produced products could be compared. Bulk produced products were investigated filling the quartz cell entirely with an aqueous solution bubbled with purified air or nitrogen for 25 minutes. A few microliters of NA, corresponding exactly to the volume needed to reach the concentration of 2 mM NA, were then added, after which the cell was stirred. The remaining gas-liquid interfaces were located into the quartz cell entries and were out of the Xenon lamp beam. However, one cannot totally exclude the hypothesis of the presence of small bubbles or micelles in the bulk of this solution. This series of experiments was performed with the NA with a purity of 97%.

As shown figure VI-12, under air all compounds seem favored in the presence of an interface with the notable exceptions of the C_{18} recombination product and the C_9 saturated mono-carbonyl compounds which were not formed at all. Under nitrogen, the influence of the interface is slightly less evident, with the same notable exception of the C_{18} recombination products and the C_9 saturated mono-carbonyl compounds, clearly enhanced in the presence of an interface. The appearance of these two products specifically under these experimental conditions suggests that their formation requires both a low oxygen concentration and concentrated NA. This is consistent with the expected mechanism which the $C_{18}O_4H_{34}$ products arises from, the recombination of two nonanoic acid radicals ($C_9O_2H_{17}^{\cdot}$) produced by an H-abstraction on two acid molecules. Such a recombination would indeed be favored where high concentration is achieved, e.g., at the interface. Even if these C_{18} products are only detected under nitrogen and not under air, this result shows that the interface is a favorable venue for radical-radical reactions. This could become of high importance for reactions able to compete with oxygen addition. A good example could be the disproportionation reaction proposed by Fu and co-workers as a radical-radical pathway leading to the unsaturated species detected in the gas phase during experiment performed under air with a photosensitizer (Fu et al., 2015).

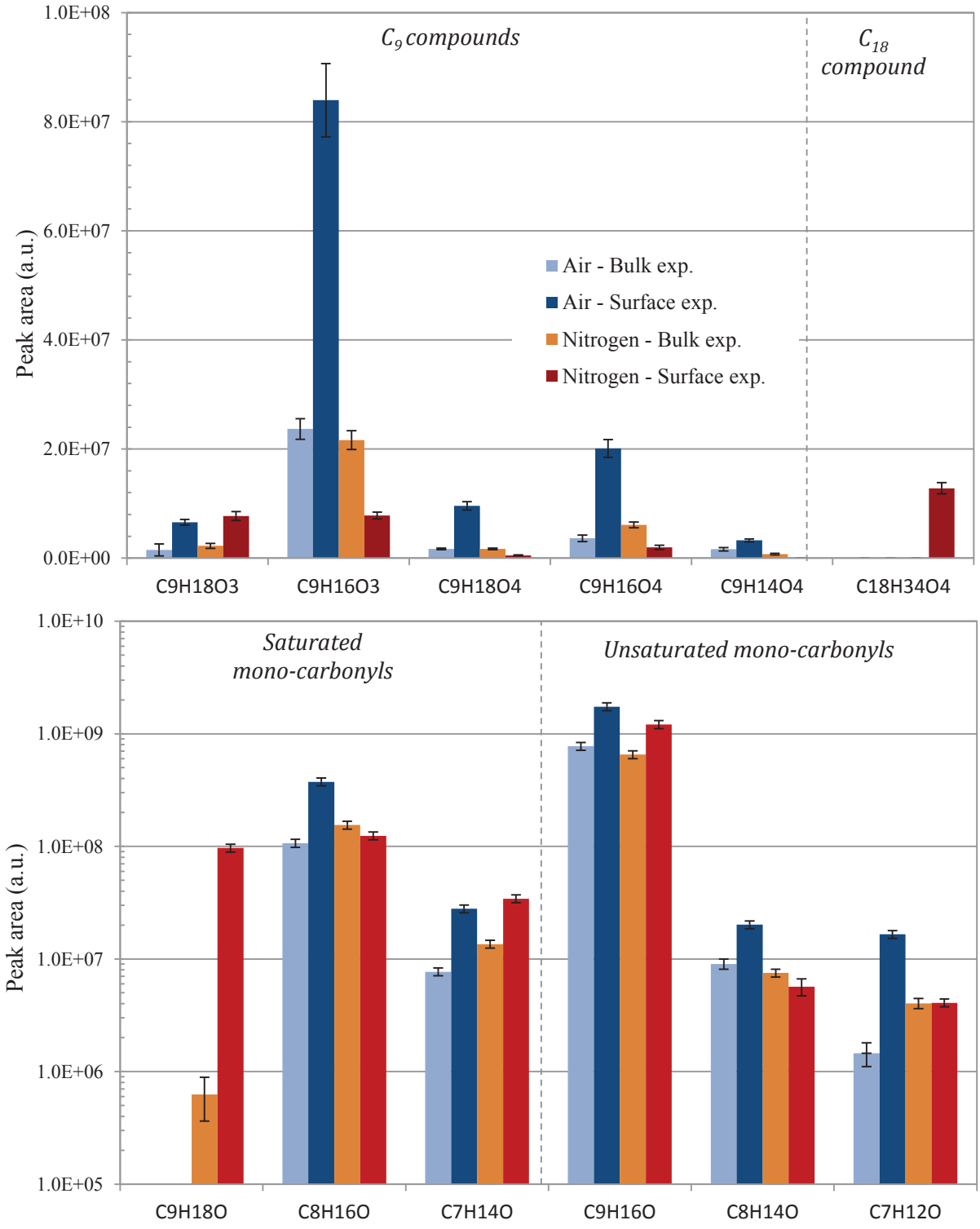

Figure VI-12: Signals obtained for selected condensed phase compounds obtained irradiating an aqueous solution of NA (97% purity) under filtered air and nitrogen, produced in the bulk (lighter colors) or in presence of an interface (darker colors). (A) detected in (-)-ionization mode and (B) detected in (+)-ionization mode after PFBHA derivatization (log_{10} scale). Error bars correspond to the estimated analytical uncertainties.

The last series of experiments probing the photochemistry of NA alone in water were performed adding a Pyrex filter at the output of the Xenon lamp to filter the radiations in the 250-290 nm range, which are not relevant for ground level photochemical processes. Comparison of the data obtained for experiments carried out (1) for 1 h without Pyrex filter, (2) for 1 h with a Pyrex filter and (3) for 5 h with a Pyrex filter, is provided Figure VI-13. A one hour irradiation time using a Pyrex filter appeared too short to produce detectable amounts of all the previously observed compounds. Nevertheless, extending this irradiation time to 5 hours, duration still relevant for environmental processes, allows the formation of most of the previously observed products.

The signals for the C_9 oxidation products, the C_{18} recombination products and the saturated carbonyl compounds obtained after 5 hours of irradiation with the Pyrex filter are of the same order of magnitude than those obtained after 1 hour without the Pyrex filter, suggesting a similar but logically slower chemistry with the filter. The unsaturated carbonyl species are formed after 5 hours with the Pyrex filter but only for the experiment conducted under nitrogen. The behavior of these compounds brings them closer to the C_{18} recombination products as these are also systematically formed only under nitrogen. This could be consistent with a formation mechanism of these unsaturated species involving radical-radical reactions.

In the hypothesis of a photochemistry initiated by NA itself, and more precisely by its absorption band centered at 270 nm, the production rate of excited states of nonanoic acid would be much higher without the Pyrex filter, and thus the related concentration of radical produced from these excited states much higher too. Under that condition, without the Pyrex filter i.e., with a relatively high concentration of radicals, disproportionation reactions appear to be significant with or without molecular oxygen in the system. On the contrary, with the Pyrex filter i.e., with a relatively low concentration of radical over the 5 hours of irradiation, these radical-radical reactions appear only competitive with other reactions, e.g. molecular oxygen addition, under nitrogen. The fact that the C_{18} compounds are not at all formed under air, even without the Pyrex filter, suggest that disproportionation reactions are faster than recombination reactions. Observations suggest that when a sufficient concentration of radicals is reached, either by removing the Pyrex filter or by adding a photosensitizer, disproportionation could significantly compete with oxygen addition to form unsaturated species (Ciuraru et al., 2015c; Fu et al., 2015).

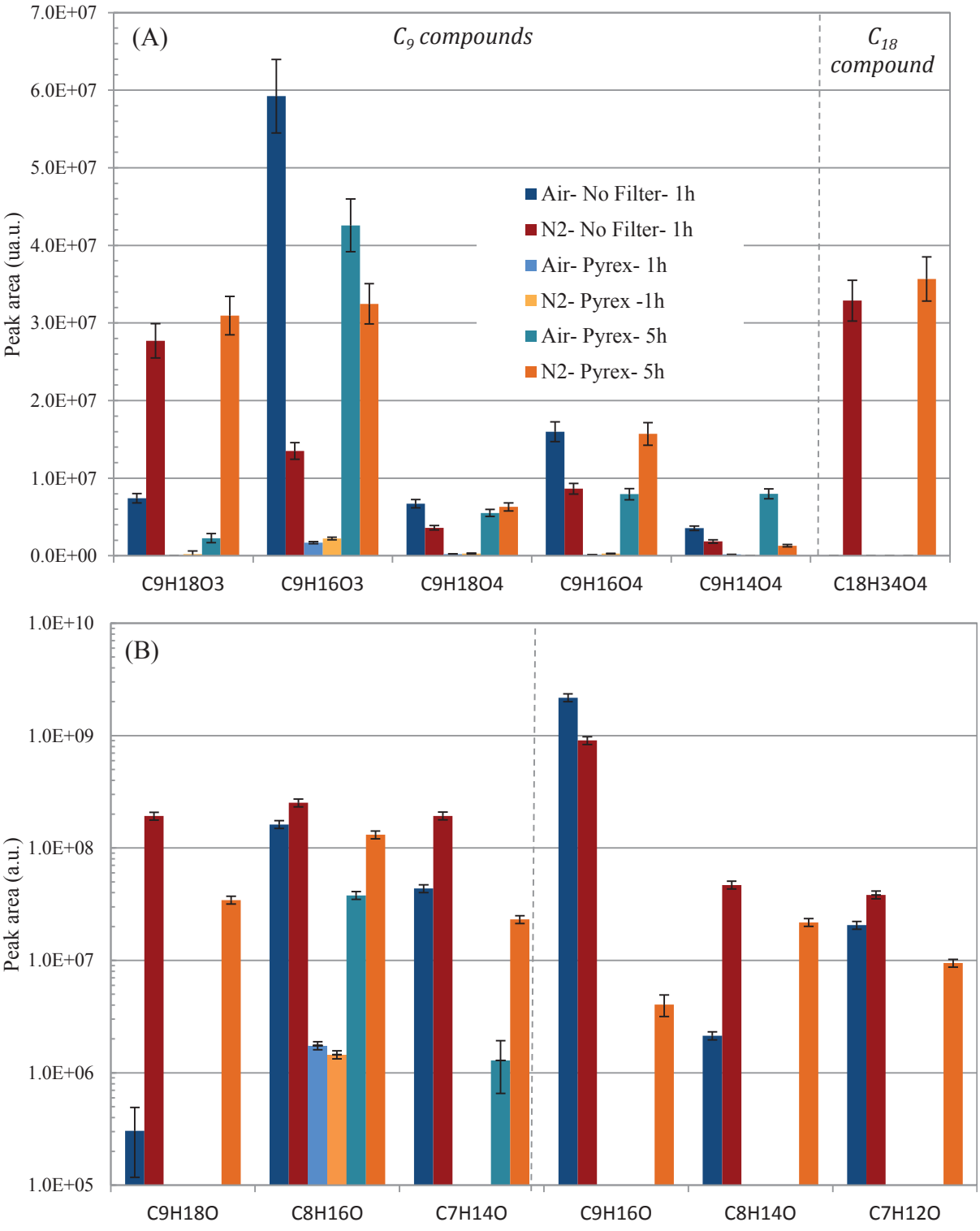

Figure VI-13: Signals obtained for selected condensed phase compounds obtained for an aqueous solution of NA alone (99.5% purity) under filtered air and under N_2, irradiated with (5h) and without (1h) the use a Pyrex filter. Products detected in (A) (-) ionization mode and (B) in (+) ionization mode after PFBHA derivatization (log_{10} scale). Error bars correspond to the estimated analytical uncertainties.

VI.3.3.b. Experiments with photo-initiator

The photochemistry of NA as surfactant alone in the presence of an air-water interface was compared with the photochemistry adding a photosensitizer. Similarly to the experiments described for the gas-phase, 4-BBA was used as photosensitizer. This series of experiments was performed under laboratory air, with the 97% purity NA and without Pyrex filter. Results are presented figure VI-14.

The list of the photo-products detected in both cases is very similar and a complete list of products observed is provided table VI-S (section VI.7). 4-BBA appears to promote the formation of the C_9 and C_8 oxidation products (carbonyl species not included). This is consistent with a formation mechanism initiated by a H-abstraction on NA by the triplet excited state of 4-BBA, followed by the addition of molecular oxygen on this alkyl radical. The similarity of the C_9 and C_8 product series points toward a similar formation mechanism as for the photochemistry of NA alone.

On the other hand, the presence of 4-BBA in the aqueous phase seems to have no or negative impact on the formation of C_{18} recombination products and carbonyls products (except for C_{18} recombination products under air). Besides, one can observe the formation of recombination products of NA molecules with 4-BBA molecules ($C_{23}O_5H_{28}$) of 4-BBA with itself ($C_{28}O_6H_{22}$). The formation of these new products could hinder the other radical-radical reactions and explain the observations.

The last series of experiments was conducted adding 10 mM of hydrogen peroxide in the aqueous phase instead of 4-BBA. Similarly, this series of experiments was performed under laboratory air, with NA of 97% purity and without Pyrex filter. Results are presented figure VI-S7 and show, as for the gas phase analysis, a poor reproducibility. Nevertheless, compared to NA alone, hydrogen peroxide favors the formation of all the C_9 and C_8 oxidation products as well as the formation of nonanoic acid radical recombination products in C_{18} (recombination of 2 NA radicals) but also in C_{27} (recombination of 3 NA radicals) even under air. The impact on the formation of carbonyl species is less clear. If the formation of $C_{<9}$ unsaturated monocarbonyl compounds appears clearly favored with H_2O_2, the formation of the C_9 one is clearly hindered. This could be a clue indicating different chemical routes for these two classes of compounds, as discussed below.

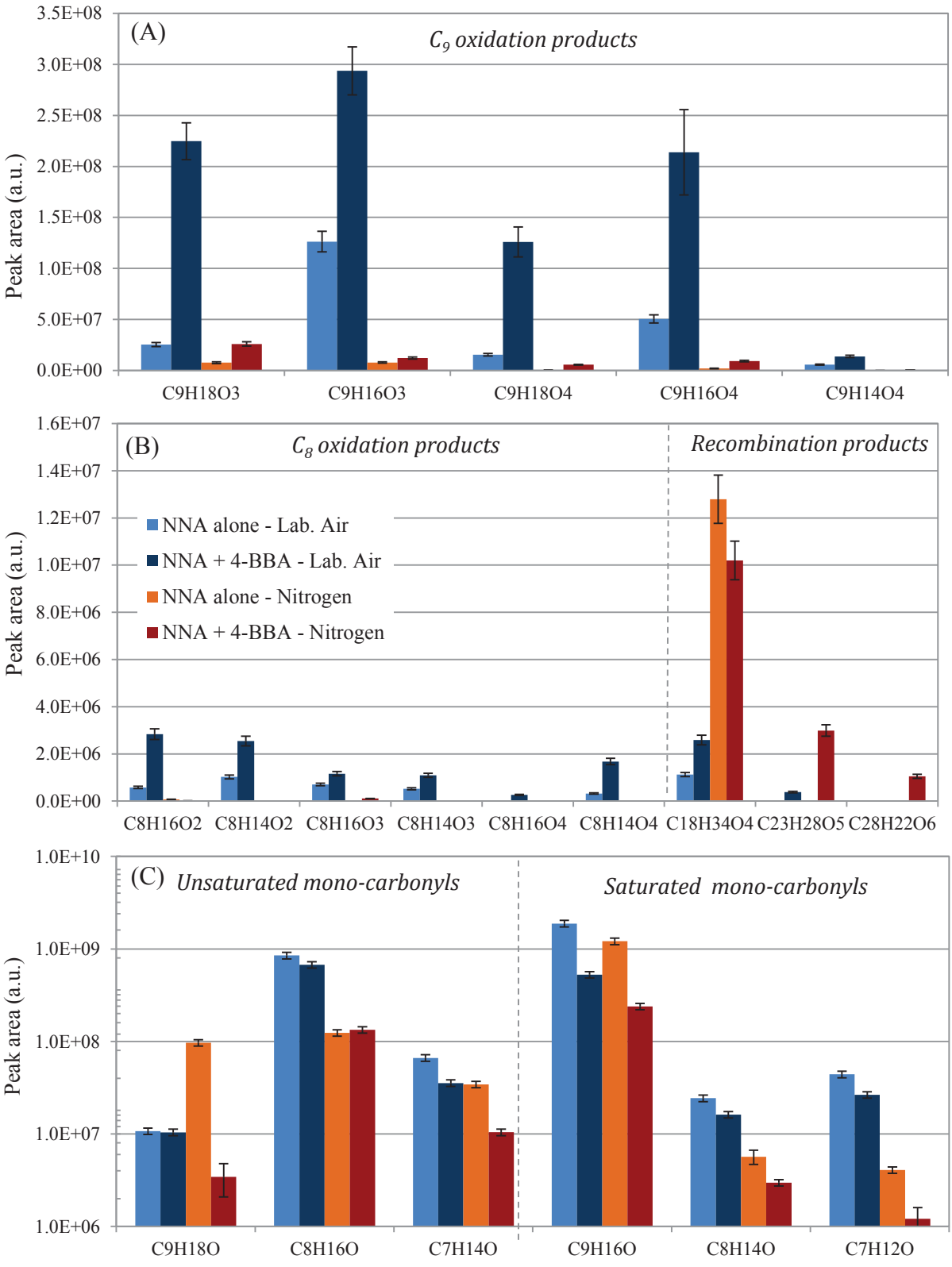

Figure VI-14: Signals of selected condensed phase compounds after irradiation (1h) of an aqueous solution of NA alone (97% purity, 2 mM) or with 0.1 mM of 4-BBA under laboratory air and N_2 detected in (A) and (B) (-) ionization mode and (C) (+) ionization after PFBHA derivatization (log_{10} scale). Error bars correspond to the estimated analytical uncertainties.

VI.3.4. Mechanistic insights

The similarity of the products formed with 4-BBA or H_2O_2 confirms an identical initial step, i.e., an H-abstraction on NA. H_2O_2 photolysis indeed rapidly forms OH radicals that are expected to exclusively react with hydrocarbons through H-abstraction (Finlayson-Pitts and Pitts Jr, 1999). The role of singlet oxygen, possibly coming from 4-BBA triplet state quenching by dissolved molecular oxygen, can be considered here as insignificant.

The absence of evidence of singlet oxygen combined with the formation of unsaturated products, points towards a particular chemistry occurring at the interface. This is supported by the observation done by Gever et al., who identified an advanced photochemical degradation of a pesticide in a microlayer to be quite different to the expected bulk processes (Gever et al., 1996).

A general mechanism explaining the observed products is shown in figure VI-15. In NA the H-abstraction is expected to occur preferentially on the α-carbon. This initial step leads to the formation of an NA alkyl radical who can undergo two competitive reaction pathways, (1) molecular oxygen addition giving rise to a peroxyl radical and (2) termination radical-radical reactions.

Two main radical-radical reactions are suggested. The first one corresponds to the recombination of two NA alkyl radical to form $C_{18}H_{34}O_4$ compounds. Experiments performed with H_2O_2 showed the recombination of up to three NA alkyl radicals, undoubtedly due to the high radical concentration involved in these experiments. It is very interesting to note that the formation of recombination products is favored by the presence of the interface (figure VI-12) and under nitrogen (Figures VI-11 to VI-14). This evidences that this kind of reaction is quite logically promoted by a high NA concentration and is in competition with molecular oxygen addition. The second possible radical-radical reaction is corresponding to a disproportionation, in which an alkyl radical abstracts a hydrogen on another alkyl radical to give rise to both saturated and unsaturated compounds. This pathway, also expected to be promoted by high NA concentration at the interface, was previously proposed by Fu et al. (2015) to explain the formation of unsaturated compounds in similar experiments. Here, the disproportionation product, nonenoic acid, was detected in the gas phase with higher intensity under nitrogen (figure VI-9 and VI-S2).

In parallel, molecular oxygen addition on the initially formed NA alkyl radical appears to be at the origin of most of the compounds detected in both gas and aqueous phases. The so formed peroxyl radical can firstly evolve toward C_9 oxidation products via peroxyl-peroxyl radical reactions. The formation of these products, bearing either hydroxyl or carbonyl function and keeping the carboxylic function of NA, was clearly observed in the aqueous phase. But peroxyl radical can also undergo fragmentation leading to the formation of octanal, when the H was abstracted on the α position of the NA parent molecule. The detection of octanal as a major compound in both phases strongly supports this pathway to be significant. Initial H-abstraction on other NA position would lead to the formation of also detected smaller aldehydes.

Each of these detected products can subsequently undergo H-abstraction followed by a similar chemistry as discussed above. Radical-radical reactions involving the alkyl radicals of saturated aldehydes are expected to lead to the formation of unsaturated aldehydes (octenal, heptenal, …), observed in both phases and which could significantly impact marine atmosphere chemistry together with other gas phase released compounds. All of these reactions are in constant competition and it is interesting to note that if these radical-radical reactions are favored under nitrogen, the formation of unsaturated aldehydes *via* this pathway requires the previous formation of the saturated aldehydes via O_2 addition and subsequent fragmentation. Contrary to NA recombination products that are hindered by the presence of O_2, the formation of unsaturated aldehydes is thus probably promoted by both O_2 and the interface as a concentrated media.

The observed alkenes can also be formed by the well described Norrish type II photochemistry of the newly formed carbonyl compounds, e.g., octanal, which has a hydrogen on the γ-position relative to the carbonyl group. This reaction then leads to the cleavage of the carbonyl compound into an alkene (C_{n-2}) and an unsaturated alcohol (C_2). But the direct fragmentation of oxy-radicals can also be invoked, also leading to an alkene and an alcohol bearing an alkyl radical (Ehrhardt and Petrick, 1984).

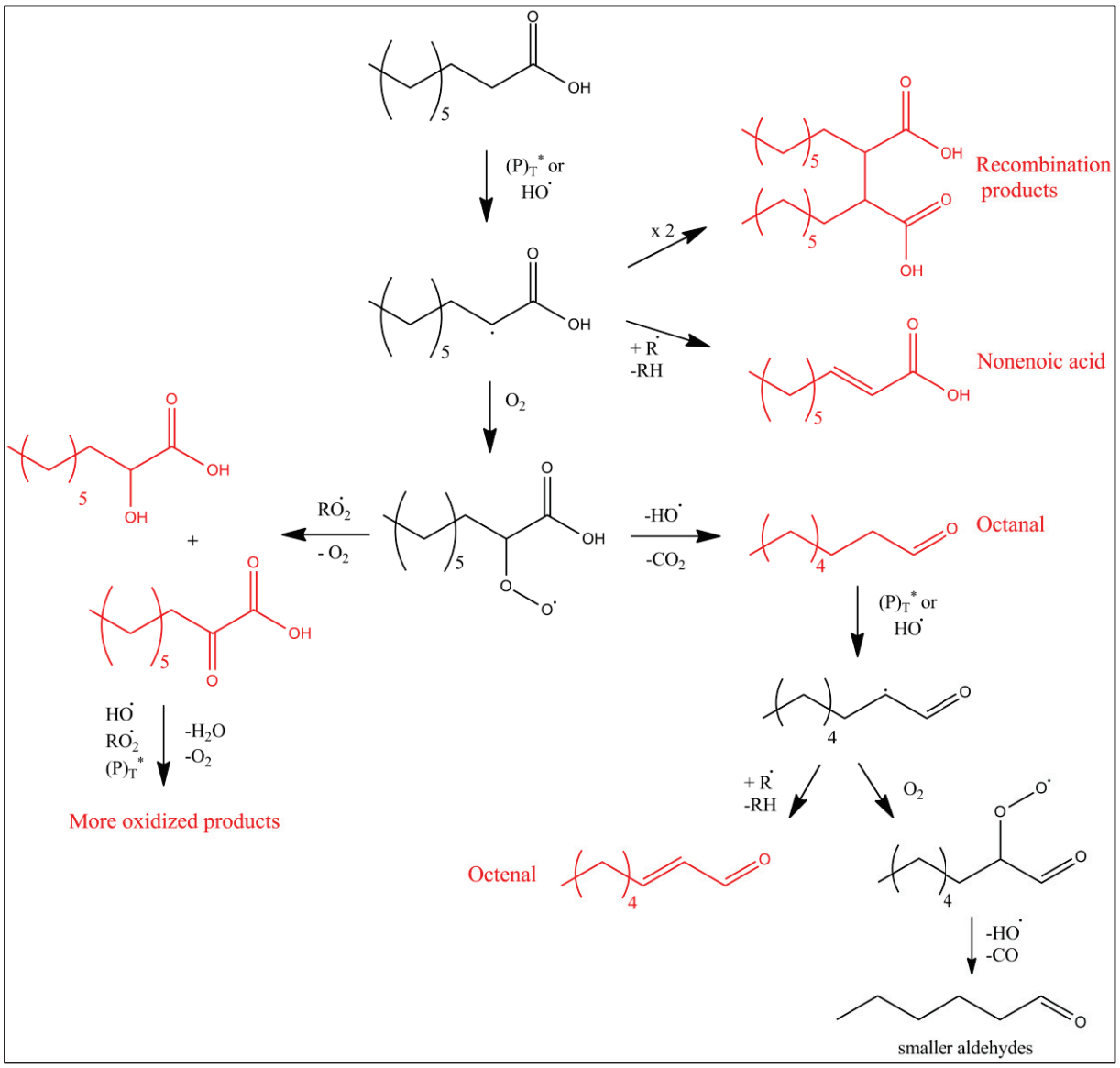

Figure VI-15: proposed mechanism for the photochemical reaction of nonanoic acid with a photosensitizer or OH-radicals leading to the formation of oxygenated and unsaturated compounds. Compounds observed are indicated in red.

The formation of nonanal and nonenal was observed to be favored in the absence of a photo-initiator. UV absorption spectrum of concentrated solution NA and neat NA have shown absorption maximum at 270 nm, this band being large enough to induce absorption until 330-340 nm. The observation of photoproducts of NA without adding any photosensitizer lead to the hypothesis that this absorption band could give rise to excited state of NA able to initiate photochemistry. Based on the literature, the figure VI-16 summarizes the identified possible fates of such a NA excited state. Norrish type I has been proposed to explain the photolytic cleavage for carboxylic acids such as isobutyric acid

(Coyle, 1978; Kaiser and Fischer, 1979). This Norrish I mechanism leads to an α-β cleavage of the aliphatic chain (figure VI-16 a) giving rise to the formation of two radicals, a carboxyl radical and, if applied to NA, an octyl radical. The octyl radical could then react with molecular oxygen to give e.g. octanal, one of the main products observed. But this mechanism alone does not explain the formation of the observed C_9 and C_{18} products.

Norrish type II reactions have also been observed for small carboxylic acids, leading to the formation of an alkene and acetic acid as shown figure VI-16 (b) (Nicholls and Leermaker, 1970). Heptene, the alkene expected to be formed from NA, was nevertheless detected only as a minor product in the gas phase, suggesting that, if occurring, this pathway is in strong competition with the other ones. On the other hand, heptene was observed in the experiments without photosensitizer but not in the experiments with 4-BBA.

A third pathway is suggested in figure VI-16 (d) and supposes that the excited NA molecule acts as photosensitizer by abstracting a hydrogen on another NA molecule, most probably from the carbon in α-position. One can consider this reaction as an intermolecular Norrish type II mechanism, promoted by the high NA concentration at the gas-water interface bringing the NA molecules in a closer arrangement. This would lead on one hand to the same NA alkyl-radical as with a photosensitizer (figure VI-16 d-1) and on the other hand to a diol radical (figure VI-16 d-2). This diol radical is of interest as it could explain the formation of the observed C_9 carbonyls in the absence of any known photosensitizer. It could indeed undergo a first H-shift leading to an alkyl radical bearing a diol function. The latter could then in his turn undergo disproportionation in the presence of another alkyl radical to give rise either to a saturated or to an unsaturated C_9 diol. As the diol function is in equilibrium with the aldehyde function by the loss of an H_2O molecule, this pathway could lead to the detected nonanal and nonenal. The pathway involving the diol radical cannot be initiated by another photo-initiator than NA and is thus specific to the NA photochemistry. It is particularly interesting to note that our experimental results are quite coherent with this proposed mechanism, as the formation of nonanal and nonenal is generally either not affected or hindered (figures VI-6 and VI-S3, VI-14 and VI-S6) when a photo-initiator is present (4-BBA or H_2O_2). This is the contrary of what it is observed for the majority of the other products that are generally promoted by the presence of a photo-initiator and whose the formation can be explain by an initial H abstraction on the NA molecule.

A fourth pathway can be proposed, figure VI-16 (c), starting with an electron release from the carboxylic function after excitation which would lead, after an internal hydrogen shift, to the formation of an nonanoic acid γ-alkyl radical and a solvated electron. The C_9 radical could then follow the same reaction scheme as proposed in the presence of a photosensitizer. It is known that certain acids, especially in their carboxylate form, can release an electron upon excitation, but it is unknown whether this also applies to NA in this case.

At this stage, it is uncertain which one of the four suggested mechanisms is the main pathway of the NA surface photochemistry in the absence of any photo-initiator, as each of them can lead to the formation of detected compounds. If the intermolecular Norrish type II mechanism appears to be the only one able to explain the formation of two specific compounds, nonanal and nonenal, this doesn't necessarily mean that it is the main reaction pathway.

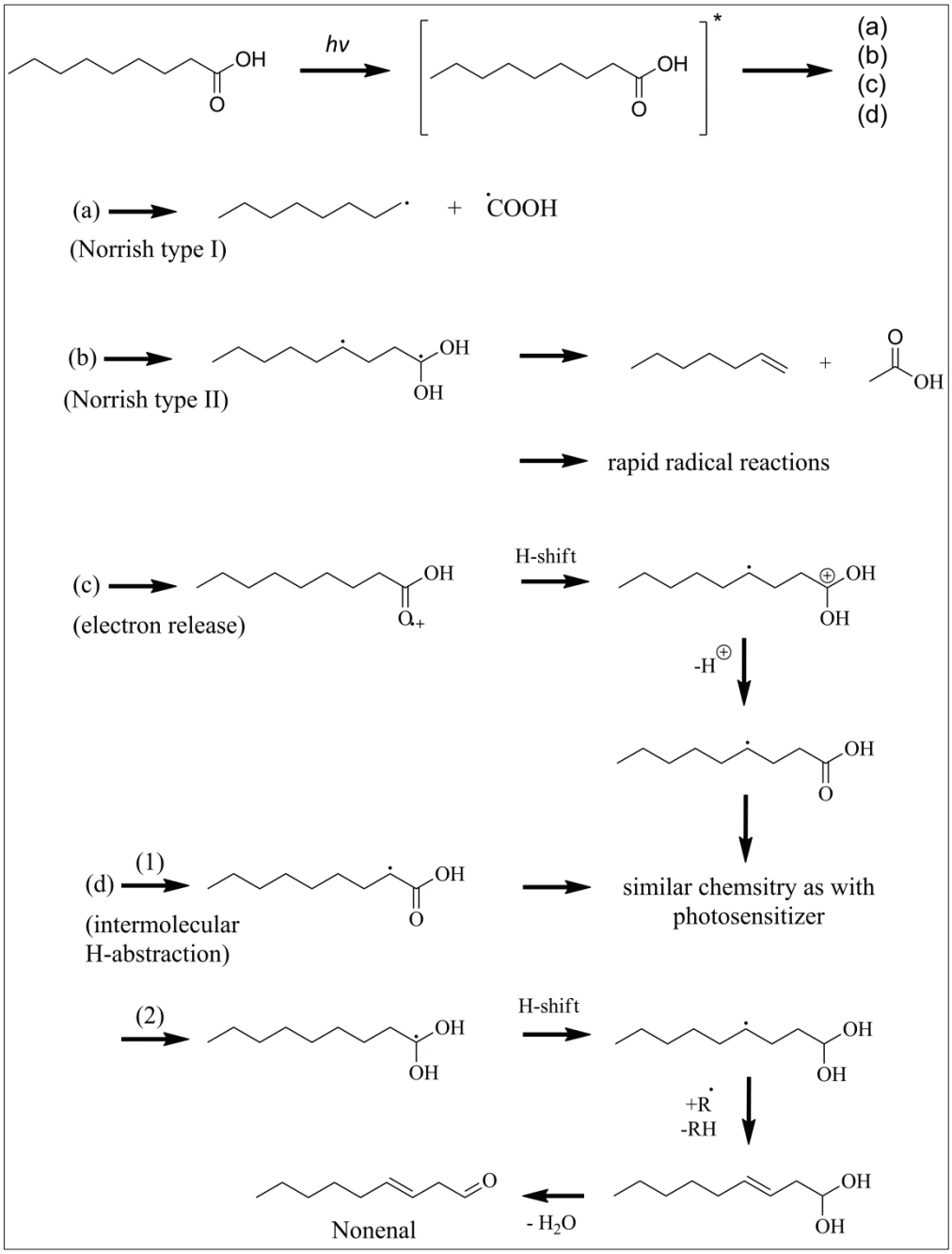

Figure VI-16: Possible initial steps for the photochemistry of nonanoic acid without photo-initiator

VI.4. Atmospheric implications and conclusions

From the experiments conducted with a carboxylic acid, nonanoic acid, in presence of a photo-initiator, it seems clear that efficient photochemistry occurs at the organic coated air-water interface. This chemistry leads to the release of functionalized and unsaturated products in the gas phase and in the underlying condensed bulk phase, confirming the observations of previous studies with an carboxylic acid as surfactant and humic acids as light active compound (Ciuraru et al., 2015a) or an alcohol with a 4-BBA as photosensitizer (Fu et al., 2015). Spectroscopic evidence show the propensity of the photosensitizer to partition quickly to the organic microlayer, enhancing the probabilities of direct reactions between the photo active organic matter and the microlayer itself. The chemistry leading to the formation of unsaturated compounds seem to be promoted by the chemical and physical characteristics of the interfacial layer and in particular the high concentrations encountered there. The formation of dimers (2 molecules of nonanoic acid) and recombination products of NA with the photosensitizer illustrate the importance of radical-radical reactions in this very unique location at the interface.

The observed photochemistry from solely a carboxylic acid as surface layer on an aqueous solution also leads to the formation of a variety of functionalized and unsaturated compounds. Although at this point the mechanism triggering this photochemistry is not yet well understood, the products formed point here again towards photo-initiated radical chain reactions. The importance of the surface excess concentration, leading to the high concentrations at the air-water interface compared to the bulk phase, seems crucial in the absorption of this carboxylic acid. The underlying water could also play a role in the formation of eventual hydrogen-bonds between two carboxylic acid molecules, leading to the observed secondary absorption peak in the near UV.

From an atmospheric point of view, the release of unsaturated compounds, such as the observed alkenes or unsaturated aldehydes and acids, is particularly interesting, as these compounds are reactive species towards gas phase oxidants and hence possible contributors to aerosol growth or even nucleation of new particles. But also the bulk condensed phase is impacted by this chemistry. The lower volatility species, as the C_9 products with up to 4 oxygens observed, partition to the bulk phase where they can influence the chemistry or even the biology.

Air-water interfaces are very largely spread over our planet and the most obvious one is constituted by the ocean surface microlayer. The chemistry reported here could thus significantly increase abiotic emission and potentially explain discrepancies between modelled and measured concentrations of VOCs above the open ocean (Beale et al., 2015; Carpenter and Nightingale, 2015). But also new particle formation observed above the open ocean could be impacted by this new source of precursors which may help to better predict particle concentrations above open oceans (Whitehead et al., 2010). Furthermore, as stated in the introduction, sea spray particle entrain organics form the SML in the troposphere, where this photochemistry could also play a significant role through heterogeneous reactions. But the photochemistry initiated by a carboxylic acid alone could of course have an even larger impact. Carboxylic acids are ubiquitous compounds and virtually present at any interface, from sea surface to leafs. If photochemistry at all these interfaces could be triggered by the mere presence of carboxylic acids, then the impacts of this photochemistry, even if relatively inefficient compared to the chemistry initiated by an efficient photosensitizer such as aromatic ketones, could be substantial.

VI.5. Affiliations of the authors

All authors :

Université de Lyon 1, Lyon, F-69626, France, CNRS, UMR5256, IRCELYON, Institut de Recherches Sur la Catalyse et l'Environnement de Lyon, Villeurbanne, F-69626, France,

Except :

[$] : Clermont Université, Université Blaise Pascal, Institut de Chimie de Clermont-Ferrand (ICCF), UMR 6296, BP 10448, 63000 Clermont Ferrand, France

[£] : Department of Chemistry, University of Toronto, 80 St. George St. Toronto, ON Canada M5S 3H6

VI.6. References

Beale, R., Dixon, J.L., Smyth, T.J. and Nightingale, P.D., 2015. Annual study of oxygenated volatile organic compounds in UK shelf waters. Marine Chemistry, 171: 96-106.

Blake, R.S., Wyche, K.P., Ellis, A.M. and Monks, P.S., 2006. Chemical ionization reaction time-of-flight mass spectrometry: Multi-reagent analysis for determination of trace gas composition. International Journal of Mass Spectrometry, 254(1–2): 85-93.

Cappellin, L. et al., 2012. On Quantitative Determination of Volatile Organic Compound Concentrations Using Proton Transfer Reaction Time-of-Flight Mass Spectrometry. Environmental Science & Technology, 46(4): 2283-2290.

Carpenter, L.J. and Nightingale, P.D., 2015. Chemistry and Release of Gases from the Surface Ocean. Chemical Reviews, 115(10): 4015-4034.

Caswell, L.R., Howard, M.F. and Onisto, T.M., 1976. Solvent and substituent effects upon the n → π* transition of aliphatic carboxylic acids and esters. The Journal of Organic Chemistry, 41(20): 3312-3316.

Ciuraru, R. et al., 2015a. Photosensitized production of functionalized and unsaturated organic compounds at the air-sea interface. Scientific Reports, 5.

Ciuraru, R. et al., 2015b. Unravelling new processes at interfaces: photochemical isoprene production at the sea surface. Environmental Science & Technology.

Ciuraru, R. et al., 2015c. Photosensitized production of functionalized and unsaturated organic compounds at the air-sea interface. Scientific Reports, 5: 12741.

Coyle, J.D., 1978. Photochemistry of carboxylic-acid derivatives. Chemical Reviews, 78: 97-123.

Cunliffe, M. et al., 2013. Sea surface microlayers: A unified physicochemical and biological perspective of the airâ€“ocean interface. Progress in Oceanography, 109(0): 104-116.

de Gouw, J. and Warneke, C., 2007. Measurements of volatile organic compounds in the earth's atmosphere using proton-transfer-reaction mass spectrometry. Mass Spectrometry Reviews, 26(2): 223-257.

de Gouw, J. et al., 2003. Sensitivity and specificity of atmospheric trace gas detection by proton-transfer-reaction mass spectrometry. International Journal of Mass Spectrometry, 223(1-3): 365-382.

de Leeuw, G. et al., 2011. Production flux of sea spray aerosol. Reviews of Geophysics, 49.

Desiraju, G.R., 1991. The C-H.cntdot..cntdot..cntdot.O hydrogen bond in crystals: what is it? Accounts of Chemical Research, 24(10): 290-296.

Desiraju, G.R., 1996. The C–H···O Hydrogen Bond: Structural Implications and Supramolecular Design. Accounts of Chemical Research, 29(9): 441-449.

Diskin, A.M., Wang, T., Smith, D. and Španěl, P., 2002. A selected ion flow tube (SIFT), study of the reactions of H3O+, NO+ and O2+ ions with a series of alkenes; in support of SIFT-MS. International Journal of Mass Spectrometry, 218(1): 87-101.

Donaldson, D.J. and Vaida, V., 2006. The influence of organic films at the air-aqueous boundary on atmospheric processes. Chemical Reviews, 106(4): 1445-1461.

Ehrhardt, M. and Petrick, G., 1984. On the sensitized photo-oxidation of alkylbenzenes in seawater. Marine Chemistry, 15: 47-58.

Ehrhardt, M. and Petrick, G., 1985. The sensitized photo-oxidation of normal-pentadecane as a model for abiotic decomposition of aliphatic-hydrocarbons in seawater. Marine Chemistry, 16: 227-238.

Fiches, G. et al., 2013. Modifying PTR-MS operating conditions for quantitative headspace analysis of hydro-alcoholic beverages. 1. Variation of the mean collision energy to control ionization processes occurring during PTR-MS analyses of 10-40% (v/v) ethanol-water solutions. International Journal of Mass Spectrometry, 356: 41-45.

Finlayson-Pitts, B.J. and Pitts Jr, J.N., 1999. Chemistry of the upper and lower atmosphere: theory, experiments, and applications. Academic press.

Fu, H. et al., 2015. Photosensitized Production of Atmospherically Reactive Organic Compounds at the Air/Aqueous Interface. Journal of the American Chemical Society, 137(26): 8348-8351.

George, C., Ammann, M., D'Anna, B., Donaldson, D.J. and Nizkorodov, S.A., 2015. Heterogeneous Photochemistry in the Atmosphere. Chemical Reviews, 115(10): 4218-4258.

Gever, J.R., Mabury, S.A. and Crosby, D.G., 1996. Rice field surface microlayers: Collection, composition and pesticide enrichment. Environmental Toxicology and Chemistry, 15(10): 1676-1682.

Guiliano, M., ElAnbaLurot, F., Doumenq, P., Mille, G. and Rontani, J.F., 1997. Photo-oxidation of n-alkanes in simulated marine environmental conditions. Journal of Photochemistry and Photobiology a-Chemistry, 102(2-3): 127-132.

Hansel, A. et al., 1995. Proton-transfer reaction mass-spectrometry - online trace gas-analysis at the ppb level. international Journal of Mass Spectrometry, 149: 609-619.

Herndon, S.C. et al., 2006. Hydrocarbon emissions from in-use commercial aircraft during airport operations. Environmental Science & Technology, 40(14): 4406-4413.

Jammoul, A., Dumas, S., D'Anna, B. and George, C., 2009. Photoinduced oxidation of sea salt halides by aromatic ketones: a source of halogenated radicals. Atmospheric Chemistry and Physics, 9(13): 4229-4237.

Jordan, A. et al., 2009. An online ultra-high sensitivity Proton-transfer-reaction mass-spectrometer combined with switchable reagent ion capability (PTR+SRI-MS). International Journal of Mass Spectrometry, 286(1): 32-38.

Kaiser, T. and Fischer, H., 1979. Norrish type-i cleavage of aliphatic carboxylic-acids and esters in solution - cidnp-study. Helvetica Chimica Acta, 62: 1475-1484.

Karl, T. et al., 2012. Selective measurements of isoprene and 2-methyl-3-buten-2-ol based on NO+ ionization mass spectrometry. Atmospheric Chemistry and Physics, 12(24): 11877-11884.

Knighton, W.B., Fortner, E.C., Herndon, S.C., Wood, E.C. and Miake-Lye, R.C., 2009. Adaptation of a proton transfer reaction mass spectrometer instrument to employ NO+ as reagent ion for the detection of 1,3-butadiene in the ambient atmosphere. Rapid Communications in Mass Spectrometry, 23(20): 3301-3308.

Liss, P.S. and Duce, R.A. (Editors), 1997. Sea Surface and Global Change. Cambridge University Press, Cambridge, 509 pp.

Mmereki, B.T. and Donaldson, D.J., 2002. Laser induced fluorescence of pyrene at an organic coated air-water interface. Physical Chemistry Chemical Physics, 4(17): 4186-4191.

Mmereki, B.T. and Donaldson, D.J., 2003. Direct observation of the kinetics of an atmospherically important reaction at the air-aqueous interface. Journal of Physical Chemistry A, 107(50): 11038-11042.

Mochalski, P., Unterkofler, K., Španěl, P., Smith, D. and Amann, A., 2014. Product ion distributions for the reactions of NO+ with some physiologically significant aldehydes

obtained using a SRI-TOF-MS instrument. International Journal of Mass Spectrometry, 363(0): 23-31.

Murov, S.L., Carmichael, I. and Hug, G.L., 1993. Handbook of Photochemistry. CRC Press, New York.

Nakabayashi, T., Kosugi, K. and Nishi, N., 1999. Liquid Structure of Acetic Acid Studied by Raman Spectroscopy and Ab Initio Molecular Orbital Calculations. The Journal of Physical Chemistry A, 103(43): 8595-8603.

Nicholls, C.H. and Leermaker, P.A., 1970. Reexamination of type-2 elimination reactions in photolysis of aliphatic carboxylic acids and amides. Journal of Organic Chemistry, 35: 2754-&.

Ovadnevaite, J. et al., 2011. Primary marine organic aerosol: A dichotomy of low hygroscopicity and high CCN activity. Geophysical Research Letters, 38.

Reeser, D.I., George, C. and Donaldson, D.J., 2009a. Photooxidation of Halides by Chlorophyll at the Air-Salt Water Interface. Journal of Physical Chemistry A, 113: 8591-8595.

Reeser, D.I. et al., 2009b. Photoenhanced Reaction of Ozone with Chlorophyll at the Seawater Surface. Journal of Physical Chemistry C, 113: 2071-2077.

Ruderman, G., Caffarena, E., Mogilner, I. and Tolosa, E., 1998. Hydrogen Bonding of Carboxylic Acids in Aqueous Solutions—UV Spectroscopy, Viscosity, and Molecular Simulation of Acetic Acid. Journal of Solution Chemistry, 27(10): 935-948.

Smith, D. and Spanel, P., 2005. Selected ion flow tube mass spectrometry (SIFT-MS) for on-line trace gas analysis. Mass Spectrometry Reviews, 24(5): 661-700.

Stemmler, K., Ammann, M., Donders, C., Kleffmann, J. and George, C., 2006. Photosensitized reduction of nitrogen dioxide on humic acid as a source of nitrous acid. Nature, 440(7081): 195-198.

Whitehead, J.D., McFiggans, G., Gallagher, M.W. and Flynn, M.J., 2010. Simultaneous coastal measurements of ozone deposition fluxes and iodine-mediated particle emission fluxes with subsequent CCN formation. Atmospheric Chemistry and Physics, 10(1): 255-266.

Wurl, O., Wurl, E., Miller, L., Johnson, K. and Vagle, S., 2011. Formation and global distribution of sea-surface microlayers. Biogeosciences, 8(1): 121-135.

Zhou, S. et al., 2014. Formation of gas-phase carbonyls from heterogeneous oxidation of polyunsaturated fatty acids at the air-water interface and of the sea surface microlayer. Atmospheric Chemistry and Physics, 14(3): 1371-1384.

VI.7. Supplementary information.

Table VI-S1: Different product ions for the considered organic molecules in the H_3O^+ and NO^+ reagent mode. Ions used for identification in this work are in bold.

VOC	Major H_3O^+ product ions [a,b]	Major NO^+ product ions [a,b]
Alcohols	$C_xH_y^+$; $(M\text{-}OH)^+$	$C_xH_y^+$; $(M\text{-}H)^+$; $(M\text{-}OH)^+$
Saturated aldehydes	**MH^+**, $(M\text{-}OH)^+$, $C_xH_y^+$	**$(M\text{-}H)^+$**
Unsaturated aldehydes	**MH^+**, $(M\text{-}OH)^+$	**$(M\text{-}H)^+$** ; MNO^+
Ketones	**MH^+**, $(M\text{-}OH)^+$	**MNO^+** ; $M^{+\bullet}$
Carboxylic acids	**MH^+**, $C_xH_y^+$	**MNO^+** ; $(M\text{-}OH)^+$
Alkenes	**MH^+**, $C_xH_y^+$	M^+; **MNO^+**

[a]: M stands for the reactant molecule. Product ions are designated as follows: MH^+ is a protonated molecule; loss of fragments is indicated between brackets; $M^{+\bullet}$ is a radical parent cation, MNO^+ is an adduct; $C_xH_y^+$ is a fragment

[b]: based on own calibrations and literature reported results (de Gouw and Warneke, 2007; Diskin et al., 2002; Mochalski et al., 2014; Smith and Spanel, 2005)

Table VI-2: Overview of the products detected during experiments with photosensitizers for the gas and the condensed phase

	Formula	Name	SRI-ToF-MS	UPLC-HRMS
Saturated aldehydes	C_3H_6O	propanal	**X**	
	C_4H_8O	butanal	**X**	
	$C_5H_{10}O$	pentanal	**X**	
	$C_6H_{12}O$	hexanal	**X**	
	$C_7H_{14}O$	heptanal	**X**	**X (or ketone)**
	$C_8H_{16}O$	octanal	**X**	**X (or ketone)**
	$C_9H_{18}O$	nonanal	**X**	**X (or ketone)**
Ketones	C_3H_6O	acetone		
	C_4H_8O	butanone	**X**	
	$C_5H_{10}O$	pentanone	**X**	
	$C_6H_{12}O$	hexanone	**X**	
	$C_7H_{14}O$	heptanone	**X**	
	$C_8H_{16}O$	octanone	**x**	
Unsaturated aldehydes	C_3H_4O	propenal	**X**	
	C_4H_6O	butenal	**X**	
	C_5H_8O	pentenal	**X**	
	$C_6H_{10}O$	hexenal	**X**	
	$C_7H_{12}O$	heptenal	**X**	**X (or ketone)**
	$C_8H_{14}O$	octenal	**X**	**X (or ketone)**
	$C_9H_{16}O$	nonenal	**X**	**X (or ketone)**
Unsaturated ketones	$C_6H_{10}O$	hexenone	**X**	
	$C_7H_{12}O$	heptenone	**X**	
	$C_8H_{14}O$	octenone	**X**	
Recombination products	$C_{18}H_{34}O_4$			**X**
	$C_{27}H_{50}O_6$			**x**

	Formula	Name	SRI-ToF-MS	UPLC-HRMS
Saturated acids	$C_4H_8O_2$	butanoic acid	X	
	$C_5H_{10}O_2$	pentanoic acid	X	
	$C_6H_{12}O_2$	hexanoic acid	X	
	$C_7H_{14}O_2$	heptanoic acid	X	
	$C_8H_{16}O_2$	octanoic acid	X	X
Unsaturated acids	$C_4H_6O_2$	butenoic acid	X	
	$C_5H_8O_2$	pentenoic acid	X	
	$C_6H_{10}O_2$	hexenoic acid	X	
	$C_7H_{12}O_2$	heptenoic acid	X	
	$C_8H_{14}O_2$	octenoic acid	X	X
	$C_9H_{16}O_2$	nonenoic acid	X	
Higher oxygenated acids	$C_8H_{16}O_3$			X
	$C_8H_{14}O_3$			X
	$C_8H_{16}O_4$			X
	$C_8H_{14}O_4$			X
	$C_9H_{18}O_3$			X
	$C_9H_{16}O_3$		X	X
	$C_9H_{18}O_4$			X
	$C_9H_{16}O_4$			X
	$C_9H_{14}O_4$			X
Alkenes	C_4H_8	butene	X	
	C_5H_{10}	pentene	X	
	C_6H_{12}	hexene	X	
	C_8H_{16}	octene	X	
	C_9H_{18}	nonene	X	

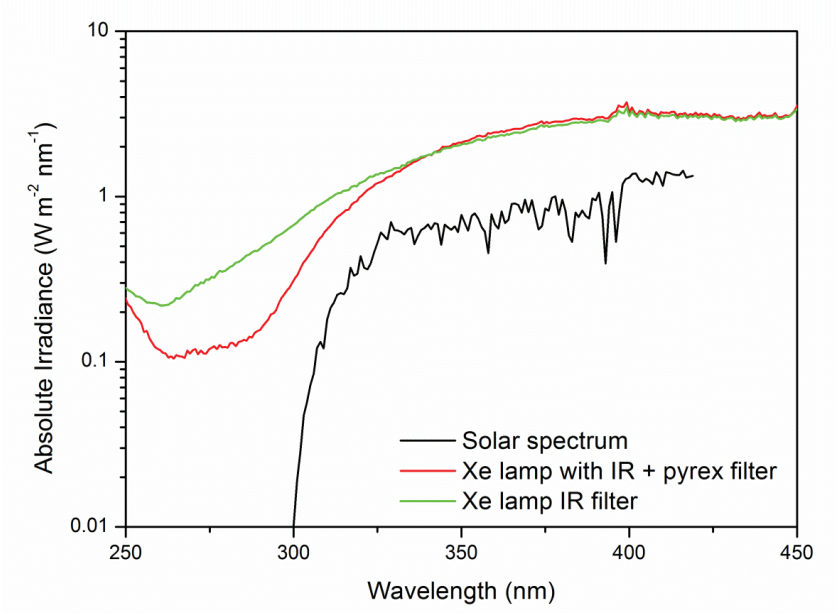

Figure VI-S1: Irradiance spectra of the Xenon lamp used in our experiments with IR water filter (green line) and with IR and pyrex filter (red line) measured at 13 cm of the output compared to the solar irradiance spectrum of the sun (black line) at ground level (latitude 45°N, calculated with Quick TUV calculator, NCAR, Boulder,Co: http://cprm.acom.ucar.edu/Models/TUV/Interactive_TUV/).

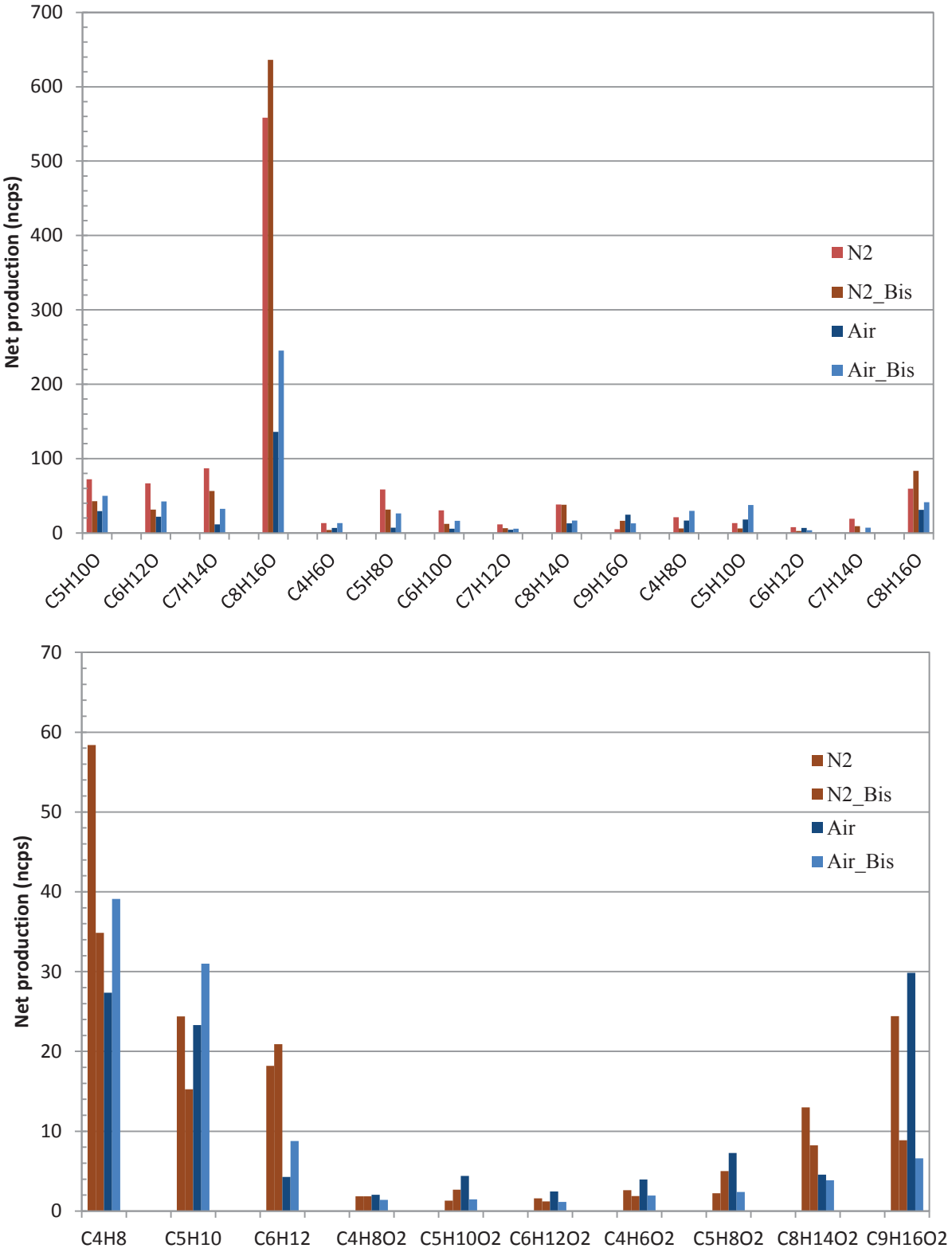

Figure VI-S2: Net production observed for selected compounds in the gas phase detected in NO^+ mode, in presence of purified air (■) and nitrogen (■) above an irradiated solution containing 2 mM NA and 10 mM H_2O_2..

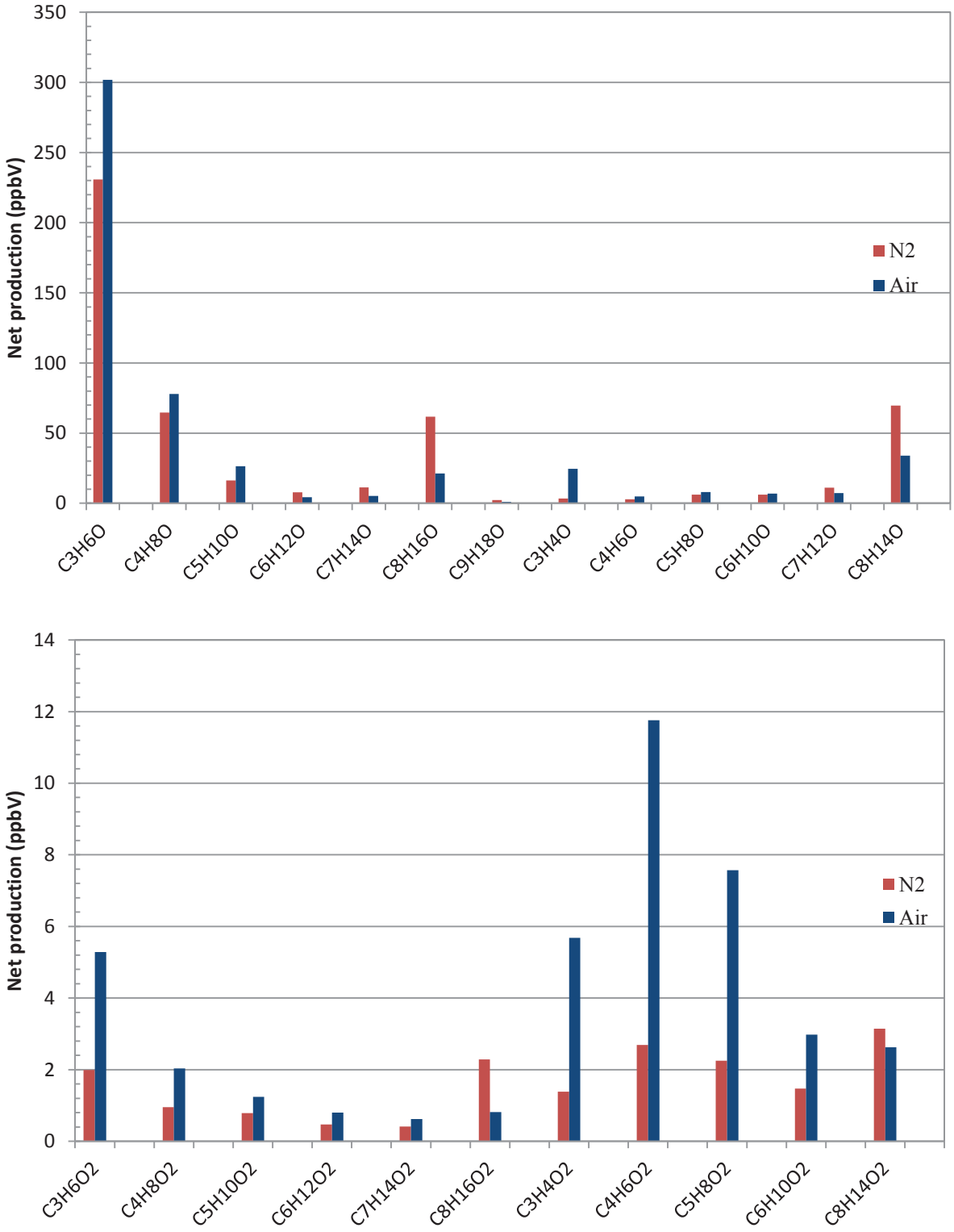

Figure VI-S3: Net production observed in two experiments for selected compounds in the gas phase detected in H_3O^+ mode, in presence of purified air (■) and nitrogen (■) above an irradiated solution containing 2 mM NA and 10 mM H_2O_2. Concentrations shown are the net increase for each ion, without corrections for fragmentations.

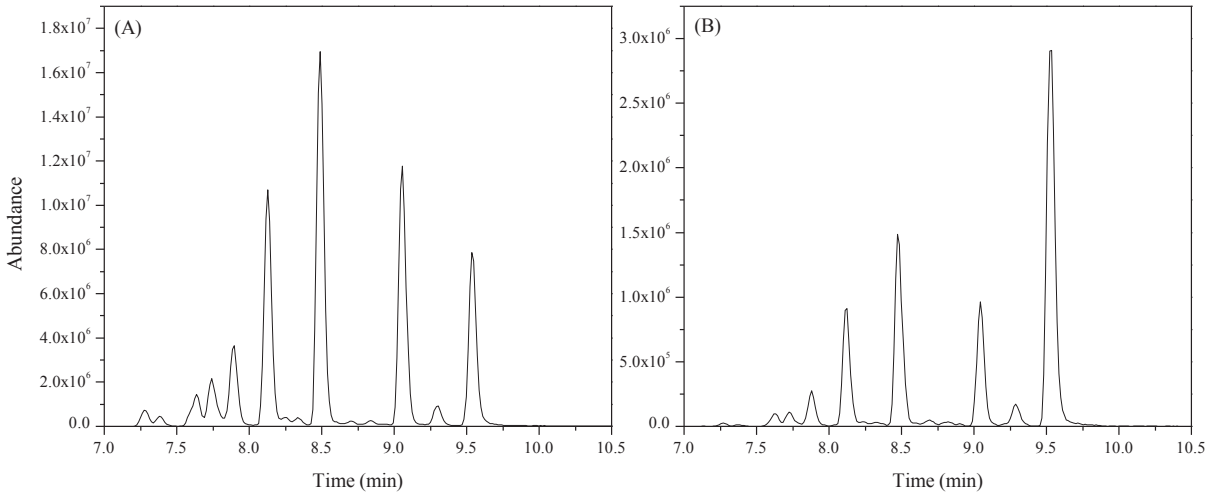

Figure S-VI-5 UHPLC-(-)HESI/HRMS extracted ion chromatograms for m/z 173.118 ($C_9O_3H_{18}$). Experiments performed with 97% purity nonanoic acid, 0.1 mM of 4-BBA and (A) under laboratory air, (B) under nitrogen.

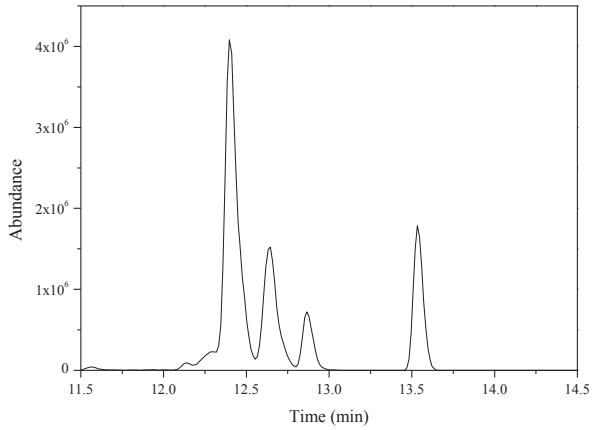

Figure S-VI-6 UHPLC-(-)HESI/HRMS extracted ion chromatograms for m/z 313.238 ($C_{18}O_4H_{34}$). Experiment performed under nitrogen with 99.5% purity nonanoic acid.

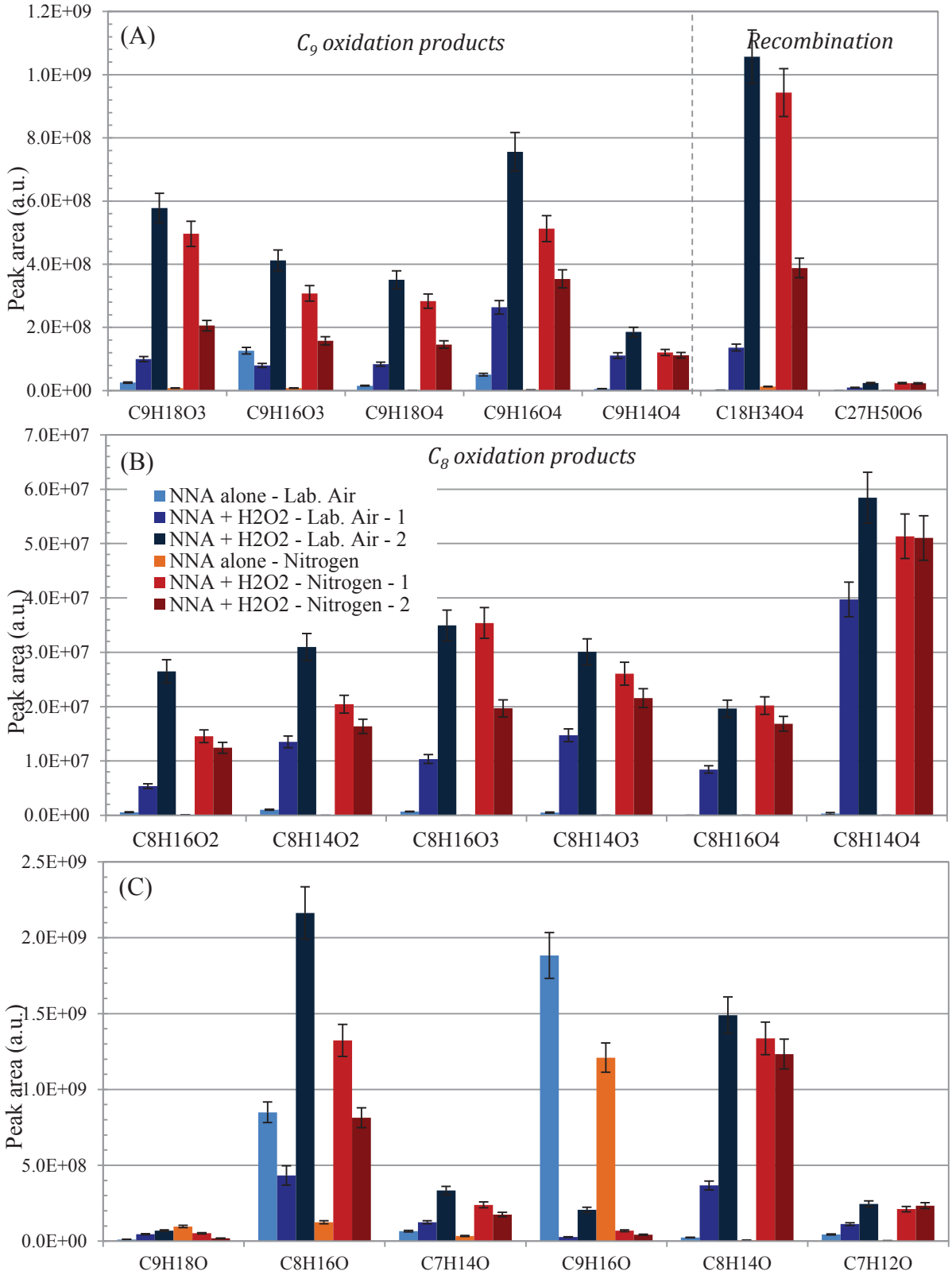

Figure S-VI-7: Signals obtained for a series of selected compounds in the condensed phase, after irradiation (1h) of NA alone (97% purity, 2 mM) or with H_2O_2 (10 mM) under laboratory air or N_2, detected in (A) and (B) (-) ionization mode and (C) (+) ionization mode after PFBHA derivatization (log_{10} scale). Error bars correspond to the estimated analytical uncertainties.

Chapter VII. Conclusion and perspectives

Chapter VII. Conclusion and perspectives.

In this work we firstly studied the photophysical and photochemical properties of two relevant photosensitizers, imidazole-2-carboxaldehyde and 6-carboxypterine in aqueous solutions. The latter proved to be moderately efficient photosensitizer towards three halides and an organics, limonene, in its triplet excited state. In its singlet excited state, CPT showed to efficiently oxidize the iodide and the four small carboxylic acids studied through a mechanism of electron transfer, leading to the formation of higher oxidized products, as showed in the case of lactic acid. The reactivity of the excited 6-carboxyoterin with limonene led to the formation of highly oxygenated products and recombination, reaction products similar to those observed for the reactions of triplet state excited imidazole-2-carboxaldehyde with the monoterpene. The formation of these products could explain the observed growth in particles containing imidazole-2-carboxaldehyde, a compound formed *in situ* in the particles, under light conditions in the presence of limonene. The observed particle growth occurs through reactive uptake of the VOC in the particulate phase, without gas phase oxidation. This second photosensitizer also showed high reactivity in its triplet state towards two halides, iodide and bromide, leading to the formation of highly reactive halogen species which can be released in the gas phase.

The reactivity of these two photosensitizers, relevant for the air-sea interface and for the particulate interface, towards halides and relevant organics, and previous works on photosensitized reactions initiated by aromatic ketones (Jammoul et al., 2009; Jammoul et al., 2008), leads to think that this type of heterogeneous photochemical reactions could be widely spread in the environment and could have a larger impact than generally known. Although models cannot account for the entire variety of organic reactions occurring in the environment, it would be useful to model the impact of these photochemical heterogeneous reactions at the surface of aerosols have, in particular on the oxidative capacity of the troposphere and on SOA formation. More research is needed to assess the importance and kinetics of such reactions at the air-sea interface, where these reactions could have a very large impact as well..

The formation of functionalized and unsaturated compounds at the interface of an organic coated aqueous solution containing a photosensitizer clearly demonstrates the important influence of photochemistry at the air-sea interface on the condensed and gas phase. It also bring into evidence that this interfacial photochemistry is specific for this region, where not only high concentrations of the surfactant, here simulated by 1-octanol or nonanoic acid, are expected but also of the photosensitizer, which partitions to this organic phase. This highly concentrated environment favors radical-radical reactions in particular which explain the observed unsaturated compounds. On the other hand oxidants from the gas phase are also readily available, leading to a large fraction of oxygenated species in addition and competition to this reduction pathway. Moreover, this chemistry has also been brought into evidence for the presence of nonanoic acid alone, opening the possibility of light induced reactions triggered by a carboxylic acid alone in a concentrated environment, e.g., the air-sea interface. Through chemical analysis of the gas and the bulk phase a general formation mechanism could be proposed explaining the formation of key compounds observed.

This chemistry can have very important repercussions on the marine boundary and the surface ocean, and by extension on all other interfaces where these type of compounds could be present, especially marine aerosols and a very wide range of potential interfaces can be relevant for the photochemistry of a carboxylic acid alone. At this stage, more work is needed to fully understand the processes at stake, to investigate their universality and to evaluate their real impact on the tropospheric chemistry and the marine environment in particular.

VII.1. References

Jammoul, A., Dumas, S., D'Anna, B. and George, C., 2009. Photoinduced oxidation of sea salt halides by aromatic ketones: a source of halogenated radicals. Atmospheric Chemistry and Physics, 9(13): 4229-4237.

Jammoul, A., Gligorovski, S., George, C. and D'Anna, B., 2008. Photosensitized heterogeneous chemistry of ozone on organic films. Journal of Physical Chemistry A, 112(6): 1268-1276.

Appendix I: Aknowledgements

This study was supported by the European Research Council under the European Union's Seventh Framework Programme (FP/2007-2013) / ERC Grant Agreement 290852 – AIRSEA, and the Marie Curie International Research Staff Exchange project AMIS (Grant 295132), and the Region Rhone Alpes.

Appendix II: Article

SO_2 uptake on oleic acid: a new pathway for organosulfate formation in the atmosphere.

Authors: Jing Shang[†¥], Monica Passananti[‡¥], Yoan Dupart[‡], Raluca Ciuraru[‡], Liselotte Tinel[‡], Stéphanie Rossignol[‡], Sébastien Perrier[‡], Tong Zhu[†], Christian George[‡]*

Article submitted to Environmental Science & Technology Letters

[†]State Key Joint Laboratory of Environmental Simulation and Pollution Control, College of Environmental Sciences and Engineering, Peking University,

Beijing, 100871, People's Republic of China

[‡]Université de Lyon 1, Lyon, F-69626, France, CNRS, UMR5256, IRCELYON, Institut de Recherches Sur la Catalyse et l'Environnement de Lyon, Villeurbanne, F-69626, France

[¥]*These authors have contributed equally to this work.*

* E-mail: *christian.george@ircelyon.univ-lyon1.fr*

ABSTRACT

Organosulfates have been detected in tropospheric particles and are thought to be products of secondary organic aerosol (SOA) formation processes. In this study, the reaction of sulfur dioxide (SO_2) with oleic acid and its possible contribution to organosulfate formation was investigated. The experiments were carried out at the gas-liquid interface with a coated-wall flow tube reactor. It was shown that SO_2 reacts efficiently with the unsaturation of oleic acid under atmospheric conditions, without the presence of ozone, with uptake coefficients in excess of 10^{-6}, decreasing with initial SO_2 concentration and linearly increasing with humidity. It was also shown that SO_2 reacts efficiently with oleic acid to form C_9 and C_{18} organosulfur products. These results tend to elucidate the role of organosulfates' interfacial chemistry, as a significant pathway for their contribution to atmospheric SOA formation.

1. INTRODUCTION

Heterogeneous reactions have attracted much attention in recent years because of their potential importance in affecting trace gas pollutants' transformation and particles' properties.[1-4] Sulfur dioxide (SO_2) is an important atmospheric pollutant. It can react at the surface of many aerosol particles such as mineral dust[5-8] and black carbon[9-11] and is, of course, at the origin of acid haze and rain.[12] But there are few studies about its heterogeneous reactions on organic surfaces, and its contribution to organosulfates is still unclear. Organosulfates are important secondary organic aerosol (SOA) components and good tracers for aerosol heterogeneous reactions.[13-14] Indeed, Liao et al. proposed that regions with elevated VOCs (Volatile Organic Compounds) and SO_2 may produce significantly more aerosol mass via some heterogeneous reaction processes.[13] Laboratory studies have also shown that the reactive uptake of carbonyls or biogenic olefins on sulfate-containing particles contributes to the formation of organosulfates.[15-17] However, the knowledge of organosulfates' spatial distribution, conditions of formation and environmental impact is limited.[14,18] It is, however, generally accepted that they are produced after the ozonolysis of unsaturated compounds (such as isoprene), with the transient epoxy compounds interacting with S-containing ions.[14,19-20] A direct chemical route from SO_2 interacting with unsaturated compounds has not been reported, but will be shown here.

Oleic acid (OA), a monounsaturated long-chain fatty acid, has been detected in urban, rural and marine aerosols.[21-23] It is the most common fatty acid found in plant membranes and in many cooking oils, and is a marker for meat cooking aerosols.[24-25] The low vapor pressure of OA makes it suitable for studies of heterogeneous chemistry. Indeed, it has been chosen as an unsaturated model compound for oxidation by atmospheric oxidants such as O_3 or NO_3 radicals.[26-29]

In this study, the heterogeneous reaction of SO_2 with OA was investigated using a coated-wall flow tube reactor, and was compared to the reactions of SO_2 with stearic acid and sodium oleate. The effects of SO_2 concentration, relativity humidity and OA mass were also investigated. The uptake coefficients of SO_2 on OA films were measured. We present a reaction scheme of SO_2 with OA based on the products identified using UHPLC-HR-MS for the liquid phase and SRI-ToF-MS for the gas phase.

2. MATERIALS AND METHODS

2.1 Heterogeneous uptake of SO_2 on oleic acid film

The uptake experiments were carried out in a coated-wall flow tube (Figure S1) coupled to an SO_2 detector (Thermo Scientific™ Model 43i SO_2 Analyzer) under atmospheric conditions (293 K; 1 atm). The flow reactor is a temperature-controlled double-walled cylindrical Pyrex tube, 22 cm in length. At the outlet of the flow tube, the temperature and relative humidity (RH) were monitored by a temperature and humidity sensor (Sensor-tec, UFT75 Sensor). Oleic acid ($C_{18}H_{34}O_2$, Alfa Aesar, 99% purity) was used to coat on the inner wall of a 20 cm long, 1.2 cm internal diameter (i.d.), Pyrex tube, then introduced into the flow tube. In order to coat the Pyrex tube, a 40 mg mL^{-1} oleic acid solution in acetone (Sigma-Aldrich, CHROMOSOLV® Plus, for HPLC, ≥ 99.9% purity) was prepared, introduced into the tube, then brushed using a Teflon rod, and finally dried. Because of the oily properties of OA, it was dispersed evenly as an oily thin film (sometimes showing little drops) with a corresponding weight ranging from 5.7 to 42.4 mg, corresponding to a film thickness between 0.04 and 0.3 μm. The SO_2 gas phase concentration (ranging from 0.3 to 11.3 molecules cm^{-3}) and the relative humidity of the airflow (RH, from 2 to 74 %) were adjusted by regulating the mixing ratios between an SO_2 standard gas tank flow (Linde France S.A., SO_2 in N_2, SO_2 concentration 10.31 ppm), a water-saturated airflow and a dry airflow (Linde France S.A., synthetic air, purity 99.9990%) using mass flow controllers. The water-saturated airflow was provided by bubbling the carrier gas in water in a humidifier at 293 ± 1 K. The resulting SO_2 flow was introduced into the flow tube through a horizontal movable injector at a flow rate of 150 or 300 mL min^{-1}.

The position of the injector was adjusted to vary the interaction length between 3.3 and 19.8 cm, leading to residence times between 0.7 and 4.5 s at a 300 mL min^{-1} flow rate and between 1.5 and 9.0 s at a 150 mL min^{-1} flow rate. A detailed description of the experimental procedure is reported in the Supporting Information. Similarly to OA films, stearic acid and sodium oleate films were prepared as follows: A 6 mg mL^{-1}stearic acid(Alfa Aesar, 98% purity) or an 8 mg mL^{-1}sodium oleate (Sigma-Aldrich, U.S., ≥ 99% purity) ethanol solution was added into a Pyrex tube until a coating of 4.5 mg or 4.9 mg was reached for stearic acid and sodium oleate, respectively.

The uptake coefficient (γ) is defined as the ratio of the molecules removed from the gas phase to the total gas surface collisions. It was determined by observing the loss of SO_2 as it was exposed to OA and was calculated from the measured first-order loss rate constant (k):[30-31]

$$\gamma = \frac{2rk}{\omega} (1)$$

where r is the radius of the flow tube (here 0.006 m) and ω is the mean molecular velocity of SO_2 (312 m s^{-1}). The uptake coefficient was determined using the geometric surface area of the coated glass tube.

2.2 Characterization of liquid phase products by UHPLC-HRMS

After the reaction of SO_2 with OA, the inner side of the flow tube was washed with methanol, then diluted with acetonitrile and ultrapure water to get a 2 mM OA solution to be analyzed by UHPLC-HESI/HRMS. All solvents were purchased from Fisher Scientific (USA) and were chemical grade Optima® LC-MS. UHPLC-HESI/HRMS analyses were performed by injecting 5 µL of samples into a DionexUltiMate 3000 UHPLC system coupled with a high

mass resolution Q-Exactive Hybrid Quadrupole-Orbitrap mass spectrometer (Thermo Scientific, USA) equipped with a Heated Electrospray Ionization source (H-ESI). The chromatographic separation was performed on a C_{18}Acquity UPLC HSS T3 column (1.8µm, 2.1 mm × 100 mm, Waters). The mobile phase was: (A) water with 0.1% formic acid and (B) acetonitrile with 0.1% formic acid and a gradient elution was applied (see Supporting Information). Electrospray ionization was performed in negative mode. The mass spectrometer was operated in full-scan mode with a scanning range from 50 to 750 m/z and a resolution of 140,000.

2.3 Characterization of gas phase products by SRI-ToF-MS

A commercially available Switchable Reagent Ion Time-of-Flight Mass Spectrometer (SRI-ToF-MS, Ionicon Analytik GmbH) using both H_3O^+ and NO^+ ionization modes was used to characterize gas phase products. The SRI-ToF-MS system was mounted at the exit of the flow reactor and sampled 80 sccm through 1.5 m of 1/4" mm i.d. peek tubing heated at 60 °C. Measurements were performed at a drift voltage of 600 V, a drift temperature of 60°C and a drift pressure of 2.25 mbar resulting in an E/N of about 130–135 Td (1 Td = 10^{-17} cm^2 V^{-1}). The resolution of the spectra was approximately 4000 at m/z 100. A more detailed description of the instrument is given elsewhere[32] (see also Supporting Information).

3. RESULTS AND DISCUSSIONS

3.1 The uptake of SO_2 on oleic acid

While no significant loss of SO_2 was observed on the clean glass insert (Figure S2), a sharp and sustained decrease was observed when exposed to an OA film (Figure S3). The SO_2 signal clearly decreased with the increasing exposed OA surface. After exposure, the injector was moved downstream and the SO_2 concentration returned to its original level, without any indication of SO_2 desorption. This suggested an irreversible uptake of SO_2 on the OA surface under our experimental conditions. These experiments were conducted under clean carrier gas, in the absence of any additional gas phase oxidants (such as ozone), and are indicative of an efficient uptake of SO_2 onto these surfaces, which is reported here for the first time under atmospheric conditions.

The measurement of the uptake coefficient was conducted by observing the decay of SO_2 concentration as a function of the injector position, i.e. of the interaction time. The SO_2 concentration decay was found to obey first-order kinetics:

$$\ln\left(\frac{C_0}{C_t}\right) = k_{obs}t \quad (2)$$

where C_0 represents the initial SO_2 concentration, C_t is the concentration of SO_2 at reaction time t, and k_{obs} is the observed first-order loss rate constant. Table S1 summarizes the uptake coefficients at different initial concentrations, humidity and OA mass conditions.

While no dependence was observed as a function of the deposited OA mass (Figure S4), Figure 1a illustrates the decrease of the uptake coefficient with increasing initial SO_2 concentration, indicative of a Langmuir-Hinshelwood-type mechanism, characterized by the adsorption of SO_2 followed by a chemical reaction (on the surface or within the bulk). OA is a

viscous liquid at room temperature, thus SO_2 could diffuse into the bulk of the film. On the other hand, increasing humidity was seen to accelerate the uptake process (Figure 1b), either by promoting the adsorption of SO_2 or by increasing the water content of the film and therefore the SO_2 solubility, and in both cases enhancing the reaction of SO_2 with OA.

3.2 Comparison of the reactivity of stearic acid, sodium oleate and oleic acid films

In order to better understand the reaction between SO_2 and OA, we measured the reactivity of stearic acid (a saturated C_{18} carboxylic acid) and sodium oleate (unsaturated C_{18} bearing a carboxylate function). For this purpose, stearic acid and sodium oleate were exposed to SO_2 as described above (Figure S5). While stearic acid did not show any reactivity, sodium oleate moderately reacted with SO_2 with a surface passivation after 23 min. In comparison, OA film sustained the reactivity for more than 3 hours. Thus, saturated compounds do not react, in contrast to the unsaturated oleic acid and sodium oleate. In addition, acidity could catalyze the uptake rate. These results highlight for the first time an efficient chemical reaction of SO_2 with unsaturated compounds.

3.3 Products, mechanism and impact

Table 1 lists the main condensed phase products, when oleic acid is exposed to synthetic air or SO_2. Under air, the UHPLC-HRMS analysis shows that OA is only slowly oxidized and that, as expected, no organosulfate products are formed. When OA is exposed to SO_2, the formation of sulfur-containing products is unambiguously observed, and the most abundant ones are detected at *m/z* 377.201 ($C_{18}H_{34}O_6S$) and *m/z* 237.080 ($C_9H_{18}O_5S$).

The product at *m/z* 377.201 is a C_{18} compound with the same degree of unsaturation as OA. It could therefore be a cyclic organosulfate, as previously observed in some photochemical reactions[33] and for SO_2 addition to double bonds.[34]

Sulfur dioxide may add to double bonds and non polar medium may promote radical reactions to form a diradical intermediate (Figure 2). In the presence of oxygen this intermediate could lead to cyclic organosulfates or to fragmentation products such as $C_9H_{18}O_5S$ (*m/z* 237.080).[33,35] The film exposure to SO_2 also increases the formation of OA oxidation products. This increase could be explained by some radical chain reactions triggered by the addition of SO_2 to the double bond. Indeed, the observed products at *m/z* 297.244 ($C_{18}H_{34}O_3$) and at *m/z* 187.098 ($C_9H_{16}O_4$) are common lipid oxidation products.[36] Gas phase products were analyzed by connecting an SRI-ToF-MS to the exit of the flow tube reactor. Both H_3O^+ and NO^+ ionization modes were used to analyze the gas phase. Gaseous sulfur-containing products were not observed, probably due to the low volatility. However, the formation of gaseous oxygenated compounds was observed. In the H_3O^+ ionization mode the main product signals detected were at *m/z* 143.134 ($(C_9H_{18}O)H^+$), *m/z* 145.122 ($(C_8H_{16}O_2)H^+$), *m/z* 131.143 ($(C_8H_{18}O)H^+$, octanol) and *m/z* 117.127 ($(C_7H_{16}O)H^+$, heptanol). In NO^+ ionization mode an increase of typical fragments of nonanoic acid and aldehydes[37-38] was observed when the film was exposed to SO_2.

To the best of our knowledge, this is the first time that a direct heterogeneous reaction between SO_2 and OA has been reported (i.e. without any further oxidant being required). This reaction leads to the formation of organosulfates and is relevant in highly polluted regions such as in some urban areas of China, where average concentrations of SO_2 and ozone of 15 ppbv and 65 ppbv, respectively, have been reported for 2014, with peak concentrations of SO_2 larger than 34 ppbv.[39] Taking into consideration the reported uptake coefficient of ozone on oleic acid at long reaction times[28] and the data presented here, it is possible to estimate that ca.

1.6–3.3 % of the double bonds will still react directly with the addition of SO_2, in regions with high sulfur loadings. [40]. As such heterogeneous SO_2 addition could certainly be generalized to other alkenes, we suggest that it should be taken into account for the atmospheric formation of organosulfates.

AUTHOR INFORMATION

Corresponding Author

*E-mail:*christian.george@ircelyon.univ-lyon1.fr* Phone: +33472445492

Notes

The authors declare no competing financial interest.

ACKNOWLEDGEMENTS

This study was supported by the Marie Curie International Research Staff Exchange project AMIS (Grant 295132), and the AgenceNationale de la Recherche through the COGNAC grant (ANR-13-BS06-0002-01), and the European Research Council under the European Union's Seventh Framework Programme (FP/2007-2013) / ERC Grant Agreement 290852 – AIRSEA.

ASSOCIATED CONTENT

Supporting Information Available: Additional information regarding the flow tube experiments and the product analysis is reported. This material is available free of charge via the Internet at http://pubs.acs.org.

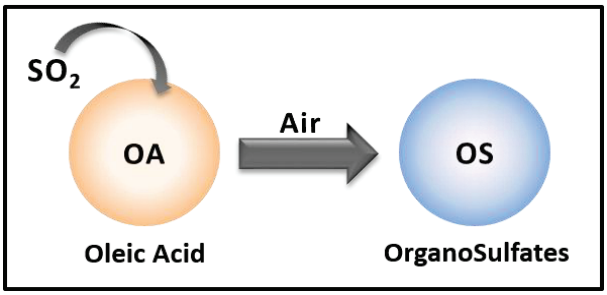

Table of Contents (TOC) Graphic

REFERENCES

1. Han, C.; Liu, Y.; Ma, J.; He, H. Key Role of Organic Carbon in the Sunlight-enhanced Atmospheric Aging of Soot by O_2. *Proc. Natl. Acad. Sci. U.S.A.* **2012**, *109*, 21250-21255.
2. Kolb, C. E.; Cox, R. A.; Abbatt, J. P. D.; Ammann, M.; Davis, E. J.; Donaldson, D. J.; Garrett, B. C.; George, C.; Griffiths, P. T.; Hanson, D. R.; and et al. An Overview of Current Issues in the Uptake of Atmospheric Trace Gases by Aerosols and Clouds. *Atmos. Chem. Phys.* **2010**, *10*, 10561-10605.
3. Rudich, Y.; Donahue, N. M.; Mentel, T. F. Aging of Organic Aerosol: Bridging the Gap between Laboratory and Field Studies. *Annu. Rev. Phys. Chem.* **2007**, *58*, 321-352.
4. George, C.; Ammann, M.; D'Anna, B.; Donaldson, D. J.; Nizkorodov, S. A. Heterogeneous Photochemistry in the Atmosphere. *Chem. Rev.* **2015**, *115*, 4218-4258.
5. Adams, J. W.; Rodriguez, D.; Cox, R. A. The Uptake of SO_2 on Saharan Dust: a Flow Tube Study. *Atmos. Chem. Phys.* **2005**, *5*, 2679-2689.
6. Li, L.; Chen, Z. M.; Zhang, Y. H.; Zhu, T.; Li, S.; Li, H. J.; Zhu, L. H.; Xu, B. Y. Heterogeneous Oxidation of Sulfur Dioxide by Ozone on the Surface of Sodium Chloride and its Mixtures with Other Components. *J. Geophys. Res.-Atmos.* **2007**, *112*, 1-13.
7. Nanayakkara, C. E.; Pettibone, J.; Grassian, V. H. Sulfur Dioxide Adsorption and Photooxidation on Isotopically-labeled Titanium Dioxide Nanoparticle Surfaces: Roles of Surface Hydroxyl Groups and Adsorbed Water in the Formation and Stability of Adsorbed Sulfite and Sulfate. *Phys. Chem. Chem. Phys.* **2012**, *14*, 6957-6966.
8. Wu, L. Y.; Tong, S. R.; Wang, W. G.; Ge, M. F. Effects of Temperature on the Heterogeneous Oxidation of Sulfur Dioxide by Ozone on Calcium Carbonate. *Atmos. Chem. Phys.* **2011**, *11*, 6593-6605.
9. Nienow, A. M.; Roberts, J. T. Heterogeneous Chemistry of Carbon Aerosols. *Annu. Rev. Phys. Chem.* **2006**, *57*, 105-128.
10. Novakov, T.; Chang, S. G.; Harker, A. B. Sulfates as Pollution Particulates: Catalytic Formation on Carbon (Soot) Particles. *Science* **1974**, *186*, 259-261.
11. Song, H.; Shang, J.; Zhu, T.; Zhao, L.; Ye, J.-H. Heterogeneous Oxidation of SO_2 by Ozone on the Surface of Black Carbon Particles. *Chem. J. Chinese U.* **2012**, *33*, 2295-2302.
12. Finlayson-Pitts, B. J.; Pitts Jr, J. N. Chapter 1 - Overview of the Chemistry of Polluted and Remote Atmospheres. In *Chemistry of the Upper and Lower Atmosphere*, Pitts, B. J. F.-P. N., Ed. Academic Press: San Diego, 2000; pp 1-14.

13. Liao, J.; Froyd, K. D.; Murphy, D. M.; Keutsch, F. N.; Yu, G.; Wennberg, P. O.; St. Clair, J. M.; Crounse, J. D.; Wisthaler, A.; Mikoviny, T.; and et al. Airborne Measurements of Organosulfates over the Continental US. *J. Geophys. Res.Atmos.* **2015**, *120*, 2990-3005.

14. Zhang, H.; Worton, D. R.; Lewandowski, M.; Ortega, J.; Rubitschun, C. L.; Park, J.-H.; Kristensen, K.; Campuzano-Jost, P.; Day, D. A.; Jimenez, J. L.; and et al. Organosulfates as Tracers for Secondary Organic Aerosol (SOA) Formation from 2-Methyl-3-Buten-2-ol (MBO) in the Atmosphere. *Environ. Sci. Technol.* **2012**, *46*, 9437-9446.

15. Liggio, J.; Li, S.-M. Organosulfate Formation During the Uptake of Pinonaldehyde on Acidic Sulfate Aerosols. *Geophys. Res. Lett.* **2006**, *33*, 1-4.

16. Liggio, J.; Li, S. M. Reversible and Irreversible Processing of Biogenic Olefins on Acidic Aerosols. *Atmos. Chem. Phys.* **2008**, *8*, 2039-2055.

17. Perri, M. J.; Lim, Y. B.; Seitzinger, S. P.; Turpin, B. J. Organosulfates from Glycolaldehyde in Aqueous Aerosols and Clouds: Laboratory Studies. *Atmos. Environ.* **2010**, *44*, 2658-2664.

18. Tolocka, M. P.; Turpin, B. Contribution of Organosulfur Compounds to Organic Aerosol Mass. *Environ. Sci. Technol.* **2012**, *46*, 7978-7983.

19. Minerath, E. C.; Elrod, M. J. Assessing the Potential for Diol and Hydroxy Sulfate Ester Formation from the Reaction of Epoxides in Tropospheric Aerosols. *Environ. Sci. Technol.* **2009**, *43*, 1386-1392.

20. Mauldin, R. L., III; Berndt, T.; Sipilae, M.; Paasonen, P.; Petaja, T.; Kim, S.; Kurten, T.; Stratmann, F.; Kerminen, V. M.; Kulmala, M. A New Atmospherically Relevant Oxidant of Sulphur Dioxide. *Nature* **2012**, *488*, 193-196.

21. Cheng, Y.; Li, S. M. Nonderivatization Analytical Method of Fatty Acids and Cis-pinonic Acid and its Application in Ambient $PM_{2.5}$Aerosols in the Greater Vancouver Area in Canada. *Environ. Sci. Technol.* **2005**, *39*, 2239-2246.

22. Graham, B.; Guyon, P.; Taylor, P. E.; Artaxo, P.; Maenhaut, W.; Glovsky, M. M.; Flagan, R. C.; Andreae, M. O. Organic Compounds Present in the Natural Amazonian Aerosol: Characterization by Gas Chromatography-mass Spectrometry. *J. Geophys. Res.Atmos.* **2003**, *108*, 1-13.

23. Schauer, J. J.; Rogge, W. F.; Hildemann, L. M.; Mazurek, M. A.; Cass, G. R.; Simoneit, B. R. T. Source Apportionment of Airborne Particulate Matter Using Organic Compounds as Tracers. *Atmos. Environ.* **1996**, *30*, 3837-3855.

24. Rogge, W. F.; Hildemann, L. M.; Mazurek, M. A.; Cass, G. R.; Simonelt, B. R. T. Sources of Fine Organic Aerosol. 1. Charbroilers and Meat Cooking Operations. *Environ. Sci. Technol.* **1991**, *25*, 1112-1125.

25. Zhao, X.; Hu, Q.; Wang, X.; Ding, X.; He, Q.; Zhang, Z.; Shen, R.; Lu, S.; Liu, T.; Fu, X.; and et al. Composition Profiles of Organic Aerosols from Chinese Residential Cooking: Case Study in Urban Guangzhou, South China. *J. Atmos. Chem.***2015**, *72*, 1-18.

26. Docherty, K. S.; Ziemann, P. J. Reaction of Oleic Acid Particles with NO_3Radicals: Products, Mechanism, and Implications for Radical-initiated Organic Aerosol Oxidation. *J. Phys. Chem. A* **2006**, *110*, 3567-3577.

27. Lee, J. W. L.; Carrascon, V.; Gallimore, P. J.; Fuller, S. J.; Bjoerkegren, A.; Spring, D. R.; Pope, F. D.; Kalberer, M. The Effect of Humidity on the Ozonolysis of Unsaturated Compounds in Aerosol Particles. *Phys. Chem. Chem. Phys.* **2012**, *14*, 8023-8031.

28. Mendez, M.; Visez, N.; Gosselin, S.; Crenn, V.; Riffault, V.; Petitprez, D. Reactive and Nonreactive Ozone Uptake during Aging of Oleic Acid Particles. *J. Phys. Chem. A* **2014**, *118*, 9471-9481.

29. Vesna, O.; Sax, M.; Kalberer, M.; Gaschen, A.; Ammann, M. Product Study of Oleic Acid Ozonolysis as Function of Humidity. *Atmos. Environ.* **2009**, *43*, 3662-3669.

30. Keyser, L. F.; Moore, S. B.; Leu, M. T. Surface Reaction and Pore Diffusion in Flow-tube Reactors. *J. Phys. Chem.* **1991**, *95*, 5496-5502.

31. Zhang, D.; Zhang, R. Y. Laboratory Investigation of Heterogeneous Interaction of Sulfuric Acid with Soot. *Environ. Sci. Technol.* **2005**, *39*, 5722-5728.

32. Fu, H.; Ciuraru, R.; Dupart, Y.; Passananti, M.; Tinel, L.; Rossignol, S.; Perrier, S.; Donaldson, D. J.; Chen, J.; George, C. Photosensitized Production of Atmospherically Reactive Organic Compounds at the Air/Aqueous Interface. *J. Am. Chem. Soc.* **2015**, *137*, 8348-8351.

33. Jones, P. W.; Adelman, A. H. A Novel Preparation of Cyclic Sulfites Through Photosulfoxidation of Alkenes. *Tetrahedron* **1974**, *30*, 2053-2055.

34. Vogel, P.; Turks, M.; Bouchez, L.; Markovic, D.; Varela-Alvarez, A.; Sordo, J. A. New Organic Chemistry of Sulfur Dioxide. *Acc. Chem. Res.* **2007**, *40*, 931-942.

35. Christl, M.; Brunn, E.; Lanzendorfer, F. Reactions of Benzvalene with Tetracyanoethylene, 2,3-Dichloro-5,6-Dicyano-p-Benzoquinone, Chlorosulfonyl Isocyanate, and Sulfur Dioxide. Evidence for Concerted 1,4-Cycloadditions to a Vinylcyclopropane System. *J. Am. Chem. Soc.* **1984**, *106*, 373-382.

36. Frankel, E. N. Volatile Lipid Oxidation Products. *Prog. Lipid Res.* **1983**, *22*, 1-33.

37. Mochalski, P.; Unterkofler, K.; Hinterhuber, H.; Amann, A. Monitoring of Selected Skin-Borne Volatile Markers of Entrapped Humans by Selective Reagent Ionization Time of Flight Mass Spectrometry in NO^+ Mode. *Anal. Chem.* **2014**, *86*, 3915-3923.

38. Mochalski, P.; Unterkofler, K.; Spanel, P.; Smith, D.; Amann, A. Product Ion Distributions for the Reactions of NO^+ with Some Physiologically Significant Aldehydes Obtained Using a SRI-TOF-MS Instrument. *Int. J. Mass Spectrom.* **2014**, *363*, 23-31.

39. MPE, Ministry of Environmental Protection the People's Republic of China, Report on the State of the Environment of China: 2014. **2014**, *http://www.mep.gov.cn/gkml/hbb/qt/201506/W020150605384146647135.pdf*, 09/09/2014.

40. Carmichael, G. R.; Ferm, M.; Thongboonchoo, N.; Woo, J. H.; Chan, L. Y.; Murano, K.; Viet, P. H.; Mossberg, C.; Bala, R.; Boonjawat, J.; and et al. Measurements of Sulfur Dioxide, Ozone and Ammonia Concentrations in Asia, Africa, and South America Using Passive Samplers. *Atmos. Environ.* **2003**, *37*, 1293-1308.

FIGURE LEGENDS

Figure 1. Dependence of the uptake coefficient on the SO_2 initial concentration (a) and relative humidity RH (b).

Figure 2. Suggested reaction mechanism and structures of the identified organosulfur derivatives.

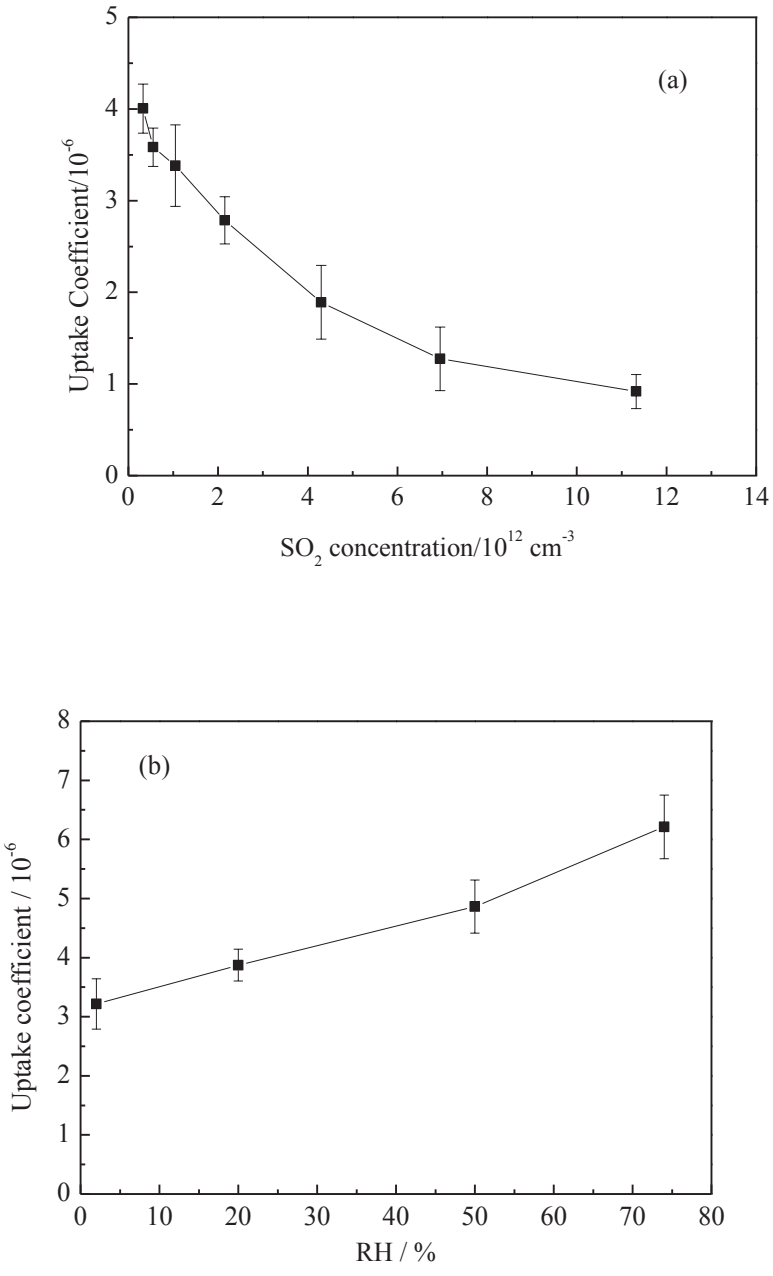

Figure 1

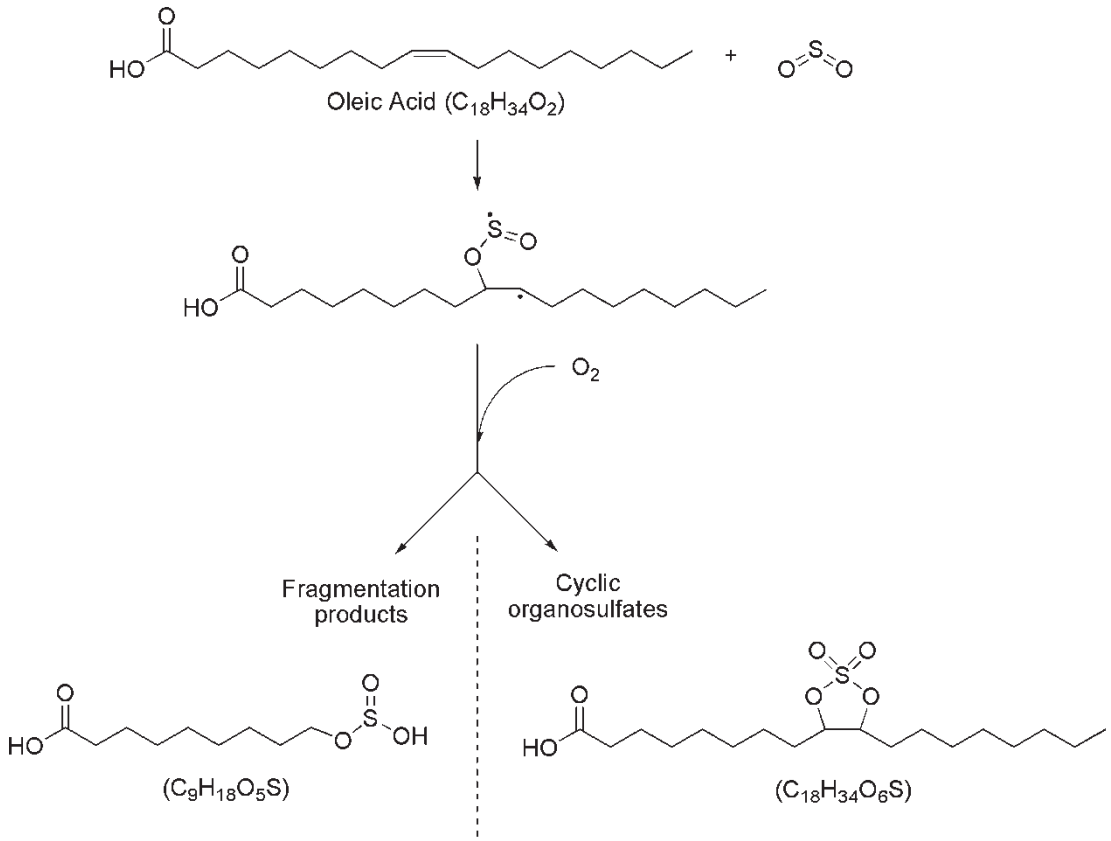
Oleic Acid ($C_{18}H_{34}O_2$)
O_2
Fragmentation products
Cyclic organosulfates
($C_9H_{18}O_5S$)
($C_{18}H_{34}O_6S$)

Figure 2

Table 1. Exact masses, detected by UHPLC-HRMS, of oleic acid film exposed to synthetic air and to SO_2 (4.3×10^{12} molecules cm^{-3}). Experimental conditions: flow rate = 150 mL min^{-1}, RH = 30%.

				Oleic acid film exposed to SO_2 in synthetic air		Oleic acid film exposed to synthetic air	
Oxidation Products	Chemical Formula	Detected mass (m/z)	Δppm	Integrated Peak Area ($\times 10^6$ a.u.)	Ratio Product/Oleic Acid	Integrated Peak Area ($\times 10^6$ a.u.)	Ratio Product/Oleic Acid
C_{18}	**$C_{18}H_{34}O_2$**	**281.249**	+ 0.4	1.71	**1.00**	1.25	1.00
	$C_{18}H_{34}O_3$	297.244	+ 0.8	49.34	**28.91**	0.72	0.57
	$C_{18}H_{34}O_4$	313.239	+ 0.8	29.83	**17.48**	2.90	2.32
	$C_{18}H_{36}O_4$	315.254	+ 0.7	3.97	**2.33**	1.81	1.45
	$C_{18}H_{32}O_4$	311.223	+ 0.9	1.84	**1.08**	0.03	0.03
	$C_{18}H_{32}O_3$	295.228	+ 0.6	15.40	**9.02**	-	-
C_9	$C_9H_{18}O_3$	173.118	+ 0.9	1.64	**0.96**	0.83	0.67
	$C_9H_{16}O_4$	187.098	+ 1.1	39.81	**23.33**	6.45	5.17
	$C_9H_{16}O_3$	171.103	+ 1.5	1.39	**0.81**	0.08	0.06
Organosulfur Products							
C_{18}	$C_{18}H_{32}O_7S$	391.180	+ 1.4	1.00	**0.59**	-	-
	$C_{18}H_{34}O_6S$	377.201	+ 1.2	15.01	**8.79**	-	-
	$C_{18}H_{34}O_7S$	393.196	+ 1.3	5.26	**3.08**	-	-
	$C_{18}H_{36}O_7S$	395.211	+ 1.2	3.41	**2.00**	-	-
C_9	$C_9H_{18}O_5S$	237.080	+ 1.1	9.35	**5.48**	-	-

Supporting information

SO_2 uptake on oleic acid: a new pathway for organosulfate formation in the atmosphere.

Jing Shang[†¥], Monica Passananti[‡¥], Yoan Dupart[‡], Raluca Ciuraru[‡], Liselotte Tinel[‡], Stéphanie Rossignol[‡], Sebastien Perrier[‡], Tong Zhu[†], Christian George[‡]*

[†]State Key Joint Laboratory of Environmental Simulation and Pollution Control, College of Environmental Sciences and Engineering, Peking University,

Beijing, People's Republic of China

[‡] Université de Lyon 1, Lyon, F-69626, France, CNRS, UMR5256, IRCELYON, Institut de Recherches Sur la Catalyse et l'Environnement de Lyon, Villeurbanne, F-69626, France

[¥]*These authors have contributed equally to this work.*

Heterogeneous uptake of SO_2 on organic films

A schematic representation of the coated-wall flow tube is shown in Figure S1.

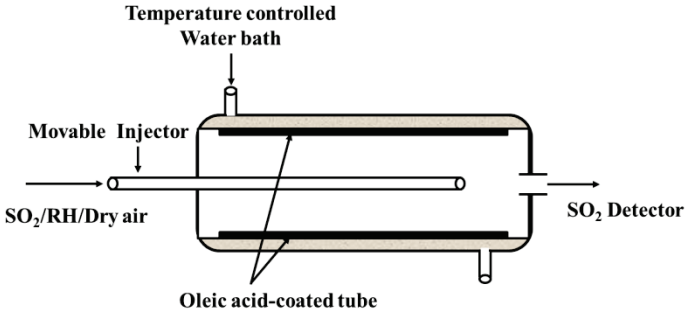

FigureS1. Schematic diagram of the flow tube reactor.

To examine whether there is adsorption of SO_2 onto the Pyrex surface, a blank experiments was conducted with about 4.6×10^{12} molecular cm^{-3} SO_2 introduced into a clean tube (washed with a NaOH solution, acetone and ultrapure water sequentially). The injector was successively withdrawn for 3.3, 9.9 and 19.8 cm length. No decrease of SO_2 was observed (Figure S2), indicating that there is no adsorption of SO_2 on the Pyrex tube.

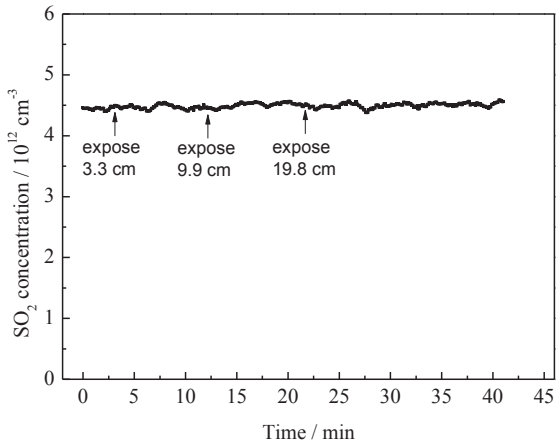

Figure S2. Time evolution of SO_2 concentration. The injector was successively withdrawn for 3.3, 9.9, 19.8 cm length over a blank Pyrex tube. Experimental conditions: SO_2 concentration = 4.6×10^{12} molecular cm^{-3}, flow rate = 150 mL min^{-1}, RH = 6 %.

All tubes used to prepare organic films were washed with a NaOH solution, acetone and ultrapure water sequentially. In a typical experiment, oleic acid was introduced into the tube adhered onto the inside of the tube. Then the tube was exposed to SO_2 with a flow rate of 300 mL min^{-1} or 150 mL min^{-1}. A steady-state flow of SO_2 was first established without exposure of the oleic acid film. When the SO_2 concentration was stable the injector was quickly withdrawn to expose 3.3 cm of the coated tube with the oleic acid film to SO_2 gas. A sharp decrease in SO_2 concentration was observed upon exposure of SO_2 to oleic acid. No obvious recovery in the SO_2 concentration was observed during the exposure. After about 10 min, the injector was moved downstream, that is, no oleic acid was exposed to

SO_2, and the SO_2 concentration returned to its original level. This withdrawing and return of the injector was repeated for 6.6, 9.9, 13.2, 16.5 and 19.8 cm respectively of the oleic acid surface exposed to SO_2 for 10 min each time (Figure S3). The SO_2 signal decay increased with the increase of oleic acid exposure length. After each 10 min exposure, the injector was pushed downstream to the original position, and a full recovery of the signal was observed every time.

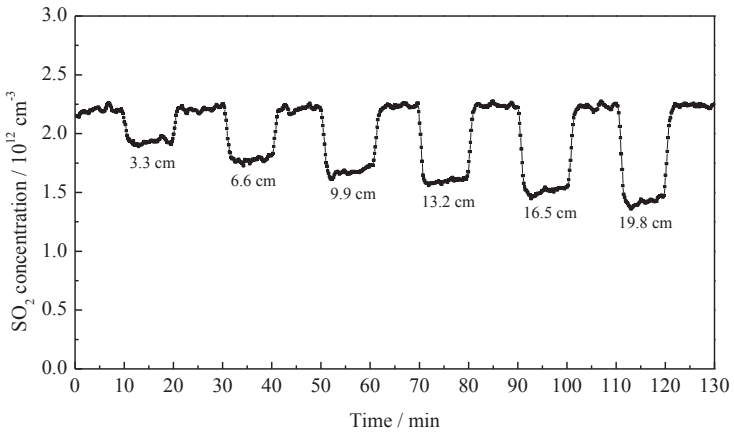

Figure S3. Uptake of SO_2 on the surface of oleic acid. The injector was withdrawn for 3.3, 6.6, 9.9, 13.2, 16.5 and 19.8 cm, respectively, over the oleic acid surface and then returned to its original position. Experimental conditions: oleic acid mass = 7.0 mg, SO_2 concentration = 2.1×10^{12} molecular cm^{-3}, flow rate = 300 mL min^{-1}, RH = 6 %.

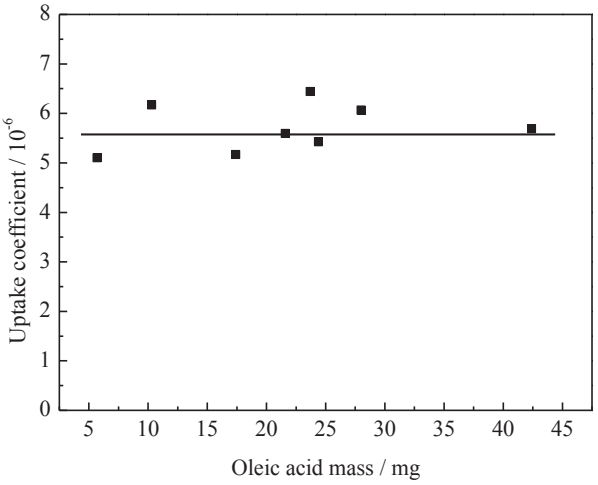

Figure S4. Dependence of uptake coefficient with oleic acid mass. Experimental Conditions: oleic acid mass = 5.7, 10.3, 17.4, 21.6, 23.7, 24.4, 28.0, 42.4 mg; RH = 3~4 %, SO_2 initial concentration = 2.0~2.1 × 10^{12} molecular cm^{-3}; flow rate = 300 mL min^{-1}.

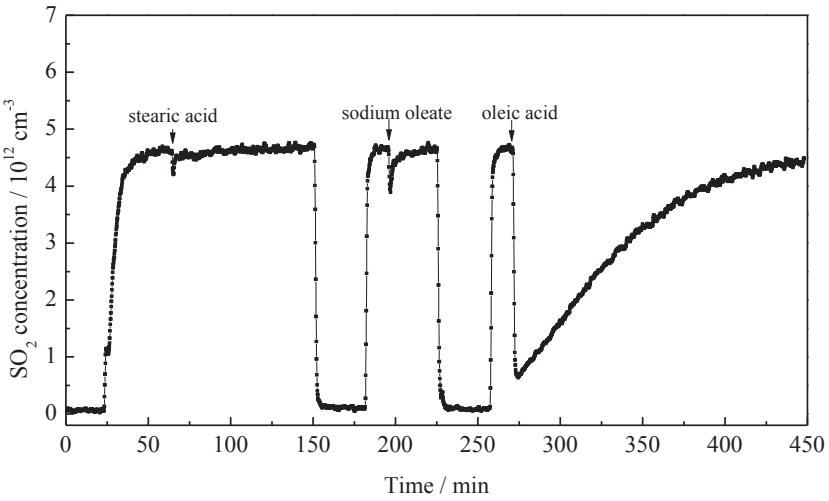

Figure S5. Uptake of SO_2 on stearic acid, sodium oleate and oleic acid films. Experimental Conditions: SO_2 initial concentration is 4.5×10^{12} molecular cm^{-3}; RH = 0.1 %; the mass of stearic acid, sodium oleate and oleic acid is 4.5, 4.9 and 3.0 mg, respectively; flow rate = 150 mL min^{-1}, exposure length 19.8 cm. The time regions of zero signal of SO_2 (background signal) during 0-25, 150-180 min and 230-260 min are the switching period for the tube.

Table S1. Summary of uptake coefficient measurements of SO_2 on oleic acid at different SO_2 concentration, RH and oleic acid mass conditions.

Parameters	SO_2 concentration ($\times 10^{12}$ molecular cm^{-3})	RH (%)	Oleic acid mass (mg)	k (s^{-1})	R^{2} *	γ ($\times 10^{-6}$)
Different SO_2 concentration	0.3	7	6.6	0.104	0.9944	4.00
	0.6	7	6.0	0.093	0.9957	3.58
	1.1	6	5.0	0.088	0.9788	3.38
	2.2	6	7.7	0.072	0.9895	2.79
	4.3	7	6.2	0.049	0.9459	1.89
	7.0	6	5.0	0.033	0.9137	1.27

	11.3	6	6.0	0.024	0.9501	0.92
Different RH	2.3	2	5.2	0.084	0.9827	3.22
	2.2	20	6.8	0.101	0.9952	3.87
	2.2	50	6.3	0.127	0.9915	4.87
	2.3	74	8.0	0.162	0.9925	6.21
Different oleic acid mass	2.1	4	5.7	0.133	0.9942	5.10
	2.0	3	10.3	0.160	0.9962	6.17
	2.1	3	17.4	0.134	0.9923	5.17
	2.1	3	21.6	0.146	0.9921	5.60
	2.1	3	23.7	0.168	0.9968	6.44
	2.1	3	24.4	0.141	0.9963	5.42
	2.1	3	28.0	0.158	0.9975	6.07

	2.0	3	42.4	0.148	0.9963	5.69

Experimental conditions: flow rate = 300 mL min^{-1} and T = 293~294 K.

* R^2 is the correlation coefficient of the line $ln\ (C_0/C_t)$~t

Analytical conditions for the condensed phase products by HPLC-HRMS

The mobile phase was: (A) water with 0.1% formic acid and (B) acetonitrile with 0.1% formic acid. Gradient elution was performed at a flow rate of 0.3 mL min^{-1}, starting at 1% B (for 2 min) linearly programmed to 100% B within 11 min, this ratio was maintained constant for 2 min before returning to initial conditions (B at 1%) in 0.1 min for 6.9 min. Electrospray ionization was performed in negative mode using the following conditions: spray voltage -3.0 kV, capillary temperature 350 °C, sheath gas (N_2) flow rate 40 (arbitrary units), auxiliary gas (N_2) flow rate 25 (arbitrary units), heater temperature 250 °C, S-lens RF level 50. The Q-Exactive mass spectrometer was calibrated externally every day by direct infusion of a sodium acetate solution (2 mM in H_2O/CH_3CN 1/1 v/v) to reach mass accuracies below 4 ppm. The data were processed using Xcalibur v. 2.2 software.

Analytical conditions for the gas phase products by SRI-ToF-MS

The reagent ions to ionize products are generated by a hollow cathode discharge ion source using water vapor in the case of H_3O^+ ionization mode and a mixture

of N_2 and O_2 in the case of NO^+ ionization mode. The settings of the source were optimized for each ionization mode in order to obtain less than 2% impurities in the primary ion signal. In the H_3O^+ mode the settings used were: source current 4 mA; source voltage 100 V; source outlet voltage 80 V ; and source valve opening at 37 % with a flow of 5.8 sccm of water vapor. In the NO^+ ionization mode, the source settings were the following: source current 5.5; source voltage 25 V; source outlet voltage 69 V and source opening valve at 36 % with flows of 5.4 sccm and 2.8 sccm for O_2 and N_2 respectively. For H_3O^+ ionization mode spectra were acquired between 1 and 350 *m/z* at a sampling frequency of 25 kHz and were registered by co-adding single TOF-extractions for a time of 1 s. In NO^+ ionization mode spectra were acquired between 1 and 400 m/z at a sampling frequency of 35 kHz and were registered by co-adding single TOF-extractions for a time of 8 s. Data were processed using PTR-MS Viewer 3.1.0.12.

Résumé :

Les travaux présentés dans cette thèse portent premièrement sur la caractérisation de nouveaux photosensibilisateurs par des méthodes spectroscopiques. Ainsi les cinétiques de la réaction d'oxydation entre deux photosensibilisateurs à l'état triplet, imidazole-2-carboxaldehyde et 6-carboxypterine, et trois halogénures ont été déterminées par photolyse laser. La réactivité de l'état singulet de la 6-carboxypterine avec les halogénures et quatre acides organiques a été étudiée par fluorimétrie. Ces photosensibilisateurs sont relevants pour la photochimie à la surface de l'océan, mais également à la surface des particules atmosphériques. Les réactions mises en évidence mènent à la formation d'espèces radicalaires très réactives, influençant ainsi la composition de la phase condensée et gazeuse de l'environnement marin. La suite de cette étude s'est focalisée sur l'analyse des produits formés à partir de processus photo-induites à interface air-eau en présence d'une microcouche de surface d'un organique, utilisant deux organiques différents, l'octanol et l'acide nonanoique. En présence d'un photosensibilisateur et de lumière UVA, les changements en phase gaz ont été suivi par SRI-ToF-MS en ligne et en phase condensée par UPLC-(ESI)-HRMS. Ainsi on a démontré que la photochimie à la surface mène à la formation de produits fonctionnalisés et insaturés initiée par une abstraction d'hydrogène sur l'organique surfactant. Ces produits, observés en phase condensée et gazeuse, ont le potentiel de contribuer à la formation d'aérosols. Etonnamment, des produits ont également été observés dans les deux phases sans l'ajout d'un photosensibilisateur et montrant une activité photochimique de l'acide nonanoique seul à l'interface air-eau. Les mécanismes potentiels et les conséquences environnementales sont discutés.

Abstract :

The works presented in this thesis concern firstly the characterization of two new photosensitizers by spectroscopic methods. This way the kinetics of the oxidation reaction between the triplet state of the photosensitizers, imidazole-2-carboxaldehyde and 6-carboxypterin, and three halides have been determined by laser flash photolysis. Also, the reactivity of the singlet state of 6-carboxypterin with halides and four organic acids has been studied by static fluorimetry. These photosensitizers are relevant for the photochemistry at the surface of the ocean, but also at the surface of atmospheric particles. The reactions evidenced by these studies lead to the formation of very reactive radical species influencing the composition of the condensed and gas phase of the marine environment. This study then focalized on the analysis of the products formed at the organic coated air-water interface through photo-induced processes. Two different organics were used as surfactants, octanol and nonanoic acid. In the presence of a photosensitizer and UVA light, the changes in the gas phase were monitored online by SRI-ToF-MS and in the condensed bulk phase by UPLC-(ESI)-HRMS offline analysis. These analysis showed that photochemical reactions at the interface lead to the formation of functionalized and unsaturated compounds initiated by a hydrogen abstraction on the organic surfactant. These products, observed in the condensed and gas phase have the potential to contribute to the formation of aerosols. Surprisingly, some of these products were also observed in the two phases without the presence of a photosensitizer, bringing into evidence a photochemistry of nonanoic acid at the air-water interface. Potential formation mechanisms of the products and environmental consequences are discussed.